Sedimentation characteristics on the Andaman shelf, Thailand: unraveling extreme events

Dissertation

Zur Erlangung des Doktorgrades

Dr. rer. nat.

der Mathematisch-Naturwissenschaftlichen Fakultät

der Christian-Albrechts Universität zu Kiel

Vorgelegt von

Daroonwan (Sakuna) Schwartz

Kiel, 2015

Referent: Prof. Dr. Karl Stattegger

Korreferent: Prof. Dr. Sebastian Krastel-Gudegast

Tag der mündlichen Prüfung: 9th November 2015

Zum Druck genehmigt: 10th November 2015

gez. Prof. Dr. Wolfgang J. Duschl, Dekan

I affirm in lieu of oath that:

i) apart of the supervisor's guidance the content and design of the paper is all the candidate's own work;

ii) the present thesis has not been submitted either partially or wholly as part of a doctoral degree to another examining body and whether it has been published or submitted for publication;

iii) the thesis has already been prepared subjected to the Rules of Good Scientific Practice of the German Research Foundation.

Kiel, den 2015

Daroonwan (Sakuna) Schwartz

Abstract

The 2004 Indian Ocean tsunami had an impact on the entire coastline of Southeast Asia. As one of several recent tsunamis, it provides unique opportunities to study the geomarine effects of such events in detail. The Andaman shelf (Thailand) was chosen to evaluate offshore tsunami deposits. Its coastline was strongly influenced by the 2004 tsunami, while the infrequent occurrence of strong storms and negligible fluvial discharge increase the preservation potential of tsunami deposits on the seafloor.

In total, 60 sediment cores and 156 seafloor sediment samples from water depth between 5-65 m, as well as 10 onshore sediment samples and supporting hydroacoustic data were available for this study. Investigations of shallow seismic data, sedimentary structures, grain size composition, physical sediment properties, element composition and Ti/Ca log-ratio as well as ^{210}Pb and AMS^{14}C dating revealed general information about the seafloor sediment distribution and its stratigraphy on the Andaman Sea shelf during the Holocene period. In the study area, the seafloor is dominated by coarse sediment (sand and boulders with coral rubbles). Partly, small incised channels are observed down to 30 m water depth. This structure has been interpreted as a remnant of an old reef platform, active during times of lower sea level. Especially within these channels, finer grained sediment, including event deposits, were trapped.

Sediment cores retrieved from shallow water down to approx. 16 m revealed three different types of event deposits that are interpreted as tsunami, storm and flash-flood deposits. Thus, the dataset allowed to discriminate and to compare recent storm and tsunami deposits. The most recent event deposits were found in core depths between 0 and 40 cm, and were interpreted as being tsunami deposits. These tsunami layers have a thickness about 12-30 cm, and are comprised of several distinct units that include sedimentary features as lamination, fining and coarsening upward, massive structure, erosional of both upper and lower contacts, terrigenous and anthropogenic components, and clasts. The different units represent different hydrodynamic conditions (probably run-up and backwash phase). In core depths between 5 and 82 cm, a second type of event layer has been found. These layers are 1-10 cm thick and mainly contain sharp and erosional lower contacts, partly massive and partly show slight lamination. These are assigned to storm deposits. Accordingly, the prominent difference between tsunami and storm deposits is the presence of clasts, terrigenous materials, anthropogenic artifacts and mud content. A third kind of event layers found in core depths between 12 and 92 cm are considered to be result of small scale events such as flash floods during summer monsoon period. These deposits have a thickness of 2-13 cm, and are mainly composed of clayey silt with few sand layers, which are commonly laminated and generally fining upward with transitional boundaries.

Zusammenfassung

Der Tsunami im Indischen Ozean 2004 hatte Auswirkungen auf die gesamte Küste Südostasiens. Er bietet als jüngster von mehreren rezenten Tsunamis einzigartige Möglichkeiten, um die geomarinen Auswirkungen solcher Ereignisse im Detail zu studieren. Der Schelfbereich der Andaman-See in Thailand wurde gewählt, um offshore Tsunami-Ablagerungen zu untersuchen. Das seltene Auftreten starker Winde und der sehr geringe Einfluss von fluviatilem Sediemnteintrag ermöglicht es Tsunamiablagerungen und Einflüsse für eine relativ lange Zeit auf dem Meeresgrund zu konservieren.

Insgesamt standen für die vorliegende Studie 60 Sedimentkerne und 156 Meeressedimentproben aus Wassertiefen zwischen 5-65 m, sowie 10 Onshore-Sedimentproben und hydroakustische Daten zur Verfügung. Durch Untersuchungen von flachseismischen Daten, Röntgenaufnahmen, dem Ti/Ca log-Verhältnis sowie ^{210}Pb und AMS^{14}C Datierungen konnten allgemeine Informationen über die Sedimentverteilung und über die Stratigraphie auf dem Meeresboden des Schelfbereichs der Andaman-See während des Holozäns gewonnen werden. Im Untersuchungsgebiet ist der Meeresboden v.a. durch grobe Sedimente, Sand und Geröll mit Korallen-Trümmern, geprägt. Teilweise wurden kleine, eingeschnittene Kanäle bis zu einer Wassertiefe von 30 m beobachtet. Diese Strukturen werden als Überbleibsel einer alten Riff-Plattform interpretiert, die in Zeiten eines niedrigeren Meeresspiegels aktiv gewesen ist. Innerhalb dieser Kanäle wurden feinkörnige Sedimente, einschließlich Ereignisablagerungen gewonnen.

Die Untersuchung von Sedimentkernen aus Wassertiefen bis zu ca. 16 m ergab drei unterschiedliche Ereignisablagerungen: Ablagerungen auf Grund eines Tsunami-Ereignisses, Ablagerungen auf Grund starker Stürme und Ablagerungen, die auf den Sommer-Monsun zurückgeführt werden könenn. So erlauben die Datensätze die Abgrenzung und den Vergleich von Ablagerungen, die durch Stürme und durch Tsunami-Ereignisse begründet sind. Die jüngsten Ablagerung, die in Kerntiefen zwischen 0 und 40 cm gefunden worden, wurden als Tsunami-Ablagerungen interpretiert. Die Tsunami-Schicht hat eine Mächtigkeit von etwa 12 bis 30 cm und besteht aus mehreren Einheiten. Die Sedimente beinhalten Laminierung, Fining- und Coarsening Upward, massive Strukturen, Erosion der oberen und unteren Kontakte, terrigene und anthropogene Komponenten und Schlammgerölle. Die verschiedenen Einheiten resultieren aus unterschiedlichen hydrodynamischen Bedingungen (wahrscheinlich Runup und Backwash). In einer Kerntiefe zwischen 5 und 82 cm hat eine zweite Art von Ereignis ihre Spuren hinterlassen. Diese Schichten sind zwischen 1-10 cm mächtig und enthalten vor allem scharfe und erodierte untere Kontaktflächen, grobe Laminierung, Rippelstrukturen und gradierte Sande. Diese Ereignisschichten konnten auf Grund einer ^{210}Pb-Datierung in Korrelation mit historischen Sturmdaten als einzelne Ablagerungen durch Stürme identifiziert werden. Ein zentraler Unterschied zwischen Ablagerungen durch Stürme einerseits und Tsunamis andererseits liegt im Vorhandensein von Schlammgeröllen und schlammigem und terrigenen Materialien. Als drittes lassen sich in Schichten in Kerntiefen zwischen 12 und 92 cm kleinere Ereignisse nachweisen, nämlich Sedimenteinträge während der Monsunperioden. Diese Einlagen haben eine Mächtigkeit von 2-13 cm, und zeichnen sich durch eine Fining-upward-Sequenz (Ton und Schluff) zum Hangenden, mit eingelagerten feinkörnigen Sedimenten, aus.

Contents

Abstract ..... **I**

Zusammenfassung ..... **III**

CHAPTER I INTRODUCTION **1**

1.1 Geology and regional setting 2

1.2 Hydrodynamics 5

CHAPTER II METHODS **7**

2.1 Hydroacoustic methods 7

2.2 Sedimentological methods 7

2.2.1 Grab samples *8*

2.2.2 Core samples *8*

2.2.3 Onshore samples *10*

CHAPTER III SEDIMENTARY DEPOSITS LEFT BY THE 2004 INDIAN OCEAN TSUNAMI ON THE INNER CONTINENTAL SHELF OFFSHORE OF KHAO LAK, ANDAMAN SEA (THAILAND) **13**

3.1 Introduction 13

3.2 Study area 14

3.3 Methods 14

3.4 Results 19

3.4.1 Sedimentary structure and grain size *19*

3.4.2 Geochemical and physical properties *20*

3.4.3 ^{210}Pb data and interpretation *20*

3.5 Discussion 22

3.5.1 Evidence of the 2004 Indian Ocean tsunami event layer *22*

3.5.2 Processes of offshore sedimentation by the tsunami *24*

3.5.3 Diagnostic features of offshore tsunami deposits *24*

3.6 Conclusions 26

References 27

CHAPTER IV INTERNAL STUCTURE OF EVENT LAYERS PRESERVED ON THE ANDAMAN SEA CONTINENTAL SHELF, THAILAND: TSUAMI VS. STORM AND FLASH-FLOOD DEPOSITS **31**

Abstract 31

4.1 Introduction 31

4.2 Regional Setting 32

4.3 Methods 34

4.4 Results 35

4.4.1 Subsurface sediment sequence *35*

4.4.2 Ti/Ca ratios and ^{210}Pb activity *42*
4.5 Discussion 43
4.5.1 Identification of event deposits *43*
4.5.2 Identification and features of the tsunami facies *44*
4.5.3 Comparison of tsunami, storm and flash-flood facies *46*
4.6 Conclusions 48
References 48
CHAPTER V NOTES ON THE DISTRIBUTION AND STRATIGRAPHY OF THE SEDIMENT ON THE ANDAMAN SEA CONTINENTAL SHELF, THAILAND 53
5.1 Introduction 53
5.2 Seafloor sediment characteristics and interpretation 53
5.3 Subsurface sediment succession and sedimentary units 54
5.4 Radionuclide data 59
5.6 Sea level observation in the Andaman Sea 59
CHAPTER VI COMPREHENSIVE CONCLUSIONS 61
REFERENCES (for chapter I, II and IV) 63
ACKNOWLEDGEMENT 69
APPENDIX
CORE CATALOG 71
ADDITIONAL PUBLICATIONS 95

CHAPTER I

INTRODUCTION

Tsunamis are relatively frequent phenomena occurring worldwide (Scheffers and Kelletat, 2003), with two devastating events in the last ten years – the 2011 Tohoku tsunami offshore Japan (Goto et al., 2014a, 2014b; Ikehara et al., 2014; Sugawara et al., 2014), and the 2004 Indian Ocean Tsunami (Paris et al., 2010; Brill et al., 2011; Feldens et al., 2012; Sakuna-Schwartz et al., 2015; Schwarzer et al., 2015). These events had large impacts on both the coastal zone and potentially the continental shelf. The history of past tsunamis is written in the deposits they leave behind: Tsunami waves and tsunami return flows can erode, transport and deposit large amounts of sediments both onshore and offshore (e.g., Paris et al., 2010; Goto et al., 2011). Due to the number of processes involved - including erosion, bed load transport, lower flow regime currents, upper flow regime currents, oscillatory flows, combined flows, bidirectional currents, mass emplacement, freezing *en masse*, setting from suspension and sand injection (Shanmugam, 2011), tsunami deposits are very complex in terms of a number of characteristics, including grain size, sedimentary structures and sediment components (e.g., Luque et al., 2001; van den Bergh et al., 2003; Fujiwara and Kamataki, 2007; Kortekaas and Dawson, 2007; Noda et al., 2007; Paris et al., 2010; Chagué-Goff et al., 2011). Geological and environmental impacts of onshore tsunami deposits have been intensively studied in recent years (see Bourgeois, 2009 for a review), whereas the offshore behaviour and effects of tsunami waves during run-up and backwash are still poorly understood.

A basic problem in studying tsunami deposits is that our knowledge of the sedimentological characteristics of offshore tsunami deposits is limited to a small number of case studies (e.g., van den Bergh et al., 2003; Noda et al., 2007; Paris et al., 2010; Sakuna et al., 2012). Tsunami impact (erosion) on the seafloor have primarily been examined indirectly through studies of onshore deposits containing marine microfossils such as foraminifera (e.g., Hawkes et al., 2007; Uchida et al., 2010) or diatoms (e.g., Dawson, 2007; Sawai et al., 2009). The offshore tsunami deposit studies that have been conducted to date have indicated that the signatures of these deposits are highly variable. For instance, a distinct sandy layer that contained tephra and pumices was deposited by a tsunami generated during the Krakatau eruption in water depths of 2 to 27 m at an embayment next to Java Island (van den Bergh et al., 2003). Around Banda Aceh, which was the most severely devastated region during the 26 December 2004 tsunami, the tsunami left large fields of boulders in various sizes (up to 15 m in diameter) both on land and offshore in water depth of 10 to 25 m (Paris et al., 2010). Displaced boulders were also previously reported by Goto et al. (2007) and Feldens et al. (2009) from the Andaman Sea coast and shelf, respectively. Sugawara et al. (2009) reported nearshore impacts of the 2004 tsunami in the Andaman Sea in water depths of 6 to 30 m based on the distribution of foraminifera tests in surface sediments. In several other studies (e.g., Abrantes et al., 2008; Goodman-Tchernov et al., 2009; Smedile et al., 2011; Sakuna et al., 2012), offshore tsunami deposits were interpreted from event layers found in water depths between 9-105 m. These tsunami deposits were composed of sediments coarser than the ambient marine sediments, contained indicators of a terrigenous provenance and specific microfossil assemblages. However, there have been no unique criteria for identifying offshore tsunami deposits. Recently, Goto et al. (2011) used repeated bathymetrical surveys and modelling and found that the amount of sediments mobilised by tsunamis is much more substantial offshore than on land. Shallow water tsunami deposits from uplifted marine sedimentary strata were investigated by Fujiwara and Kamataki (2007) in Japan, and by Cantalamessa and Celma (2005) and Le Roux and Vargas (2005) in Chile. However, these older deposits can be reinterpreted: This was the case with inferred

backwash deposits in a shallow marine Miocene setting on the Mejillones Peninsula in northern Chile (Cantalamessa and Celma, 2005), which were recently found to be debris flow deposits with no evidence permitting an interpretation as tsunami deposits of any kind (Bahlburg et al., 2010). This comes as no surprise – how can paleo-tsunami deposits be interpreted when even modern deposits are difficult to identify?

The examples mentioned above indicate the limitations of our understanding of the processes of erosion and deposition in shallow marine settings during tsunami events and the difficulties of identifying offshore tsunami deposits. Prior studies show that the interpretation has to consider the local environment as well as a series of proxies (e.g. van den Bergh et al., 2003; Abrantes et al., 2008; Goodman-Tchenov et al., 2009; Paris et al., 2010; Smedile et al., 2011 after Sakuna et al., 2012).

Recently, there have been several well-documented case studies of tsunami events that offered an opportunity to examine tsunami deposits and its geomarine effects. This study focuses on the effects of the 2004 Indian Ocean Tsunami offshore Thailand, during which the Andaman Sea coastline of Thailand especially in the Phang Nga area was heavily affected (Szczuciński et al., 2006). The seafloor geomorphology and shelf configurations are key factors strongly affecting tsunami waves and the propagation (Di Geronimo et al., 2009). However, the seafloor geomorphology is not well known on the Andaman Sea area. It is therefore necessary to construct a detailed geomorphology and sedimentology of the local conditions parallel to tsunami studies.

Based on an extensive dataset comprising hydroacoustic, sedimentological, geochemical and ^{210}Pb activity, the four major tasks of this study are:

1. To provide evidence that the impact of the 2004 Indian Ocean tsunami can be identified in offshore deposits by using sedimentological methods and geochemical proxies;
2. To relate event layers in sediment cores between 5 and 60 m water depth to tsunami and storm events;
3. To compare the characteristics of storm and tsunami deposits within the same offshore location;
4. To characterize sedimentological and geochemical properties of the deposited sediment in the study area.

Results are presented in 3 separated chapters. Following an introduction of the investigation area and the used methodology, in chapter 3, detailed grain size, X-radiographic and geochemical proxies with supplementary ^{210}Pb activity evidence will be examined to address the modern offshore tsunami deposits. In chapter 4, extensive sediment core studies provide an opportunity to compare and discuss potential ways to discriminate tsunami and storm deposits at the same offshore locations. In chapter 5 the distribution and stratigraphy of Holocene and late Pleistocene sediment on the Andaman Sea continental shelf (Thailand) will be shown.

1.1 Geology and regional setting

The Andaman Sea (Fig. 1) locates in the northeastern Indian Ocean, surrounded by Myanmar in the north, and Sumatra in the south. The eastern part of the basin is bounded by Thailand and Malaysia, and the Andaman and Nicobar Island chain on the west, which are the subaerial expressions of the Andaman-Nicobar Ridge separating the basin from the Bay of Bengal (Rodolfo, 1969). It occupies an area of about 6×10^5 km^2; the average depth is about 1,100 m with a maximum depth of about 4,400

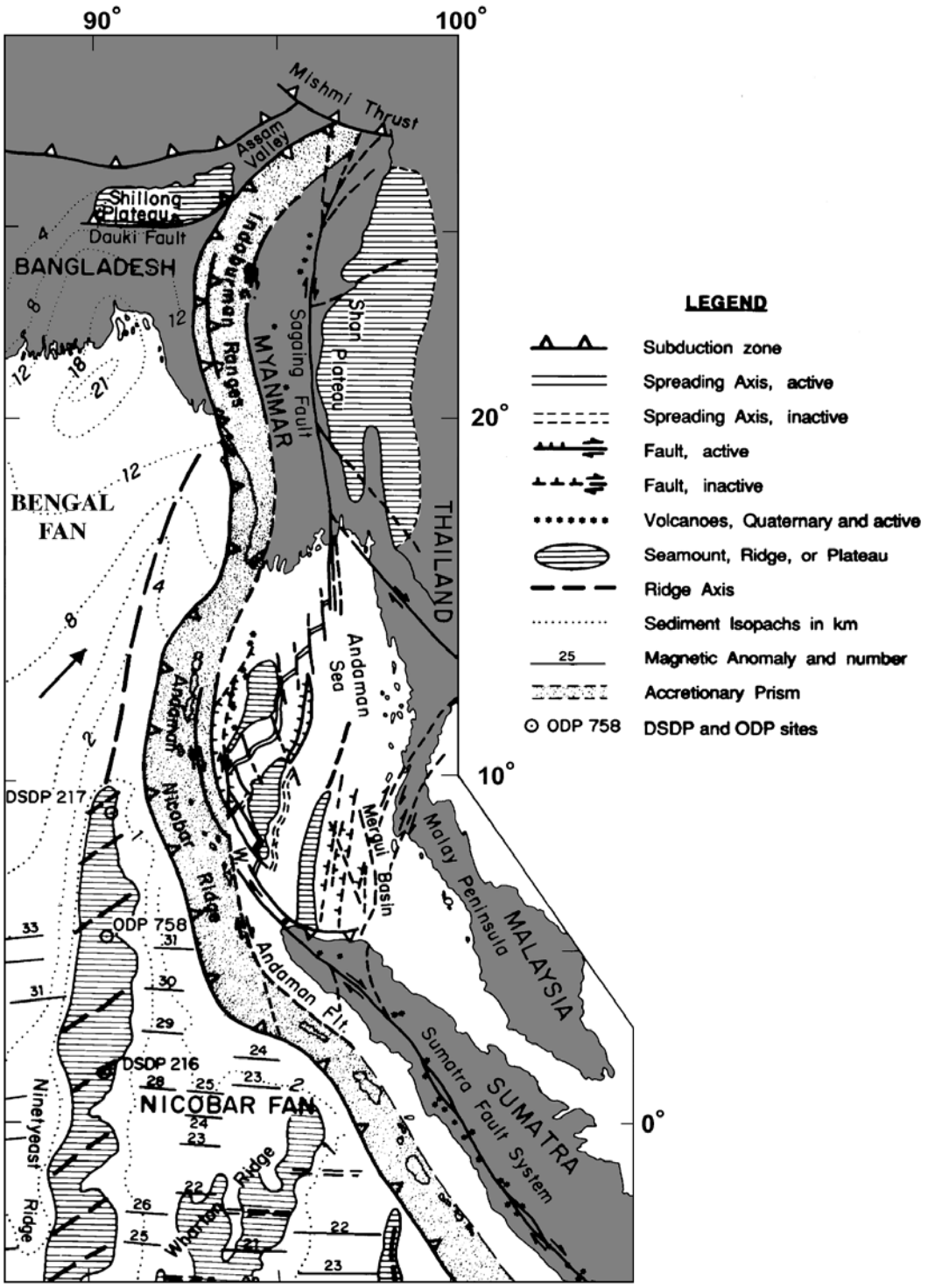

Fig. 1 Tectonic map of part of the northern Indian Ocean (modified from Curray, 2005).

m in the west (Dutta et al., 2007). The area is rifting and extensional from Mergui Basin over the East Andaman Basin, due to oblique convergent margin between Australian or Indian plate and the Eurasian or Southeast Asian plate (Curray, 2005). Dominated NE-SW trending extensional faults in the East Andaman Basin cause the input of fine grained terrigenous materials from the Ayeyarwady-Salween river system restricted to the area off the ridge and direct transfer to the deeper parts of the Andaman Sea by submarine canyons (Schwab et al., 2012). Another source of terrigenous input in the southern part of the Andaman Sea is the Malacca Strait (Curray, 2005),

delivering fine grained terrigenous materials to the deeper parts of the Andaman Sea Basin (Keller and Richard, 1967). Therefore, the shelf along western Myanmar and the Thai-Malay peninsula are described as sediment starved (Rodolfo, 1969; Ramaswamy et al., 2004; Rao et al., 2005), whereas the adjacent East Andaman Sea Basin is one of the main depocenters in the Andaman Sea (Morley et al., 2011).

The geology of the investigation area, offshore Khao Lak (Fig. 2) is poorly known, with most information gathered during tin mining exploration activities in the last century (compiled by Usiriprisan et al., 1987) and recently during studies on the impact of the 2004 Indian Ocean tsunami (Di Geronimo et al., 2009; Sugawara et al., 2009; Feldens et al., 2012). The area is situated

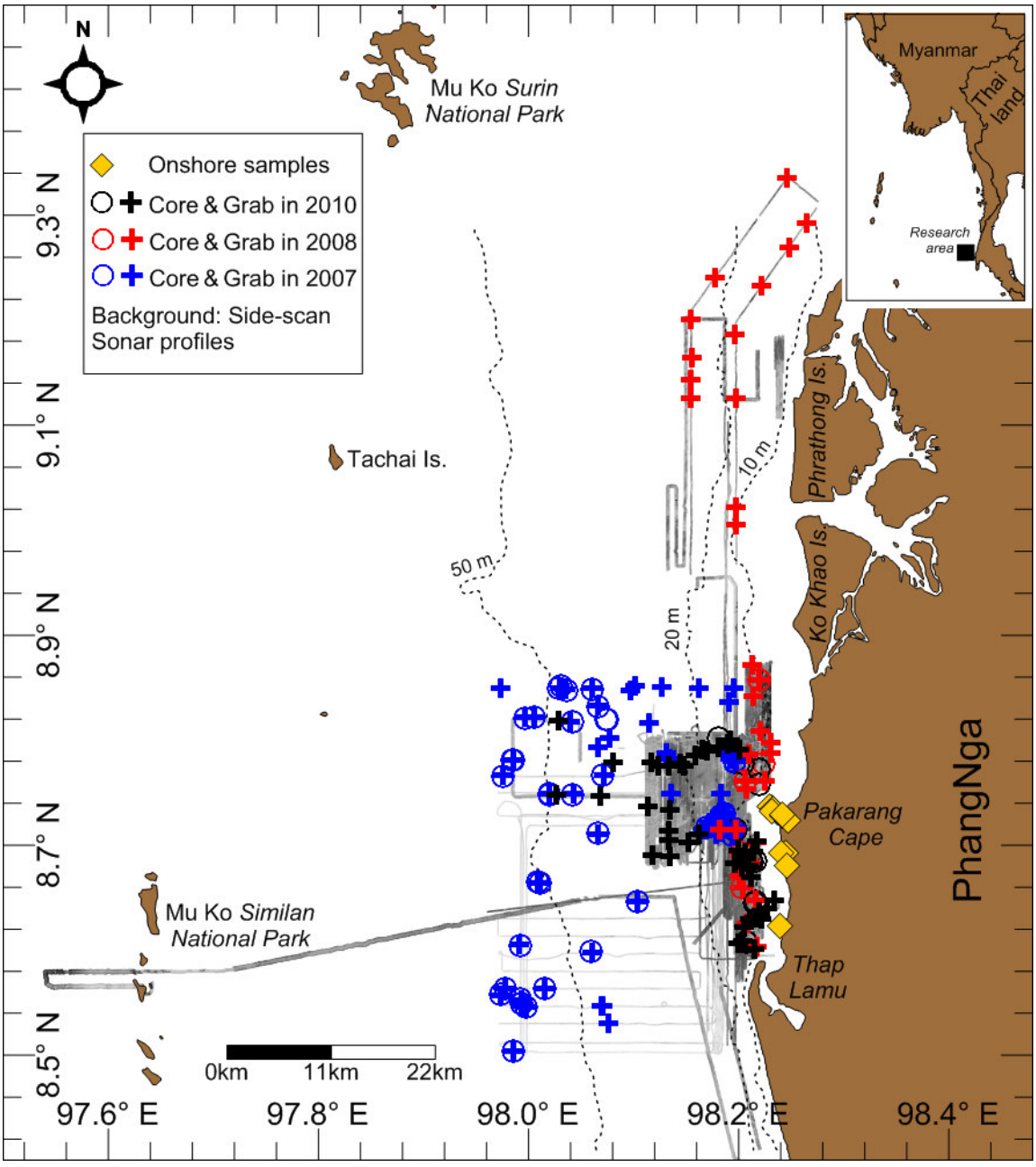

Fig. 2 Overview map of the investigation area including sampling stations and side-scan sonar tracklines. The bathymetric data are based on the nautical chart 353. The sediment samples taken during the three years research periods are ordered due to the 3 different cruises in difference colors except onshore sediment samples which taken in 2007.

on the western side of the South Thai-Malay peninsula offshore Phang Nga province. The coastal area is composed of embayed areas with sandy beaches commonly separated by rocky headlands. In general the shelf is gently dipping offshore, reaching water depths of 60 m within a distance of 30 km from the coastline. Discontinuous muddy sediment patches and a channel system incised into an old paleo-reef exist in water depths between 5 to 15 m. These patches are present north and south of Pakarang Cape and host preserved 2004 tsunami deposits (Sakuna et al., 2012). Several granite outcrops are scattered on the inner shelf at water depth of 5-10 m and on the mid shelf at water depth of about 30 m. Sand ridges striking oblique to the coastline in NE-SW direction are observed commonly between Thap Lamu and Pakarang Cape (Feldens et al. 2010). The onset of the ridges is found at about 15 m water depth however their extension to water depths exceeding 30 m is unknown.

1.2 Hydrodynamics

In the Andaman Sea and as well as in the other part of the southeast Asian waters, the pressure distribution is very stationary over the year and therefore reversal changing of wind dominates the season and ocean hydrodynamics in this region. The Northeast (hereafter NE) monsoon is active from December through February and full developed in January. The winds are directed from the north and northeast which bring dried-cold and clam conditions to the region. During the NE monsoon, the north equatorial current is strongly developed and in the Bay of Bengal a large anticyclonic eddy is formed. The current is drifting to the southwest and also extending over the equator to the south, joining with the south equatorial current to the west that flow into the Andaman Sea from the northeast side of the Malacca Strait (Fig. 3a). Therefore the net surface current flows out of the shelf causing an upwelling region along the west coast of Myanmar and Thailand (Wyrtki, 1961). By May, the strong southwesterly winds lead to high precipitation over the most of Southeast Asia, introducing the Southwest (hereafter SW) monsoon season that is active from May to September. The monsoon reaches its full development in July and August. During the SW monsoon the strong north equatorial circulation is highly piling up f water along the eastern side of the Bay of Bengal. Part of this water flows through the Andaman Sea and is deflected to the south when approaching the west corner of Sumatra and joining with the south equatorial current (Fig. 3b). In the Malacca Strait, the surface current is always flowing in northwest direction to the Andaman Sea since the sea surface elevation in the South China Sea is higher than in the Andaman Sea (Rizal et al., 2012). In general, these circulation patterns agree well within an open ocean area while on the shelf area longshore currents are directed to the north (Choowong et al., 2009; Di Geronimo et al., 2009; Feldens et al., 2012).

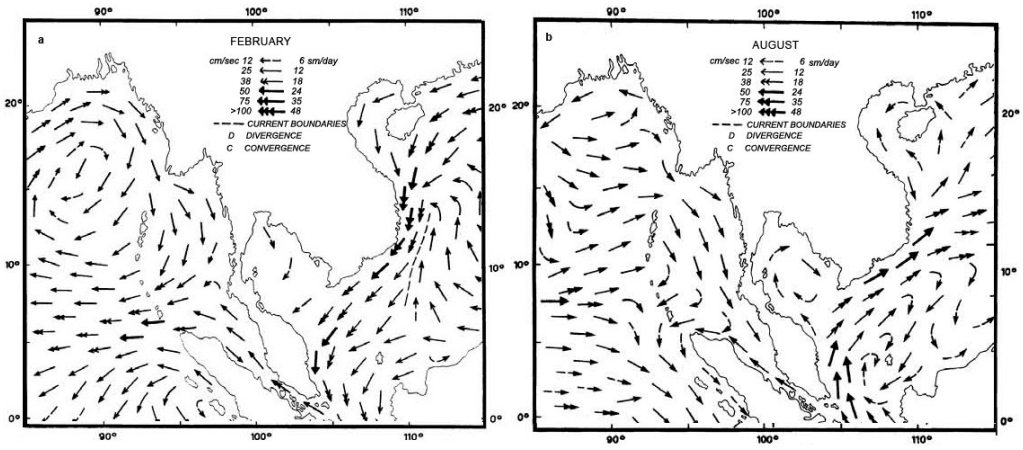

Fig. 3 Surface currents during a) February and b) August (modified from Wyrtki, 1961).

The exchange of water mass with the Indian Ocean occurs at sills in the Andaman-Nicobar Ridge and is restricted at water depth around 1800 m however a uniform well mixed water mass is present in the deepest parts throughout the Andaman Sea which probably has its origin in large amplitudes of internal waves (Dutta et al., 2007). Semidiurnal tide is found in the Andaman Sea (Fig. 4) with most days having two high tides and two low tides of almost equal amplitude (Rizal et al., 2012).

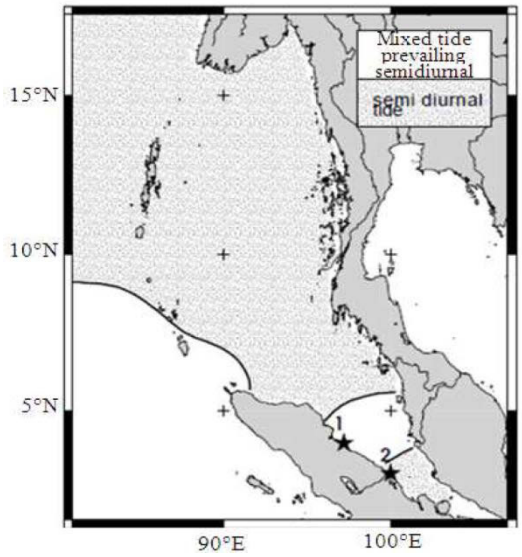

Fig. 4 Tidal type distribution from Rizal et al. (2012).

CHAPTER II

METHODS

Three research cruises in 2007 (November to December), 2008 (November to December) and 2010 (February to March) were conducted to obtain high-resolution hydroacoustic data and sediment samples, the latter including sampling by grab samplers and short gravity cores. The interpretation of the hydroacoustic data formed the basis for the selection of sediment sampling sites. Thus, it could be ensured that unusual and small-scale morphological and sedimentological patterns that may be related to the 2004 tsunami event could be sampled.

2.1 Hydroacoustic methods

A side scan sonar emits high frequency (100 – 1000 kHz) acoustic signals and records the return signal (backscatter) from the seabottom to obtain data of the acoustic properties of the sediment surface building up the seafloor. Normally side-scan sonars consist of two transducers mounted in a sonar "fish" which is towed behind a ship or mounted below or alongside. Each transducer is capable of sending and receiving acoustic signals. The transducers insonify an area of the seafloor perpendicular to the tow direction, with narrow horizontal directivity and wide vertical directivity, thus allowing to rapidly cover large areas of the seafloor. In combination with ground truthing by visual observation or sediment samples, these images are then related to sediment (and partly biological) properties including grain size. Further, objects elevated from the seafloor (e.g. boulders or artificial objects) or depressions can be easily detected. The side scan sonar system used in this work included a Klein 595 dual frequency side scan sonar (only 384 kHz was used) and a Benthos 1624 dual frequency sonar emitting sound pulses around 100 and 400 kHz. Processing of the side scan sonar data followed standard procedures (Blondel, 2009). Generally, backscatter data are displayed inverted in this study, with areas of low backscatter intensity displayed in lighter colors.

Seismic systems (reflection seismic and subbottom profilers) are used to visualize the geological/sedimentological built up of the seafloor. The boomer system which was used emits a sound pulse directed normal to the seafloor surface. Due to its low frequency, it penetrates into the subsurface. Part of the acoustic energy is reflected at lithological boundaries as the impedance of different layers differs from each other. The reflected energy is recorded by hydrophone arrays towed behind the ship ("streamer"). Profiles shown in this study were recorded using an EG&G boomer system with a CEA power supply emitting sound pulses with frequencies between approx. 1 and 15 kHz and a C-Boom low voltage boomer with a frequency of 1.76 kHz. Processing of the seismic data included the application of a lowpass filter to remove swell, a bandpass filter with 400 to 800 Hz on the lower and 4000 to 8000 Hz on the upper flank, as well as application of a time-varying gain and 3 fold stacking.

2.2 Sedimentological methods

Three types of sediment samples were used for this study: surface sediment samples were used for ground truthing of the side scan sonar data and the determination grain size distribution patterns across the shelf; sediment cores were used for investigation of the subsurface sedimentary structures, and onshore samples from various environments that had been subjected to tsunami erosion (pre-tsunami soils, mangrove soils, sand from the coastal plain) provided data on terrigenous geochemical end-members.

2.2.1 Grab samples

A total of 156 grab samples on selected position based on the side-scan mosaic were taken using a Van-Veen type grab sampler. The grain size distribution of these samples was determined mostly following the ASTM standard; however, sediment <63µm were removed prior to sieving instead of <40 µm. For sieving between 2 cm and <63 µm an interval of 0.25Φ was used. Statistical parameters of the grain size distributions were calculated in phi (Φ) units with $\Phi=-\log_2 d$ (d being the grain size in mm, Krumbein, 1938), using the logarithmic method of moments available with the GRADISTAT software (Blott and Pye, 2001).

2.2.2 Core samples

Sixty sites in water depths of 5 to 65 m were cored with a 2 m long Rumohr-type gravity corer (8 cm diameter). All sediment cores were first split and photographed. Forty three cores were selected for detailed analysis at a 1 cm interval in the laboratory according to the following scheme (Table 1). A Multi-sensor core logger (MSCL, Fig. 4) was used to measure basic physical and acoustical sediment properties i.e. bulk density, gamma-ray attenuation, magnetic susceptibility and *p*-wave velocity. These properties are commonly used to identify distinct layers such as debris flows and turbidites within sediment cores (Weber et al., 1997; Best and Gunn, 1999; Hofmann et al., 2005). An X-ray fluorescence (XRF) core scanner (Fig. 5) was used to semi-quantitatively assess chemical element composition which can serve as a tool for differentiating terrigenous from marine constituents (Lamy et al., 2001; Bahr et al., 2005; Ohta and Arai, 2007). About 1 cm thick slabs of the sediment cores were radiographed to detect any internal sedimentary structures or unconformities (Fig. 6). Grain size composition from 15 cores was determined every centimetre

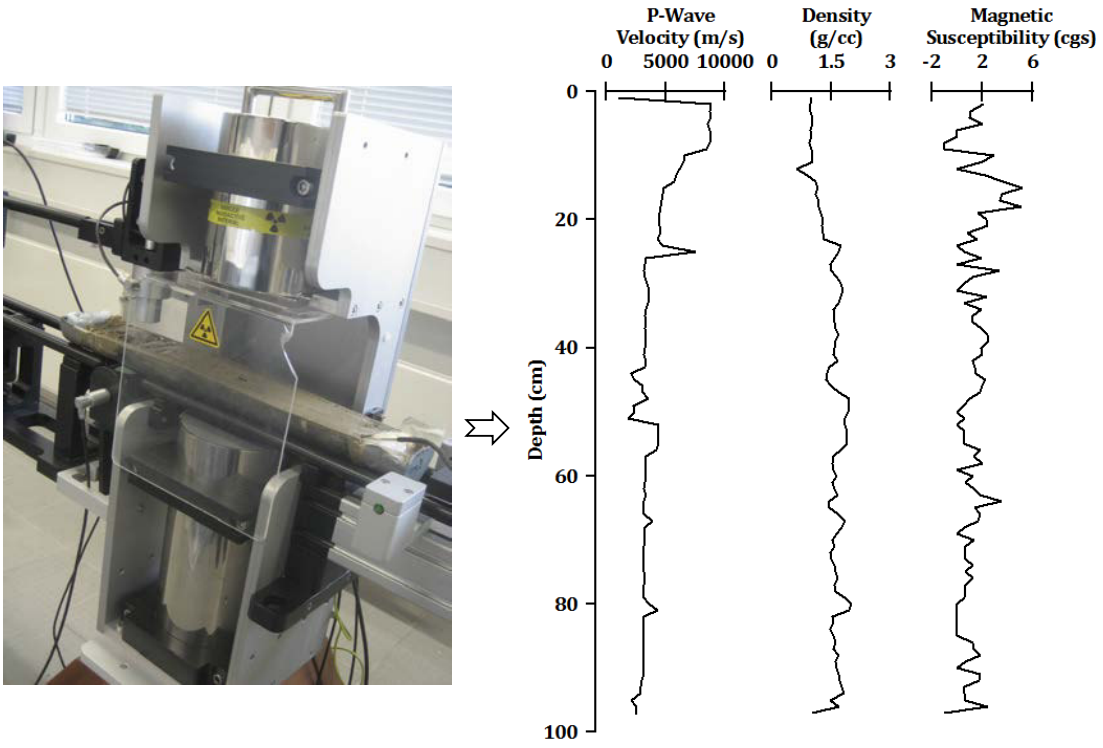

Fig. 4 Multi-sensor core logger. The core moves past stationary sensor systems that measure P-wave velocity, Attenuated Gamma and Magnetic Susceptibility. A data example is displayed on the right.

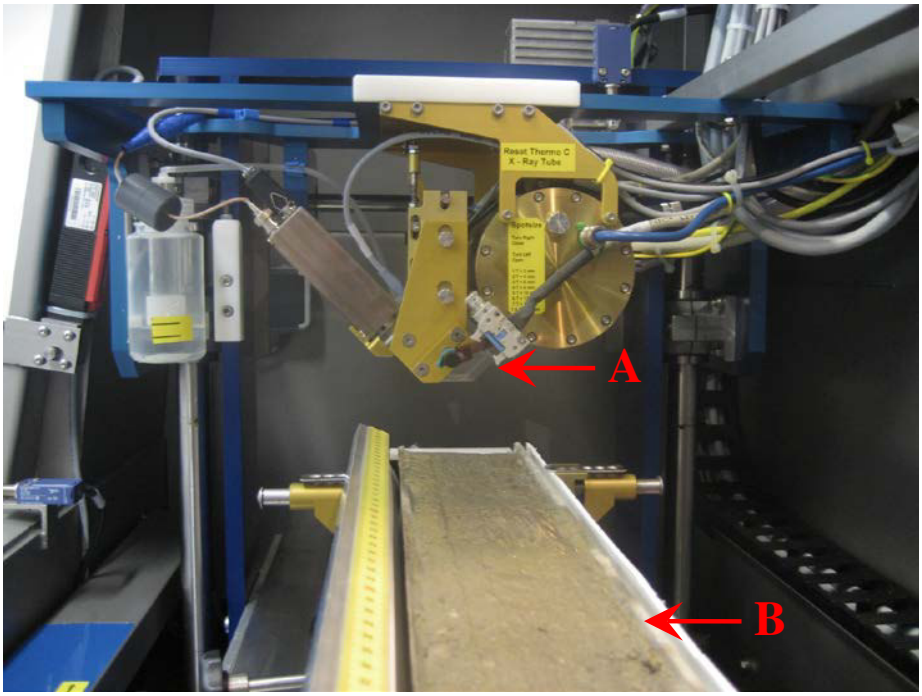

Fig. 5 Inside of X-ray fluorescence (XRF) core scanner. A= XRF detector. B= split-core surface covered with a thin film.

with a Coulter LS-13320 laser-based particle sizer. The materials were chemically treated prior of the measurement, in order to remove carbonate shell fragments and organic matter.

Measurements of ^{210}Pb activity were carried out on four cores, three from the inner shelf (core 030310-C3, core 050310-C4 and core 050310-C6) and one from the mid shelf (core 031207-22), by using gamma spectrometry at the Leibniz-Laboratory for Radiometric Dating and Isotope Research (Kiel, Germany). The ^{137}Cs supported activity was mostly below the detection limits and therefore it could not serve as an independent tracer. The sediment accumulation rate (SAR) was estimated from the decline in the excess ^{210}Pb activities following the equations used by Robbins and Edgington (1975) and McKee et al. (1983),

$$SAR = \lambda \times z \times \left[\ln \left(A_0 / A_z \right) \right]^{-1},$$

where λ is the decay constant (= 0.0311 year^{-1}); z is the depth in the core (cm); A_0 is the specific activity of excess ^{210}Pb at a particular reference horizon (Bq kg^{-1}) and A_z is the specific activity of excess ^{210}Pb at depth z below the reference horizon (Bq kg^{-1}).

The age of the Andaman Sea sediment was determined by the accelerator mass spectrometry (AMS) radiocarbon dating of 3 samples taken from core 031207-22. Wood fragments were selected for dating because no suitable carbonate shells were found. Studies from the South China Sea (Hanebuth et al., 2000; Schimanski and Stattegger, 2005) proved that remained plants and wood fragments can provide reliable ages. The AMS ^{14}C dating was measured at the Leibniz-Laboratory for Radiometric Dating and Isotope Research (Kiel University, Germany). Samples were cleaned (alkali residue extraction) by using 1% HCl, 1% NaOH at 60° C and again 1% HCl. The alkali residue was then combusted to CO_2 in an evacuated, flame sealed quartz tube with CuO and silver wool at 900° C for 4 hours. The CO_2 was reduced to graphite with H_2 at 600° C on an iron catalyst, and the

resulting graphite-iron powder was pressed into aluminium target holder. The pressed samples were measured with a 3 MV Tandetron 4130 ccelerator mass spectrometry (AMS) system from High Voltage Engineering Europa. The analytical precision for modern samples is better than 0.5% which equals ±40 years for the 1-σ statistical uncertainty of the measured age (Nadeau, 1997; Nadeau, 1998). The measured AMS ^{14}C ages were converted into calendar years BP applying the CALIB version 5.0.1 software (Stuiver and Reimer, 1993) and the INTCAL04 calibration curve (Reimer et al., 2004) for the reservoir effect.

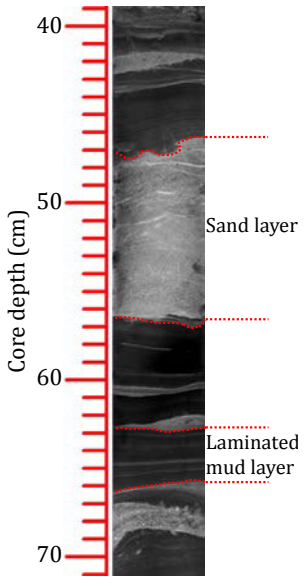

Fig. 6 An example X-radiograph of sediment core 030310-C3.

2.2.3 Onshore samples

The sediment samples taken onshore were pressed as pellets before the element compositions were measured using the XRF scanner. The setting of the device was the same as for the core samples. The relative concentrations of eight elements (Al, Si, S, K, Ca, Ti, Mn and Fe) were analysed later using principal component analysis (PCA) to evaluate the sediment provenance (Marques et al., 2008; Heise et al., 2010). Four elements were not used, due to either very low concentrations in some samples (at detection limits: P, V, Cr, Rh) or possible changes due to sample preparation (Cl). PCA is a data reduction technique used to convert a large number of geochemical variables into a small set of new variables called principal components or factors (PC) and to group samples based on their geochemical composition (Ohta and Arai, 2007; Reid and Spencer, 2009).

Table 1 Summary of the methods used on the whole set of retrieved sediment cores, except the sediment cores are shorter than 10 cm.

SFT=Seafloor type†, P=Photo, R=X-radiograph image, X=XRF, M=MSCL, G=Grain size, B=^{210}Pb, C=^{14}C, F=Microfossil

Core No.	Sampler	Sampling date	Latitude (N)	Longitude (E)	Water depth (m)	Core recovery (cm)	SFT	Methods							
								P	R	X	M	G	B	C	F
011207-02	core 1	01.12.07	08° 50.952'	98° 01.703'	54.50	76.00	H	*	*	*	*				
011207-02	core 2	01.12.07	08° 51.073'	98° 01.826'	55.40	146.00	H	*	*	*	*	*			
011207-04	core 1	01.12.07	08° 49.886'	98° 03.964'	47.50	70.00	H	*	*	*	*				
011207-05	core 1	01.12.07	08° 50.928'	98° 03.608'	48.70	69.00	H	*	*	*	*				
021207-16	core 1	02.12.07	08° 49.178'	98° 04.515'	45.30	45.00	H	*	*	*	*	*			
021207-16	core 2	02.12.07	08° 49.176'	98° 04.437'	45.50	43.00	H	*	*	*	*				
021207-18	core 1	02.12.07	08° 49.032'	98° 02.528'	52.00	71.00	H	*	*	*	*				
031207-19	core 1	03.12.07	08° 49.330'	98° 00.314'	56.50	67.50	H	*	*	*	*				
071207-20	core 1	02.12.07	08° 49.275'	97° 59.768'	57.90	75.50	H	*	*	*	*				

Table 1 (continue).

Core No.	Sampler	Sampling date	Latitude (N)	Longitude (E)	Water depth (m)	Core re-covery (cm)	SFT	Methods							
								P	R	X	M	G	B	C	F
031207-22	core 1	03.12.07	08° 46.829'	97° 59.094'	62.10	69.00	H	*	*	*	*				
031207-22	core 2	03.12.08	08° 46.884'	97° 59.164'	61.90	116.00	H	*	*	*	*	*	*	*	*
031207-23	core 1	03.12.07	08° 44.879'	98° 01.173'	57.00	71.50	H	*	*	*	*	*			
031207-30	core 2	03.12.07	08° 43.702'	98° 11.010'	21.50	17.00	SR	*	*	*	*				
051207-31	core 1	05.12.07	08° 47.176'	98° 11.724'	15.90	71.00	B	*	*	*	*				
051207-32	core 2	05.12.07	08° 46.725'	98° 11.814'	14.40	30.00	B	*	*	*	*	*			
051207-32	core 3	05.12.07	08° 46.770'	98° 11.810'	14.60	46.00	A	*	*	*	*				
051207-37	core 2	05.12.07	08° 43.762'	98° 11.089'	16.60	42.00	SR	*	*	*	*	*			
071207-49	core 1	07.12.07	08° 30.250'	97° 59.142'	61.40	49.00	H	*	*	*	*				
071207-51	core 1	07.12.07	08° 32.943'	97° 59.572'	58.20	74.00	H	*	*	*	*				
071207-52	core 1	07.12.07	08° 33.202'	97° 59.542'	59.60	74.00	H	*	*	*					
071207-54	core 1	07.12.07	08° 33.834'	97° 58.687'	63.20	74.00	H	*	*	*	*				
071207-55	core 1	07.12.07	08° 33.818'	98° 00.908'	57.50	82.00	H	*	*	*	*				
071207-62	core 1	07.12.07	08° 36.283'	97° 59.552'	57.90	70.00	H	*	*	*	*				
071207-64	core 1	07.12.07	08° 39.873'	98° 00.510'	48.90	50.00	H	*	*	*	*				
081207-76	core 1	08.12.07	08° 42.915'	98° 11.713'	13.00	18.00	A	*	*	*	*				
081207-77	core 1	08.12.07	08° 42.569'	98° 11.680'	13.90	30.00	C	*	*	*	*				
071208-02	core 1	07.12.08	08° 39.602'	98° 12.206'	13.00	20.00	A	*	*	*	*				
071208-04	core 1	07.12.08	08° 41.567'	98° 12.169'	11.60	28.00	A	*	*	*	*	*			
071208-05	core 1	07.12.08	08° 42.918’	98° 11.851’	14.10	28.00	A	*	*	*	*	*			
071208-07	core 1	07.12.08	08° 45.644’	98° 12.352’	13.20	65.00	A	*	*	*	*				
071208-08	core 3	07.12.08	08° 51.418’	98° 13.168’	11.50	57.00	A	*	*	*	*				
030310-C2	core 1	03.03.10	08° 36.474'	98° 12.454'	11.50	23.00	A	*	*	*	*				
030310-C2	core 2	03.03.10	08° 36.451'	98° 12.472'	11.10	25.00	A	*	*	*	*				
030310-C3	core 1	03.03.10	08° 38.708'	98° 12.931'	9.50	97.00	A	*	*	*	*	*	*		*
030310-C6	core 1	03.03.10	08° 41.128'	98° 12.976'	9.30	32.00	F	*		*	*				
030310-C7	core 1	03.03.10	08° 41.192'	98° 12.689'	12.50	34.00	A	*	*	*	*				
030310-C7	core 3	03.03.10	08° 41.052'	98° 12.763'	11.90	65.00	A	*	*	*	*	*			
040310-C2	core 3	04.03.10	08° 42.918'	98° 11.841'	13.50	650.00	A	*	*	*	*	*			

Table 1 (continue).

Core No.	Sampler	Sampling date	Latitude (N)	Longitude (E)	Water depth (m)	Core re-covery (cm)	SFT	Methods							
								P	R	X	M	G	2	C	F
050310-C1	core 1	05.03.10	08° 48.142'	98° 10.856'	19.20	20.00	I	*	*	*	*				
050310-C2	core 1	05.03.10	08° 45.438'	98° 13.186'	9.80	75.00	A	*	*	*	*	*			
050310-C3	core 1	05.03.10	08° 46.352'	98° 13.182'	11.20	52.00	A	*	*	*	*	*			
050310-C4	core 1	05.03.11	08° 46.659'	98° 12.269'	15.30	56.00	A	*	*	*	*	*	*		*
050310-C6	core 1	05.03.10	08° 38.761'	98° 12.967'	9.60	99.00	A	*	*	*	*	*	*		

† seafloor type details in chapter V

Earth Planets Space, **64**, 931–943, 2012

CHAPTER III

SEDIMENTARY DEPOSITS LEFT BY THE 2004 INDIAN OCEAN TSUNAMI ON THE INNER CONTINENTAL SHELF OFFSHORE OF KHAO LAK, ANDAMAN SEA† (THAILAND)

D. Sakuna[1,2], W. Szczuciński[3], P. Feldens[1], K. Schwarzer[1], and S. Khokiattiwong[2]

[1]*Institute of Geosciences Sedimentology, Coastal and Continental Shelf Research, University of Kiel, Otto-Hahn-Platz 1, D-24118 Kiel, Germany*
[2]*Oceanography and Environment Unit, Phuket Marine Biological Center, P.O. Box 60, Phuket 83000, Thailand*
[3]*Institute of Geology, Adam Mickiewicz University, Maków Polnych 16, 61-606 Poznań, Poland*

(Received November 24, 2010; Revised May 3, 2011; Accepted June 15, 2011; Online published October 24, 2012)

Tsunami waves leave sedimentary signatures both onshore and offshore, although the latter are hardly known. The objective of the present study is to provide new evidence for the 2004 Indian Ocean tsunami deposits left on the inner continental shelf of the Andaman Sea (Thailand) and to identify diagnostic sedimentological and geochemical properties of these deposits. Based on extensive seafloor mapping, three sediment cores were selected for study and were analysed for their sedimentary structures, grain size composition, chemical elemental composition, physical properties and ^{210}Pb activity. Sediment cores retrieved from shallow water (9–15 m) within 7.5 km off the shore revealed distinct event layers, which were interpreted as being tsunami deposits. These 20–25 cm thick deposits were already covered with post-tsunami marine sediments. They were composed of several units, marine sand layers alternating with poorly sorted mud with terrigenous and anthropogenic components, representing different hydrodynamic conditions (probably during run-up and backwash phase). These sedimentological observations were supported by geochemical and physical data and were confirmed using ^{210}Pb dating. A sediment core taken from a depth of 57 m at a distance of 25 km offshore did not reveal clear event deposits. Comparisons with available data from offshore tsunami deposits showed that there is no single set of signatures that could be applied to identify this kind of deposits.

Key words: 2004 Indian Ocean tsunami, offshore tsunami deposits, sedimentology, Khao Lak, Thailand.

3.1 Introduction

Tsunamis are relatively frequent phenomena that occur worldwide (Scheffers and Kelletat, 2003). Recent examples of tsunamis include the 2004 Indian Ocean tsunami, tsunamis in Java in 2006 and Samoa in 2009, the Chilean tsunami in 2010 and the 2011 Tohoku tsunami in Japan. These events can have potentially large impacts on both the coastal zone and the continental shelf. As tsunami waves propagate into shallower water, they can erode, transport and deposit large amounts of sediments both onshore and offshore (e.g., Paris et al., 2010, Goto et al., 2011). Due to the number of processes involved (Shanmugam, 2011), tsunami deposits are very complex in terms of a number of characteristics, including grain size, sedimentary structures and sediment components (e.g., Luque et al., 2001, van den Bergh et al., 2003, Fujiwara and Kamataki, 2007, Kortekaas and Dawson, 2007, Noda et al., 2007, Paris et al., 2010, Chagué-Goff et al., 2011). Geological and environmental impacts of onshore tsunami deposits have been intensively studied in recent years (see Bourgeois, 2009 for a review), whereas the offshore behaviour and effects of tsunami waves during run-up and backwash are still poorly understood.

A basic problem in studying tsunamis is that our knowledge of the sedimentological features of offshore tsunami deposits is limited to a small number of case studies (e.g., van den Bergh et al., 2003, Noda et al., 2007, Paris et al., 2010). Tsunami impacts (erosion) on the seafloor have primarily been examined indirectly through studies of onshore deposits containing marine microfossils such as foraminifera (e.g., Hawkes et al., 2007, Uchida et al., 2010) or diatoms (e.g., Dawson, 2007, Sawai et al., 2009). The studies of shallow marine tsunami deposits that have been conducted to date have indicated that there is a large variability in the characteristics of these deposits. For instance, a distinct sandy layer was deposited by a tsunami generated during the Krakatau eruption in an embayment next to Java

†Reprinted with permission of TERRAPUB (Terra Scientific Publishing Company). The original article is published in Earth Planets Spaces, vol. 64, p. 931-943, 2012.

Island (van der Bergh et al., 2003). Around Banda Aceh, which was the most severely devastated region during the 26 December 2004 tsunami, the tsunami left large fields of boulders on land and offshore (Paris et al., 2010). Displaced boulders were also previously reported by Goto et al. (2007) and Feldens et al. (2009) from the Andaman Sea coast and shelf, respectively. Sugawara et al. (2009) reported nearshore impacts of the 2004 tsunami in the Andaman Sea in water depths of 6 to 30 m based on the distribution of foraminifera tests in surface sediments. In several other studies (e.g., Abrantes et al., 2008, Goodman-Tchernov et al., 2009, Smedile et al., 2011), offshore tsunami deposits were interpreted from event layers composed of sediments that were coarser than the ambient marine sediments, contained indicators of a terrigenous provenance and specific microfossil assemblages. However, there have been no unique criteria for identifying offshore tsunami deposits. Recently, Goto et al. (2011) used repeated bathymetrical surveys and modelling and found that the amount of sediments mobilised by tsunamis is much more substantial offshore than on land.

Shallow water tsunami deposits from uplifted marine sedimentary strata were investigated by Fujiwara and Kamataki (2007) in Japan, and by Cantalamessa and Celma (2005) and Le Roux and Vargas (2005) in Chile. However, these older deposits can be reinterpreted, as in the case of backwash deposits in a shallow marine Miocene setting on the Mejillones Peninsula in northern Chile (Cantalamessa and Celma, 2005), which were recently found to be debris flow deposits with no evidence permitting an interpretation as tsunami deposits of any kind (Bahlburg et al., 2010).

The above examples indicate the limitations of our understanding of the processes of erosion and deposition in shallow marine settings during tsunami events and the difficulties of identifying offshore tsunami deposits. Significant progress in the search for diagnostic criteria may be accomplished only through an increased number of well-documented case studies of modern tsunami deposits. The objective of this study is to provide evidence that the impact of the 2004 Indian Ocean tsunami can be identified in shallow water deposits offshore of Khao Lak by using sedimentological methods and geochemical proxies.

3.2 Study area

The study area is located on the continental shelf of the Andaman Sea offshore Khao Lak (Phang Nga province, Thailand) and extends to a distance of about 25 km offshore (Fig. 1). The coast is composed of embayed areas with sandy beaches separated by rocky headlands. The shelf is relatively flat and sloping offshore, reaching water depths of 50 m at a distance of 25 km from the coastline. The sea bottom is mainly composed of sand, sandy mud, muddy sand and bedrock outcrops (Usiriprisan et al., 1987, Di Geronimo et al., 2009, Feldens et al., 2009, in press EPS). In some regions, the seabed was subjected to offshore tin mining (Usiriprisan et al., 1987). The climate of this region is dominated by monsoons, with the southwest monsoon remaining active from May to September and generating heavy rainfall during this period. The northeast monsoon lasts from December to February and results in a calm, dry season (Khokiattiwong et al., 1991). The study area is located next to the area in Thailand most damaged during the 2004 Indian Ocean tsunami (Bell et al., 2005, Szczuciński et al., 2006). Moreover, strong storms are rare in this area, increasing the preservation of potential tsunami deposits on the seafloor (Jankaew et al., 2008, Kumar et al., 2008). Previous post-tsunami seafloor mapping surveys (Di Geronimo et al., 2009, Feldens et al., 2009) reported discontinuous muddy sediment patches and a channel-like system next to an ancient reef platform located in shallow water (5 to 15 m). Consolidated mud deposits containing grass, wood and shell fragments, likely transported by the backwash flow in the 2004 tsunami, were reported in grab samples and short cores (Feldens et al. 2009). Based on these data and further hydroacoustic surveys (Feldens et al., in press EPS), new target areas for sediment coring were selected (Figs. 1 and 2) to examine modern offshore tsunami deposits.

3.3 Methods

High resolution hydroacoustic mapping (Feldens et al., 2009, Feldens et al., in press EPS) was performed during three research cruises (Nov.-Dec. 2007, Nov.-Dec. 2008 and Feb.-Mar. 2010). Data from these surveys form the basis for the selection of sediment coring sites. Sixty sediment cores were collected using a 2 m long

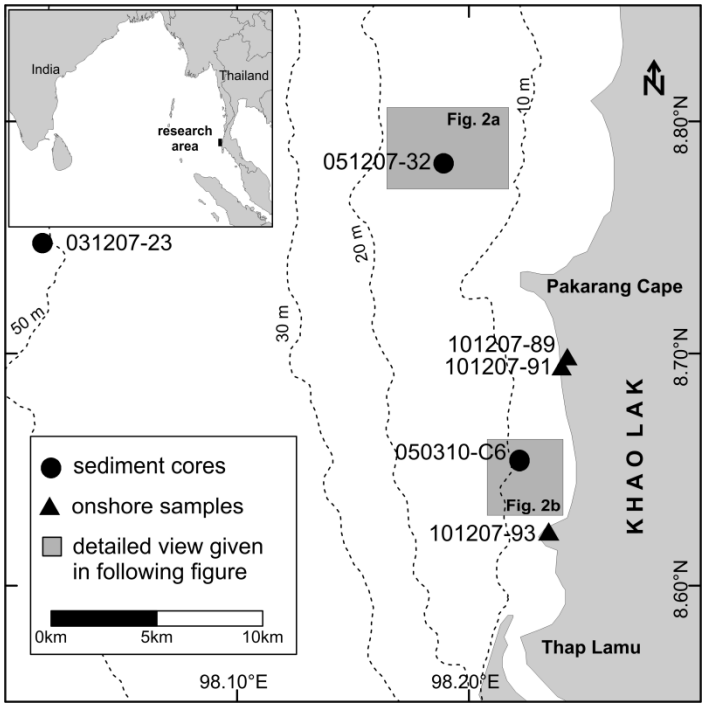

Fig. 1 Overview of the investigation area. Bathymetric data are based on nautical chart. The inset shows location of the study area within the Indian Ocean basin.

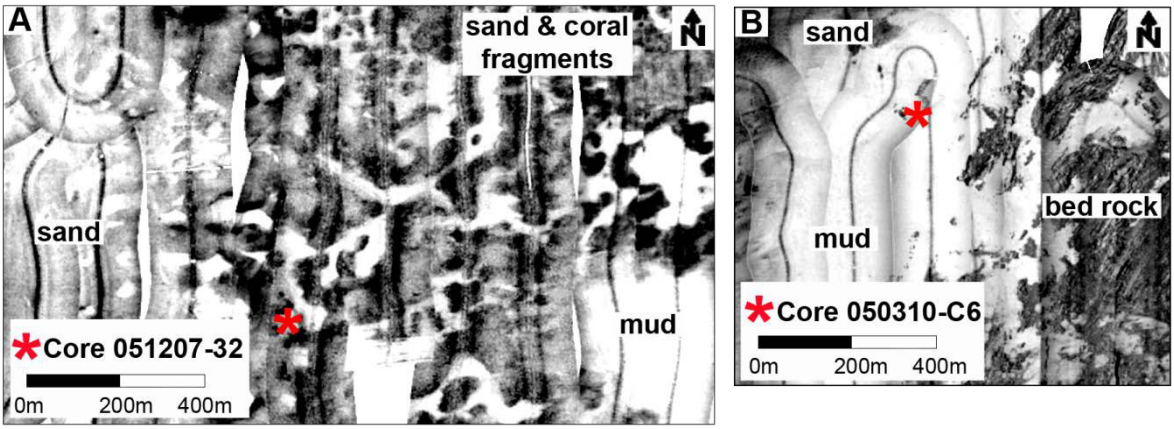

Fig. 2 Side scan sonar mosaics (refer to Fig. 1 for positions). The images show the location of sediment cores. A) Sediment core 051207-32 was retrieved from a small mud-filled channel (displayed in light grey). The channels are separated by coarse sand, frequently containing coral fragments (displayed in dark grey). Further offshore, medium to coarse sands are deposited (displayed in intermediate grey). B) Sediment core 050310-C6 was retrieved from a large patch covered by silty sediments (displayed in light gray) seaward of granitic bedrock outcrops. Coarse sands are deposited further offshore (displayed in dark grey).

Rumohr type gravity corer in water depths of 5 to 70 m. Three cores were selected for the present study (Figs. 1 and 2, Table 1), two of which were obtained in water depths of 9.6 and 14.4 m, located 3.1 and 7.2 km offshore, respectively, while the third core was collected further offshore at a water depth of 57 m, 25.5 km offshore. Moreover, three samples from sites located within various onshore environments that had been subjected to tsunami erosion (pre-tsunami soils, mangrove soils, coastal plain sands) were obtained to provide data on terrigenous geochemical end-members (Fig. 1).

Table 1 List of the analyzed sediment cores.

Core No.	Sampling year	Latitude (N)	Longitude (E)	Water Depth (m)	Core recovery (cm)	Distance offshore (km)
050310-C6	2010	08°38.761'	98°12.967'	9.6	99	3.1
051207-32	2007	08°46.725'	98°11.814'	14.4	30	7.2
031207-23	2007	08°44.879'	98°01.173'	57.0	70	25.5

The cores were first analysed using non-destructive techniques; a Multi-sensor core logger (MSCL) and an X-ray fluorescence (XRF) core scanner. The following basic physical and acoustical sediment properties were measured: bulk density, gamma-ray attenuation, magnetic susceptibility and *p*-wave velocity. These physical properties are commonly used to find distinct layers such as debris flows and turbidites within sediment cores (Weber et al., 1997, Best and Gunn, 1999, Hofmann et al., 2005). An XRF core scanner was used to semi-quantitatively assess sediment composition; this method can serve as a tool for differentiating terrigenous materials from marine sediments (Lamy et al., 2001, Bahr et al., 2005, Ohta and Arai, 2007). The measurements were taken every centimetre directly at the surface of a split core. The instrument was set to a count time of 30 s with a voltage of 10 kV. At this setting, the measurement range covered thirteen elements (Al, Si, P, S, Cl, K, Ca, Ti, V, Cr, Mn, Fe and Rh). Data were provided as relative element intensities in counts per second (cps). These intensities depend mainly on element concentration, matrix effects and physical properties, as well as sample geometry (Jansen et al., 1998, Weltji and Tjallingii, 2008).

The relative concentrations of eight elements, Al, Si, S, K, Ca, Ti, Mn and Fe from onshore samples (101207-89, 101207-91 and 101207-93) and samples from core 050310-C6, were analysed using principal component analysis (PCA) to evaluate the sediment provenance (Marques et al., 2008, Heise et al., 2010). Four elements were not used, due to either very low concentrations in some samples (at detection limits: P, V, Cr, Rh) or possible changes due to sample preparation (Cl). PCA is a data reduction technique used to convert a large number of geochemical variables into a small set of new variables called principal components or factors (PC) and to group samples based on their geochemistry (Ohta and Arai, 2007, Reid and Spencer, 2009).

Digital X-radiography images were obtained from 1 cm thick slabs taken from the surface of split sediment cores. This technique is used to detect any internal sedimentary structures or unconformities not visible to the naked eye. The images (Figs. 3-5) show the relative change in sediment bulk density. High bulk density sediment, such as pebbles, shell fragments or sand, reduce X-ray penetration and are displayed in light grey, whereas low bulk density sediment, as observed for fine-grained sediments, is represented by dark grey or black (Bouma, 1964).

To determine the grain size distribution, core materials were sampled in 1 cm intervals. The materials were digested with HCl and H_2O_2 to remove carbonates and organic matter prior to analysis with a Coulter LS-13320 laser-based particle sizer device with a measuring range of 0.04 to 2000 µm. In core 050310-C6, samples composed mainly of grains in excess of sand size (27-38, 40-41, 72-73 and 87-88 cm) were not analysed. Statistical parameters of the grain size distribution (Figs 3-5) were calculated using the logarithmic method of moments in GRADISTAT software (Blott and Pye, 2001).

^{210}Pb dating has been widely used for the assessment of sediment accumulation rates over the last 100 years. Total ^{210}Pb activity in the recent sediments comes primarily from two sources: supported (autochthonous) ^{210}Pb is produced by the radioactive decay of uranium radioactive chain isotopes in sediments and excess (allochthonous) ^{210}Pb is produced by the decay of ^{222}Rn, mostly in the atmosphere, and is then deposited with the sediments. The excess ^{210}Pb activity profile in the sediments is commonly characterised by the maximum activity at the surface and by the exponential

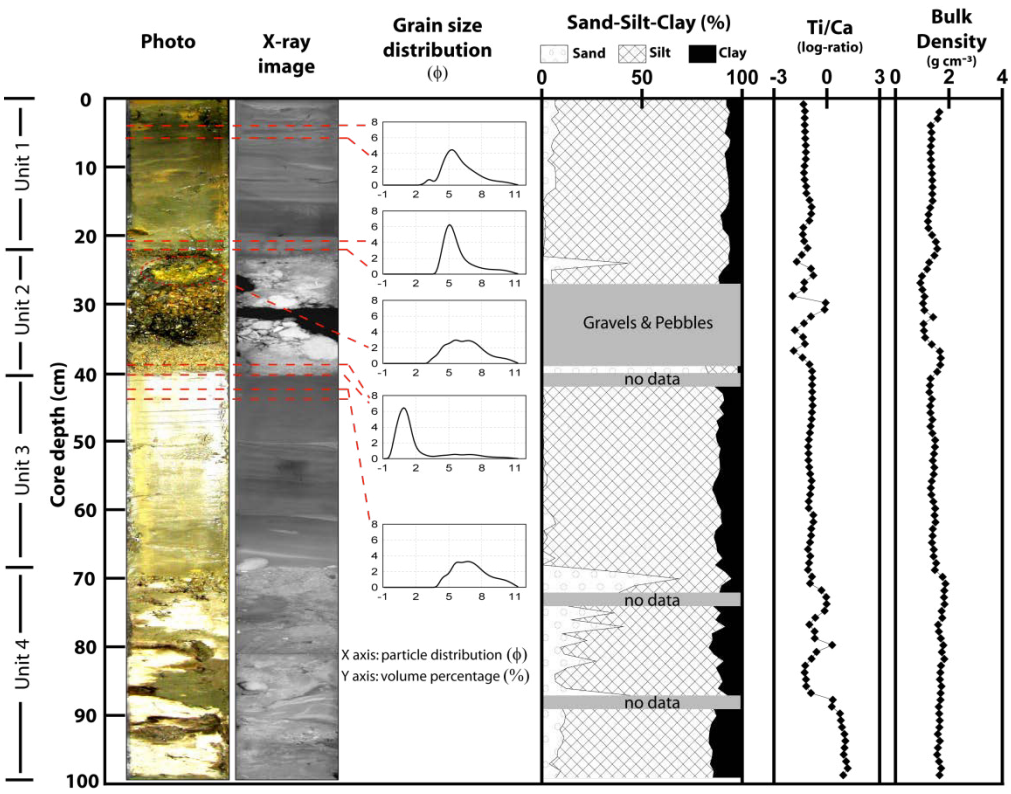

Fig. 3 Properties of sediments in core 050310-C6: division into sedimentary units, photo, X-ray image, typical grain size distributions (ϕ), amount of sand, silt and clay fraction (%), Ti/Ca log-ratio and bulk density.

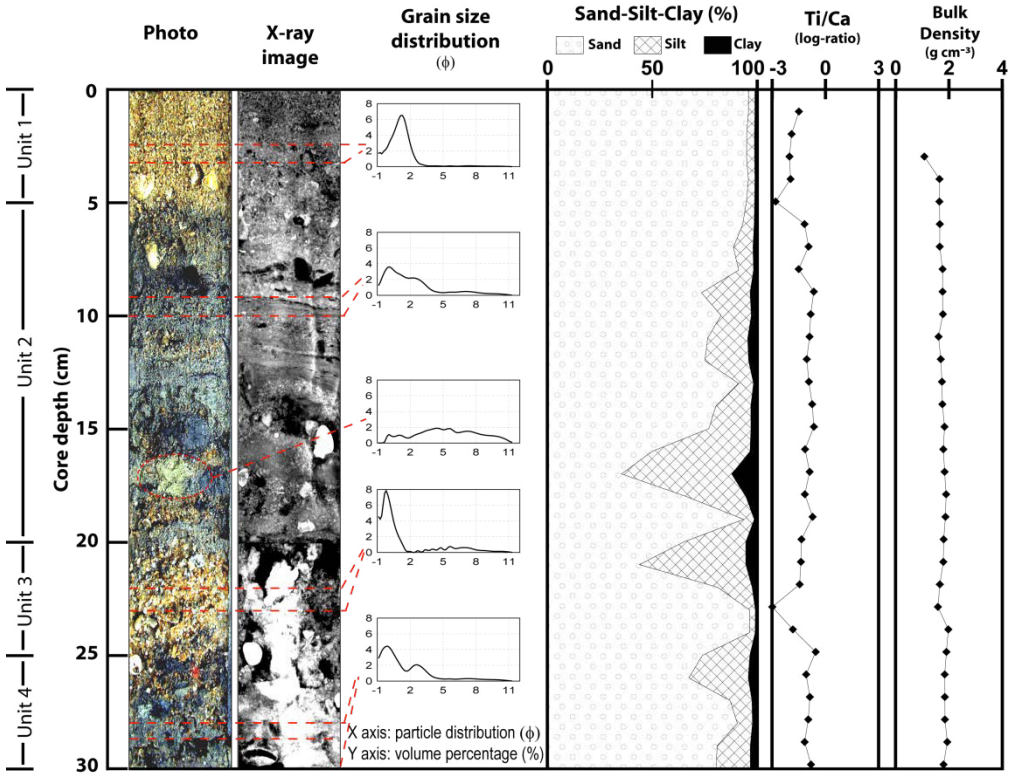

Fig. 4 Properties of sediments in core 051207-32: division into sedimentary units, photo, X-ray image, typical grain size distributions (ϕ), amount of sand, silt and clay fraction (%), Ti/Ca log-ratio and bulk density.

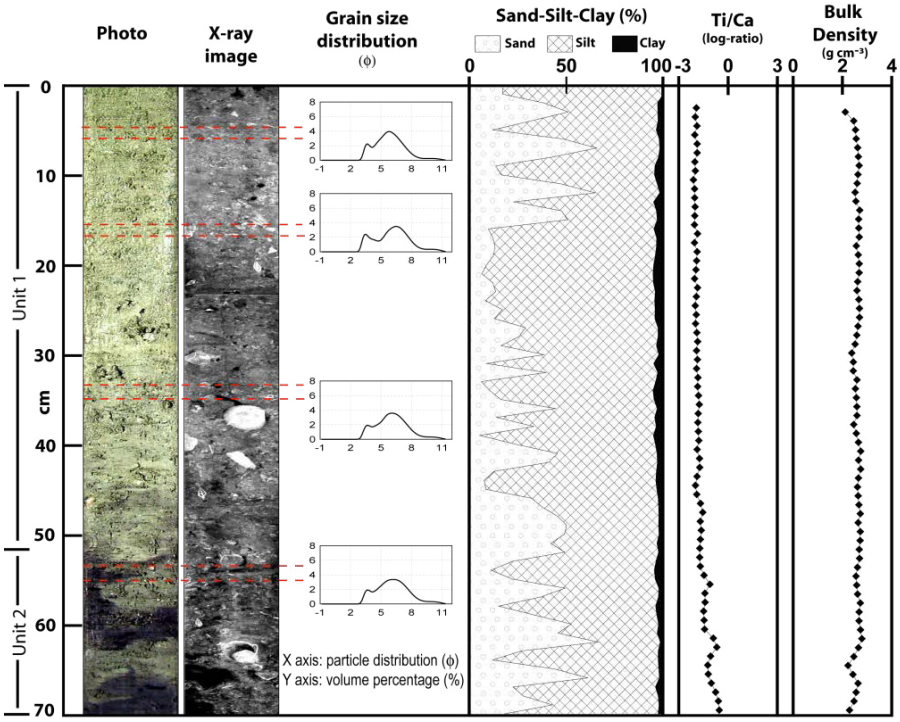

Fig. 5 Properties of sediments in core 031207-23: division into sedimentary units, photo, X-ray image, typical grain size distributions (ϕ), amount of sand, silt and clay fraction (%), Ti/Ca log-ratio and bulk density.

decay, and is used for the assessment of sediment accumulation rates under several assumptions, depending on the applied model (Robbins and Edgington, 1975, Nittrouer et al., 1979, Carpenter et al. 1982). However, the shape of the ^{210}Pb profile may also reveal information on changes in sediment accumulation rates, the presence of major erosional events and the presence of event layers (e.g., Nittrouer et al., 1979, Jaeger et al., 1998, Sommerfield and Nittrouer, 1999, Crockett et al., 2008, Szczuciński et al., 2009). An event layer can usually be observed in the portion of the ^{210}Pb activity profile that shows no change downcore (usually due to rapid deposition during the event). However, more frequently, ^{210}Pb depletion is observed due to dilution processes in larger sediment masses and/or the admixture of sediments containing low ^{210}Pb activity due to a coarser grain size fraction.

^{210}Pb activity was measured for samples from core 050310-C6 using gamma spectrometry at the Leibniz-Laboratory for Radiometric Dating and Isotope Research (Kiel, Germany). The ^{210}Pb supported activities in the present study were assessed from minimum activities (40 Bq kg^{-1}) found in the sediment core, which are similar to the supported activities reported for similar sediments in the region (Szczuciński, 2010). However, supported activities are typically ascertained by averaging the nearly uniform, low-level ^{210}Pb activities below the region of radioactive decay or through independent measurements of ^{226}Ra (often through ^{214}Pb and ^{214}Bi; e.g., Zaborska et al., 2007, Szczuciński et al., 2009). Because the uniform activities in the lowermost part of the core were not reached and the ^{226}Ra was not measured, a precise estimation of ^{210}Pb supported activities could not be obtained. Supported ^{210}Pb activity values in the order of 10 to 26 Bq kg^{-1} were also reported by Kennedy et al. (2008) from the nearshore sediments on the Andaman Sea coast and are considered in the discussion of the calculated accumulation rates. The linear sediment accumulation rate (SAR) was determined from the decline in the excess ^{210}Pb activities using the following equation (Robbins and Edgington, 1975, McKee et al., 1983):

$$\mathrm{SAR} = \lambda \times z \times \left[\ln(A_0 / A_z)\right]^{-1}$$

where λ is the decay constant (= 0.0311 year^{-1}); z is the depth in the core (cm); A_0 is the specific activity of excess ^{210}Pb at a particular reference horizon (Bq kg^{-1}); and A_z is the specific activity of excess ^{210}Pb at depth z below the reference horizon (Bq kg^{-1}).

Along with ^{210}Pb, ^{137}Cs activity was measured using gamma spectrometry.

3.4 Results

In water depths of 5 to 20 m, several regions covered with mud or revealing a channel-like morphology (Di Geronimo et al., 2009, Feldens et al., 2009, 2010, in press EPS), were found to host tsunami deposits. Representative sediment cores from these regions were selected for the present study (core 050310-C6 from a mud patch and core 051207-32 from the channel).

3.4.1 Sedimentary structure and grain size

Core 050310-C6, with a length of 99 cm, was retrieved from a water depth of 9.6 m (see Figs. 1 and 2 and Table 1). The core was subdivided into four major sedimentary units (Fig. 3).

- The first, unit 1 (0-22 cm), was composed of brown, poorly sorted laminated silt that contained up to 10.8 % clay and up to 8.4 % sand. Only a few bioturbation traces were preserved. This unit was divided into three subunits. The upper part (subunit 1a, 0-15 cm) was very finely laminated. It contained both horizontal and cross laminations, as well as erosional surfaces. Grey-scale changes of the x-ray image suggested slight upward fining within the laminae. The second subunit (1b, 15-20 cm) was composed mostly of silt. In comparison to the units located above and below this subunit, it was slightly depleted in sand and enriched in clay. It contained very gently marked horizontal laminations. The upper contact was transitional while the lower contact was sharp. The lower subunit (1c, 20-22 cm) was composed of slightly coarser silt than the subunit above. The sediment was fining upward and conformably overlaid the sediments of unit 2.

- Unit 2 (22-40 cm) was composed of sand, gravel, clay clasts, pieces of laterites, rocks and shells. The arrangement of these particles was subhorizontal, with the largest clasts being up to 3 cm in diameter. Based on a detailed analysis, this unit was divided into two subunits. The upper subunit 2a (22-38 cm) was composed of sediments ranging from normal grading gravels to fine sand. The lower contact with subunit 2b was erosional. Subunit 2b (38-40 cm) was composed of laminated medium to coarse sand.

- Unit 3 (40-69 cm) was represented by laminated silt and clayey silt that was slightly finer than the sediment forming unit 1. Its upper contact was erosional and the basal contact was sharp. Within this unit, at least three fining-upward sequences were differentiated (3a: 40-50 cm, 3b: 50-61 cm, and 3c: 61-69 cm). These sequences began with thin sandy silt laminae and became finer with decreasing depth, eventually becoming clayey silt. Moreover, in subunit 3b, an erosional surface was preserved in the middle of the subunit. The lamination in the unit was slightly inclined, and few small vertical burrows were preserved. A 2 cm-diameter gravel was found at the bottom of this unit.

- Unit 4 (69-99 cm) was composed of laminated muddy sand, which was partly intercalated with consolidated mud that was almost white. The layering and laminations were partly disturbed. In the upper 10 cm of this unit, white consolidated mud did not extend continuously in the horizontal plane, while the lowermost 5 cm of the sediment in the core was composed entirely of this type of sediment. Some small gravel components were found at a depth of 92-94 cm.

Core 051207-32 was retrieved from a water depth of 14.4 m and was 30 cm in length (Figs. 1 and 2, Table 1). This core also revealed several different sediment types, and was therefore divided into four units (Fig. 4):

- Unit 1 (0-5 cm) was composed of a yellowish medium to coarse sand with shell fragments. This unit had a massive structure and conformably overlaid the upper surface of unit 2.

- Unit 2 (5-20 cm) had a relatively complex composition. It was composed of stiff muddy sand, sandy mud and sand. It was variable in

colour, ranging from yellow or light green to olive or black. It was partly laminated, but also contained muddy clasts, pieces of wood, laterites and red brick fragments (artefacts). Sand appeared in the form of intercalations. Moreover, gravel and small pebbles were scattered throughout the entire unit. The grain size in this unit did not show normal grading, except for the upper part. The lower contact was sharp and uneven.

- Unit 3 (20-25 cm) was a massive layer of heterogeneous coarse sand and gravels.

- Unit 4 (25-30 cm) was composed of muddy sand and was very similar to unit 2. The upper part contained admixtures of coarse sand from unit 3.

Core 031207-23 was retrieved from a water depth of 55.4 m and was 70 cm long (Figs. 1 and 5, Table 1). It was composed of poorly sorted sandy silt and silty sand, with only 5.2% clay. Shells were abundant in this core, and it was possible to distinguish two units.

- Unit 1 (comprising the upper approx. 51 cm) was composed mostly of silty sand with intercalations of sandy silt. Laminations were poorly preserved and shells were less abundant than in the lower unit. No distinct boundary was observed between units, the change was transitional, and the lower boundary was selected in conjunction with changes in geochemistry. The upper part of the unit contains sandy intercalations of several cm-thick. The lowest sand content was found at a depth of 20-30 cm.

- Unit 2 (approx. 51-70 cm) was also composed of silty sand intercalated with sandy silt. The intercalations appeared in the form of poorly preserved layering. The unit contained more shell fragments than unit 1.

3.4.2 Geochemical and physical properties

Log-ratios of titanium (Ti) and calcium (Ca), which represent the relative variations of terrigenous versus marine constituents, are shown in Figs 3-5. Ti is enriched in tropical soils in the form of laterites and bauxites and is relatively inert against diagenetic processes (Calvert and Pedersen, 2007), whereas Ca reflects the occurrence of $CaCO_3$, which is mainly produced under marine conditions (Hofmann et al., 2005, Weltji and Tjallingii, 2008). In all of the studied cores, changes in the Ti/Ca log-ratio roughly reflected the sedimentary units described above. In core 050310-C6 (Fig. 3), the ratio was stable in units 1 and 3, variable in unit 2 and generally elevated in unit 4. In core 051207-32 (Fig. 4), this ratio was slightly lower in the sandy, shell-rich units (units 1 and 3). This ratio was mostly uniform in core 031207-23 (Fig. 5), where only a slight downward increase was observed in unit 2.

The PCA revealed that two principal components of onshore and core 050310-C6 sediment samples (PC1 and PC2) explained 80.5 % of the cumulative variance. PC1 (accounting for 69.7 % of the variance) had highly negative factor scores for terrestrial elements, such as Al, Si, S, K, Ti, Mn and Fe. PC2 (accounting for 10.8 % of the variance) had highly positive factor scores for Ca and Si. This finding indicates that PC2 was characterised by a marine component, and Si was most likely associated with marine sands. Plotting these two main factors together (Fig. 6) indicated the grouping of sediment samples (circled on the graph). Samples from unit 2 of core 050310-C6 and onshore sediments had positive values for PC1, which indicated a stronger terrestrial influence than units 1 and 3. For PC2, most of units 1, 2 and 3 of core 050310-C6 had positive values, whereas onshore samples had negative values. This finding suggests that unit 2 of core 050310-C6 also had marine components. Therefore, sediments from unit 2 of core 050310-C6 were a mixture of terrestrial and marine components.

The bulk density of the studied cores was generally uniform, with the exception of slight variations in units 2 and 4 of core 050310-C6. The other measured physical properties did not reveal significant changes.

3.4.3 ^{210}Pb data and interpretation

The total ^{210}Pb activity profile of core 050310-C6 (Fig. 7) revealed a general decline of activities with depth, interrupted by one major and several minor anomalies that were interpreted as being event layers or periods of accelerated sediment accumulation. These event layers reflect a non-steady sedimentation regime.

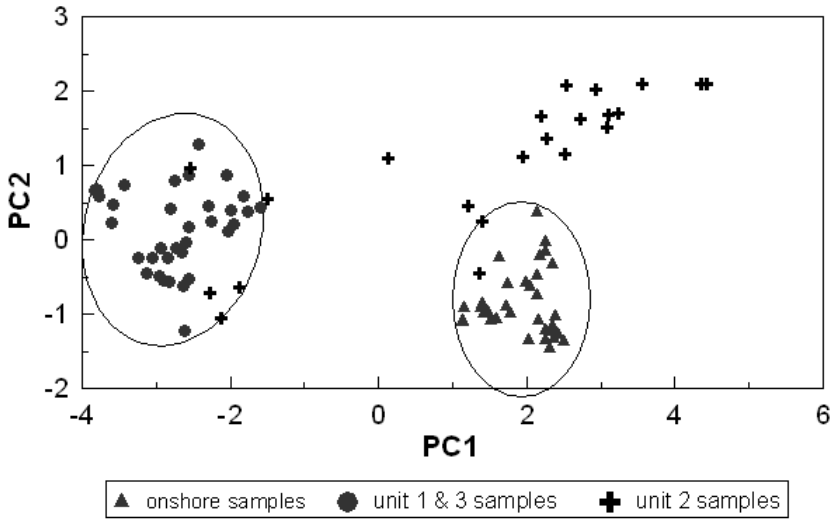

Fig. 6 PCA for chemical elemental composition data (from XRF core scanner) of onshore sediment samples which were retrieved from Khao Lak coastline (101207-89, 101207-91 and 101207-93; see position on Fig. 1) and offshore sediment samples from unit 1, 3 and 2 of core 050310-C6. Unit 1 and 3 are interpreted as post- and pre-tsunami deposits and unit 2 as tsunami deposits.

Using data on sedimentary structures as supporting information, the total ^{210}Pb profile was divided into three major parts, referred to as sedimentary units 1, 2 and 3 (Fig. 3).

- The upper portion of unit 1 was composed of three sediment segments (approximately 0-15 cm, 15-20 cm and 20-22 cm), which were most likely deposited during events or periods of accelerated accumulation, as indicated by step-like activity profiles. The uppermost segment could also be interpreted as a surface mixed layer; however, the well-preserved laminations suggest that sediment mixing due to bioturbation was not significant. Precise calculations of sediment accumulation rates were not possible since the accumulation was not steady and the background activities were only assumed. Depending on the ^{210}Pb supported activities used and considering the analytical accuracy, the calculated sediment accumulation rates were in the range of 1.3 to 5.7 cm y^{-1}. In general, the lower the supported activities applied, the higher the accumulation rate that we obtain. Since the assumptions for this method were not fully met (the accumulation was not steady), the results should be regarded as an approximation; we can infer from these results that the accumulation rate occurring is in the order of a few cm per year. This finding suggests that the unit had to be deposited over a period of several to a dozen years. Considering that the core was sampled in 2010, it is possible that the sediments in unit 1 were deposited after 2004.

- Unit 2 (around 22 to 40 cm) was partly composed of coarse sediments, which do not contain excess ^{210}Pb, as indicated by a sample taken from a depth of 38 cm which showed only the activity of supported ^{210}Pb. The activities in the upper part of the unit and below it are similar. Therefore, this unit was assumed to be an event layer. Moreover, similar ^{210}Pb activities in the lowermost part of unit 1 and in the uppermost part of unit 3 also suggested that the event that created unit 2 was effectively depositional and caused little or no erosion of the older sediments.

- Unit 3 (below 40 cm) revealed a general decline of ^{210}Pb activity with depth; however, there were three segments with slightly reversed trends. Those segments were found at approximately the following sediment depths: 40-50, 50-61 and 61-69 cm. These segments roughly corresponded to the fining-upward subunits 3a, 3b and 3c and most likely represented sedimentary events or periods of accelerated deposition. The calculations of sediment accumulation rates in this unit, under the conditions

specified above, indicated rates of approximately 0.7 to 2.4 cm y^{-1}.

The ^{137}Cs values indicated very low activities, often close or below minimum detection activity levels (Fig. 7). However, the presence of ^{137}Cs throughout the core supports a ^{210}Pb-based interpretation of a high accumulation rate since ^{137}Cs has been present in the environment since the early 1950s (Robbins et al., 1978). The very low activities observed were due in part to high accumulation rates and the dilution effect of the radioisotope in the large mass of sediment, and in part to generally low ^{137}Cs fallout at this latitude (see discussion in Szczuciński et al., 2009).

3.5 Discussion

3.5.1 Evidence of the 2004 Indian Ocean tsunami event layer

Cores were collected within three to six years after the 2004 Indian Ocean tsunami. In the period between the tsunami and the time of collection, neither big storms nor intense anthropogenic offshore activities affected the region. Several tropical cyclones were recorded during the 20th century and passed near the study area; the last major cyclone in this region was Cyclone Gay in 1989 (Kumar et al., 2008; Brand, 2009). However, despite the fact that these events were recorded in middle continental shelf deposits (Szczuciński, 2010), they have not been found to cause significant sedimentological change in the eastern coastal region of the Andaman Sea due to their westward-oriented tracks (Brand, 2009). Consequently, the documented sedimentary event layers found in the inner shelf cores are considered to represent potential effects of the 2004 tsunami, when maximum water velocities over the inner shelf were modelled and in the order of several m s^{-1} (Suppasri et al., 2011).

In core 050310-C6, the most likely result of deposition by the 2004 tsunami was sediment unit 2, which was composed of poorly sorted sand and gravel between fine-grained deposits. This event layer contains compounds of a terrestrial and marine origin: clay clasts, pieces of laterites, rocks and shells. The mixed provenance of the sediments was supported by the PCA evaluating their chemical composition. These sediments were similar to samples taken from potential onshore sources, as well as marine sands (Fig. 6). Unit 2 is also marked by similar ^{210}Pb activities above and below the unit and by anomalously low ^{210}Pb activity in some samples taken from the unit, which supports the event origin of this unit. The neighbouring deposits (units 1 and 3) represent rapidly accumulating sediments (>1 cm y^{-1}) with episodes of erosion and sedimentation indicated by sedimentary structures seen in X-radiographs (Fig. 3) and reflecting the dynamic nature of shallow water environments (water depths of approximately 10 m). The ^{210}Pb-based assessment of accumulation rates confirmed, within error ranges, that unit 2 was several years old and could have been generated by the 2004 Indian Ocean tsunami.

Core 051207-32 was sampled within three years of the tsunami. The sand layer forming the uppermost portion of this core was very similar to sediments covering most of the continental shelf at water depths of 15 to 22 m (e.g., Feldens et al., 2009, 2010 and in press EPS). This layer conformably covers units 2, 3 and 4 (>25 cm in thickness), which revealed many features of event deposits, such as poorly sorted sediments ranging from mud to gravel, muddy clasts, pieces of wood, laterites and pieces of red brick. The latter suggests that the sediments had material of terrigenous origin included. The changing character of the deposits (mud/sand/mud) may reflect changing flow velocities and directions, while minor changes in the Ti/Ca log-ratio may reflect changes in sediment sources. Based on this evidence and the assumptions presented above, units 2-4 are interpreted as having been deposited during the passage of the tsunami wave train.

The potential tsunami deposits in the two cores differed from one another in terms of the number of units with event deposits, their sedimentary characteristics and the relative input of terrestrial material. These characteristics may have been related to the various water depths (9.6 and 14.4 m), the distance offshore (3.1 and 7.2 km), and variations in the hydrodynamics of tsunami waves. The video records of the 2004 tsunami offshore of Khao Lak revealed a high variability in flow patterns, including the formation of giant gyres (e.g., Di Geronimo et al., 2009). Although there is a supporting age control for one core (in core 051207-32, it was not possible to evaluate this factor due to the lack of suitable sediments above and below the event layer) and there was no evidence of recent heavy

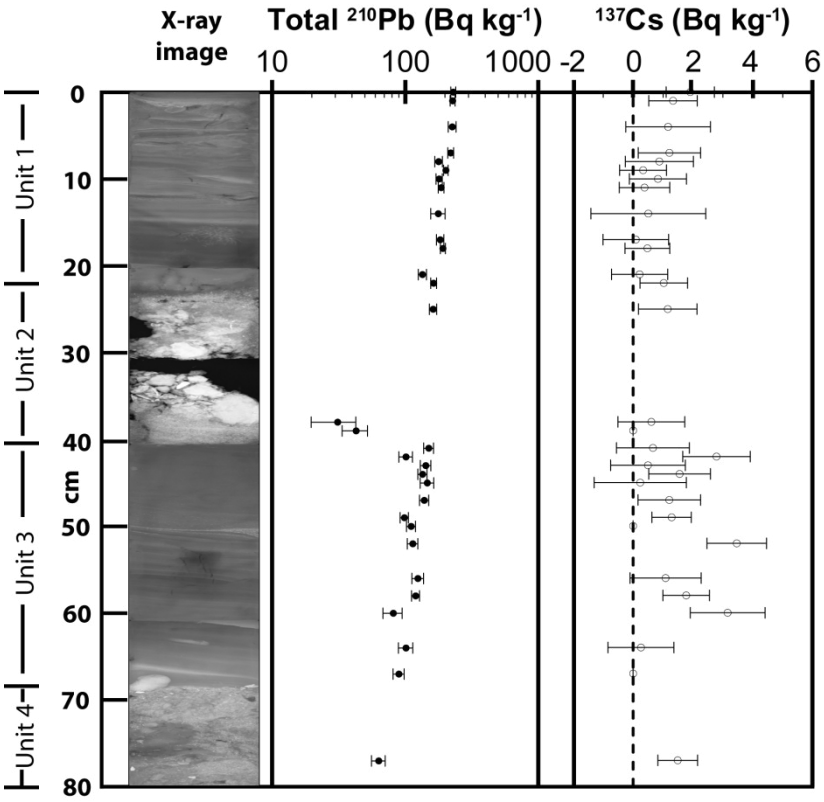

Fig. 7 Total ^{210}Pb activity (Bq kg^{-1}) profile, ^{137}Cs activity profile and X-ray image of core 050310-C6. The lowest total ^{210}Pb activity was measured in the sand layer (38-40 cm depth), and is close to assumed supported ^{210}Pb activity.

storms in the area, one may consider that the event deposits were formed by storms or cyclones. Storm deposits (tempestites) in shallow environments may reveal many various features depending on local conditions. There are no studies of storm deposits on the inner shelf in the Andaman Sea. However, in general, shallow water storm deposits may be sandy or muddy and often have basal erosional contact, normal gradation, plane lamination, wave ripples, thicknesses ranging from a few to more than 30 cm and hummocky cross stratification (e.g., Einsele et al., 1991; Weidong et al., 1997, Allison et al., 2005). Storm deposits may contain only one or many of these features. Moreover, as indicated by modern examples (e.g., Allison et al., 2005), changing flow conditions are also observed during a hurricane, and near-bottom velocities can reach more than 1 m s^{-1}. Thus, many characteristics of storms and tsunamis over the continental shelf that affect sedimentation may be similar. The major features observed in the documented event layers, which are less likely, or unlikely, in storm deposits are: the frequent presence of terrestrial components, poor sorting and a massive character of some layers. Terrestrial components may be found in storm deposits if there is a big river nearby and can also occur due to coastal erosion. However, storms primarily tend to erode the coastline (beach, dune), while tsunamis may also deliver terrestrial material further inland such as human artefacts and plants. The poor sorting and massive character of sediments may indicate a kind of sediment gravity mass flow (expected during backwash). Gravity mass flows are also known to be generated by storms, for instance in form of wave-induced fluid mud flows (e.g., Nittrouer et al., 2007). However, the fluid mud flow deposits are usually better sorted, do not include oversized clasts and contain less terrestrial material when compared with tsunami deposits.

Sediments in core 031207-23 were taken from a water depth of 57 m. Distinct event layers were not recognised in this core, suggesting that the 2004 tsunami had no or very limited depositional effect in this region. Confirming conclusion reached by Szczuciński (2010) based on ^{210}Pb analyses of sediment cores from the mid continental shelf.

3.5.2 Processes of offshore sedimentation by the tsunami

Assuming that the interpretation of the event layers as tsunami deposits in cores 050310-C6 (unit 2) and 051207-32 (units 2-4) is correct, these deposits may serve as a source of information about tsunami sedimentation processes.

In core 050310-C6 (water depth 9.6 m, 3.1 km offshore), unit 2 (interpreted as being a tsunami deposit) began with a subunit that is approximately 2 cm thick (2b), which is composed of horizontally laminated medium to coarse sand. This subunit showed no indication that it had a terrigenous origin (the Ti/Ca ratio was similar to that in the sediments beneath it). There are several processes able of forming laminated sandy deposits, including flows in the upper and lower flow regimes, storms and turbidity currents (Reineck and Wunderlich, 1998). In the case presented in this study, it is likely that the sand was transported from water depths of 15-22 m, where medium and coarse sands are common (Feldens et al., in press EPS), toward the shoreline during the run-up phase. To confirm this fact, a detailed analysis of microfossils is recommended in the future. The transport of sand could occur as a unidirectional flow in lower or upper plane bed conditions. Later on, an erosional surface was created, along with the deposition of unit 2a (approximately 16 cm thick). The subunit is likely to have been deposited as a result of decelerating flow conditions because it revealed a normal gradation. Considering the largest size of pebbles found in the lower part of the unit, the water velocity had to be at least in the order of several tens of cm s^{-1}. This subunit contains many terrigenous components; moreover, its chemical composition is similar to the onshore sediments analysed (Fig. 6). Therefore, it is very likely that this unit was created during the backwash flow.

Units 2-4 in core 051207-32 (water depth 14.4 m, located 7.2 km offshore) could be interpreted as tsunami deposits. Because the retrieved sediment core does not reach below unit 4, it is unclear how the sequence of tsunami deposits begins. The lowermost unit is composed of massive stiff mud with scattered gravel, pieces of wood, mud clasts and red brick fragments. Its chemical composition also suggests a terrigenous origin, and thus, this unit was most likely formed during backwash. This finding is supported by the presence of over-sized clasts "floating" in the finer sediment mass and relatively high sediment consolidation. This subunit was approximately 5 cm thick and was covered by coarse sand and gravel with a massive appearance. The Ti/Ca log-ratio in this thin layer was lower than that of the layer below, so these sediments may have no, or a lower, terrigenous contribution. This layer may have been transported from offshore and deposited during the tsunami run-up flow. The lack of clear lamination suggests that the deposition was rapid. The sand was covered by a complex, stiff mud with many over-sized compounds of sand and gravel (unit 2), which is very similar to the lowermost portion of unit 4. This finding is interpreted as being an effect of the backwash flow, although the terrestrial contribution is not clear in the sediment geochemistry. However, during the backwash from the second wave, the inundated land was already mostly covered with water (e.g., Choowong et al., 2008), so there was much less erosion on land than during the first wave backwash phase. The upper part of this unit was partly laminated and reflected an upward fining in grain size. It is possible that the sediment-gravity flow evolved, due to a decrease in flow density, into simple settling from suspension, or that the unit represents two (or more) events (or pulses).

3.5.3 Diagnostic features of offshore tsunami deposits

Onshore tsunami deposits are characterised by a complex set of diagnostic features that have been presented in many studies (e.g., Dawson and Shi, 2000, Goff et al., 2001, Shiki et al., 2008, Bourgeois, 2009, Mamo et al., 2009, Chagué-Goff, 2010, Goto et al., 2010, Chagué-Goff et al., 2011). However, such criteria have not yet been summarised for offshore tsunami deposits, and the published data are limited. In the literature, offshore tsunami deposits are frequently related not only to the direct effect of deposition from tsunami-induced water flow (run-up or backwash), but also to tsunami-induced secondary processes such as turbidity currents (Dawson and Stewart, 2007, Shiki et al., 2008) and formation processes of so-called "homogenites" (Cita et al., 1996). The present discussion is limited to the recent shallow water

Table 2 Comparison of selected signatures of offshore tsunami deposits.

Source of data	van den Bergh *et al.* (2003)	Abrantes *et al.* (2008)	Goodman-Tchernov *et al.* (2009)	Paris *et al.* (2010)	Smedile *et al.* (2011)	Present study
Region	Java, Indonesia	Portuguese shelf off Lisbon	coastal zone of Israel, Eastern Mediterranean	Sumatra, Indonesia	Augusta Bay, Eastern Sicily, Italy	Andaman Sea, Thailand
Age of tsunami (AD)	1883	1755, 1969	1630-1550 BC, 115 AD, 551 AD	2004	1169, 1693, 1908, and 8 other events	2004
Distance offshore (km)	3-14	6-15	~ 4	0-5	2	3-7
Water depth (m)	2 - 27	88 - 105	10 - 20	10 - 25	72	9 - 15
Type of sedimentary contacts	lower - sharp, often erosional; upper sharp or blurred due to bioturbations	no visible contact, sharp contact, erosional surface	erosional lower contact	sharp	not visible, sharp	lower - sharp, erosional; upper - sharp
Grain size	sand, gravel (mainly carbonate) and mud size tephra	mud, sand and gravels	sandy mud, muddy sand, pebbles	sand, boulders of various sizes (up to 15 m)	sandy mud; often with bimodal grain size distribution	mud, sand, gravels and pebbles
Sediment sorting	poorly sorted	well sorted, poorly sorted	poorly sorted	poorly sorted	moderately to poorly sorted	poorly sorted
Terrigenous components	volcanic rock fragments	no	organic material, pumice	trees	no	wood, mud clasts, laterite
Anthropogenic artifacts	no	no	pottery	yes	no	brick pieces
Fossils	abundant broken shells; presence of	shell fragments	molluscs; change in foraminifera and	coral boulders	significant amount of displaced	shells
Geochemical indicators	variable Ca and Mn	variable Fe and Ca content	not studied	not studied	no	variable Ti/Ca ratio
Number of layers	1 - >6	1	1 - 2	1	1	2 - >3
Sedimentary structures	fining upward, laminated, coarsening upward at the base, shell layers	laminations, turbidite	imbrication, rip-up clasts, fining upward sequence	lobe shaped boulders arrangement; segregation of boulders with distance	not reported	laminations, massive structures, fining upward sequence, internal erosional
Presence of tephra layer	tephra and pumices	no	pumices	no	tephra is present but not related to the tsunami deposits	no
Presence of ^{210}Pb event like profile	^{210}Pb used for age control	yes	not studied	not studied	no	yes

deposits most likely formed due to direct deposition from tsunamis.

Table 2 summarises major features of tsunami deposits on the inner shelf or within 15 km of land that were generated by the eruption of Santorini in ca. 1630-1550 BC (Goodman-Tchernov et al., 2009), the eruption of Krakatau in 1883 (van den Bergh et al., 2003), earthquakes on the Portuguese margin in 1755 and 1969 (Abrantes et al., 2008), several tsunamis in the Mediterranean (Smedile et al., 2011) and the 2004 Indian Ocean tsunami (Paris et al., 2010 and present study). Several sedimentological studies (e.g., Massari and D'Alessandro, 2000, Takashimizu and Masuda, 2000, Fujiwara and Kamataki, 2007) on potential shallow marine tsunami deposits from the geological past are not included in the discussion because they are not related to a specific tsunami event but are interpreted as being tsunami-generated based on sedimentological properties. The comparison proves how variable offshore tsunami deposits can be. The deposits may form an event layer several cm, several tens of cm or even over 1 m thick. The layers tend to have sharp lower contacts, which are often erosional. The upper contact may be blurred by bioturbations. They are composed of all grain size classes; often several classes are present in one layer resulting in poor sorting. Frequently, offshore tsunami deposits contain some typical terrigenous particles (wood, plants, etc.) and, if available, human-made pottery, brick, etc. This finding suggests the important role of tsunami backwash flows in the formation of these deposits. The fossil assemblage within the event layers may represent organisms from various environments. There was a high degree of variation in typical geochemical indicators of marine (Ca) or terrestrial origin (Fe, Mn, Ti). The tsunami deposits may appear in the form of a single layer or several layers and may present the whole range of sedimentary structures: laminations, fining or coarsening upward, a massive structure, erosional surfaces, imbrications, lag deposits, etc. Finally, the key to the interpretation of these structures is accurate dating, with analyses such as ^{210}Pb activity profiles being particularly helpful. For instance, in the case of 1969 tsunami deposits on the Portuguese shelf, there was no visible change in sediment properties apart from a slight change in the ^{210}Pb profile (Abrantes et al., 2008).

The presented comparison of offshore tsunami deposit characteristics reveals that their interpretation may be even more difficult than in the case of onshore tsunami deposits. It appears that the identification will always have to be based on several characteristics and a broad knowledge of local conditions. Distinguishing offshore tsunami and storm deposits will be a considerable challenge for future studies.

3.6 Conclusions

The present study provided new evidence of probable 2004 Indian Ocean tsunami deposits left on the inner shelf of the Andaman Sea (Thailand) and identified the diagnostic sedimentological and geochemical properties of these deposits. The deposits were restricted to the shallow marine environment (water depths of 9-15 m) within 8 km of the shoreline. Deposition occurred during the run-up phase, causing landward redeposition of marine sand, and during backwash flow events, which also deposited terrigenous sediments. The transport and deposition of sediments were driven by several processes, including unidirectional flow in various flow regimes and high-density sediment-gravity flow.

Typical features of these event deposits included the following: a thickness in the order of 20-25 cm, a wide range of grain sizes and poor sorting, in contrast to underlying and overlying sediments, the presence of several layers, marine sand alternating with poorly sorted mud with terrigenous and anthropogenic components, representing different hydrodynamic conditions (run-up and backwash phase).

Geochemical and geophysical analyses, and particularly ^{210}Pb activity measurements, were helpful supplementary tools in the identification of event layers. However, the analysis of available data on offshore tsunami deposits showed that there is no single set of signatures that could be universally applied to identify these deposits. Future studies will need to include more proxies (microfossils and advanced geochemistry in particular) to establish an identification key for offshore tsunami deposits.

Acknowledgements. We are grateful to Phuket Marine Biological Center (PMBC) for supporting us with ship time of RV Chakratong Tongyai and RV Boonlert Pasook as well as with other facilities during field campaigns. We further thank Dr. Warner Brückmann and Dr. Dieter Garbe-Schönberg for supporting the MSCL and XRF scanner measurements. Gratitude is also expressed to Dr. Nils Anderson and Dr. Helmut Erlenkeuser for their helpful comments and ^{210}Pb determination. We thank Dr. Björn Heise and Daniel Unverricht for their tremendous help and inspiring ideas. Acknowledgements are due to Dr. P.M. De Martini and Dr. C. Chagué-Goff for their very constructive and detailed reviews. This research was funded by Deutsche Forschungsgemeinschaft (DFG) grant SCHW 572/11 and DAAD (Deutscher Akademischer Austausch Dienst) fellowship provided to Ms. Daroonwan Sakuna for a Ph.D. study at Kiel University.

References

Abrantes, F., Alt-Epping, U., Lebreiro, S., Voelker, A. and Schneider, R., Sedimentological record of tsunamis on shallow-shelf areas: The case of the 1969 AD and 1755 AD tsunamis on the Portuguese Shelf off Lisbon, *Marine Geology*, **249**, 283-293, 2008.

Allison, M.A., Sheremet, A., Goñi, M.A. and Stone, G.W., Storm layer deposition on the Mississippi-Atchafalaya subaqueous delta generated by Hurricane Lili in 2002, *Continental Shelf Research*, **25**, 2213-2232, 2005.

Bahlburg, H., Spiske, M. and Weiss, R., Comment on "Sedimentary features of tsunami backwash deposits in a shallow marine Miocene setting, Mejillones Peninsula, northern Chile" by G. Cantalamessa and C. Di Celma [Sedimentary Geology 178 (2005) 259--273], *Sedimentary Geology*, **228**, 77-80, 2010.

Bahr, A., Lamy, F., Arz, H., Kuhlmann, H. and Wefe, G., Late glacial to Holocene climate and sedimentation history in the NW Black Sea, *Marine Geology*, **214**, 309-322, 2005.

Bell, R., Cowan, H., Dalziell, E. and Evans, N., Ó Leary, M., Rush, B. and Yule, L., Survey of impacts on the Andaman Coast, Southern Thailand following the great Sumatra-Andaman earthquake and tsunami of December 26, 2004, *Bull. of The New Zealand Soc. For Earthquake Eng.*, **38**, 123-148, 2005.

Best, A.I. and Gunn, D.E., Calibration of marine sediment core loggers for quantitative acoustic impedance studies, *Marine Geology*, **160**, 137-146, 1999.

Blott, S.J. and Pye, K., Gradistat: a grain-size distribution and statistics package for the analysis of unconsolidated sediments, *Earth Surf. Process. Landforms*, **26**, 1237-1248, 2001.

Bouma, A.H., Notes on X-ray interpretation of marine sediments, *Marine Geology*, **2**, 278-309, 1964.

Bourgeois, J., Geologic effects and records of tsunamis, In: *The Sea, Volume 15: Tsunamis*, Edited by Robinson, A.R. and Bernard, E.N., 53-91 pp., Harvard University press, Amsterdam, 2009.

Brand, S., Typhoon havens handbook, In: *http://www.nrlmry.navy.mil/port_studies/Havens_Handbook/thh-nc/0start.htm*, Edited by Brand, S., 2009.

Calvert, S.E. and Pedersen, T.F., Elemental proxies for paleoclimatic and paleoceanographic variability in marine sediments: interpretation and application, In: *Developments in Marine Geology*, Edited by Hillaire-Marcel, C. and de Vernal, A., 567-644 pp., 2007.

Cantalamessa, G. and Celma, C.D., Sedimentary features of tsunami backwash deposits in a shallow marine Miocene setting, Mejillones Peninsula, northern Chile, *Sedimentary Geology*, **178**, 259-273, 2005.

Carpenter, R., Peterson, M.L. and Bennett, J.T., 210Pb-derived sediment accumulation and mixing rates for the Washington continental slop, *Marine Geology*, **48**, 135-164, 1982.

Chagué-Goff, C., Chemical signatures of paleootsunamis: A forgotten proxy?, *Marine Geology*, **271**, 67-71, 2010.

Chagué-Goff, C., Schneider J.-L., Goff J.R., Dominey-Howes D., Strotz L., Expanding the proxy toolkit to help identify past events – Lessons from the 2004 Indian Ocean Tsunami and the 2009 South Pacific Tsunami, *Earth-Science Reviews*, **doi**: 10.1016/j.earscirev.2011.03.007, 2011.

Choowong, M., Murakoshi, N., Hisada, K., Charusiri, P., Charoentitirat, T., Chutakositkanon, V., Jankaew, K., Kanjanapayont, P. and Phantuwongraj, S., 2004 Indian Ocean tsunami inflow and outflow at Phuket, Thailand, *Marine Geology*, **248**, 179-192, 2008.

Cita, M.A., Camerlenghi, A. and Rimoldi, B., Deep-sea tsunami deposits in the eastern Mediterranean: new evidence and depositional models, *Sedimentary Geology*, **104**, 155-173, 1996.

Crockett, J.S., Nittrouer, C.A., Ogston, A.S. and Goni, M.A., Variable styles of sediment accumulation impacting strata formation on a clinoform: Gulf of Papua, Papua New Guinea, In: *The Fly River, Papua New Guinea: Environmental Studies in an Impacted Tropical River System*, Edited by Bolton, B., 177-207 pp., Elsevier, Amsterdam, 2008.

Dawson, A.G. and Shi, S., Tsunami deposits, *Pure and Applied Geophysics*, **157**, 875-897, 2000.

Dawson, A.G. and Stewart, I., Tsunami deposits in the geological record, *Sedimentary Geology*, **200**, 166-183, 2007.

Dawson, S., Diatom biostratigraphy of tsunami deposits: Examples from the 1998 Papua New Guinea Tsunami, *Sedimentary Geology*, **200**, 328-335, 2007.

Di Geronimo, I., Choowong, M. and Phantuwongraj, S., Geomorphology and Superficial Bottom Sediments of Khao Lak Coastal Area (SW Thailand), *Polish J. of Environmental Studies*, **18**, 111-121, 2009.

Einsele, G., Ricken, W. and Seilchaer, A., In: *Cycles and events in stratigraphy*, Edited by Einsele, G., Ricken, W. and Seilchaer, A., 955 pp., Springer-Verlag, Berlin, Heidelberg, New York, 1991.

Feldens, P., Schwarzer, K., Szczuciński, W., Stattegger, K., Sakuna, D. and Somgpongchaiykul, P., Impact of 2004 Tsunami on Seafloor Morphology and Offshore Sediments, Pakarang Cape, Thailand, *Polish J. of Environmental Studies*, **18**, 63-68, 2009.

Feldens, P., Sakuna, D., Somgpongchaiykul, P. and Schwarzer, K., Shallow water structures in a tsunami-affected area (Pakarang Cape, Thailand), *Coastline Reports*, **16**, 15-24, 2010.

Feldens, P., Schwarzer, K., Sakuna, D., Szczuciński, W. and Somgpongchaiykul, P., Identification of offshore tsunami deposits on the shelf off Khao Lak (Thailand), *Earth, Planets and Space* (in press).

Fujiwara, O. and Kamataki, T., Identification of tsunami deposits considering the tsunami waveform: an example of subaqueous tsunami deposits in Holocene shallow bay on southern Bobo Penisular, Central Japan, *Sedimentary Geology*, **200**, 295-313, 2007.

Goff, J.C., Chagué-Goff, C. and Nichol, S., Paleotsunami deposits; a New Zealand Perspective, *Sedimentary Geology*, **143**, 1-6, 2001.

Goodman-Tchernov, B.N., Dey, H.W., Reinhard, E.G., McCoy, F. and Mart, Y., Tsunami waves generated by the Santorini eruption reached Eastern Mediterranean shores, *Geology*, **37**, 943-946, 2009.

Goto, K., Chavanich, S.A., Imamura, F., Kunthasap, P., Matsui, T., Minoura, K., Sugawara, D., Yanagisawa, H., Distribution, origin and transport process of boulders deposited by the 2004 Indian Ocean tsunami at Pakarang Cape, Thailand, *Sedimentary Geology*, **202**, 821-837, 2007.

Goto, K., Kawana, T. and Imamura,F., Historical and geological evidence of boulders deposited by tsunamis, southern Ryukyu Islands, Japan, *Earth-Science Reviews*, **102**, 77-99, 2010.

Goto, K., Takahashi, J., Oie, T. and Imamura, F., Remarkable bathymetric change in the nearshore zone by the 2004 Indian Ocean tsunami: Kirinda Harbor, Sri Lanka, *Geomorphology*, **127**, 107-116, 2011.

Hawkes, A.D., Bird, M., Cowie, S., Grundy-Warr, C., Horton, B.P., Hwai, A., Law, L., Macgregor, C., Nott, J., Ong, J.E., Rigg, J., Robinson, R., Tan-Mullins, M., Sa, T.T., Yasin, Z. and Aik, L.W., Sediments deposited by the 2004 Indian Ocean Tsunami along the Malaysia-Thailand Penisula, *Marine Geology*, **242**, 169-190, 2007.

Heise, B., Bobertz, B. and Harff, J., Classification of the Perl River Estuary via Principal Component Analysis and Regionalisation, *J. of Coastal Research*, **26**, 769-779, 2010.

Hofmann, D.I., Fabian, K., Schneider, F., Donner, B. and Bleil, U., A stratigraphic network across the Subtropical Front in the central South Atlantic: Multi-parameter correlation of magnetic susceptibility, density, X-ray fluorescence and $\delta^{18}O$ records, *Earth Planet. Sci. Lett.*, **240**, 694-709, 2005.

Jaeger, J.M., Nittrouer, C.A., Scott, N.D. and Milliman, J.D., Sediment accumulation along a glacially impacted mountainous coastline: north-east Gulf of Alaska, *Basin Research*, **10**, 155-173, 1998.

Jankaew, K., Atwater, B.F., Sawai, Y., Choowong, M., Charoentitirat, T., Martin, M.E. and Prendergast, A., Medieval forewarning of the 2004 Indian Ocean tsunami in Thailand, *Nature*, **455**, 1228-1231, 2008.

Jansen, J.H.F., Van der Gaast, S.J., Koster, B. and Vaars, A.J., CORTEX, a shipboard XRF-scanner for element analyses in split sediment cores, *Marine Geology*, **151**, 143-153, 1998.

Kennedy, J., Barry, B., Markwitz, A., Srisuksawad, K. and Limsakul, A., Pixe analysis of sediments affected by the December 2004 Indian Ocean Tsunami, *International Journal of PIXE*, **18**, 227-240, 2008.

Khokiattiwong, S., Limpsaichol, P., Petpiroon, S., Sojisuporn, P. and Kjerfve, B., Oceanographic variations in Phangnga Bay, Thailand under monsoonal effects, *Phuket Marine Biological Center Research Bulletin*, **55**, 43-76, 1991.

Kortekaas, S. and Dawson, A.G., Distinguishing tsunami and storm deposits: An example from Martinhal, SW Portugal, *Sedimentary Geology*, **200**, 208-221, 2007.

Kumar, V.S., Babu, V.R., Babu, M.T., Dhinakaran, G. and G.V. Rajamanickam, Assessment of Storm Surge Disaster Potential for the Andaman Islands, Journal of Coastal Research, 24, 171-177, 2008.

Lamy, F., Hebbeln, D., Röhl, U. and Wefer, G., Holocene rainfall variability in southern Chile: a marine record of latitudinal shifts of the Southern Westerlies, Earth Planet. Sci. Lett., 185, 369-382, 2001.

Le Roux, J.P. and Vargas, G., Hydraulic behaviour of tsunami backflows: insights from their modern and ancient deposits, *Environmental Geology*, **49**, 65-75, 2005.

Luque, L., Lario, J., Zazo, C., Goy, J.L., Dabrio, C.J. and Silva, P.G., Tsunami deposits as paleoseismic indicators: examples from the Spanish coast, *Acta Geologica Hispanica*, **36**, 197-211, 2001.

Mamo, B., Strotz, L. and Dominey-Howes, D., Tsunami sediments and their foraminiferal assemblages, *Earth-Science Reviews*, **96**, 263-278, 2009.

Marques, W.S., Sial, A.N., Menor, E.A., Ferreira, V.P., Freire, G.S.S., Lima, E.A.M. and Manso, V.A.V., Principal component analysis (PCA) and mineral associations of litoraneous facies of continental shelf carbonates from northeastern Brazil, *Continental Shelf Research*, **28**, 2709-2717, 2008.

Massari, F. and D'Alessandro, A., Tsunami-related scour-and-drape undulations in Middle Pliocene restricted-bay carbonate deposits (Salento, south Italy), *Sedimentary Geology*, **135**, 265-281, 2000.

McKee, B.A., Nittrouer, C.A. and DeMaster, D.J., The concepts of sediment deposition and accumulation applied to the continental shelf near the mouth of the Yangtze River, *Geology*, **11**, 631-633, 1983.

Nittrouer, C.A., Austin, J.A., Field, M.E., Kravitz, J.H., Syvitski, J.P.M. and Wiberg, P., In: *Continental margin sedimentation*, Edited by Nittrouer, C.A., Austin, J.A., Field, M.E., Kravitz, J.H., Syvitski, J.P.M. and Wiberg, P., 560 pp., International Association of Sedimentologists, Spec. Publ., 37, 2007.

Nittrouer, C.A., Sternberg, R.W., Carpenter, R. and Bennett, J.T., The use of Pb-210 geochronology as a sedimentological tool: application to the Washington continental shelf, *Marine Geology*, **31**, 297-316, 1979.

Noda, A., Katayama, H., Sagayama, T., Suga, K., Uchida, Y., Satake, K., Abe, K. and Okamura, Y., Evaluation of tsunami impacts on shallow marine sediments: An example from the tsunami caused by the 2003 Tokachi-oki earthquake, northern Japan, *Sedimentary Geology*, **200**, 314-327, 2007.

Ohta, T. and Arai, H., Statistical empirical index of chemical weathering in igneous rocks: A new tool for evaluating the

degree of weathering, *Chemical Geology*, **240**, 280-297, 2007.

Paris, R., Fournier, J., Poizot, E., Etienne, S., Mortin, J., Lavigne, F. and Wassmer, P., Boulder and fine sediment transport and deposition by the 2004 tsunami in Lhok Nga (western Banda Aceh, Sumatra, Indonesia): A coupled offshore-onshore model, *Marine Geology*, **268**, 43-54, 2010.

Reid, M.K. and Spencer, K.L., Use of principal components analysis (PCA) on estuarine sediment datasets: The effect of data pre-treatment, *Environmental Pollution*, 157, 2275-2281, 2009.

Reineck, H.E. and Wunderlich, F., Lamination and Laminated Rhythmites in Water-laid Sands, *Senckenbergiana maritima*, 28, 227-235, 1998.

Robbins, J.A. and Edgington, D.N., Determination of recent sedimentation rates in Lake Michigan using Pb-210 and Cs-137, *Geochimica et Cosmochimica Acta*, 39, 285-304, 1975.

Robbins, J.A., Edgington, D.N. and Kemp, A.L.W., Comparative ^{210}Pb, ^{137}Cs, and pollen geochronologies of sediments from Lakes Ontario and Erie, *Quaternary Research*, **10**, 256-278, 1978.

Sawai Y., Jankaew, K., Martin, M.E., Prendergast, A., Choowong, M. and Charoentitirat, T., Diatom assemblages in tsunami deposits associated with the 2004 Indian Ocean tsunami at Phra Thong Island, Thailand, *Marine Micropaleontology*, **73**, 70-79, 2009.

Scheffers, A. and Kelletat, D., Sedimentological and geomorphologic tsunami imprints worldwide- a review, *Earth-Science Reviews*, **63**, 83-92, 2003.

Shanmugam, G., Process-sedimentological challenges in distinguishing paleo-tsunami deposits, *Natural Hazards*, **doi:** 10.1007/s11069-011-9766-z, 2011.

Shiki, T.,Tsuji, Y., Yamazaki, T. and Minoura, K., In: *Tsunamiites - Features and Implications*, Edited by Shiki, T.,Tsuji, Y., Yamazaki, T. and Minoura, K., 425 pp., Elsevie, Amsterdam, 2008.

Smedile, A., De Martini, P.M., Pantosti, D., Bellucci, L., Del Carlo, P., Gasperini, L., Pirrotta, C., Polonia, A. and Boschi, E., Possible tsunami signatures from an integrated study in the Augusta Bay offshore (Eastern Sicily-Italy), *Marine Geology*, **281**, 1-13, 2011.

Sommerfield, C.K. and Nittrouer, C.A., Modern accumulation rates and sediment budget for the Eel shelf: a flood-dominated depositional environment, *Marine Geology*, **154**, 227-241, 1999.

Sugawara, D., Minoura, K., Nemoto, N., Tsukawaki, S., Goto, K. and Imamura, F., Foraminiferal evidence of submarine sediment transport and deposition by backwash during the 2004 Indian Ocean tsunami), *Island Arc*, **18**, 513-525, 2009.

Suppasri, A., Koshimura, S. and Imamura, F., Developing tsunami fragility curves based on satellite remote sensing and the numerical modeling of the 2004 Indian Ocean tsunami in Thailand, *Natural Hazards and Earth System Sciences*, **11**, 173-189, 2011.

Szczuciński, W., Impacts of 2004 Indian Ocean tsunami on mid continental shelf of Andaman Sea, In: *The 3rd International Tsunami Field Symposium*. Program and abstracts, Sendai, Japan, 10-11 April, 2010, 57-58 pp., 2010.

Szczuciński, W., Chaimanee, N., Niedzielski, P., Rachlewicz, G., Saisuttichai, D., Tepsuwan, T., Lorenc, S. and Siepak, J., Environmental and Geological Impacts of the 26 December 2004 Tsunami in Coastal Zone of Thailand – Overview of Short and Long-Term Effects, *Polish J. of Environmental Studies,* **15**, 793-810, 2006.

Szczuciński, W., Stattegger, K. and Scholten, J., Modern sediments and sediment accumulation rates on the narrow shelf off central Vietnam, South China Sea, *Geo-Marine Letters*, **29**, 47-59, 2009.

Takashimizu, Y. and Masuda, F., Depositional facies and sedimentary successions of earthquake-induced tsunami deposits in Upper Pleistocene incised valley fills, central Japan, *Sedimentary Geology*, **135**, 231-239, 2000.

Tjallingii, R., Stattegger, K., Wetzel, A. and Phach, P. V., Infilling and flooding of the Mekong River incised valley during deglacial sea-level rise, *Quaternary Science Reviews*, **29**, 1432-1444, 2010.

Tsuji, Y., Namegaya, Y., Matsumoto, H., Iwasaki, S.I., Kanbua, W., Sriwichai, M. and Meesuk, V., The 2004 Indian tsunami in Thailand: surveyed runup heights and tide gauge records, *Earth Planets and Space*, **58**, 223--232, 2006.

Uchida J.I., Fujiwara, O., Hasegawa, S. and Kamataki, T., Sources and depositional processes of tsunami deposits: Analysis using foraminiferal tests and hydrodynamic verification, *Island Arc*, **19**, 427-442, 2010.

Usiriprisan, C., Chiemchindaratana, S., Shoosuwan, S. and Chatrapakpong, Y., *Offshore exploration for tin and heavy minerals in the Andaman Sea*, 224 pp., Department of Mineral Resources, Bangkok and UNDP, New York, 1987.

van den Bergh, G. D., Boer, W., de Haas, H., van Weering, Tj. C. E. and van Wijhe, R., Shallow marine tsunami deposits in Teluk Banten (NW Java, Indonesia), generated by the 1883 Krakatau eruption, *Marine Geology*, **197**, 13-34, 2003.

Weber, M.E., Niessen, F., Kuhn, G. and Wiedicke, M., Calibration and application of marine sedimentary physical properties using a multi-sensor core logger, *Marine Geology*, **136**, 151-172, 1997.

Weidong, D., Baoguo, Y. and Xiaogen, W., Studies of storm deposits in China: a review, *Continental Shelf Research*, **17**, 1645-1658, 1997.

Weltji, G.J. and Tjallingii, R., Calibration of XRF core scanners for quantitative geochemical logging of sediment cores: Theory and application, *Earth Planet. Sci. Lett.*, **274**, 423-438, 2008.

Zaborska, A., Caroll, J., Papucci, C. and Pempowiak J., Intercomparison of alpha and gamma spectrometry techniques used in ^{210}Pb geochronology, *Journal of Environmental Radioactivity*, **93**, 38-50, 2007.

Nat. Hazards Earth Syst. Sci., 15, 1181–1199, 2015
www.nat-hazards-earth-syst-sci.net/15/1181/2015/
doi:10.5194/nhess-15-1181-2015

Natural Hazards and Earth System Sciences
Open Access

CHAPTER IV

INTERNAL STUCTURE OF EVENT LAYERS PRESERVED ON THE ANDAMAN SEA CONTINENTAL SHELF, THAILAND: TSUAMI VS. STORM AND FLASH-FLOOD DEPOSITS‡

D. Sakuna-Schwartz[1,*], P. Feldens[1], K. Schwarzer[1], S. Khokiattiwong[2], and K. Stattegger[1]

[1]Institute of Geosciences, Kiel University, Otto-Hahn-Platz 1, 24118 Kiel, Germany
[2]Oceanography Unit, Phuket Marine Biological Center, P.O. Box 60, Phuket 83000, Thailand
* now at: Oceanography Unit, Phuket Marine Biological Center, P.O. Box 60, Phuket 83000, Thailand

Correspondence to: D. Sakuna-Schwartz (daroonwans@gmail.com)

Received: 10 September 2014 – Published in Nat. Hazards Earth Syst. Sci. Discuss.: 1 December 2014
Accepted: 20 May 2015 – Published: 12 June 2015

Abstract

Tsunami, storm and flash-flood event layers, which have been deposited over the last century on the shelf offshore Khao Lak (Thailand, Andaman Sea), are identified in sediment cores based on sedimentary structures, grain size compositions, Ti/Ca ratios and ^{210}Pb activity. Individual offshore tsunami deposits are 12 cm to 30 cm in thickness and originate from the 2004 Indian Ocean Tsunami. They are characterized by 1) the appearance of sand layers enriched in shells and shell debris and 2) the appearance of mud and sand clasts. Storm deposits found in core depths between 5 and 82 cm could be attributed to recent storm events by using ^{210}Pb profiles in conjunction with historical data of typhoons and tropical storms. Massive sand layers enriched in shells and shell debris characterize storm deposits. The last classified type of event layer represents reworked flash-flood deposits, which are characterized by a fining-upward sequence of muddy sediment. The most distinct difference between storm and tsunami deposits is the lack of mud and sand clasts, mud content and terrigenous material within storm deposits. Terrigenous material transported offshore during the tsunami backwash is therefore an important indicator to distinguish between storm and tsunami deposits in offshore environments.

4.1 Introduction

Tsunami waves propagating into shallow waters as well as related backwash flows can erode, transport and deposit significant amounts of sediments in the inner-shelf environment (e.g., Paris et al., 2010; Goto et al., 2011), here defined as 0 m to 30 m water depth. The behavior of tsunami waves is controlled by the source earthquake or landslide and the ocean basin's morphology on a larger scale, and by the inner shelf and coastal bathymetry as well as the hydrological conditions on a local scale (Cheng and Weiss, 2013; Spiske et al., 2013; Goto et al., 2014). Coastal and inner-shelf bathymetry is the most important factor controlling backwash flow (Le Roux and Vargas, 2005; Paris et al., 2010; Feldens et al., 2012; Spiske et al., 2014).

The structure and texture of tsunami deposits in offshore areas mainly depend on the local sediment sources, the geomorphology of the seafloor, the tsunami wave height and the number of waves in the case of more than one wave hitting the shoreline during the run-up and backwash (Sakuna et al., 2012). Both the bathymetry and available sediments are highly variable in shallow marine environments (e.g., Dartnell and Gardner, 2004). A complex composition of offshore tsunami deposits is therefore expected, with potentially quick changes both in space and time (Shanmugam, 2011). A tsunami's impact in deeper waters may

‡Reprinted with permission of Copernicus Publications on behalf of the European Geosciences Union. The original article is published in Nat. Hazards Earth Syst. Sci., vol. 15, p. 1181-1199, 2015.

be preserved within sediments below the storm wave base (e.g., Weiss and Bahlburg, 2006; Weiss, 2008). However, while the tsunami's impact increases with decreasing water depth towards the coastline, only very few offshore tsunami deposits have been reported until now. Therefore, it is not surprising that the described offshore deposits of historical tsunami - not considering inferred tsunami paleorecords on geological timescales (Le Roux and Vargas, 2005; Fujiwara and Kamataki, 2007; Spiske et al., 2014) - are highly variable in thickness, texture and structure (e.g., van den Bergh et al., 2003; Abrantes et al., 2008; Goodman-Tchenov et al., 2009; Paris et al., 2010; Smedile et al., 2011; Sakuna et al. 2012; Milker et al., 2013). Reported offshore tsunami deposits range from centimeters to 1 m in thickness while spanning grain sizes from mud to boulders, including terrigenous and marine sediments over one or several layers. The depositions are composed of different fossil assemblages and different sedimentary structures (Sakuna et al., 2012). One reason for the scarcity of reported offshore tsunami deposits is their potentially low preservation in shallow waters due to reworking and transport by currents, waves (Weiss and Bahlburg, 2006), tides and gravity flows which disperse sediment and shape continental shelf settings. Reworking of event layers is intensified by bioturbation especially in areas with low accumulation rates, where deposits cannot quickly escape the surface mixing layer (Wheatcroft and Drake, 2003).

A further problem is the differentiation of tsunami layers from other event-related deposition and accumulation, with storms and flash floods arguably most important in inner-continental-shelf settings. The differentiation of tsunami deposits from tempestites has been widely discussed for deposits left on land (e.g., Nott, 2003; Goff et al., 2004; Kortekaas and Dawson, 2007; Morton et al., 2007; Switzer and Jones, 2008; Lario et al., 2010; Lorang, 2011; Richmond et al., 2011; Phantuwongraj and Choowong, 2012; Ramírez-Herrera et al., 2012; Brill et al., 2014a). However, there is no consensus yet on reliable sedimentological criteria to distinguish between offshore storm and tsunami deposits. Generally, shallow-water, proximal tempestites are characterized by basal erosional contacts and a sequence from normal gradation to cross-stratification to plane lamination, with frequently preserved ripples at the top (Einsele et al. 1991; Allison et al., 2005). Not all tempestites comprise all these features, and they may also be observed in offshore tsunami deposits (Sakuna et al. 2012). Flash floods can comprise a large percentage of a river's yearly discharge and can form hyperpycnal flows due to high suspension load (Mulder et al., 2003; Bourrin et al., 2008). These criteria have also been established for tsunami backwash flows (Le Roux and Vargas, 2005). In monsoon-dominated areas, flash-flood deposits occur frequently in front of river mouths or through ephemeral streams (Kale, 2003; Malmon et al., 2004). Their deposits have to be considered while identifying offshore backflow tsunami deposits. Flash-flood deposits are typically coarse-grained (Postma, 2001) or alternating sand and mud layers (Martin, 2000), but they also comprise stratified deposits of silty clay within mud belts (Cutter and Diaz, 2000; Hill et al., 2007).

The Andaman Sea (Thailand) is an area where tsunami, storm and flash-flood deposits can be studied. It was subjected to few strong storms over the last decades and is regularly impacted by the northeast and southwest monsoons, with the latter causing flash floods. It was strongly affected by the 2004 Indian Ocean Tsunami, and preserved event deposits are accessible closely beneath the surface of the seafloor due to low riverine sediment delivery. Based on a collection of six sediment cores, the objectives of this study are to a) identify, describe and discuss tsunami, storm and flash-flood deposits in sediment cores and b) to identify proxies that can be used to distinguish tsunami, storm and flash-flood deposits from each other.

4.2 Regional Setting

The investigation area near Pakarang Cape (hereafter PC) is located on the western side of the southern Thai-Malay Peninsula offshore Phang Nga province (Fig. 1). The Ayeyarwady-Salween river system is the main source supplying fine-grained sediment into the Andaman Sea (Rodolfo, 1969; Colin et al., 1999), which is highly seasonal with more than 80% of the annual discharging during the SW monsoon (Ramaswamy et al., 2004). The majority of the Andaman shelf is classified as sediment starved (Rodolfo, 1969; Panchang et al., 2008; Schwab et al., 2012). The coastline north and south of PC represents an embayed coast with sandy beaches

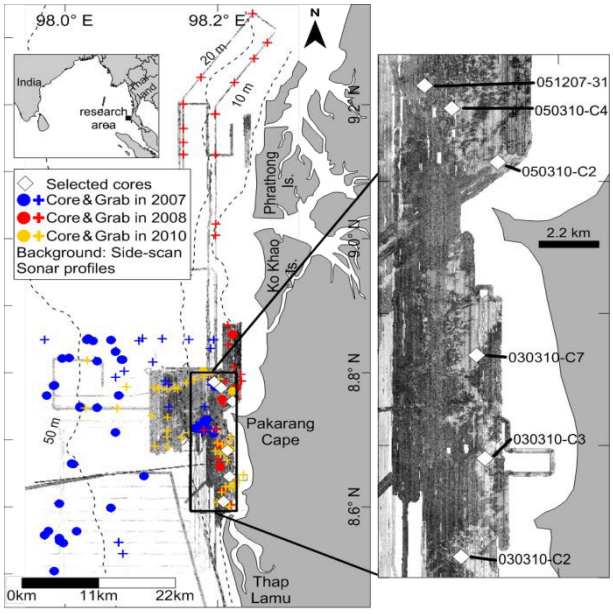

Fig. 1 Overview map of the investigation area including sampling stations. The bathymetric data are based on nautical charts. The sediment samples taken during the three year research period are ordered due to the 3 different cruises in difference colours.

commonly separated by rocky headlands. In general, the shelf gently dips offshore, reaching 60 m water depths within a distance of 30 km from the coastline. PC itself is surrounded by a 3 km long reef platform (Goto et al., 2007; Choowong et al., 2009; Di Geronimo et al., 2009). The tides in this area are mixed semidiurnal tides, with most days having two high tides and two low tides. The mean tidal range extends from 1.1 m during neap tide to 3.6 m during spring tide (Thampanya et al., 2006). Based on geomorphological evidence from sandy hooks and spits, northward-directed current-induced longshore sediment transport occurs in the study area (Choowong et al., 2009; Brill et al., 2014b). Maps of the nearshore bathymetry and sediment distribution have been created following the 2004 Indian Ocean Tsunami (e.g., Di Geronimo et al., 2009; Feldens et al., 2009, 2012), but these maps cover only a small percentage of the Andaman Sea Shelf. According to these studies, mud patches are widespread in water depths between 5 m and 15 m north and south of PC. Several granite outcrops are scattered along the inner shelf at water depths of 5-10 m and on the midshelf at a water depth of approximately 30 m. Extensive cassiterite mining both on- and offshore affected the area over the last century (Hylleberg et al., 1985; Usiriprisan et al., 1987). Offshore, visible remnants of the mining activities include up to 7 m deep holes at water depths of 20-25 m NW of PC (Feldens et al., 2009).

The climate of this region is influenced by the tropical monsoon, with the northeast monsoon lasting from December to February, causing dry weather conditions, and the southwest monsoon lasting from May to September, bringing strong westerly winds and heavy rainfall (Khokiattiwong et al., 1991). While no studies on flash floods have been published for the Andaman Coast, they are expected to occur during the southwest monsoon (Lim and Boochabun, 2012) and have been reported by the local population. Storms and typhoons commonly form in the South China Sea during the northeast monsoon but tend to lose their energy while crossing the Thai-Malay Peninsula (data compiled by TMD, 2012). In additional, cyclone tracks originating within the Bay of Bengal are predominantly directed towards the coast of India, Bangladesh and Myanmar (Singh et al., 2000, Brill et al., 2011). The Andaman Shelf is therefore seldom affected by severe storms and typhoons, and only nine strong storm events have been recorded within a 180-nautical-mile radius of Phuket between 1945 and 1996 (Table 1).

Table 1 History of nine tropical storms and typhoons that ap- proached within a 180-nautical-mile radius of Phuket during the 52-year period (1945–1996). Modified from the Typhoon Havens Handbook (Brand, 2009).

Storm	Date	Maximum wind speed at storm center (knot)
Harriet	26 Oct 1962	30
Lucy	1 Dec 1962	20
Gloria	21 Dec 1965	30
Sally	5 Dec 1972	40
Sarah	12 Nov 1973	25
Gay	4 Nov 1989	100
Forrest	15 Nov 1992	55
Manny	16 Dec 1993	20
Ernie	18 Nov 1996	22

The coastal area of the Andaman Sea was seriously affected by the 2004 Indian Ocean Tsunami (Chavanich et al., 2005; Siripong, 2006; Szczuciński et al., 2006; Choowong et al., 2007; Goto et al., 2007; Umitsu et al., 2007). Since then, several studies (Di Geronimo et al., 2009; Sugawara et al., 2009; Feldens et al., 2009, 2012) have focused on the tsunami's impact on the shelf area offshore Khao Lak. Only little influence and

Table 2 List of the analysed sediment cores.

Core No.	Sampling year	Latitude (N)	Longitude (E)	Water Depth (m)	Core recovery (cm)	Distance offshore (km)
051207-31	2007	08°47.176'	98°11.724'	15.9	70	7.2
030310-C2	2010	08°36.474'	98°12.454'	11.5	23	3.3
030310-C3	2010	08°38.708'	98°12.931'	9.5	97	3.2
030310-C7	2010	08°41.053'	98°12.763'	11.9	65	2.9
050310-C2	2010	08°45.438'	98°13.186'	9.8	75	4.1
050310-C4	2010	08°46.659'	98°12.269'	15.3	55	6.3

few deposits related to the 2004 tsunami could be found 3 to 5 years later offshore between 5 and 70 m water depths (Di Geronimo et al., 2009; Sugawara et al., 2009; Feldens et al., 2012; Sakuna et al., 2012; Milker et al., 2013). Due to the reworking of shelf sediments (Sakuna et al., 2012) and the re-establishment of the coastline (Choowong et al., 2009; Grzelak et al., 2009) following the tsunami, the remaining offshore tsunami deposits have been chiefly found in locally sheltered positions adjacent to granitic outcrops, within an incised channel system and in areas of locally higher sediment accumulation rates (Feldens et al., 2012; Sakuna et al., 2012; Milker et al., 2013).

4.3 Methods

During three research cruises in December 2007, December 2008 and February-March 2010, side-scan sonar data were obtained using a Klein 595 side-scan sonar (384 kHz) and a Benthos 1624 side-scan sonar (100 kHz and 400 kHz). The instruments were towed behind the vessel with approximately 10 m to 50 m offset from the GPS antenna. This offset was accounted for by a constant value for each profile when calculating the position of the tow fish. Side-scan sonar data were recorded in digital format, employing the Isis software package Triton Elics Int. The data were processed and geo-referenced using the same software to create side-scan sonar mosaics of the study area. In this study, areas of higher backscatter are displayed with darker colors.

A total of 60 gravity cores using a Rumohr-type gravity corer (8 cm diameter) were collected (see Fig. 1) based on the on-site interpretation of the side-scan sonar images and previous shallow seismic mapping (Feldens et al. 2009, Feldens et al. 2012). Gravity cores could be retrieved only from fine-grained (silt and finer) seafloor sediments, as the corer could not penetrate into the seafloor composed of sand. In all the cores, the sediment water interface was preserved. The split sediment cores were first photographed and analyzed at a 1 cm interval in the laboratory according to the following scheme. A multi-sensor core logger (MSCL) was used to obtain data about physical sediment properties (Weber et al., 1997; Best and Gunn, 1999; Hofmann et al., 2005). Chemical element composition to differentiate between terrigenous versus marine constituents (Lamy et al., 2001; Bahr et al., 2005; Ohta and Arai, 2007; Tjallingi et al., 2010) was determined by an X-ray fluorescence (XRF) core scanner. The sediment slabs were radiographed to detect internal sedimentary structures and unconformities.

Six cores are presented in this study (Fig. 1, Table 2). For the selected cores, grain size composition was determined every 1 cm with a laser-based particle sizer device with a measuring range of 0.04 to 2000 µm. Therefore, grains larger than 2000 µm were separated prior to the measurements. The statistical parameters of the grain size distributions were calculated in phi (Φ) units with $\Phi = -\log_2 d$ (d being the grain size in mm; Krumbein, 1938), using the logarithmic method of moments available with the GRADISTAT software (Blott and Pye, 2001). Measurements of ^{210}Pb activity were done for two sediment cores (030310-C3 and 050310-C4) to assess sediment accumulation rates. The sediment samples were dried, ground and analyzed using gamma spectrometry at the Leibniz Laboratory for Radiometric Dating and Isotope Research, Kiel, Germany. As the ^{137}Cs activity was mostly below the detection limits it could not serve as an independent tracer. The sediment accumulation rate (SAR) was estimated from the decline in the excess ^{210}Pb activity following the equations used by Robins and Edington (1975) and McKee et al. (1983).

$$SAR = \lambda \times z \times \left[\ln(A_0 / A_z)\right]^{-1},$$

Where λ is the decay constant (= 0.0311 year^{-1}); z is the depth in the core (cm); A_0 is the specific activity of excess ^{210}Pb at a particular reference horizon (Bq kg^{-1}); and A_z is the specific activity of excess ^{210}Pb at depth z below the reference horizon (Bq kg^{-1}).

4.4 Results

4.4.1 Subsurface sediment sequence

The description of the sediment sequence in the cores is based on structure and texture analyses of photos and X-radiographic images. The depth values in the following section refer to core depths. Core positions are indicated in Fig. 1 and an overview of all the available core details is given in Fig. 2, while the side-scan sonar data showing the sediment distribution from the areas where the cores have been taken are shown in Fig. 3. The sedimentary features and the interpretation of all the studied cores are summarized in Table 3 and Fig. 5.

Core 030310-C3 (Fig. 2)

Core 030310-C3 (97 cm in length) was collected 3.2 km offshore at a water depth of 9.5 m, ca. 100 m west of a granitic outcrop (Fig. 3a). In the vicinity of the coring position, the backscatter in the side-scan sonar is low, representing silt and fine sand, proven by grab samples and grain size analyses.

The lowermost 2 cm of the core is composed of massive fine-grained sediment. At 95 cm, an erosional contact with laminated sediments above exists. These laminated sediments extend up to 82 cm (facies D, Table 3a-VI). The laminations are slightly inclined, and the sediment is fining upward. Traces of bioturbation are not observed. Above a wavy and erosional contact at 82 cm, a massive sand layer including few shells extends up to 79 cm (facies C, Table 3a-V). The upper boundary of this sand layer is sharp. Above, fining-upward laminated mud extends from 79 cm to 70 cm (facies D). No traces of bioturbation are observed here either. Notably, a large sand clast can be observed from 77 cm to 73 cm in this core section. Laminations bend around the base of this clast and onlap at both sides. At 70 cm, a sharp contact separates the laminated mud from a massive sand layer that extends up to 67 cm (facies C, Table 3a-IV). While half of its upper boundary appears transitional, this is likely related to disturbance (smearing) during the sampling procedure. Above 67 cm, laminated sediment prevails up to 56 cm (facies D). Interbedded sand layers at 66 cm, from 63 to 62 cm and from 61 to 60 cm show preserved wavy structures, each forming a sharp upper contact. An erosive unconformity separates a 9 cm thick laminated sand layer at 56 cm in which shells or bioturbation traces do not appear. The lower 4 cm of this sand layer appears massive (facies C, Table 3a-III). Above, laminated sediment is present from 47 cm to 36 cm (facies D), where it is terminated by an erosional boundary. In this interval, massive sand layers are interbedded from 43 to 42 cm with sharp upper and lower contacts, and from 39 to 38.5 cm layer with an irregularly sharp lower contact and a transitional upper contact are observed. Mud clasts have been found between 35 cm and 31 cm (facies B, Table 3a-II), with the diameter increasing in the upper layer. Above a transitional boundary, a sand layer rich in shell debris is present between 31 cm and 29 cm (facies A, Table 3a-II). No bioturbation traces are observed within this layer. Above a sharp contact at 29 cm, laminated mud is deposited up to 26 cm (facies B, Table 3a-I). Here, a sand layer 2 cm in thickness is observed above an erosional contact (facies A, Table 3a-I). Its upper sharp contact at 24 cm is ripple-shaped. Above the contact at 24 cm, laminated material extends up to ca. 6 cm (facies E). Single bioturbation traces are observed between 17 cm and 16 cm core depth. In this interval, no lamination is recognized. Apparently, the deformed features in the upper 13 cm of the core are related to disturbances during coring. A highly irregular boundary from ca. 8 cm to 6 cm separates the laminated material from more homogeneous sediment that includes few coarser sand grains. Above a sharp boundary at 1 cm, homogeneous fine-grained material is observed.

Core 030310-C2 (Fig. 2)

Core 030310-C2, with a length of 23 cm, was retrieved from a silty seafloor at 11.5 m water depth, 3.3 km offshore the navigational entrance to Thap Lamu harbor (Fig. 1). Due to strong fishing activities with fixed nets, no side scan-sonar surveys could be carried out here.

From the base of this core to 17 cm, bioturbated fine sand is observed. Few shells are scattered throughout the layer which is assigned to facies E.

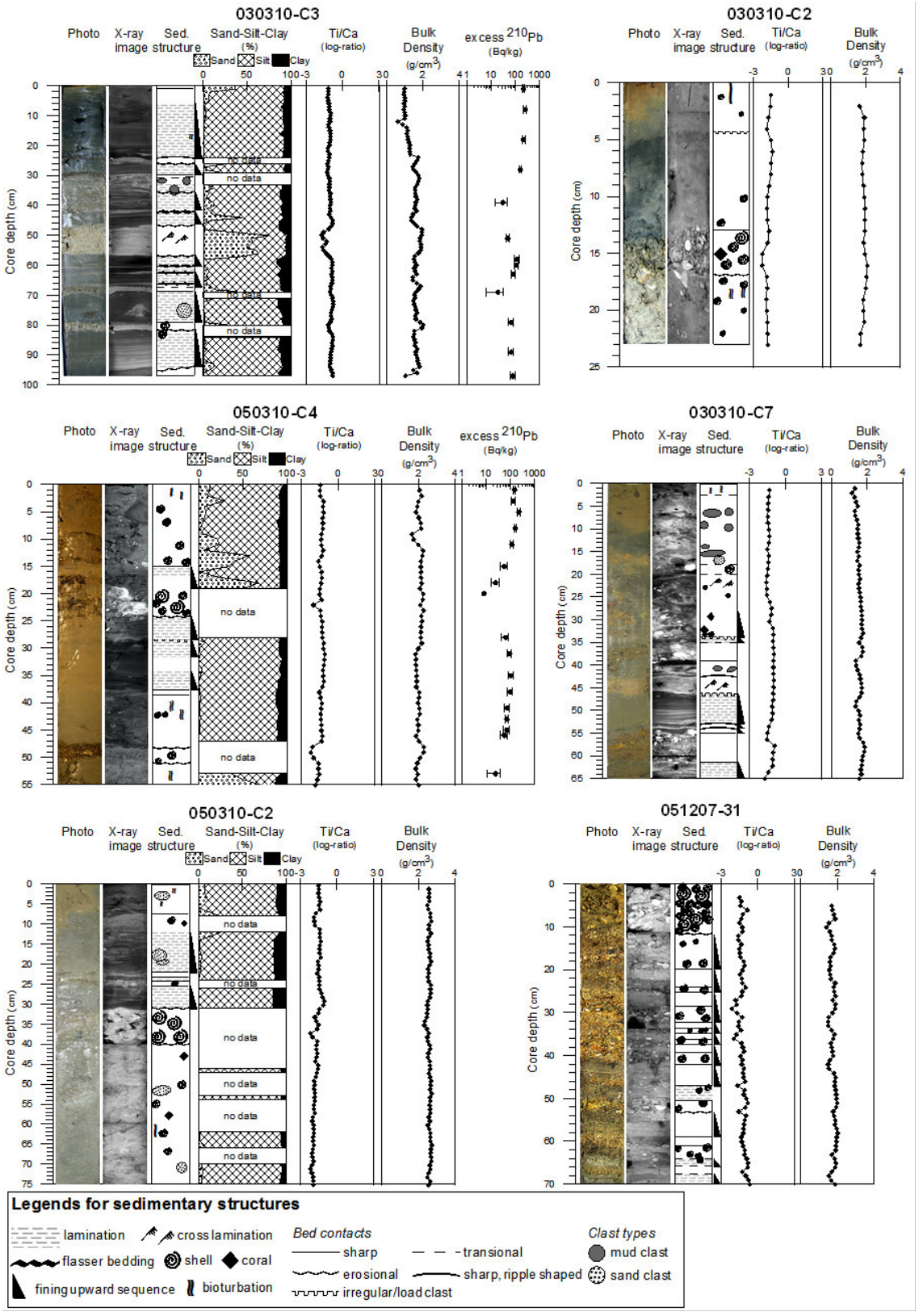

Fig. 2 Interpretation of the sediment cores.

A 4 cm thick layer composed of coarse sand and gravel including shells, laterite fragments and coral debris, which are all typical indicators for facies A is separated from the fine sand layer below (facies A, Table 3b-II). Above an erosional boundary at 13 cm, an 8.5 cm thick layer of muddy fine sand including few shell fragments is observed (facies B, Table 3b-I). A sharp boundary with an irregular shape - interpreted as a load clast - appears at 4.5 cm. At the top of the core, homogeneous silt to fine sand with frequent traces of bioturbation is present (facies E).

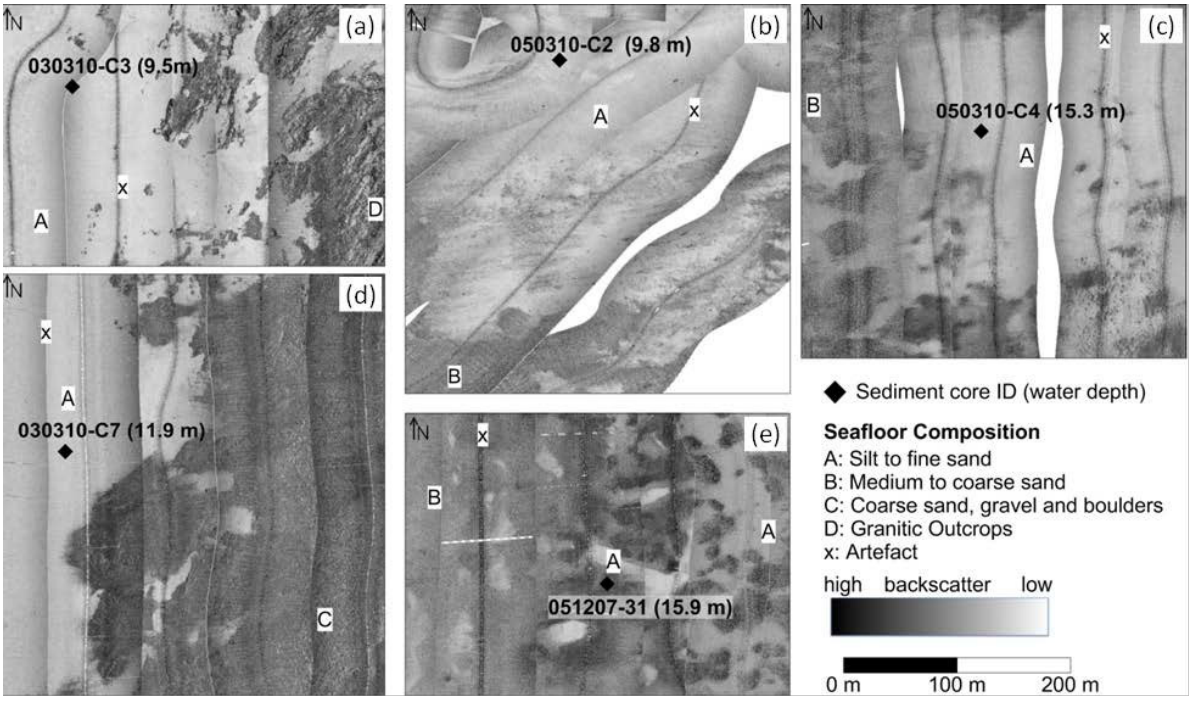

Fig. 3 Cut outs of the side scan sonar mosaic showing the sediment distribution at the coring positions. No data are available for core 030310-C2. The composition of the seafloor was established based on the ground truthing of the backscatter data with grab samples and underwater video images (Feldens et al., 2012).

Core 050310-C4 (Fig. 2)

Core 050310-C4, with a length of 55 cm, was retrieved 6.3 km offshore at a water depth of 15.3 m. The position is located within a patch of silt to fine sand that is surrounded by patches of medium to coarse sand (see Fig. 3c).

The lowermost part of the core (55 - 51.5 cm) consists of silty to sandy sediment with traces of bioturbation included. At 51.5 cm, a layer of coarse sand, 3 cm in thickness, is separated from the sediment above and beneath by sharp erosional contacts. The layer appears massive and small shells are observed (facies C, Table 3c-IV). A layer composed of silty sediment is deposited above 48.5 cm. This layer is characterized by the occurrence of few shells and frequent bioturbation traces (facies E). At 37.5 cm, a sharp contact separates a 3 cm thick layer of laminated fine-grained sediment (facies C, Table 3c-III). The single laminae could not be sampled individually due to their small thickness of 1 mm to 5 mm. Above, a 6 cm thick layer of fine sediment is separated by upper and lower sharp contacts, the latter with ripple shapes (facies D). Few shells are present in the layer as well. At 28.5 cm, a sharp but irregular contact - interpreted as load cast - separates coarse sediment (facies B, Table 3C-II). At 24 cm, an erosional contact separates a 7 cm thick admixture layer of sand, gravel, laterites and shells (facies A, Table 3c-II). Laminated sediment is found again from 17 cm to 15 cm. Following a sharp boundary, coarse sediment including minor components of shells is deposited above 15 cm (facies B, Table 3c-I). Due to disturbances during sampling in the field, the upper boundary of the layer is not clearly visible. However, based on the abundance of shells, it is likely situated at ca. 2 cm. The upper 2 cm of the core comprises fine-grained sediment with few bioturbation traces (facies E).

Core 030310-C7 (Fig. 2)

Core 030310-C7, with a length of 65 cm, was retrieved from a water depth of 11.9 m, 2.9 km offshore (ca. 4.9 km south of PC), in an area where the seafloor is composed of silty to fine sediment. The boundary between silt- and fine-sand-covered seafloor and coarse sand, gravel and boulders is situated ca. 70 m to the southeast. Granitic outcrops appear ca. 500 m to the east (see Fig. 3d).

Table 3 Characteristics of the sedimentary deposit in shallow water and their event interpretation.

Core No.	Photo	X-ray image	Section depth (cm)	Type of sedimentary contact	Sediment description	Identified event
030310-C3 (a-I) 5 cm		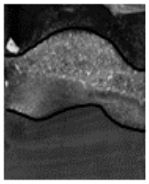	23-28	upper: sharp lower: erosional	Top: a 2 cm thick layer of shell debris sand Bottom: laminated mud	Tsunami (2004) Top: facies A Bottom: facies B
(a-II) 10 cm		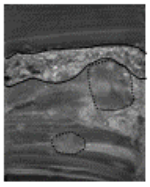	27-37	upper: sharp lower: erosional	Top: a 2 cm thick layer of shell debris sand Bottom: laminated mud with mud clasts	Tsunami (2004) Top: facies A Bottom: facies B
(a-III) 10 cm		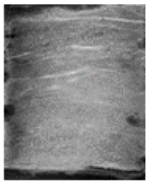	47-57	upper: erosional lower: erosional	Massive sand layer with clear cross lamination that is observed in the upper five centimetres	Storm
(a-IV) 5 cm		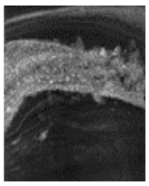	66-71	upper: transitional (due to smearing) lower: sharp	Massive sand layer	Storm
(a-V) 5 cm		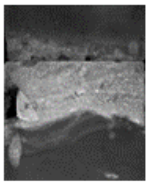	78-83	upper: sharp lower: erosional	Massive sand layer including few shells	Storm
(a-VI) 10 cm		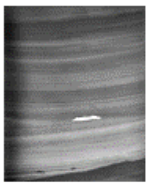	85-95	lower: erosional	Fining upward sequence laminated mud with no bioturbation	Flash flood (monsoon)
030310-C2 (b-I) 10 cm		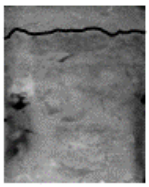	3-13	upper: sharp	Homogenous fine sand	Tsunami facies B (2004)

At the base of the core, laminated material is fining upward from 65 cm to 61 cm. At 61 cm, a sharp contact with a 6 cm thick layer composed of coarse sand and occasional gravel exists (facies C, Table 3d-VI). This layer is not massive and no clear fining-upward or -downward trend can be recognized. The layer is draped by a centimetre-thick unit of muddy material on its top. Cross-laminations of coarser sediment are identified from light scattering in X-ray images at 54 cm and 53 cm (facies D, Table 3d-V). A sharp contact has been found at 53 cm that separates a 6 cm thick fining-upward sequence of laminated fine-grained material, which shows no sign of bioturbation traces (facies D, Table 3d-V). At 47 cm, an irregular sharp contact separates the laminated sediment from a layer of sand, in which faint indications of

Table 3 (continue).

Core No.	Photo	X-ray image	Section depth (cm)	Type of sedimentary contact	Sediment description	Identified event
030310-C2 (cont.) (b-II)		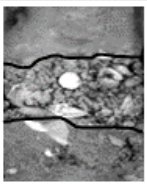	10-20	upper: erosional lower: erosional	A 4 cm thick layer of shell fragments with admixture of gravels, laterites, corals and sand	Tsunami facies A (2004)
050310-C4 (c-I)	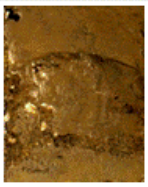		6-16	upper: sharp lower: erosional	Massive sandy mud with shell fragments scatter through the layer and laminated mud	Tsunami facies B (2004)
(c-II)		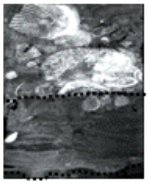	19-29	upper: erosional lower: sharp	Top: Shell deposit in admixture of gravels, laterites and mud Bottom: coarse sediment	Tsunami (2004) Top: facies A Bottom: facies B
(c-III)			33-38	upper: sharp lower: sharp	Laminated fine grain sediment	Flash flood (monsoon)
(c-IV)	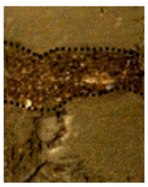	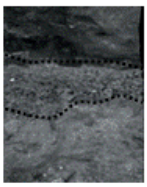	47-52	upper: erosional lower: sharp	Massive coarse sand layer	Storm
030310-C7 (d-I)		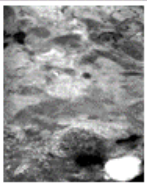	9-19	upper: transitional (due to bioturbation) lower: transitional	Massive sediment that contains sandy and mud clasts scatter throughout the layer	Tsunami facies B (2004)
(d-II)		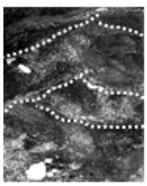	20-30	upper: transitional lower: transitional	Mud, sand and gravel partly cross laminated with generally fining upward grain size	Tsunami facies A (2004)

cross-laminations are observed (facies C, Table 3d-IV). At the top of the sand layer at 42.5 cm, ripple structures draped by a 0.5 cm thick layer of mud are preserved. Between 42 cm and 39 cm, a mixture of sand and mud clasts prevails (facies B, Table 3d-III). Above a sharp contact at 39 cm, a 4 cm thick layer comprising coarse sand and pebbles exists (facies A). A transitional contact at 35 cm separates sand layer from a 1 cm thick layer of slightly laminated silty fine sediment (facies B, Table 3d-III). A fining-upward sequence of coarse sand, partly pebble-size corals and pebbles exists from 34 cm to 28 cm (facies A, Table 3d-II). Above 28 cm, an 8 cm thick sequence of cross-laminated bedforms is observed with several corals and shells scattered throughout (facies A, Table 3d-II).

Table 3 (continue).

Core No.	Photo	X-ray image	Section depth (cm)	Type of sedimentary contact	Sediment description	Identified event
030310-C2 (cont.) (b-II) 10 cm		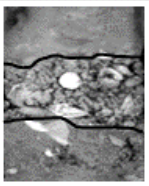	10-20	upper: erosional lower: erosional	A 4 cm thick layer of shell fragments with admixture of gravels, laterites, corals and sand	Tsunami facies A (2004)
050310-C4 (c-I) 10 cm	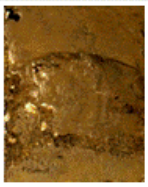		6-16	upper: sharp lower: erosional	Massive sandy mud with shell fragments scatter through the layer and laminated mud	Tsunami facies B (2004)
(c-II) 10 cm		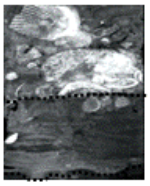	19-29	upper: erosional lower: sharp	Top: Shell deposit in admixture of gravels, laterites and mud Bottom: coarse sediment	Tsunami (2004) Top: facies A Bottom: facies B
(c-III) 5 cm			33-38	upper: sharp lower: sharp	Laminated fine grain sediment	Storm
(c-IV) 10 cm	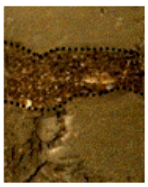	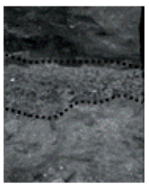	47-52	upper: erosional lower: sharp	Massive coarse sand layer	Storm
030310-C7 (d-I) 10 cm		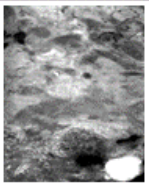	9-19	upper: transitional (due to bioturbation) lower: transitional	Massive sediment that contains sandy and mud clasts scatter throughout the layer	Tsunami facies B (2004)
(d-II) 10 cm		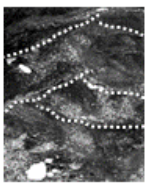	20-30	upper: transitional lower: transitional	Mud, sand and gravel partly cross laminated with generally fining upward grain size	Tsunami facies A (2004)

Up to 19 cm, the layer is covered by sand. Above 19 cm, a layer of mixed clasts composed of sand and mud exists, with few shells scattered throughout (facies B, Table 3d-I). Few bioturbation traces are observed at the top 3 cm of the layer (facies E).

Core 051207-31 (Fig. 2)

Core 051207-31, with a length of 70 cm, was retrieved 7.2 km offshore at a water depth of 15.9 m at a boundary of patches that are composed of silt to fine sand and partly coarse sand (Fig. 3e). From sub-bottom profiler data it is known that this position is located in a partly filled incised channel system (Feldens et al., 2012).

Table 3 (continue).

Core No.	Photo	X-ray image	Section depth (cm)	Type of sedimentary contact	Sediment description	Identified event
051207-31 (cont.) (e-IV) 5 cm			57-62	upper: sharp lower: erosional	Massive coarse sand	Storm
(e-V) 5 cm		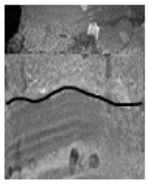	65-70	upper: transitional	Laminated fine-grained material	Flash flood (monsoon)
050310-C2 (f-I) 5 cm		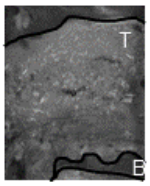	7-12	upper: sharp lower: disturbed during sampling	Top: sand layer with corals and shell fragments Bottom: mud layer (left part was disturbed during sampling)	Tsunami (2004) Top: facies A Bottom: facies B
(f-II) 10 cm		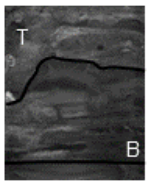	11-21	upper: sharp lower: disturbed during the slab preparation	Top: silty to fine sand with shell fragments Bottom: laminated mud with sand clasts	Tsunami (2004) Top: facies A Bottom: facies B
(f-III) 10 cm		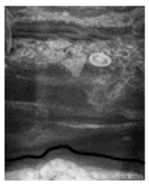	22-32	lower: erosional	Sequence deposition of sand and fine grain layer	Flash flood (monsoon)
(f-IV) 10 cm	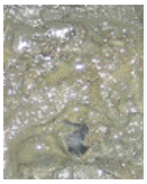		30-40	upper: erosional lower: erosional	Shell deposit in sandy maxtrix	Storm

At the core base, laminated fine-grained material exists from 70 cm to 68 cm (facies D, Table 3e-V). A transitional boundary separates a 2 cm thick layer of massive coarse grains extending from 68 cm to 66 cm. With transitional lower and upper boundaries, the sediment, mainly composed of muddy sand with few shells incorporated, is fining upwards between 66 cm and 64 cm. Sediment changes into a 2.5 cm thick layer of massive coarse sand at approximately 61 cm (facies C, Table 3e-IV). Above 58.5 cm, the sediment is gradually fining upward. At 53 cm, an erosive contact separates the fining-upward sequence from a 3 cm thick layer comprising pebbles, coarse sand and shell fragments (facies C, Table 3e-III). Laminated material is present above, up to 47 cm. Few shells are located within this layer. Following a sharp contact at 47 cm, a coarse, fining-upward sequence is present, capped by a sharp boundary at 45 cm (facies C, Table 3e-II). Fining-upward sequences with a sharp boundary composed of pebbles, coarse sand and shell fragments exist within 41-38 cm, 38-34.5 cm, 34.5-32 cm, 32-25 cm, 25-20 cm, 20-15.5 cm and 15.5-11.5 cm. All these units are assigned to facies E. At 11.5 cm, an erosional contact separates a fining-upward sequence from a layer of shells that forms the upper part of this core (facies A, Table 3e-I).

Core 050310-C2 (Fig. 2)

Core 050310-C2, with a length of 75 cm, was collected at a water depth of 9.8 m, located 1.5 km northeast of PC. The seafloor at the sampling position is composed of silt to fine sand (Fig. 3b).

The lower part of the core from 75 cm to 40 cm comprises a silty matrix with few corals and abundant shells scattered throughout. A bioturbation trace is found from 63 cm to 60 cm. The whole unit belongs to facies E. Above an erosional contact at 40 cm, a 9 cm thick layer, mainly composed of large shells in a sandy matrix, is observed (facies C, Table 3f-IV). Above an erosional boundary at 31 cm, laminated mud is observed. Between a sharp upper and lower contact, a sand layer in which shells are present extending from 25 cm to 24 cm. The sand layer is draped by a 1 cm thick layer of fine-grained, laminated sediment. A similar sequence is observed above: a 1 cm thick layer of sand (23 cm to 22 cm) with a sharp upper and lower boundary is draped by laminated muddy material that reaches up to ~20 cm (facies D, Table 3f-III). The depth of the upper boundary is an approximation, because the sediment was disturbed during the slab preparation. From 20 cm to 14 cm, several centimeter-thick clasts composed of sandy material disrupt the laminations (facies B, Table 3f-II). Above a sharp contact at 14 cm, a 2 cm thick sequence of likely silty to fine sand material including shell fragments exists (facies A, Table 3f-II). At 12 cm, a 0.5 cm thick homogenous mud layer is draped on the layer beneath (facies B, Table 3f-I). However, it is difficult to determine whether this layer extends along the whole core width, as the left part of the core was disturbed during sampling. Above, a coarser sand layer with a sharp upper contact is deposited from 11.5 cm to 7.5 cm, which includes pieces of corals and shell fragments (facies A, Table 3f-I). The top of the core (above 7.5 cm core depth) was partly disturbed during sampling, but it apparently consists of bioturbated but otherwise homogeneous fine-grained material, with the exception of few sandy clasts with a diameter of 1-5 mm (facies E).

Summary of core description

While the cores appear highly diverse, in general, five different facies are recognized within the presented cores, which are termed facies A to E. In several cores, several centimeter thick layers comprised of shells and shell debris with variable fraction of coarse sand and gravel exist. These are assigned to tsunami deposits, named facies A. Poorly sorted sediment units comprising mud to sand and including mud and sand clasts are found, assigned as well to tsunami deposits, facies B.

Sand layers that are partly massive and partly show slight lamination occur. Shells are scattered throughout the sand layers. At the top, rippled shapes draped with mud are partly preserved. These structures are related to storm deposits, named facies C.

Most frequently occurring are layers composed of mainly clayey silt with few sand layers, which are commonly laminated and generally fining upward with transitional boundaries (individual laminae could not be sampled). Bioturbation is rarely observed in this facies, named facies D, representing partly reworked flash-flood deposits.

All other layers, which could not be assigned to event deposits, are regular shelf deposits, assigned to facies E. Depending on their location, these layers are composed of sandy to muddy sediment, containing fragments of corals and shells, and show bioturbation. Transitional and sharp contacts to layers above and below are common.

4.4.2 Ti/Ca ratios and ^{210}Pb activity

The Ti/Ca log ratios displayed in Fig. 2 in all six cores are stable (Ti/Ca log ratios are about -1.6 to -1.1) throughout finer sediments (facies B and D), while coarse sediment layers (Facies A, C, E) show Ti/Ca log ratios varying between -2.8 and -0.1.

The excess ^{210}Pb activity profiles measured in core 030310-C3 and 050310-C4 (Fig. 4) reveal a decline of activity downcore with several anomalies, the latter being interpreted as event layers. Given an unsteady sedimentation, the presence of event layers and the lack of an independent age control, which is required for ^{210}Pb dating (Smith, 2001), absolute dates cannot be given for particular core sections. However, the presence of excess ^{210}Pb confirms – assuming supported ^{210}Pb similar to values measured in coarse-grained event layers – that the sampled sediments have been deposited over the last century. Precise calculation of sediment

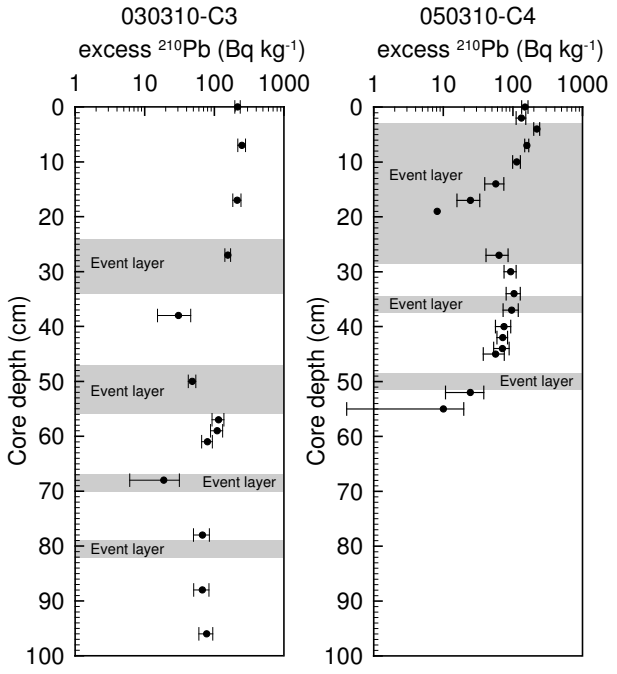

Fig. 4 Excess ^{210}Pb activity profiles with 2σ uncertainty ranges observed in the shallow water cores 030310-C3 and 050310-C4.

accumulation rates are not possible as the accumulation is not steady, based on the interpretation of X-Ray images, and uniform conditions were not encountered in the lowermost part of the core; the given values only represent rough estimations. However, some important indications may be drawn from the measured ^{210}Pb activity profiles. The estimated average accumulation rate for the upper 27 cm of core 030310-C3 (Fig. 4) is about 2.6 cm y^{-1} when considering a mixing surface layer of ~7 cm and using the surficial sediment for reference activity. The upper segment (0-28 cm) of the activity profile of core 050310-C4 (Fig. 4) shows a general decrease in the excess ^{210}Pb activity, which correlates with an increase in sand content. Using the surficial sediment for reference activity, an accumulation rate of 0.5 cm y^{-1} may be assumed for the uppermost centimeters of the sediment above the first event layer. Below 37 cm, the profile approaches supported ^{210}Pb activity as observed in the coarse-grained event layers.

4.5 Discussion

4.5.1 Identification of event deposits

The analyzed core data allow differentiating between three types of event deposits which are related to (1) flash floods, (2) storms and typhoons and (3) the 2004 Indian Ocean Tsunami.

The majority of the laminated fine-grained sediments of facies D (Fig. 2, 5 and Table 3) are interpreted as reworked flash-flood deposits which have not been described from the Andaman Sea yet. In general, the most important source from which fine sediment is supplied to accumulate on continental shelves is river discharge (Kuehl et al., 1985; Wright and Nittrouer, 1995; Geyer et al., 2004; Crokett and Nittrouer, 2004; Palinkas et al., 2006), which is minor in the investigation area (Jankaew et al., 2008; Feldens et al., 2009; Brill et al., 2011). However, anthropogenic activities that have been increasing during the last century such as tin mining on and offshore, construction of tourist resorts, deforestation, agriculture and urbanization all cause river discharge due to increased exposure to weathering and erosion of fine-grained sediment (Wolanski and Spagnol, 2000). In the course of flash floods during the southwest monsoon (rainy season), these fine sediments are subsequently transported through ephemeral channels towards the sea (e.g., Curran et al., 2002; Mulder et al., 2003; Malmon et al., 2004; Owen, 2005; Hill et al., 2007). Enhanced sedimentation due to anthropogenic impacts has been observed in different settings such as tropical estuaries in Papua New Guinea, Vietnam, Australia and Indonesia (Wolanski and Spagnol, 2000); the Pearl River in Hong Kong (Owen and Lee, 2004; Owen, 2005); and the Waiapu River in New Zealand (Wadman and McNinch, 2008). Offshore Khao Lak, Feldens et al. (2012) found sediment distributions composed of silt and fine sand deposited above 15 m water depth that were orientated parallel to the shoreline. These fine sediments offshore Khao Lak, which show little cohesiveness due to a high percentage of coarse silt and fine sand, were deposited during a multitude of small-scale events (Table 3a-V, 3c-IV, 3d-V and 3e-VI and Fig. 5). In the X-ray images, they are recognized as laminated sections of mud, silt and fine sand. Regular reworking and re-deposition from suspension are indicated by the frequent occurrence of fining-upward sequences, showing a distinct absence of bioturbation. This indicates episodically high accumulation rates (Wheatcroft and Drake, 2003), supported by the tsunami layers buried to depths >20 cm in some cores (this study; Sakuna et al., 2012). Notable is the

frequent occurrence of thin sand layers less than 1 cm in thickness with sharp upper and lower boundaries within the laminated core sections in core 051207-31. Based on side-scan sonar images, this core is situated close to a boundary of fine and coarse sediment (Fig. 3), which explains the transport of sand into areas covered by finer sediment in the range of annual cycles without exceptional storm events, as demonstrated by repeated side-scan sonar mapping offshore Khao Lak (Feldens et al., 2012).

In the sedimentary record, ideal proximal tempestites comprise an erosional lower contact, a graded or massive lower section, cross-stratification and plane laminations, and they frequently have ripple structures at their top (e.g., Einsele et al., 1991; Krassay, 1994; Weidong et al., 1997; Allison, 2005). Layers showing parts of these characteristics comprise facies C and are frequently observed in the X-ray images (Table 3a-II, 3a-III, 3a-IV, 3c-IV, 3d-IV, 3d-VII and 3e-III and Fig. 5), including sharp and partly erosional lower contacts, preserved cross-laminations, ripples and graded-bedded sand without mud content. Based on measurable ^{210}Pb activity throughout the core, several proposed event deposits in the cores 030310-C3 and 050310-C4 are less than 100 years old but are older than the 2004 Indian Ocean Tsunami, even when accounting for intermittent sedimentation. During the 52-year period from 1945 to 1996, only nine tropical storms passed through the investigation area (Brand, 2009; see Table 1). Therefore, it is very likely that these storms are responsible for the deposition of facies C. It should be noted that more storms than event layers occurred during the period documented, although the lower parts of the sediment cores may be expected to reach back to 1945 based on measurable excess ^{210}Pb activities of fine-grained sediment in the lower core sections (Fig. 4). This can be explained either by storms not leaving traces at the coring sites or, considering low accumulation between individual storm events, by the erosion and reworking of older event deposits.

Several event layers attributed to facies A and B in the uppermost part of the cores (Table 4 and Fig. 5) show different characteristics from the event layers beneath, which are attributed to storm events. They display a larger variability, ranging from 10 cm thick shell deposits to mud

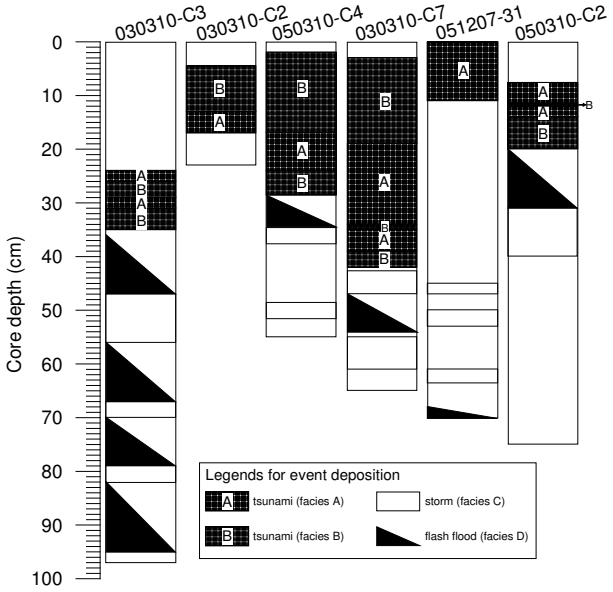

Fig. 5 Event sequence log diagram for sediment cores taken in shallow water (<15 m water depth).

deposits including coarse sand grains, laterites and shell debris as well as clasts of various compositions. The different depth beneath the seafloor of these events layers may be due to expected small-scale changes in sediment accumulation rates (also indicated by excess ^{210}Pb) across the shelf. Based on the accumulation rates estimated for core 030310-C3 and 050310-C4, the age of these deposits is 9 and 4 years, respectively. Despite the large uncertainties in ^{210}Pb dating at this location, the absence of large storms between the tsunami and our sampling in 2010 and the partly different sedimentary characteristics observed in X-ray images suggest that the uppermost event layer in these cores is the result of the 2004 Indian Ocean Tsunami.

4.5.2 Identification and features of the tsunami facies

Event deposits attributed to the 2004 Indian Ocean Tsunami based on ^{210}Pb dating are grouped into facies A and B (Table 4 and Fig. 5) representing the variable characteristics of offshore tsunami deposits.

Except in core 030310-C3, the inferred tsunami deposit sequences show sand enriched with shells or shell debris (facies A) at their base. Seafloor dominated by shells, coral rubble and sand is frequent between 15 m to 20 m water depth offshore Khao Lak (Feldens et al., 2012). Therefore, this layer is likely to be eroded

Table 4 Tsunami facies types.

Tsunami deposits facies types	X-ray images	Core no.	Section depth (cm)	Sediment description
A: sand enriched with shells or shell debris	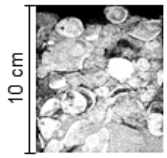 10 cm	051207-31	0-10	A 10 cm thick of shell deposit at the top of core with a lower erosional contact
	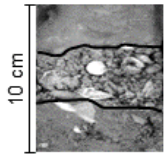 10 cm	030310-C2	10-20	A 4 cm thick layer of shell fragments with admixture of gravels, laterites, corals and sand
	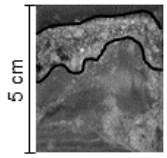 5 cm	030310-C3	29-34	A 2 cm thick layer of shell debris sand with sharp boundary at the top and bottom layer
	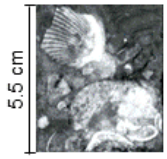 5.5 cm	050310-C4	18.5-24	Shell deposit in admixture of gravels, laterites and mud
	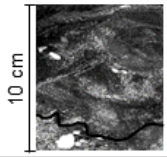 10 cm	030310-C7	20-30	Mud, sand and gravel partly cross laminated with generally fining upward grain size
B: massive layers common with mud or sand clasts	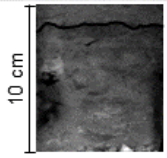 10 cm	030310-C2	3-13	Homogenous fine sand with an irregular sharp contact
	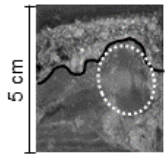 5 cm	030310-C3	29-34	Laminated mud with mud clasts
	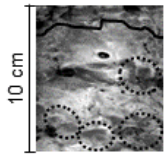 10 cm	030310-C7	2-12	Homogenous mud with several mud clasts
	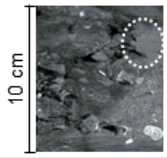 10 cm	050310-C4	6-16	Massive mud with shell fragments scatter through the layer and mud clast

during the propagation of tsunami waves from the open ocean to shallow waters. Considering a change of grain size, a marine origin of these deposits may eventually be indicated by generally lower Ti/Ca ratios in the massive sand layer (facies A) compared to the surrounding muddy layers (Fig. 2). Despite promising first results (Sakuna et al. 2012), Ti/Ca ratios appear unsuited to identify offshore tsunami deposits in a shallow-water setting, where tsunami deposits mainly comprise marine sands or backwash material, which is an admixture of marine and terrigenous material, and considering that several wave trains hit the coastline. However, foraminifera transfer functions further support a transport of facies A material from these water

depths (Milkler et al., 2013). A depth of ca. 20 m is substantially lower compared to the depths found during previous studies of tsunami impact based on wave theory and the analysis of microfossils (e.g., Nanayama and Shigeno, 2006; Weiss and Bahlburg, 2006; Weiss, 2008; Uchida et al., 2010). It is unknown whether the local shelf morphology offshore Khao Lak prohibited the substantial erosion of material from deeper waters or whether the sediments transported onshore from deeper waters were not preserved. As no storm event occurred between the 2004 tsunami and the time of sampling, the latter appears unlikely, suggesting that the preserved tsunami deposits offshore Khao Lak are in fact limited to shallow water depths. However, it cannot be ruled out that tsunami deposits exist beneath the shelf break, but no samples are available from that area. Further, facies A in core 050310-C2 is located in a core depth of 30 cm and is covered by a fining-upward sequence. Therefore, it is likely that it was deposited by a storm event and would have similar sedimentary characteristics to parts of the more clearly identifiable tsunami deposits. This indicates that tsunami run-up deposits may be hard to distinguish from tempestites in sediment cores, even a few years after a tsunami event.

Sediments from facies A are mostly covered by massive deposits commonly including mud and/or sand clasts (facies B). Those clasts are widely used as a sedimentological proxy to identify tsunami deposits and are interpreted as relating to hyperpycnal tsunami backwash flows (Goff et al., 2004; Le Roux and Vargas, 2005; Morton et al., 2007; Goodman-Tchernov et al., 2009; Sakuna et al., 2012). Clasts are found in the uppermost part of the tsunami sequence and include material transported during the backwash, as shown by foraminifera composition (Milker et al., 2013) and the presence of laterites and grass (Feldens et al., 2012; Sakuna et al., 2012). The Ti/Ca ratios in this facies type are not noticeably different from the inferred flash floods deposits, which have to originate from onshore sediment as well (Fig. 2). An inverted sequence in core 030310-C3 may be explained by three wave trains approaching the coastline, causing several cycles of onshore–offshore transport directions. However, clasts are not observed within all the cores. The absence of backwash deposits in core 051207-31 may be related to subsequent erosion, with the tsunami deposits exposed at the seafloor.

Intensive cross-lamination in a layer sandwiched between the tsunami facies A and B is observed within core 030310-C7. It may be assumed that the cross-bedding is related to multiple flow reversals between the run-up and backwash of the three wave trains approaching the coastline during the 2004 tsunami event (e.g., Siripong, 2006). Cross-bedding is a common feature for onshore tsunami deposits, where it was widely used to indicate the hydrodynamic regime during the deposition (Dawson et al., 1996; Nanayama et al., 2000; Goff et al., 2001; Bahlburg and Weiss, 2007; Engel and Brückner, 2011).

4.5.3 Comparison of tsunami, storm and flash-flood facies

On the Andaman Sea shelf, the presence of deposits related to tsunami, tropical storms and annual flash floods during the summer monsoon season allows us to compare the sedimentary signatures of these events at the same offshore location. The distinction of tsunami deposits from those deposited by other high-energy events, such as storms or hurricanes, are still problematic, even for deposits on land (Nanayama et al., 2000; Kortekaas and Dawson, 2007; Morton et al., 2007; Switzer and Jones, 2008; Phantuwongraj and Choowong, 2012). Previous studies proved that a series of proxies must be applied, e.g., the geomorphological setting, sedimentary structures, microfossil assemblages and geochemical components (Goff et al., 2004, 2012; Kortekaas and Dawson, 2007; Morton et al., 2007; RamÍrez-Herrera et al., 2012; Chagué-Goff et al., 2011; Richmond et al., 2011, Sakuna et al. 2012). The different signatures of the identified event deposits are summarized in Table 5. In particular, the differentiation between tsunami facies type A and storm deposits appears to be problematic. Storms raise water levels due to their low atmospheric pressure and cause coastal flooding (Ogston et al., 2000; Harris and Heap, 2009). Sediment is kept in suspension and deposited with waning energy levels. This results in deposits of graded sand, frequently showing cross-bedding. Wave ripple marks draped with mud are frequently only preserved at the top of the storm deposit sequence (Weidong et al., 1997). While a tsunami event may comprise several waves, thus allowing the deposition of several mud drapes, it is expected that later waves erode the previously deposited mud drapes. Distinct lamina of shells and their fragments are common in storm deposits,

Table 5 Differences between the sedimentary features of flash flood, tsunami and storm deposits on the Andaman Sea shelf.

Deposition characteristics	**Flash flood (monsoon effect)**	**Tsunami**	**Tropical storm**
Age of events (AD)	-	2004	1962-1965, 1972-1973, 1989
Occurrence (max. observed water depth)	16 m	16 m	45 m
Deposit thickness	1-12 cm	12-30 cm	2-9 cm
Sedimentary contact	transitional	sharp, erosional	sharp, erosional
Grain size range	mud	mud to gravels	silt to coarse sand
Sediment sorting	poorly sorted but better than tsunami deposits	poorly sorted	poorly sorted but better than tsunami deposits
Sedimentary structure	laminated, fining upward sequences	laminated, massive structures, fining upward sequence, internal erosional surfaces	rippled, cross laminated, graded sand
Presence of rip-up clast	no	yes	no
Terrigenous component	no	wood and laterites	no
Anthropogenic artifact	no	pieces of brick	no
Presence of carbonate material	occasionally shell fragments	pieces of boken shells and corals	complete shells and their fragments (typical for beach sand)
Presence of mud	yes	yes	no
Presence of sand	no	yes	yes

most likely because of high-frequency waves (Morton et al., 2007), and have also been observed in tsunami deposits offshore Khao Lak (this study). Therefore, neither the observed cross-laminated sections nor the presence of sand, rich in shells or shell debris (facies A), are suitable as a proxy to distinguish tsunami and storm deposits. In contrast, mud and sand clasts (facies B) were previously used to discriminate storm and tsunami deposits (e.g., Morton et al., 2007; Phantuwongraj and Choowong, 2012), as were terrestrial components and anthropogenic artifacts. The backwash transports a variety of material from the hinterland towards offshore, and the high-density backwash flows support the formation of clasts (Dawson and Stewart, 2007; Morton et al., 2007; Shanmugam, 2011; RamÍrez-Herrera et al., 2012). In contrast, erosion during storms is focused on the shoreface and the beach (Snedden et al., 1988; Allison et al., 2005); thus, clasts and terrestrial material are expected to appear less frequently within storm deposits. This highlights the importance of material deposited during the tsunami backwash for the identification of past tsunami events. Further proxies using the increased occurrence of terrestrial material for the discrimination of offshore tsunami and storm deposits could be plants, anthropogenic material (for recent events) and geochemical proxies such as (PAH; Tipmanee et al., 2012) or microfossils (Milker at al., 2013). Tsunami backwash deposits have to be differentiated from flash floods, which can also deposit terrigenous material out of hyperpycnal density flows (Mulder et al., 2003; Bourrin et al., 2008). In fact, little difference exists in the Ti/Ca ratios between flash-flood and tsunami deposits offshore PC. However, flash floods differ from the identified tsunami deposits sedimentologically: they are generally better sorted than tsunami deposits and include less sand, likely related to the higher energy of the tsunami backwash flow. The higher energy of the backwash flow is further reflected by the generally sharp and erosional boundaries of the backwash deposits, while flash-flood deposits show mostly transitional

boundaries. Additionally, mud clasts are absent in the observed flash-flood deposits.

4.6 Conclusions

On the Andaman Sea continental shelf, tsunami, storm and flash-flood deposits have been preserved in close vicinity to each other, allowing us to compare their sedimentological characteristics. Flash-flood deposits comprise laminated, fining-upward mud with occasional shell fragments. Large storm or typhoon deposits show typically sharp and partly erosional lower contacts and are composed of rippled, cross-laminated and graded sand without mud. The 2004 Indian Ocean Tsunami left two different sedimentary facies, including 1) sand enriched in shell and shell debris and 2) layers including mud and sand clasts. From this study, the most prominent difference between the storm and tsunami deposits offshore Khao Lak area is the presence of terrestrial components, anthropogenic artifacts and mud in the latter.

Acknowledgements. The authors wish to thank the Phuket Marine Biological Center (PMBC) for supporting us with ship time of RV *ChakratongTongyai* and RV *BoonlertPasook* as well as with other facilities during field campaigns. This study was funded by the Deutsche Forschungsgemeinschaft (DFG) grant SCHW 572/11, the National Research Council of Thailand (NRCT) and the DAAD (Deutscher Akademischer Austauschdienst) fellowship provided to D. Sakuna-Schwartz for a PhD study at Kiel University.

References

Abrantes, F., Alt-Epping, U., Lebreiro, S., Voelker, A. and Schneider, R.: Sedimentological record of tsunamis on shallow-shelf areas, The case of the 1969 AD and 1755 AD tsunamis on the Portuguese Shelf off Lisbon, Marine Geology, 249, 283-293, 2008.

Allison, M.A., Sheremet, A., Goñi, M.A. and Stone, G.W.: Storm layer deposition on the Mississippi-Atchafalaya subaqueous delta generated by Hurricane Lili in 2002, Continental Shelf Research, 25, 2213-2232, 2005.

Bahlburg, H. and Weiss, R.: Sedimentology of the December 26, 2004, Sumatra tsunami deposits in easternIndia (Tamil Nadu) and Kenya, International Journal of Earth Sciences, 96, 1195-1209, 2007.

Bahr, A., Lamy, F., Arz, H., Kuhlmann, H. and Wefe, G.: Late glacial to Holocene climate and sedimentation history in the NW Black Sea, Marine Geology, 214, 309-322, 2005.

Best, A.I. and Gunn, D.E.: Calibration of marine sediment core loggers for quantitative acoustic impedance studies, Marine Geology, 160, 137-146, 1999.

Blott, S.J. and Pye, K.: Gradistat, a grain-size distribution and statistics package for the analysis of unconsolidated sediments, Earth Surface Processes and Landforms, 26, 1237-1248, 2001.

Bourrin, F., Friend, P.L., Amos, C.L., Manca, E., Ulses, C., Palanques, A., Durrieu de Madron, X. and Thompson, C.E.L.: Sediment dispersal from a typical Mediterranean flood, The Têt River, Gulf of Lions, Continental Shelf Research, 28, 1895-1910, 2008.

Brand, S. (Eds.): Tropical cyclones affecting Phuket, http://www.nrlmry.navy.mil/port_studies/thh-nc/thailand/phuket/text/frame.htm, last access: 11 June 2015, 2009.

Brill, D., Brückner, H., Jankaew, K., Kelletat, D., Scheffers, A. and Scheffers, S.: Potential predecessors of the 2004 Indian Ocean Tsunami - Sedimentary evidence of extreme wave events at Ban Bang Sak, SW Thailand, Sedimentary Geology, 239, 146-161, 2011.

Brill, D., Pint, A., Jankaew, K., Frenzel, P., Schwarzer, K., Vött, A. and Brückner, H.: Sediment transport and hydrodynamic parameters of Tsunami waves recorded in offshore Geoarchives - a case study from Thailand, Journal of Coastal Research, 30, 922-941, 2014a.

Brill, D., Jankaew, K., Neubauer, N.P., Kelletat, D., Scheffers, A., Vött, A. and Brückner, H.: Holocene coastal evolution of southwest Thailand - implications for the site-specific preservation of palaeotsunami deposits, Zeitschrift für Geomorphologie, 58, 273-303, 2014b.

Chagué-Goff, C., Schneider, J.L., Goff, J.R., Dominey-Howes, D. and Strotz, L.: Expanding the proxy toolkit to help identify past events - Lessons from the 2004 Indian Ocean Tsunami and the 2009 South Pacific Tsunami, Earth-Science Reviews, 107, 107-122, 2011.

Chavanich, S., Siripong, A., Sojisuporn, P. and Menasaveta, P.: Impact of tsunami on the seafloor and corals in Thailand, Coral Reefs, 24, 535, doi: 10.1007/s00338-005-0016-2, 2005.

Cheng, W. and Weiss, R.: On sediment extent and runup of tsunami waves, Earth and Planetary Science Letters, 362, 305-309, 2013.

Choowong, M., Murakoshi, N., Hisada, K., Charusiri, P., Daorerk, V., Charoentitirat, T., Chutakositkanon, V., Jankaew, K. and Kanjanapayont, P.: Erosion and deposition by the 2004 Indian Ocean tsunami in Phuket and Pang-nga Provinces, Thailand. Journal of Coastal Research, 23, 1270-1276, 2007.

Choowong, M., Phantuwongraj, S., Charoentitirat, T., Chutakositkanon, V., Yumuang, S. and Charusiri, P.: Beach recovery after 2004 Indian Ocean tsunami from Phang-nga, Thailand. Geomorphology, 104, 134-142, 2009.

Colin, C., Turpin, L., Bertaux, J., Desprairies, A., and Kissel, C.: Erosional history of the Himalayan and Burman ranges during the last two glacial-interglacial cycles, Earth and Planetary Science Letters, 171, 647-660, 1999.

Crokett, J.S. and Nittrouer, C.A.: The sandy inner shelf as a repository for muddy sediment, an example from Northern California, Continental Shelf Research, 24, 55-73, 2004.

Curran, K.J., Hill, P.S. and Milligan, T.G.: Fine-grained suspended sediment dynamics in the Eel River flood plume, Continental Shelf Research, 22, 2537-2550, 2002.

Cutter Jr, G.R. and Diaz, R.J.: Biological alteration of physically structured flood deposits on the Eel margin, northern California, Continental Shelf Research, 20, 235-253, 2000.

Dartnell, P. and Gardner, J.V.: Predicting Seafloor Facies from Multibeam Bathymetry and Backscatter Data, Photogrammetric Engineering & Remote Sensing, 70, 1081-1091, 2004.

Dawson, A.G. and Stewart, I.: Tsunami deposits in the geological record, Sedimentary Geology, 200, 166-183, 2007.

Dawson, A.G., Shi, S., Dawson, S., Takahashis, T. and Shutos, N.: Coastal sedimentation associated with the June 2nd and 3rd, 1994, tsunami in Rajegwesi, Java, Quaternary Science Reviews, 15, 901-912, 1996.

Di Geronimo, I., Choowong, M. and Phantuwongraj, S.: Geomorphology and Superficial Bottom Sediments of KhaoLak Coastal Area (SW Thailand), Polish Journal of Environmental Studies, 18, 111-121, 2009.

Einsele, G., Ricken, W. and Seilacher, A. (Eds.).: Cycles and events in stratigraphy, Springer-Verlag, Berlin, Heidelberg, New York, 955 pp., 1991.

Engel, M. and Brückner, H.: The identification of palaeo-tsunami deposits - a major challenge in coastal sedimentary research, Coastline Reports, 17, 65-80, 2011.

Feldens, P., Schwarzer, K., Sakuna, D., Szczuciński, W. and Somgpongchaiykul, P.: Identification of offshore tsunami deposits on the shelf off KhaoLak (Thailand), Earth, Planets and Space, 64, 875-887, 2012.

Feldens, P., Schwarzer, K., Szczuciński, W., Stattegger, K., Sakuna, D. and Somgpongchaiykul, P.: Impact of 2004 Tsunami on Seafloor Morphology and Offshore Sediments, Pakarang Cape, Thailand, Polish Journal of Environmental Studies, 18, 63-68, 2009.

Fujiwara, O. and Kamataki, T.: Identification of tsunami deposits considering the tsunami waveform, an example of subaqueous tsunami deposits in Holocene shallow bay on southern Bobo Penisular, Central Japan, Sedimentary Geology, 200, 295-313, 2007.

Geyer, W.R., Hill, P.S. and Kineke, G.C.: The transport, transformation and dispersal of sediment by buoyant coastal flows, Continental Shelf Research, 24, 927-949, 2004.

Goff, J., Chagué-Goff, C. and Nichol, S.: Paleotsunami deposits, a New Zealand perspective, Sedimentary Geology, 143, 1-6, 2001.

Goff, J., Chagué-Goff, C., Nichol, S., Jaffe, B. and Dominey-Howes, D.: Progress in palaeotsunami research, Sedimentary Geology, 243-244, 70-88, 2012.

Goff, J., McFadgen, B.G. and Chagué-Goff, C.: Sedimentary differences between the 2002 Easter storm and the 15th-century Okoropunga tsunami, southeastern North Island, New Zealand, Marine Geology, 204, 235-250, 2004.

Goodman-Tchernov, B.N., Dey, H.W., Reinhard, E.G., McCoy, F. and Mart, Y.: Tsunami waves generated by the Santorini eruption reached Eastern Mediterranean shores, Geology, 37, 943-946, 2009.

Goto, K., Chavanich, S.A., Imamura, F., Kunthasap, P., Matsui, T., Minoura, K., Sugawara, D. and Yanagisawa, H.: Distribution, origin and transport process of boulders deposited by the 2004 Indian Ocean tsunami at Pakarang Cape, Thailand, Sedimentary Geology, 202, 821-837, 2007.

Goto, K., Hashimoto, K., Sugawara, D., Yanagisawa, H. and Abe, T.: Spatial thickness variability of the 2011 Tohoku-oki tsunami deposits along the coastline of Sendai Bay, Marine Geology, 358, 38-48, 2014.

Goto, K., Takahashi, J., Oie, T. and Imamura, F.: Remarkable bathymetric change in the nearshore zone by the 2004 Indian Ocean tsunami, Kirinda Harbor, Sri Lanka, Geomorphology, 127, 107-116, 2011.

Grzelak, K., Kotwicki, L. and Szczuciński, W.: Monitoring of Sandy Beach Meiofaunal Assemblages and Sediments after the 2004 Tsunami in Thailand, Polish Journal of Environmental Studies, 18, 43-51, 2009.

Harris, P.T. and Heap, A.D.: Cyclone-induced net sediment transport pathway on the continental shelf of tropical Australia inferred from reef talus deposits, Continental Shelf Research, 29, 2011-2019, 2009.

Hill, P.S., Fox, J.M., Croeckett, J.S., Curran, K.J., Friedrich, C.T., Geyer, W.R., Milligan, T.G., Ogston, A.S., Puig, P., Scully, M.E., Traykovski, P.A. and Wheatcroft, R.A.: Sediment delivery to the seabed on continental margins, in: Continental Margin Sedimentation, Nittrouer, C.A., Austin, J.A., Field, M.E., Kravitz, J.H., Syvitski, J.P.M. and Wiberg, P.L. (Eds.), IAS Special Publication 37, pp. 49-99, 2007.

Hofmann, D.I., Fabian, K., Schneider, F., Donner, B. and Bleil, U.: A stratigraphic network across the Subtropical Front in the central South Atlantic, Multi-parameter correlation of magnetic susceptibility, density, X-ray fluorescence and $\delta^{18}O$ records, Earth and Planetary Science Letters, 240, 694-709, 2005.

Hylleberg, J., Nateewathana, A. and Chatananthawej, B.: Temporal changes in the macrobenthos on the West Coast

of Phuket Island, with emphasis on the effects of offshore tin mining, Phuket Marine Biological Center Research Bulletin, 37, 1-16, 1985.

Jankaew, K., Atwater, B.F., Sawai, Y., Choowong, M., Charoentitirat, T., Martin, M.E. and Prendergast, A.: Medieval forewarning of the 2004 Indian Ocean tsunami in Thailand, Nature, 455, 1228-1231, 2008.

Kale, V.S.: Geomorphic Effects of Monsoon Floods on Indian Rivers, Natural Hazards, 28, 65-84, 2003.

Khokiattiwong, S., Limpsaichol, P., Petpiroon, S., Sojisuporn, P. and Kjerfve, B.: Oceanographic variations in Phangnga Bay, Thailand under monsoonal effects, Phuket Marine Biological Center Research Bulletin, 55, 43-76, 1991.

Kortekaas, S. and Dawson, A.G.: Distinguishing tsunami and storm deposits, An example from Martinhal, SW Portugal, Sedimentary Geology, 200, 208-221, 2007.

Krassay, A.A.: Storm features of siliciclastic shelf *sedimentation* in the mid-Cretaceous epeiric seaway of northern Australia, *Sedimentary Geology*, 89, 241-264, 1994.

Krumbein, W. C.: Size frequency distribution of sediments and the normal phi curve, Journal of Sedimentary Petrology, 8, 84-90, 1938.

Kuehl, S.A., Nittrouer, C.A., Allison, M.A., Ercilio, L., Faria, C., Dukat, D.A., Jaeger, J.M., Pacioni, T.D., Figueiredo, A.G. and Underkoffler, E.C.: Sediment deposition, accumulation, and seabed dynamics in an energetic, fine-grained, coastal environment, Continental Shelf Research, 16, 787-815, 1985.

Lamy, F., Hebbeln, D., Röhl, U. and Wefer, G.: Holocene rainfall variability in southern Chile, a marine record of latitudinal shifts of the Southern Westerlies, Earth and Planetary Science Letters, 185, 369-382, 2001.

Lario, J., Luque, L., Zazo, C., Goy, J.L., Spencer, C., Cabero, A., Bardají, T., Borja, F., Dabrio, C.J., Civis, J., González-Delgado, J.A., Borja, C. and Alonso-Azcárate, J.: Tsunami vs. storm surge deposits, a review of the sedimentological and geomorphological records of extreme wave events (EWE) during the Holocene in the Gulf of Cadiz, Spain. Zeitschrift für Geomorphologie, 54, 301-316, 2010.

Le Roux, J.P. and Vargas, G.: Hydraulic behavior of tsunami backflows, insights from their modern and ancient deposits, Environmental Geology, 49, 65-75, 2005.

Lim, H.S. and Boochabun, K.: Flood generation during the SW monsoon season in northern Thailand. Geological Society Special Publication, 361, 7-20, 2012.

Lorang, M.S.: A wave-competence approach to distinguish between boulder and megaclast deposits due to storm waves versus tsunamis, Marine Geology, 283, 90-97, 2011.

Malmon, D.V., Reneau, S.L. and Dunne, T.: Sediment sorting and transport by flash floods, Journal of Geophysical Research, 109, F02005, doi: 10.1029/2003JF000067, 2004.

Martin, A.J.: Flaser and wavy bedding in ephemeral streams, a modern and an ancient example, Sedimentary Geology, 136, 1-5, 2000.

McKee, B.A., Nittrouer, C.A. and DeMaster, D.J.: The concepts of sediment deposition and accumulation applied to the continental shelf near the mouth of the Yangtze River, Geology, 11, 631-633, 1983.

Milker, Y., Wilken, M., Schumann, J., Sakuna, D., Feldens, P., Schwarzer, K. and Schmiedl, G.: Sediment transport on the inner shelf off KhaoLak (Andaman Sea, Thailand) during the 2004 Indian Ocean tsunami and former storm events, Evidence from foraminiferal transfer functions, Nat. Hazards Earth Syst. Sci., 13, 3113-3128, 2013.

Morton, R.A., Gelfenbaum, G. and Jaffe, B.E.: Physical criteria for distinguishing sandy tsunami and storm deposits using modern examples, Sedimentary Geology, 200, 184-207, 2007.

Mulder, T., Syvitski, J.P.M., Migeon, S., Fauge`res, J.C. and Savoye, B.: Marine hyperpycnal flows: initiation, behavior and related deposits: A review, Marine and Petroleum Geology, 20, 861-882, 2003.

Nanayama, F. and Shigeno, K.: Inflow and outflow facies from the 1993 tsunami in southwest Hokkaido, Sedimentary Geology, 187, 139-58, 2006.

Nanayama, F., Shigeno, K., Satake, K., Shimokaka, K., Koitabashi, S., Miyasaka, S. and Ishii, M.: Sedimentary differences between the 1993 Hokkaido-nansei-oki tsunami and the 1959 Miyakojima typhoon at Taisei, southwestern Hokkaido, northern Japan, Sedimentary Geology, 13, 255-264, 2000.

Nott, J.F.: Waves, boulders and the importance of the pre-transport setting, Earth and Planetary Science Letters, 210, 269-276, 2003.

Ogston, A.S., Cacchione, D.A., Sternberg, R.W. and Kineke, G.C.: Observations of storm and river flood-driven sediment transport on the northern California continental shelf, Continental Shelf Research, 20, 2141-2162, 2000.

Ohta, T. and Arai, H.: Statistical empirical index of chemical weathering in igneous rocks, A new tool for evaluating the degree of weathering, Chemical Geology, 240, 280-297, 2007.

Owens, P.N.: Soil erosion and sediment fluxes in river basins: the influence of anthropogenic activities and climate change, in: Soil and Sediment Remediation: Mechanisms, Technologies and Applications, Lens P, Grotenhuis T, Malina G, Tabak H (Eds.), IWA Publishing, London, 418-434, 2005.

Owen, R.B. and Lee, R.: Human impacts on organic matter sedimentation in a proximal shelf setting, Hong Kong, Continental Shelf Research, 24, 583-602, 2004.

Palinkas, C.M., Nittrouer, C.A. and Walsh, J.P.: Inner shelf sedimentation in the Gulf of Papua, New Guinea, a mud-rich

shallow shelf setting, Journal of Coastal Research, 22, 760-772, 2006.

Panchang, R., Nigam, R., Raviprasad, G. V., Rajagopalan, G., Ray, D. K., and Hla, U. K. Y.: Relict faunal testimony for sea-level fluctuations off Myanmar (Burma), J. Palaeon. Soc. India, 53, 185-195, 2008.

Paris, R., Fournier, J., Poizot, E., Etienne, S., Mortin, J., Lavigne, F. and Wassmer, P.: Boulder and fine sediment transport and deposition by the 2004 tsunami in LhokNga (western Banda Aceh, Sumatra, Indonesia), A coupled offshore-onshore model, Marine Geology, 268, 43-54, 2010.

Phantuwongraj, S. and Choowong, M.: Tsunamis versus storm deposits from Thailand, Natural Hazards, 63, 31-50, 2012.

Postma, G.: Physical climate signatures in shallow- and deep-water deltas, Global and Planetary Change, 28, 93-106, 2001.

Ramaswamy, V., Rao, P.S., Rao, K.K., Swe Thwin, Rao, N.S. and Raiker, V.: Tidal influence on suspended sedimen distribution and dispersal in the northern Andaman Sea and Gulf Martaban, Marine Geology, 208, 33-42, 2004.

Ramírez-Herrera, M.-T., Lagos, M., Hutchinson, I., Kostoglodov, V., Machain, M. L., Caballero, M., Goguitchaichvili, A., Aguilar, B., Chagué-Goff, C., Goff, J., Ruiz-Fernández, A. -C., Ortiz, M., Nava, H., Bautista, F., Lopez, G. I. and Quintana, P.: Extreme wave deposits on the Pacific coast of Mexico, tsunamis or storms? - A multi-proxy approach, Geomorphology, 139-140, 360-371, 2012.

Richmond, B.M., Watt, S., Buckley, M., Jaffe, B.E., Gelfenbaum, G. and Morton, R.A.: Recent storm and tsunami coarse-clast deposit characteristics, southeast Hawaii, Marine Geology, 283, 79-89, 2011.

Robbins, J.A. and Edington, D.N.: Determination of recent sedimentation rates in Lake Michigan using Pb-210 and Cs-137, Geochimicaet Cosmochimica Acta, 39, 285-304, 1975.

Rodolfo, K.S.: Bathymetry and Marine Geology of the Andaman Basin, and Tectonic Implications for Southeast Asia, Geological Society of America Bulletin, 80, 1203-1230, 1969.

Sakuna, D., Szczuciński, W., Feldens, P., Schwarzer, K. and Khokiattiwong, S.: Sedimentary deposits left by the 2004 Indian Ocean tsunami on the inner continental shelf offshore of KhaoLak, Andaman Sea (Thailand), Earth, Planets and Space, 64, 931-943, 2012.

Schwab, J.M., Krastel, S., Grün, M., Gross, F., Pananont, P., Jintasaeranee, P., Bunsomboonsakul, S., Weinrebe, W. and Winkelmann, D.: Submarine mass wasting and associated tsunami risk offshore western Thailand, Andaman Sea, Indian Ocean. Nat. Hazards Earth Syst. Sci., 12, 2609-2630, 2012.

Shanmugam, G.: Process-sedimentological challenges in distinguishing paleo-tsunami deposits, Natural Hazards, 63, 5-30, 2011.

Singh, O.P., Ali Khan, T.M. and Rahman, M.S.: Changes in the frequency of tropical cyclones over the North Indian Ocean, Meteorology and Atmospheric Physics, 75, 11-20, 2000.

Siripong, A.: Andaman Sea coast of Thailand Field Survey after the December 2004 Indian Ocean Tsunami, Earthquake Spectra, 22, 187-202, 2006.

Smedile, A., De Martini, P.M., Pantosti, D., Bellucci, L., Del Carlo, P., Gasperini, L., Pirrotta, C., Polonia, A. and Boschi, E.: Possible tsunami signatures from an integrated study in the Augusta Bay offshore (Eastern Sicily-Italy), Marine Geology, 281, 1-13, 2011.

Smith, J.N.: Why should we believe ^{210}Pb sediment geochronologies?, Journal of Environmental Radioactivity, 55, 121-123, 2001.

Snedden, J.W., Nummedal, D. and Amos, A.F.: Storm- and fair-weather combined flow on the central Texas continental shelf, Journal of Sedimentary Petrology, 58, 580-595, 1988.

Spiske, M., Bahlburg, H. and Weiss, R.: Pliocene mass failure deposits mistaken as submarine tsunami backwash sediments - an example from Hornitos, Northern Chile, Sedimentary Geology, 305, 69-82, 2014.

Spiske, M., Piepenbreier, J., Benavente, C. and Bahlburg, H.: Preservation potential of tsunami deposits on arid siliciclastic coasts, Earth-Science Reviews, 126, 58-73, 2013.

Sugawara, D., Minoura, K., Nemoto, N., Tsukawaki, S., Goto, K. and Imamura, F.: Foraminiferal evidence of submarine sediment transport and deposition by backwash during the 2004 Indian Ocean tsunami), Island Arc, 18, 513-525, 2009.

Switzer, A.D. and Jones, B.G.: Large-scale washover sedimentation in a freshwater lagoon from the southeast Australian coast, sea-level change, tsunami or exceptionally large storm?, The Holocene, 18, 787-803, 2008.

Szczuciński, W., Chaimanee, N., Niedzielski, P., Rachlewicz, G., Saisuttichai, D., Tepsuwan,T., Lorenc, S. and Siepak, J.: Environmental and Geological Impacts of the 26 December 2004 Tsunami in Coastal Zone of Thailand - Overview of Short and Long-Term Effects, Polish Journal of Environmental Studies, 15, 793-810, 2006.

Thai Meteorological Department (TMD): The Climate of Thailand, http://www.tmd.go.th/en/archive/thailand_climate.pdf, last access: 11 June 2015, 2012.

Thampanya, U., Vermaat, J.E., Sinsakul, S. and Panapitukkul, N.: Coastal erosion and mangrove progradation of Southern Thailand, Estuarine, Coastal and Shelf Science, 68, 75-85, 2006.

Tipmanee, D., Deelaman, W., Pongpiachan, S., Schwarzer, K. and Sompongchaiyakul, P.: Using Polycyclic Aromatic Hydrocarbons (PAHs) as a chemical proxy to indicate Tsunami 2004 backwash in KhaoLak coastal area, Thailand, Nat. Hazards Earth Syst. Sci., 12, 1441-1451, 2012.

Tjallingii, R., Stattegger, K., Wetzel, A. and Phach, P.V.: Infilling and flooding of the Mekong River incised valley during deglacial sea-level rise, Quaternary Science Reviews, 29, 1432-1444, 2010.

Uchida J.I., Fujiwara, O., Hasegawa, S. and Kamataki, T.: Sources and depositional processes of tsunami deposits, Analysis using foraminiferal tests and hydrodynamic verification, Island Arc, 19, 427-442, 2010.

Umitsu, M., Tanavud, C. and Patanakanog, B.: Effects of landforms on tsunami flow in the plains of Banda Aceh, Indonesia, and Nam Khem, Thailand, Marine Geology, 242, 141-153, 2007.

Usiriprisan, C., Chiemchindaratana, S., Shoosuwan, S. and Chatrapakpong, Y.: Offshore exploration for tin and heavy minerals in the Andaman Sea, Department of Mineral Resources, Bangkok and UNDP, New York, 224 pp., 1987.

van den Bergh, G. D., Boer, W., de Haas, H., van Weering, Tj. C. E. and van Wijhe, R.: Shallow marine tsunami deposits in Teluk Banten (NW Java, Indonesia), generated by the 1883 Krakatau eruption, Marine Geology, 197, 13-34, 2003.

Wadman, H.M. and McNinch, J.E.: Stratigraphic spatial variation on the inner shelf of a high-yield river, Waiapu River, New Zealand: Implications for fine-sediment dispersal and preservation, Continental Shelf Research, 28, 865-886, 2008.

Weber, M.E., Niessen, F., Kuhn, G. and Wiedicke, M.: Calibration and application of marine sedimentary physical properties using a multi-sensor core logger, Marine Geology, 136, 151-172, 1997.

Weidong, D., Baoguo, Y. and Xiaogen, W.: Studies of storm deposits in China, a review, Continental Shelf Research, 17, 1645-1658, 1997.

Weiss, R. and Bahlburg, B.: A note on the preservation of offshore tsunami deposits, Journal of Sedimentary Research, 76, 1267-1273, 2006.

Weiss, R.: Sediment grains moved by passing tsunami waves, Tsunami deposits in deep water, Marine Geology, 250, 251 – 257, 2008.

Wheatcroft, R.A. and Drake, D. E.: Post-depositional alteration and preservation of sedimentary event layers on continental margins, I. The role of episodic sedimentation, Marine Geology, 199, 123-137, 2003.

Wolanski, E. and Spagnol, S.: Environmental degradation by mud in tropical estuaries, Regional Environmental Change, 1, 152-162, 2000.

Wright, L.D. and Nittrouer, C.A.: Dispersal of river sediments in coastal seas, six contrasting cases, Estuaries, 18, 494-508, 1995.

CHAPTER V

NOTES ON THE DISTRIBUTION AND STRATIGRAPHY OF THE SEDIMENT ON THE ANDAMAN SEA CONTINENTAL SHELF, THAILAND

5.1 Introduction

The Andaman Sea continental shelf offshore western Thailand was severely damaged during the 2004 Indian Ocean tsunami event especially in the Phang Nga area. Since this tsunami event, several studies (e.g. Bell et al., 2005; Tsuji et al., 2006; Hawkes et al., 2007; Jankaew et al., 2008; Sawai et al., 2009; Sugawara et al., 2009; Choowong et al., 2009; Brill et al., 2011) focused on tsunami impact on the shelf area offshore Khao Lak. During these studies it became apparent that little information on the geological background of this area is available, with most information gathered during tin mining exploration activities in the last century (compiled by Usiriprisan et al., 1987) and recently on the nearshore and shallow water environment (Di Geronimo et., 2009). The latter information is scattered over a number of tsunami-related research articles. Partly, this background information contributed to our following articles: 1) Feldens et al. (2009): Impact of the 2004 Tsunami on Seafloor Morphology and Offshore Sediments, Pakarang Cape, Thailand, 2) Feldens et al. (2010): Shallow water sediment structures in a tsunami-affected area, Pakarang Cape, Thailand, 3) Feldens et al. (2012): Sediment distribution on the inner continental shelf off Khao Lak (Thailand) after the 2004 Indian Ocean Tsunami, 4) Milker et al. (2012): Sediment transport on the inner shelf off Khao Lak (Andaman Sea, Thailand) during the 2004 Indian Ocean tsunami and former Storm events: Evidence from foraminiferal transfer functions, 5) Sakuna et al. (2012): Sedimentary deposits left by the 2004 Indian Ocean tsunami on the inner continental shelf offshore of KhaoLak, Andaman Sea (Thailand), 6) Sakuna-Schwartz et al. (2015): Internal structure of event layers preserved on the Andaman Sea continental shelf, Thailand: Tsunami vs. Storm and Flash-flood deposits and 7) Schwarzer et al. (2015): The Indian Ocean Tsunami 2004: Identification of tsunami deposits offshore in the Andaman Sea by different proxies.

However a lot of information acquired during our study remains unpublished. Therefore this chapter summarizes the information about the geological background and stratigraphy offshore Khao Lak, based on hydroacoustic surveys, shallow seismic data, X-radiography, Ti/Ca log-ratio, ^{210}Pb and AMS^{14}C dating, and a number of sedimentological methods. The chapter starts with an overview of seafloor sediment types and their distribution followed by the classification of sedimentary units in the sediment cores and a short discussion concerning deglacial sea level rise in the Andaman Sea region.

5.2 Seafloor sediment characteristics and interpretation

Nine seafloor-types could be classified and differentiated offshore Khao Lak based on the side scan sonar images and the sedimentary composition of grab samples (Fig. 1, classification following Feldens et al., 2012): A) silt to fine sand B) coarse sand with coral fragments C) coarse sand, coral fragments and boulders D) medium to coarse sand E) medium sand F) bedrock outcrop G) carboniferous reef platform H) fine to medium sand and I) remnants of tin mining activities.

A patchy sediment cover (seafloor type A), characterized by low and homogenous backscatter intensities, commonly occurs along north and south of Pakarang Cape. It is situated in water depths between 5 and 15 m. The extension of these patches reaches up to 6 km offshore. Five sediment samples collected from this seafloor-type show that it is mainly composed of very fine sandy to coarse silt with the first mode at 2.6 Φ (Fig. 2). These sediments are interpreted as clastic materials filled in the channel system that formed small creeks dividing the surrounding reef platforms in the past. Due to a lack of large rivers discharging in the investigation area, which are the most important source for fine sediment entering the continental shelves (Kuehl et al., 1985; Wright and Nittrouer, 1995; Geyer et al., 2004; Crokett and Nittrouer, 2004; Palinkas et al., 2006). It is therefore that these fine sediments were previously attributed to increased anthropogenic run-off that

deposits fine-grained sediment in the near shore and shallow local incisions (Feldens et al., 2012). Anthropogenic enhanced sedimentation was observed as well in other tropical estuaries in Papua New Guinea, Vietnam, Australia and Indonesia (Wolanski and Spagnol, 2000) and the Pearl river in Hong Kong (Owen and Lee, 2004). North of Pakarang Cape, sediments of seafloor type A are surrounded by coarse sand with coral fragments (seafloor type B) that covers approximately 9 km^2.

In the side-scan sonar mosaic seafloor type B and C are represented by similar high backscatter intensities and mostly sharp boundaries with seafloor type A. The seafloor of type C (first mode of 0.1Φ) is generally finer than type B (first mode of 2Φ). Boulders are observed within its boundaries (Fig. 2). Bedrock outcrops in water depth < 15 m are frequent south of the cape. Those areas are classified as seafloor type F. Pakarang Cape itself is built up from carboniferous reef materials and classified as seafloor type G. In water depths between 15-30 m and 5-12 km offshore, medium to coarse sandy sediment (seafloor type D) is the most common sediment type north of Pakarang Cape. Within this facies type, in water depths of 20 to 25 m, remnants of tin mining activities (seafloor type I) can be easily recognized in the side scan sonar mosaics and bathymetric data. These remnants form holes up to 7 m deep. Towards offshore, distinct, elongated shapes (SW-NE direction) of low to medium backscatter intensities are recognized. This sediment comprises well sorted medium sand and is classified as seafloor type E (Fig. 1).

These sediments are deposited on the steep northern slope of SW-NE striking sand ridges. It is shown that the inner shelf seabed mainly consists of seafloor type B, C and D especially in the northern part of the investigation area. Seafloor type B, C and D forms the main component of the inner shelf seabed especially in the northern part of the investigation area. These seafloor types comprise fine to coarse sand, partly including coral rubble, deposited due to Holocene coastal development. This inferred that the inner shelf is a sediment starving shelf, characterized by a lack of deposition since the time of lower sea level in the Holocene period.

From 30 to 70 m water depth, the seafloor is mainly covered with silty sand that is classified as seafloor type H. The material forming this seafloor type is interpreted as hemipelagic sediments deposited during the Holocene sea level rise. Moreover, elongated fields of stones and boulders appear in the side scan sonar image at water depth of 30-35 m.

5.3 Subsurface sediment succession and sedimentary units

Forty three working sediment cores are composed of sediments that were grouped into five different sedimentary units (Fig. 3). Sedimentary units could be classified base on the digital radiographic images and the sedimentary composition (Table 1). The thickness of the different sedimentary units varies greatly between the individual coring locations. Unit I-III describe the main sedimentological characteristics of the inner shelf between 9 m and 16 m water depth, while unit IV and V are found in the mid shelf setting beneath 45 m down to 62 m water depth. The whole set of sediment cores which have been analyzed are shown in the appendix and in prior chapters.

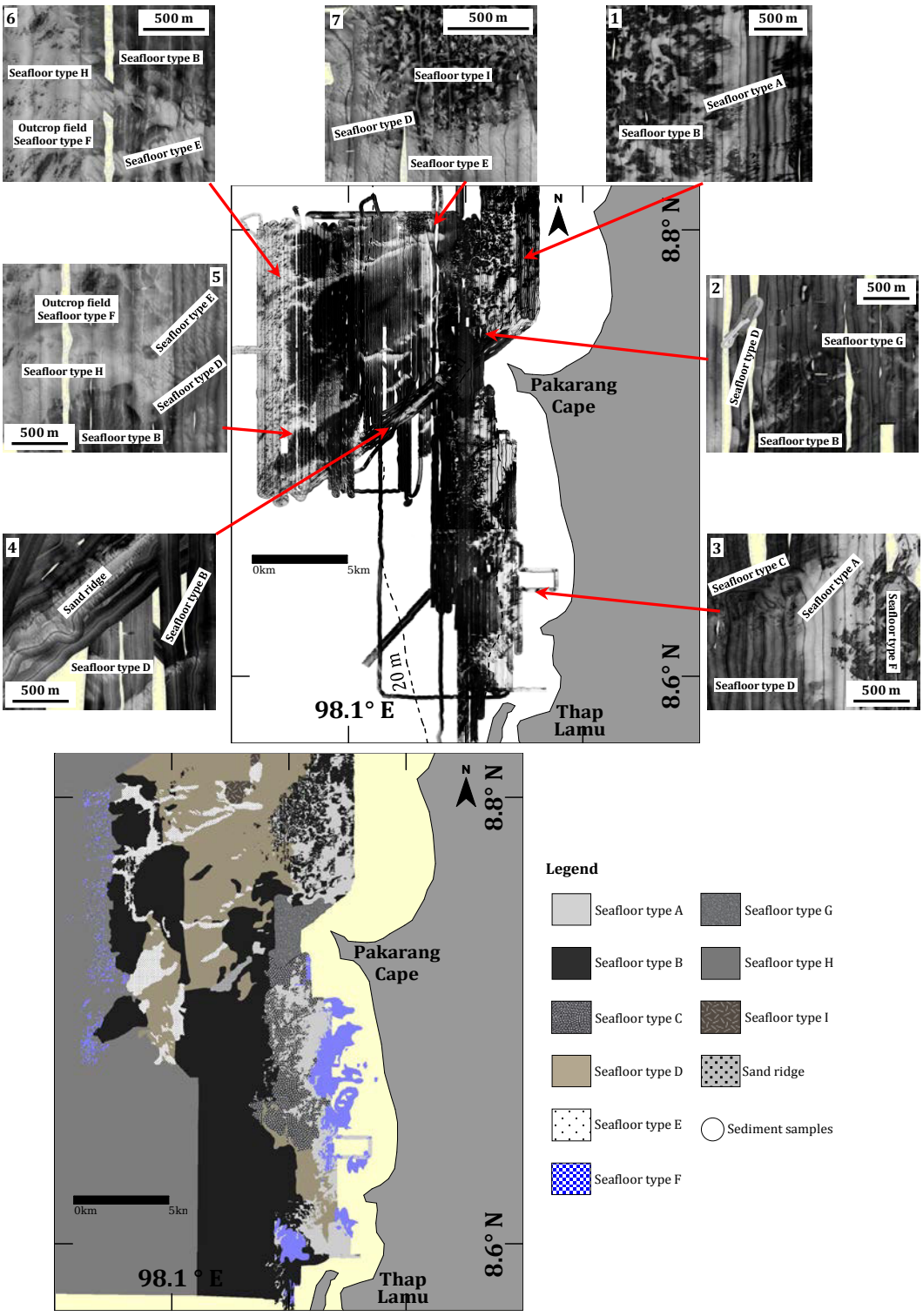

Fig. 1 Side scan sonar image of the working area and examples of side scan sonar features that were interpreted as nine differences seafloor types (above). An interpretation as a map of different seafloor types (below). The map is enlarged from the study of Feldens et al. (2012) and also merged with morphology base map of Di Geronimo et al. (2009). The seafloor types are identified from the classification of side scan sonar mosaics and verified by surface sediment samples

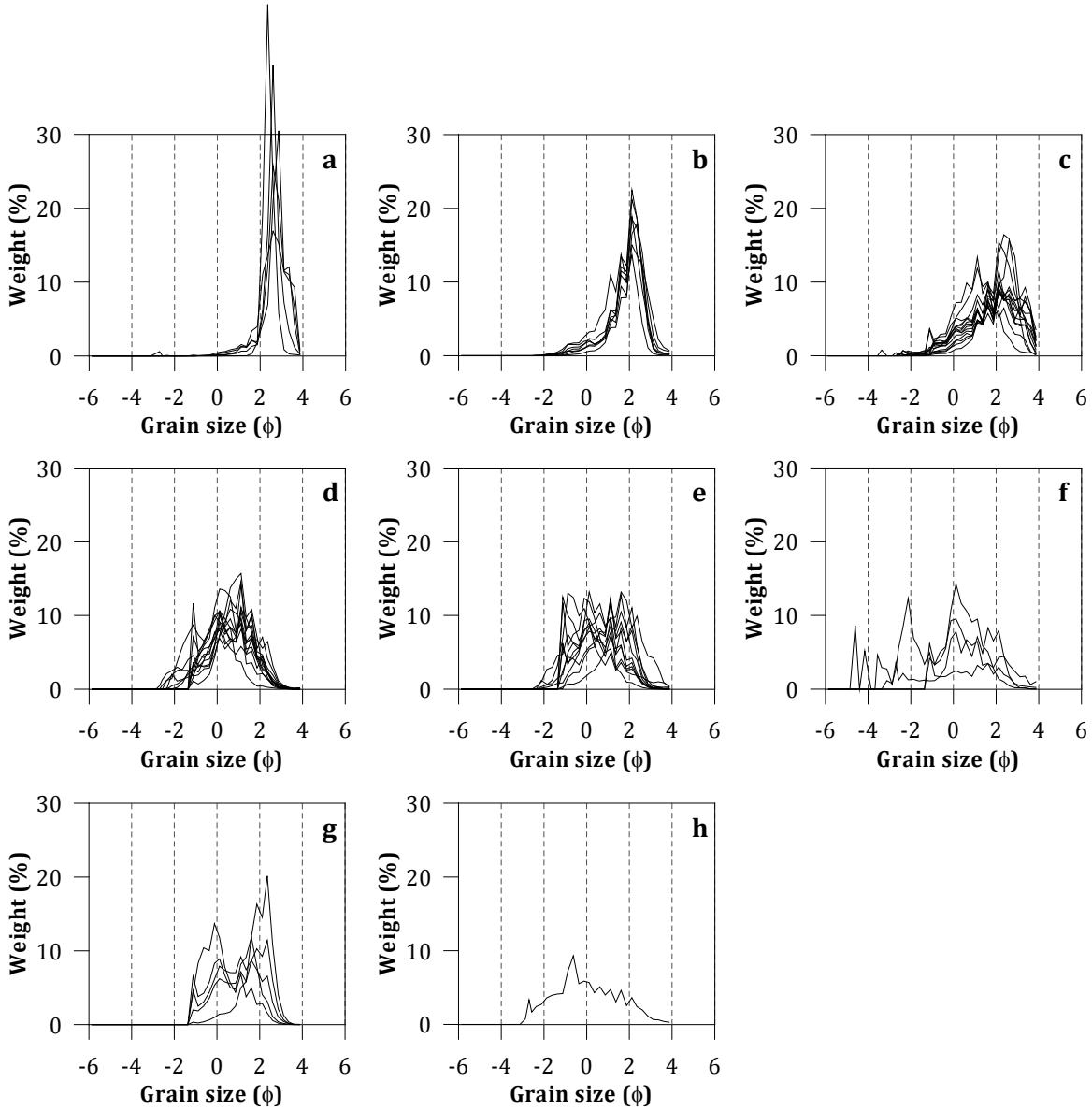

Fig. 2 Grain size distributions of sediment from different seafloor type (based on sieving results), a: silt to find sand (seafloor type A), b: fine and medium sand (seafloor type H), c: medium sand (seafloor type E), d: medium and coarse sand (seafloor type D), e: coarse sand with coral fragments (seafloor type B), f: coarse sand, coral fragments and boulders (seafloor type C), g: mud and coarse sand (sand ridge) h: sediment surrounding bedrock outcrops (seafloor type F)

- Unit I (0 cm to 24 cm core depth): the unit represents the present inner shelf surface sediments that are composed of mud (unit Ia; see cores i.e. 081207-76, 071208-02, 071208-04, 071208-05, 071208-07, 071208-08, 030310-C3, 030310-C7 core1&3, 040310-C2, 050310-C2, 050310-C3, 050310-C4 and 050310-C6) or fine sand (unit Ib; see cores i.e. 031207-30, 051207-32 core3, 030310-C2 core1&2 and 050310-C1) or coarse sand (unit Ic; see cores i.e. 051207-31, 051207-37, 051207-32 core2, 081207-77, and 030310-C6). Unit Ia is deposited near the coastline in a channel system and shallow depressions that occur down to 15 m water depth. These sediments were previously attributed to increased anthropogenic run-off leading to the deposition of fine-grained sediment in the near shore and shallow local incisions (Feldens et al., 2012). The fine sand of unit Ib forms the main

component of the seabed of the inner shelf especially in the northern part of the investigation area. These fine sands are easily mobilized and transported in the nearshore environment even under low-energy conditions. Coarse sand included in unit Ic is interpreted as a lag deposit from times of lower sea level, arising from local coral reefs that are still preserved at the seafloor (Di Geronimo et al., 2009; Feldens et al., 2012) and thus their deposition is not related to high energy events.

- Unit II (16 cm to 46 cm core depth): this unit is a distinct layer, separated from under- and overlying units by sharp and erosional contacts. Mud and sand clasts, gravel, shell debris and laterites, as well as terrigenous and anthropogenic materials are commonly found in it. ^{210}Pb activities above and below the supposed tsunami layer confirm that it was deposited within a range of a few years prior to sampling period. Therefore unit II is attributed to the 2004 Indian Ocean Tsunami (see cores i.e. 051207-32 core 2, 030310-C2 core1, 030310-C3, 030310-C6, 030310-C7 core3, 040310-C2, 050310-C2, 050310-C3, 050310-C4 and 050310-C6).

- Unit III *(29 cm to 97 cm core depth)*: the unit is composed of two subunits: subunit IIIa comprises clayey silt to fine sand with transitional boundaries. Fine lamination and generally fining upward are commonly observed (individual laminae could not be sampled). This is assigned to reworked flash-flood deposits (see core i.e. 051207-31, 051207-32 core3, 030310-C3, 030310-C7 core3, 050310-C4 and 050310-C6). Subunit IIIb contains medium to poorly sorted sand and shell fragments which are scattered throughout the unit. Massive sand layers and partly slight lamination are the main sedimentary structures with occasionally rippled shapes draped with mud at the top of the layer. These structures are related to storm deposits (see core i.e. 051207-31, 030310-C3, 030310-C7 core3, 050310-C2, 050310-C3, 050310-C4 and 050310-C6).

- Unit IV *(0 cm to 85 cm core depth)*: the unit is observed in sediment cores from the mid shelf area only (see cores i.e. 011207-02 core1&2, 011207-04, 011207-05, 021207-16 core1&2, 021207-18, 031207-19, 031207-20, 031207-22 core1&2, 031207-23, 071207-49, 071207-51, 071207-52, 071207-54, 081207-62 and 081207-64). It is composed mostly of silty sand with a silt content ranging from 26-89% and a sand content ranging from 3.6-77%. Laminations are poorly preserved, shell material is distributed throughout the unit. The change to underlying Unit V is transitional and can only be observed by changes in color. Microfossil studies of unit IV indicate that it was deposited under fully marine conditions (Milker et al., 2012). However, this unit of core 021207-16, which was retrieved from water depth of approx. 45 m, contains a distinct coarse layer that is comprised of coarse sand with abundant shell fragments at 3-8 cm core depth. Based on ^{210}Pb activity measured in the mid shelf core 031207-22 core2, this layer is older than a dozen years but less than a century; therefore it is related to storm deposits.

- Unit V (85 cm to 146 cm core depth): again, the unit is found in sediment cores from the mid shelf area. It consists mainly of dark sandy silt with a silt content ranging from 60-95% and clay content up to 9%. Plant remains and buried pieces of wood are commonly observed in this unit while shells are lacking. This unit represents a paleo-soil which was formed before the marine transgression confirmed by an abrupt change of Ti/Ca ratios and radio- carbon dating from core 021207-22 core2 (see cores i.e. 011207-02 core2 and 031207-22 core2).

Table 1 Examples of the identified sedimentary units

Unit	Photo		X-ray images		Thickness of the unit (cm)	Type of sedimentary contact	Occurrence (water depth)	Sediment description
	a	b	c	d				
Ia	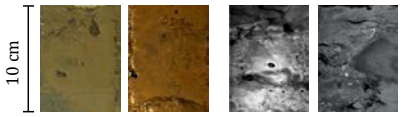 a,c = core 030310-C7 core3 c,d = core 050310-C4 core1				7-22	lower-sharp	small channels, 11-16 m	brown, poorly sorted silt to fine sand. Very fine laminated sediments are found in some cores and more often, the sediment is slightly fining upward within the laminae.
Ib	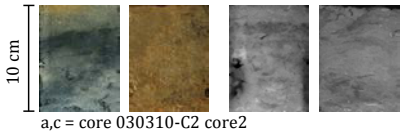 a,c = core 030310-C2 core2 c,d = core 031207-30 core1				15	lower-sharp, erosional	9 m	fine sand
Ic	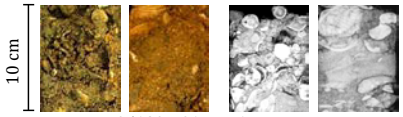 a,c = core 051207-31 core1 c,d = core 081207-77 core1				24.5	lower-sharp	15 m	Coarse sand with shells and their fragments
II	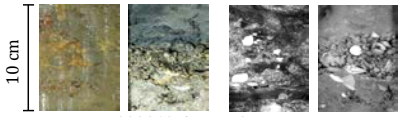 a,c = core 030310-C7 core3 c,d = core 030310-C2 core1				4.5-33	upper-sharp; lower-sharp, erosional	9-16 m	poorly sorted mud to small gravels with laterites, shell fragments, rocks, clay clasts and occasional anthropogenic materials.
IIIa	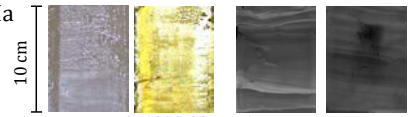 a,c = core 071208-08 core3 c,d = core 050310-C6 core1				3.5-16	upper-sharp, transitional; lower-sharp, transitional,	9-16 m	clayey silt to fine sand with common fine laminated and generally fining upward.
IIIb	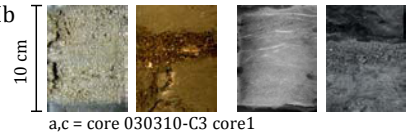 a,c = core 030310-C3 core1 c,d = core 050310-C4 core1				2-9	upper-sharp, erosional; lower-sharp, erosional	9-16 m	medium to poorly sorted sand with shell fragments scattered throughout the unit.
IV	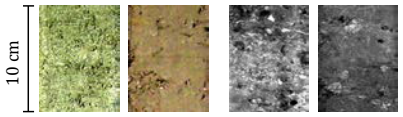 a,c = core 31207-23 core1 c,d = core 31207-22 core1				39-108	lower-transional, sharp in some cores	45-63 m	very to poorly sorted medium silt to fine sand. Laminations are poorly preserved with shells
V	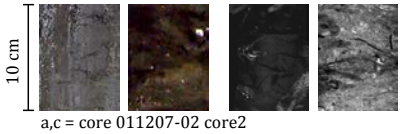 a,c = core 011207-02 core2 c,d = core 031207-22 core2				31-37	upper-transitional, sharp in some cores	55-62 m	Poorly sorted dark organic rich materials with silt content of 60-95% and a clay content up to 9%. The unit contains frequently plant remains while shell material is absent.

5.4 Radionuclide data

Three sediment cores from the inner shelf area including cores 030310-C3, 050310-C4 and 050310-C6, were measured for ^{210}Pb activity. The activity profiles and their interpretation are contained in chapter III and IV.

The ^{210}Pb measurements were carried out for one core from the mid shelf area (core 031207-22 core2) for the upper 20 cm of the core as low accumulation rates are expected in this area. The excess ^{210}Pb activity profile shows a general decline of activities with depth, whereas sediment at the depth below 9 cm almost contains no excess ^{210}Pb (Fig. 4).

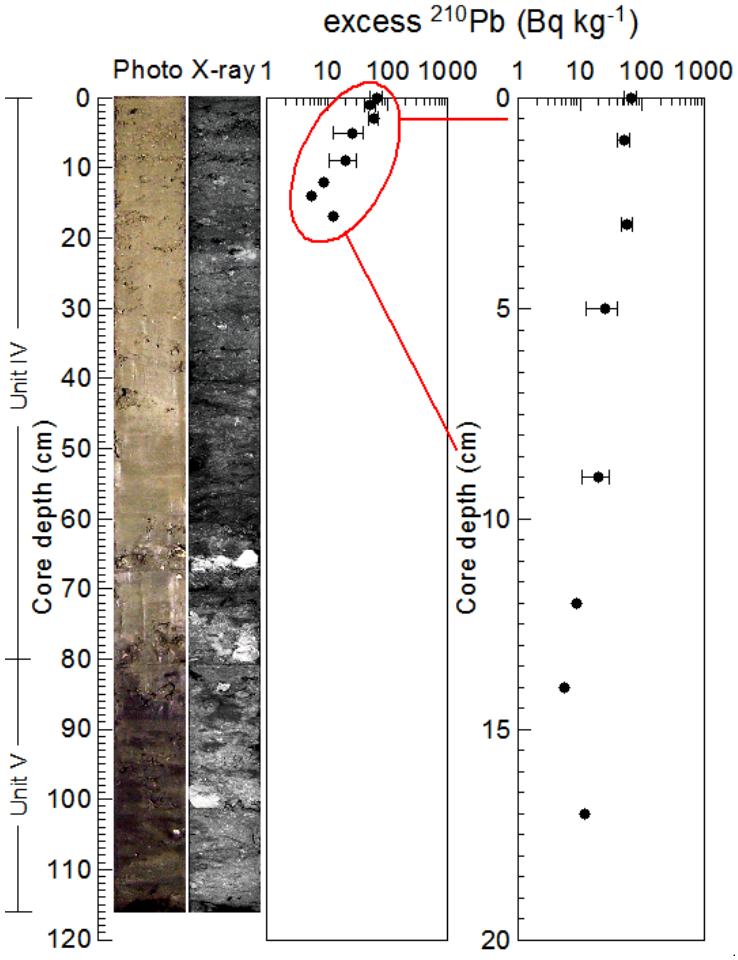

Fig. 4 The excess ^{210}Pb activity profiles with 2σ uncertainty ranges observed in sediment core 021207-22 core2 (61.9 m water depth).

Pieces of buried wood found at 82 and 92 cm core depth of core 031207-22 core2 were treated with chemical reagent as mentioned in chapter II before the accelerator mass spectrometry (AMS) ^{14}C measurement was carried out. The result has been converted into calendar years BP using the CALIB 5.0.1 software and calibrated for the reservoir effect by the intercal04 calibration curve with a 2σ uncertainty (Table 2).

5.6 Sea level observation in the Andaman Sea

Two sediment cores from mid shelf area (core 011207-02 core2 and 031207-22 core2 at the water of 55.4 m and 61.9 m, respectively) reveal a change from fluvial to marine sediment (unit V). This transition is marked by abruptly increasing Ti/Ca ratios that is typically for marine transgression

(Tjallingii et al., 2010). The transgressive surface is found at 107 cm and 82 cm core depth of core 011207-02 core2 and 031207-22 core2 respectively (Fig. 5). Hence, a slight age reversal in one wood sample from 82 cm core depth of core 031207-22 core2 (Table2) could be caused by sediment reworking during the transgression. Therefore, deglacial marine flooding of the Andaman Sea shelf occur around 13 cal ka BP by passing the present-day water depth of 63 m, which is quite similar to the flooding history of the Vietnam shelf in South China Sea (Tjallingii et al., 2014).

Table 2 AMS^{14}C dates from sediment core 021207-22

Lab code	Material type	Water Depth (m)	Sample depth (cm)	mg C	δ^{13}C (‰)	^{14}C age (yr BP)	Cal. age (yr BP: 2σ)
KIA45569	Wood [a]	61.9	82	3.1	-24.60±0.09	11439±53	13427-13178
KIA45569	Wood [b]	61.9	82	2.5	-25.85±0.15	11013±47	13080-12725
KIA45570	Wood	61.9	92	1.2	-28.64±0.20	11141±61	13202-12799

[a] *wood fraction 1*

[b] *wood fraction 2*

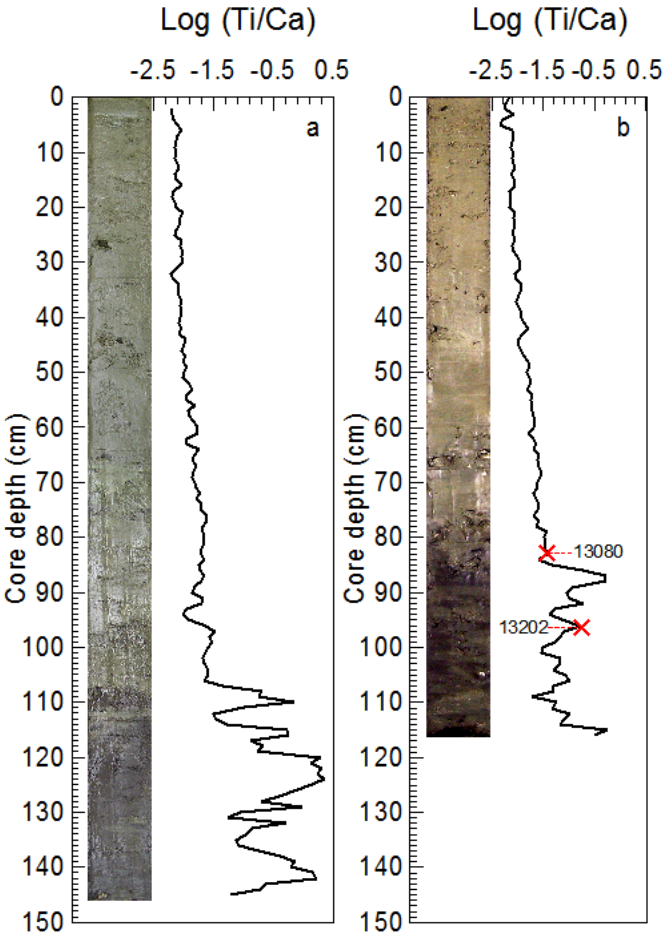

Fig. 5 Ti/Ca log ratio of sediment core a) 011207-02 core2 and b) 031207-22 core2 with calibrated age point in calendar years BP (red cross).

CHAPTER VI

COMPREHENSIVE CONCLUSIONS

Sediment samples from water depth between 5-65 m on the Andaman Sea continental shelf, offshore of Khao Lak (Thailand) have been investigated with sedimentological, geochemical and geophysical methods. This investigation is the first detail study to characterize the modern offshore tsunami deposits. Based on this study the major features of tsunami deposits on the Andaman Sea continental shelf due to the 2004 Indian Ocean tsunami were concluded:

The deposits were restricted to the shallow marine environment (water depths of 9-15 m) within 8 km of the shore line;

- Deposition occurred during the run-up phase, causing landward redeposition of marine sand and during backwash flow events, which deposited terrigeneous sediments. The transport and deposition of sediments were driven by several processes, including unidirectional flow in the various flow regimes and high-density sediment gravity flow;

- Typical features of tsunami deposits included a thickness in the order of 20-25 cm, a wide range of grain size and poor sorting, in contrast to underlying and overlying sediments, the presence of several layers, marine sand alternating with poorly sorted mud with terrigenous and anthropogenic components, representing different hydrodynamic conditions (probably during run-up and backwash phase). These observations were supported by geochemical and physical data, and were confirmed by ^{210}Pb dating;

- Comparisons with available data from offshore sediment cores (water depth > 30 m) showed that there is no single set of signatures that could be applied to identify these deposits.

With knowledge of tsunami deposits in shallow water and ^{210}Pb dating in conjunction with historical data of typhoons and tropical storms that passed the study area, distinguishing tsunami, storm and flash-flood or monsoon deposit is possible.

- The preserved sedimentary sequence includes several event layers deposited in the last 100 years that could be related to individual, historical storm events. Deposits of the 2004 Indian Ocean tsunami could be identified in water depth less than 16 m;

- Sedimentary features of the tsunami layer are highly variable both spatially and within individual cores and include lamination, fining or coarsening upward, a massive structure, erosional surfaces and clasts etc. Storm deposits in the same location commonly comprise of medium to poorly sorted sand without mud content;

- The most prominent difference between storm and tsunami deposits offshore Khao Lak area terrestrial component, anthropogenic artifacts, clasts and mud content that are not found within the storm deposits.

Based on hydroacoustic surveys, shallow-water reflection-seismic data, X-radiography, Ti/Ca log-ratio, ^{210}Pb and AMS^{14}C dating, and a number of sedimentological methods, the geological background and the stratigraphy offshore Khao Lak can be summarized:

- Five main sedimentary units are defined due to their genesis that was interpreted based on grain size distribution, digital radiographic images, water depth as well as the relative weight content of broken shells: unit I-III describe the main sedimentological characteristics of the inner shelf (between 9 m and 16 m water depth) while unit IV and V are found in the mid shelf setting (beneath 45 m down to 62 m water depth);

- The shelf has been characterized as wave dominated with a relatively low accumulation rate. The interpretation is confirmed by old drowned reefs found in offshore area covered with little recent hemipelagic sedimentation;
- The deglacial sea level rise in the Andaman Sea passed the level of 63 m about 13 cal ka BP, at the same time as reported from the Vietnam Shelf in South China Sea.

REFERENCES

Abrantes, F., Alt-Epping, U., Lebreiro, S., Voelker, A., Schneider, R.: Sedimentological record of tsunamis on shallow-shelf areas: The case of the 1969 AD and 1755 AD tsunamis on the Portuguese Shelf off Lisbon, *Marine Geology*, 249, 283-293, 2008.

Bahlburg, H., Spiske, M., Weiss, R.: Comment on "Sedimentary features of tsunami backwash deposits in a shallow marine Miocene setting, Mejillones Peninsula, northern Chile" by G. Cantalamessa and C. Di Celma [Sedimentary Geology 178 (2005) 259--273], *Sedimentary Geology*, 228, 77-80, 2010.

Bahr, A., Lamy, F., Arz, H., Kuhlmann, H., Wefe, G.: Late glacial to Holocene climate and sedimentation history in the NW Black Sea, *Marine Geology*, 214, 309-322, 2005.

Bell, R., Cowan, H., Dalziell, E., Evans, N., Ó Leary, M., Rush, B., Yule, L.: Survey of impacts on the Andaman Coast, Southern Thailand following the great Sumatra-Andaman earthquake and tsunami of December 26, 2004, *Bull. of The New Zealand Soc. For Earthquake Eng.*, 38, 123-148, 2005.

Best, A.I., Gunn, D.E.: Calibration of marine sediment core loggers for quantitative acoustic impedance studies, *Marine Geology*, 160, 137-146, 1999.

Blondel, P.: *The Handbook of Sidescan Sonar*. Springer, Berlin, Heidelberg, New York, 316 pp, 2009.

Blott, S.J., Pye, K.: Gradistat: a grain-size distribution and statistics package for the analysis of unconsolidated sediments. *Earth Surface Processes and Landforms*, 26, 1237-1248, 2001.

Bourgeois, J.: Geologic effects and records of tsunamis. In: Robinson, A.R., Bernard, E.N. (Eds.), *The Sea, Volume 15: Tsunamis*. Harvard University press, Amsterdam, pp. 53-91, 2009.

Brill, D., Brückner, H., Jankaew, K., Kelletat, D., Scheffers, A. and Scheffers, S.: Potential predecessors of the 2004 Indian Ocean Tsunami - Sedimentary evidence of extreme wave events at Ban Bang Sak, SW Thailand, *Sedimentary Geology*, 239, 146-161, 2011.

Cantalamessa, G., Celma, C.D.: Sedimentary features of tsunami backwash deposits in a shallow marine Miocene setting, Mejillones Peninsula, northern Chile, *Sedimentary Geology*, 178, 259-273, 2005.

Chagué-Goff, C., Schneider, J.L., Goff, J.R., Dominey-Howes, D., Strotz, L.: Expanding the proxy toolkit to help identify past events - Lessons from the 2004 Indian Ocean Tsunami and the 2009 South Pacific Tsunami, *Earth-Science Reviews*, 107, 107-122, 2011.

Choowong, M., Phantuwongraj, S., Charoentitirat, T., Chutakositkanon, V., Yumuang, S., Charusiri, P.: Beach recovery after 2004 Indian Ocean tsunami from Phang-nga, Thailand. *Geomorphology*, 104, 134-142, 2009.

Crokett, J.S., Nittrouer, C.A.: The sandy inner shelf as a repository for muddy sediment, an example from Northern California, *Continental Shelf Research*, 24, 55-73, 2004.

Curray, J.R.: Tectonics and history of the Andaman Sea region. *J. of Asian Earth Sciences*, 25, 187-232, 2005.

Dawson, A.G., Stewart, I.: Tsunami deposits in the geological record, *Sedimentary Geology*, 200, 166-183, 2007.

Di Geronimo, I., Choowong, M., Phantuwongraj, S.: Geomorphology and Superficial Bottom Sediments of KhaoLak Coastal Area (SW Thailand), *Polish Journal of Environmental Studies*, 18, 111-121, 2009.

Dutta, K., Bhushan, R., Somayajulu, B.L.K.: Rapid vertical mixing rates in deep waters of the Andaman Basin. *Sci. Total Eviron.*, 384, 401-408, 2007.

Feldens, P., Schwarzer, K., Szczuciński, W., Stattegger, K., Sakuna, D., Somgpongchaiykul, P.: Impact of 2004 Tsunami on Seafloor Morphology and Offshore Sediments, Pakarang Cape, Thailand, *Polish Journal of Environmental Studies*, 18, 63-68, 2009.

Feldens, P., Sakuna, D., Somgpongchaiykul, P., Schwarzer, K.: Shallow water structures in a tsunami-affected area (Pakarang Cape, Thailand), *Coastline Reports*, 16, 15-24, 2010.

Feldens, P., Schwarzer, K., Sakuna, D., Szczuciński, W., Somgpongchaiykul, P.: Identification of offshore tsunami deposits on the shelf off KhaoLak (Thailand), *Earth, Planets and Space*, 64, 875-887, 2012.

Fujiwara, O., Kamataki, T.: Identification of tsunami deposits considering the tsunami waveform, an example of subaqueous tsunami deposits in Holocene shallow bay on southern Bobo Penisular, Central Japan, *Sedimentary Geology*, 200, 295-313, 2007.

Geyer, W.R., Hill, P.S., Kineke, G.C.: The transport, transformation and dispersal of sediment by buoyant coastal flows, *Continental Shelf Research*, 24, 927-949, 2004.

Goodman-Tchernov, B.N., Dey, H.W., Reinhard, E.G., McCoy, F., Mart, Y.: Tsunami waves generated by the Santorini eruption reached Eastern Mediterranean shores, *Geology*, 37, 943-946, 2009.

Goto, K., Chavanich, S.A., Imamura, F., Kunthasap, P., Matsui, T., Minoura, K., Sugawara, D., Yanagisawa, H.: Distribution, origin and transport process of boulders deposited by the 2004 Indian Ocean tsunami at Pakarang Cape, Thailand, *Sedimentary Geology*, 202, 821-837, 2007.

Goto, K., Hashimoto, K., Sugawara, D., Yanagisawa, H., Abe, T.: Spatial thickness variability of the 2011 Tohoku-oki tsunami deposits along the coastline of Sendai Bay, *Marine Geology*, 358, 38-48, 2014a.

Goto, K., Ikehara, K., Goff, J., Chagué-Goff, C., Jaffe, B.: The 2011 Tohoku-oki tsunami - Three years on, *Marine Geology*, 358, 2-11, 2014b.

Goto, K., Takahashi, J., Oie, T., Imamura, F.: Remarkable bathymetric change in the nearshore zone by the 2004 Indian Ocean tsunami, Kirinda Harbor, Sri Lanka*, Geomorphology*, 127, 107-116, 2011.

Hanebuth, T., Stattegger, K., Grootes, P.M.: Rapid flooding of the Sunda shelf: a late-glacial sea-level record. *Science*, 288, 1033-1035, 2000.

Hawkes, A.D., Bird, M., Cowie, S., Grundy-Warr, C., Horton, B.P., Hwai, A., Law, L., Macgregor, C., Nott, J., Ong, J.E., Rigg, J., Robinson, R., Tan-Mullins, M., Sa, T.T., Yasin, Z., Aik, L.W.: Sediments deposited by the 2004 Indian Ocean Tsunami along the Malaysia-Thailand Penisula, *Marine Geology*, 242, 169-190, 2007.

Heise, B., Bobertz, B., Harff, J.: Classification of the Perl River Estuary via Principal Component Analysis and Regionalisation, *J. of Coastal Research*, 26, 769-779, 2010.

Hofmann, D.I., Fabian, K., Schneider, F., Donner, B., Bleil, U.: A stratigraphic network across the Subtropical Front in the central South Atlantic, Multi-parameter correlation of magnetic susceptibility, density, X-ray fluorescence and $\delta^{18}O$ records, *Earth and Planetary Science Letters*, 240, 694-709, 2005.

Ikehara, K., Irino, T., Usami, K., Jenkins, R., Omura, A. and Ashi, J.: Possible submarine tsunami deposits on the outer shelf of Sendai Bay, Japan resulting from the 2011 earthquake and tsunami off the Pacific coast of Tohoku, *Marine Geology*, 358, 120-127, 2014.

Jankaew, K., Atwater, B.F., Sawai, Y., Choowong, M., Charoentitirat, T., Martin, M.E., Prendergast, A.: Medieval forewarning of the 2004 Indian Ocean tsunami in Thailand, *Nature*, 455, 1228-1231, 2008.

Keller, G. H., Richards, A. F.: Sediments of the Malacca Strait, *Southeast Asia, J. Sediment. Res.*, 37, 102–127, 1967.

Kortekaas, S., Dawson, A.G.: Distinguishing tsunami and storm deposits: An example from Martinhal, SW Portugal, *Sedimentary Geology*, 200, 208-221, 2007.

Krumbein, W. C.: Size frequency distribution of sediments and the normal phi curve, *Journal of Sedimentary Petrology*, 8, 84-90, 1938.

Kuehl, S.A., Nittrouer, C.A., Allison, M.A., Ercilio, L., Faria, C., Dukat, D.A., Jaeger, J.M., Pacioni, T.D., Figueiredo, A.G., Underkoffler, E.C.: Sediment deposition, accumulation, and seabed dynamics in an energetic, fine-grained, coastal environment, *Continental Shelf Research*, 16, 787-815, 1985.

Lamy, F., Hebbeln, D., Röhl, U., Wefer, G.: Holocene rainfall variability in southern Chile, a marine record of latitudinal shifts of the Southern Westerlies, *Earth and Planetary Science Letters*, 185, 369-382, 2001.

Le Roux, J.P., Vargas, G.: Hydraulic behavior of tsunami backflows, insights from their modern and ancient deposits, *Environmental Geology*, 49, 65-75, 2005.

Luque, L., Lario, J., Zazo, C., Goy, J.L., Dabrio, C.J., Silva, P.G.: Tsunami deposits as paleoseismic indicators: examples from the Spanish coast, *Acta Geologica Hispanica*, 36, 197-211, 2001.

Marques, W.S., Sial, A.N., Menor, E.A., Ferreira, V.P., Freire, G.S.S., Lima, E.A.M., Manso, V.A.V.: Principal component analysis (PCA) and mineral associations of litoraneous facies of continental shelf carbonates from northeastern Brazil, *Continental Shelf Research*, 28, 2709-2717, 2008.

McKee, B.A., Nittrouer, C.A., DeMaster, D.J.: The concepts of sediment deposition and accumulation applied to the continental shelf near the mouth of the Yangtze River, *Geology*, 11, 631-633, 1983.

Milker, Y., Wilken, M., Schumann, J., Sakuna, D., Feldens, P., Schwarzer, K., Schmiedl, G.: Sediment transport on the inner shelf off KhaoLak (Andaman Sea, Thailand) during the 2004 Indian Ocean tsunami and former storm events, Evidence from foraminiferal transfer functions, *Nat. Hazards Earth Syst. Sci.*, 13, 3113-3128, 2013.

Morley, C. K., Charusiri, P., Watkinson, I.: Structural geology of Thailand during the Cenozoic, in: *The geology of Thailand*, edited by: Barber, A. J. and Ridd, F. D., Geological Society of London, London, United Kingdom, pp. 539–571, 2011.

Nadeau, M.J., Grootes, P.M., Schleicher, M., Hasselberg, P., Rieck, A., Bitterling, M.: Sample Throughput and data quality at the Leibniz-Labor AMS facility, *Radiocarbon*, 40, 239-245, 1988.

Nadeau, M.J., Schleicher, M., Grootes, P.M., Erlenkeuser, H., Gottdang, A., Mous, D.J.W., Sarnthein, J.M., Willkomm, H.: The Leibniz-Labor AMS facility at the Christian-Albrechts University, *Nuclear Instruments and Methods in Physics Research Section B, Kiel, Germany*, 123, 22-30, 1997.

Noda, A., Katayama, H., Sagayama, T., Suga, K., Uchida, Y., Satake, K., Abe, K., Okamura, Y.: Evaluation of tsunami impacts on shallow marine sediments: An example from the tsunami caused by the 2003 Tokachi-oki earthquake, northern Japan, *Sedimentary Geology*, 200, 314-327, 2007.

Ohta, T., Arai, H.: Statistical empirical index of chemical weathering in igneous rocks: A new tool for evaluating the degree of weathering, *Chemical Geology*, 240, 280-297, 2007.

Owen, R.B., Lee, R.: Human impacts on organic matter sedimentation in a proximal shelf setting, Hong Kong, *Continental Shelf Research*, 24, 583-602, 2004.

Palinkas, C.M., Nittrouer, C.A., Walsh, J.P.: Inner shelf sedimentation in the Gulf of Papua, New Guinea, a mud-rich shallow shelf setting, *Journal of Coastal Research*, 22, 760-772, 2006.

Paris, R., Fournier, J., Poizot, E., Etienne, S., Mortin, J., Lavigne, F., Wassmer, P.: Boulder and fine sediment transport and deposition by the 2004 tsunami in LhokNga (western Banda Aceh, Sumatra, Indonesia), A coupled offshore-onshore model, *Marine Geology*, 268, 43-54, 2010.

Ramaswamy, V., Rao, P.S., Rao, K.K., Swe Thwin, Rao, N.S., Raiker, V.: Tidal influence on suspended sedimen distribution and dispersal in the northern Andaman Sea and Gulf Martaban, *Marine Geology*, 208, 33-42, 2004.

Rao, P.S., Ramaswamy, V., Thwin, S.: Sediment texture, distribution and transport on the Ayeyarwady continental shelf, Andaman Sea. *Marine Geology*, 216, 239-247, 2005.

Reid, M.K., Spencer, K.L.: Use of principal components analysis (PCA) on estuarine sediment datasets: The effect of data pre-treatment, *Environmental Pollution*, 157, 2275-2281, 2009.

Reimer, P.J., Baillie, M.G.L., Bard, E., Bayliss, A., Beck, J.W., Bertrand, C.J.H., Blackwell, P.G., Buck, C.E., Burr, G.S., Cutler, K.B., Damon, P.E., Edwards, R.L., Fairbanks, R.G., Friedrich, M., Guilderson, T.P., Hogg, A.G., Hughen, K.A., Kromer, B.,McCormac, F.G., Manning, S.W., Ramsey, C.B., Reimer, R.W., Remmele, S., Southon, J.R., Stuiver, M., Talamo, S., Taylor, F.W., van der Plicht, J., Weyhenmeyer, C.E.: IntCal04 Terrestrial radiocarbon age calibration, 26-0 ka BP, *Radiocarbon*, 46, 1029-1058, 2004.

Rizal, S., Damm, P., Wahid, M.A., Sundermann, J., Ilhamsyah, Y., Iskandar, T., Muhammad, T.: General circulation in the Malacca Strait and Andaman Sea: A numerical model study. *American J. of Environmental Science*, 8, 479-488, 2012.

Robbins, J.A., Edgington, D.N.: Determination of recent sedimentation rates in Lake Michigan using Pb-210 and Cs-137, *Geochimica et Cosmochimica Acta*, 39, 285-304, 1975.

Rodolfo, K.S.: Bathymetry and Marine Geology of the Andaman Basin, and Tectonic Implications for Southeast Asia, *Geological Society of America Bulletin*, 80, 1203-1230, 1969.

Sakuna, D., Szczuciński, W., Feldens, P., Schwarzer, K., Khokiattiwong, S.: Sedimentary deposits left by the 2004 Indian Ocean tsunami on the inner continental shelf offshore of KhaoLak, Andaman Sea (Thailand), *Earth, Planets and Space*, 64, 931-943, 2012.

Sakuna-Schwartz, D., Feldens, P., Schwarzer, K., Khokiattiwong, S., Stattegger, K.: Internal structure of event layers preserved on the Andaman Sea continental shelf, Thailand: Tsunami vs. Storm and Flash-flood deposits, *Nat. Hazards Earth Syst. Sci.*, 15, 1181-1199, 2015.

Sawai Y., Jankaew, K., Martin, M.E., Prendergast, A., Choowong, M., Charoentitirat, T.: Diatom assemblages in tsunami deposits associated with the 2004 Indian Ocean tsunami at Phra Thong Island, Thailand, *Marine Micropaleontology*, 73, 70-79, 2009.

Scheffers, A., Kelletat, D.: Sedimentological and geomorphologic tsunami imprints worldwide- a review, *Earth-Science Reviews*, 63, 83-92, 2003.

Schimanski, A., Stattegger, K.: Deglacial and holocene evolution of the vietnam shelf: stratigraphy, sediments and sea-level change, *Marine Geology*, 214, 365-387, 2005.

Schwab, J.M., Krastel, S., Grün, M., Gross, F., Pananont, P., Jintasaeranee, P., Bunsomboonsakul, S., Weinrebe, W., Winkelmann, D.: Submarine mass wasting and associated tsunami risk offshore western Thailand, Andaman Sea, Indian Ocean. *Nat. Hazards Earth Syst. Sci.*, 12, 2609-2630, 2012.

Schwarzer, K., Feldens, P., Sakuna-Schwartz, D., Pongpiachan, S., Milker, Y., Tipmanee, D.: Identification of tsunami deposits offshore in the Andaman Sea by different proxies. In: Wang, P., Rosati, J.D., Cheng, J. (Eds.), *The Proceedings of the Coastal Sediments 2015*. San Diego, 11-15 May, World Scientific, doi: 10.1142/9789814689977_0184, 2015.

Shanmugam, G.: Process-sedimentological challenges in distinguishing paleo-tsunami deposits, *Natural Hazards*, 63, 5-30, 2011.

Smedile, A., De Martini, P.M., Pantosti, D., Bellucci, L., Del Carlo, P., Gasperini, L., Pirrotta, C., Polonia, A., Boschi, E.: Possible tsunami signatures from an integrated study in the Augusta Bay offshore (Eastern Sicily-Italy), *Marine Geology*, 281, 1-13, 2011.

Stuiver, M., Reimer, P.J.: Extended ^{14}C data-base and revised calib 3.0 ^{14}C age calibration program, *Radiocarbon*, 35, 215-230, 1993.

Sugawara, D., Minoura, K., Nemoto, N., Tsukawaki, S., Goto, K., Imamura, F.: Foraminiferal evidence of submarine sediment transport and deposition by backwash during the 2004 Indian Ocean tsunami), *Island Arc*, 18, 513-525, 2009.

Sugawara, D., Takahashi, T. and Imamura, F.: Sediment transport due to the 2011 Tohoku-oki tsunami at Sendai: Results from numerical modeling, *Marine Geology*, 358, 18-37, 2014.

Szczuciński, W., Chaimanee, N., Niedzielski, P., Rachlewicz, G., Saisuttichai, D., Tepsuwan,T., Lorenc, S., Siepak, J.: Environmental and Geological Impacts of the 26 December 2004 Tsunami in Coastal Zone of Thailand - Overview of Short and Long-Term Effects, *Polish Journal of Environmental Studies*, 15, 793-810, 2006.

Tjallingii, R., Stattegger, K., Wetzel, A., Phach, P.V.: Infilling and flooding of the Mekong River incised valley during deglacial sea-level rise, *Quaternary Science Reviews*, 29, 1432-1444, 2010.

Tjallingii, R., Stattegger, K., Stocchi, P., Saito, Y., Wetzel, A.: Rapid flooding of the southern Vietnam shelf during the early to mid-Holocene. *Journal of Quaternary Science*, 29, 581-588, 2014.

Tsuji, Y., Namegaya, Y., Matsumoto, H., Iwasaki, S.I., Kanbua, W., Sriwichai, M., Meesuk, V.: The 2004 Indian tsunami in Thailand: surveyed runup heights and tide gauge records, *Earth, Planets and Space*, 58: 223-232, 2006.

Uchida J.I., Fujiwara, O., Hasegawa, S., Kamataki, T.: Sources and depositional processes of tsunami deposits: Analysis using foraminiferal tests and hydrodynamic verification*, Island Arc*, 19, 427-442, 2010.

Usiriprisan, C., Chiemchindaratana, S., Shoosuwan, S. and Chatrapakpong, Y.: *Offshore exploration for tin and heavy minerals in the Andaman Sea*, Department of Mineral Resources, Bangkok and UNDP, New York, 224 pp., 1987.

van den Bergh, G. D., Boer, W., de Haas, H., van Weering, Tj. C. E., van Wijhe, R.: Shallow marine tsunami deposits in Teluk Banten (NW Java, Indonesia), generated by the 1883 Krakatau eruption, *Marine Geology*, 197, 13-34, 2003.

Weber, M.E., Niessen, F., Kuhn, G., Wiedicke, M.: Calibration and application of marine sedimentary physical properties using a multi-sensor core logger, *Marine Geology*, 136, 151-172, 1997.

Wolanski, E., Spagnol, S.: Environmental degradation by mud in tropical estuaries, *Regional Environmental Change*, 1, 152-162, 2000.

Wright, L.D., Nittrouer, C.A.: Dispersal of river sediments in coastal seas, six contrasting cases, *Estuaries*, 18, 494-508, 1995.

Wyrtki, K.: *Physical Oceanography of the Southeast Asian waters. Scripps Institution of Oceanography*. UC San Diego: Scripps Institution of Oceanography. Retrieved from: http://escholarship.org/uc/item/49n9x3t4, 1961.

ACKNOWLEDGEMENT

I always fascinated to do research in the field of sedimentology. Although I did my undergraduate studies in chemical oceanography, now I did get the chance to fulfill my wish. For that, I thank Dr. Klaus Schwarzer and Prof. Dr. Karl Stattegger. Through their engaging scientific discussions, I have managed to grasp vast amounts of knowledge in the sedimentology which I gratefully appreciate and will certainly be helpful for my future undertakings. The efforts taken by Dr. Peter Feldens to mentor me during my PhD work will not be easily forgotten. I thank him sincerely for investing his precious time in assisting me whenever I needed help and foremost, for his friendship.

Dr. Witek Szczuciński for an excellent advice, and all the support he gave me especially during my first paper. The discussion of the data together with Witek had a great influence on the interpretation of Pb210-dating and tsunami deposit offshore in this thesis. You are a great teacher!!!

I also owe a great deal of gratitude to Dr. Warner Brückmann and Janne Lorenzen for the MSCL measurements and to Dr. Rik Tjallingii for teaching me how to measure with the XRF scanner. Many thanks as well to Dr. Nils Anderson for conducting Pb210 analyses.

Next I like to thank staffs at PMBC for all their help and organized throughout the three year duration of filed campaigns in the Andaman Sea. Many thanks as well to the crews of RV Boonlerd and MV Fasai, who always helped us whenever needed. I am also deeply obliged to thank Dr. Somkiat Khokiattiwong, my boss in PMBC and Prof. Dr. Claudio Richter at AWI without their kindly support, my study in Germany won't exit.

This work was also made possible with the support of Daniel Unverricht, with whom I spent a lot of time arguing about numerous scientific and non-scientific subjects. I also express my gratitude to my friends at the Sedimentology, Coastal- and Continental Shelf Research group for their excellent collaboration and friendship. To Reiner and Rattana Rocynski and Wisanukorn Poonchai, I am indebted for their kindly hospitality, which made my stay at their home in Hamburg feel like my own home.

Finally, and this is very important for me, I am very grateful thank to my parents, my brother Oat and my dearest husband Frederico, for all their loving support through all my study time, especially over the last year which have not always been easy.

APPENDIX

CORE CATALOG

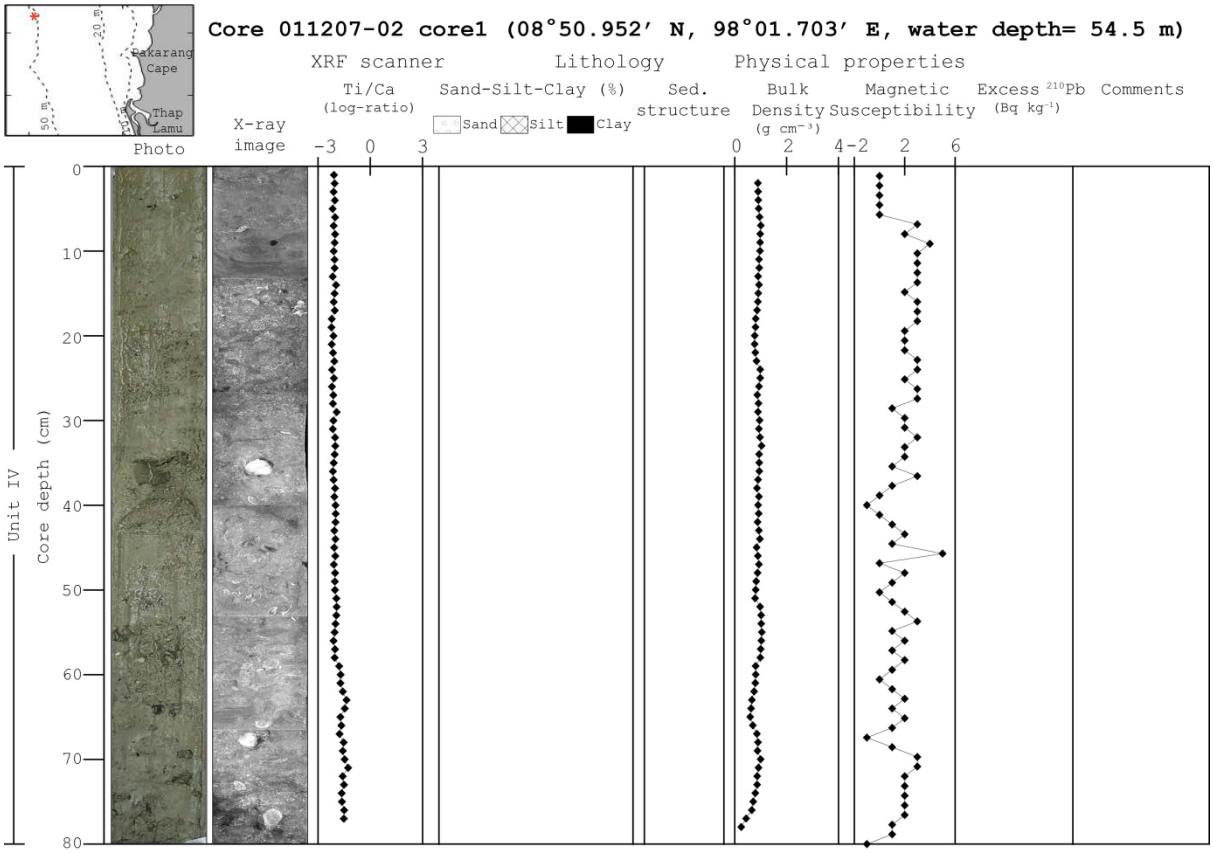
Core 011207-02 core1 (08°50.952′ N, 98°01.703′ E, water depth= 54.5 m)
XRF scanner
Lithology
Physical properties
Ti/Ca (log-ratio)
Sand-Silt-Clay (%)
Sand
Silt
Clay
Sed. structure
Bulk Density (g cm⁻³)
Magnetic Susceptibility
Excess ²¹⁰Pb (Bq kg⁻¹)
Comments
X-ray image
Photo
Core depth (cm)
Unit IV
Pakarang Cape
Thap Lamu
20 m
50 m

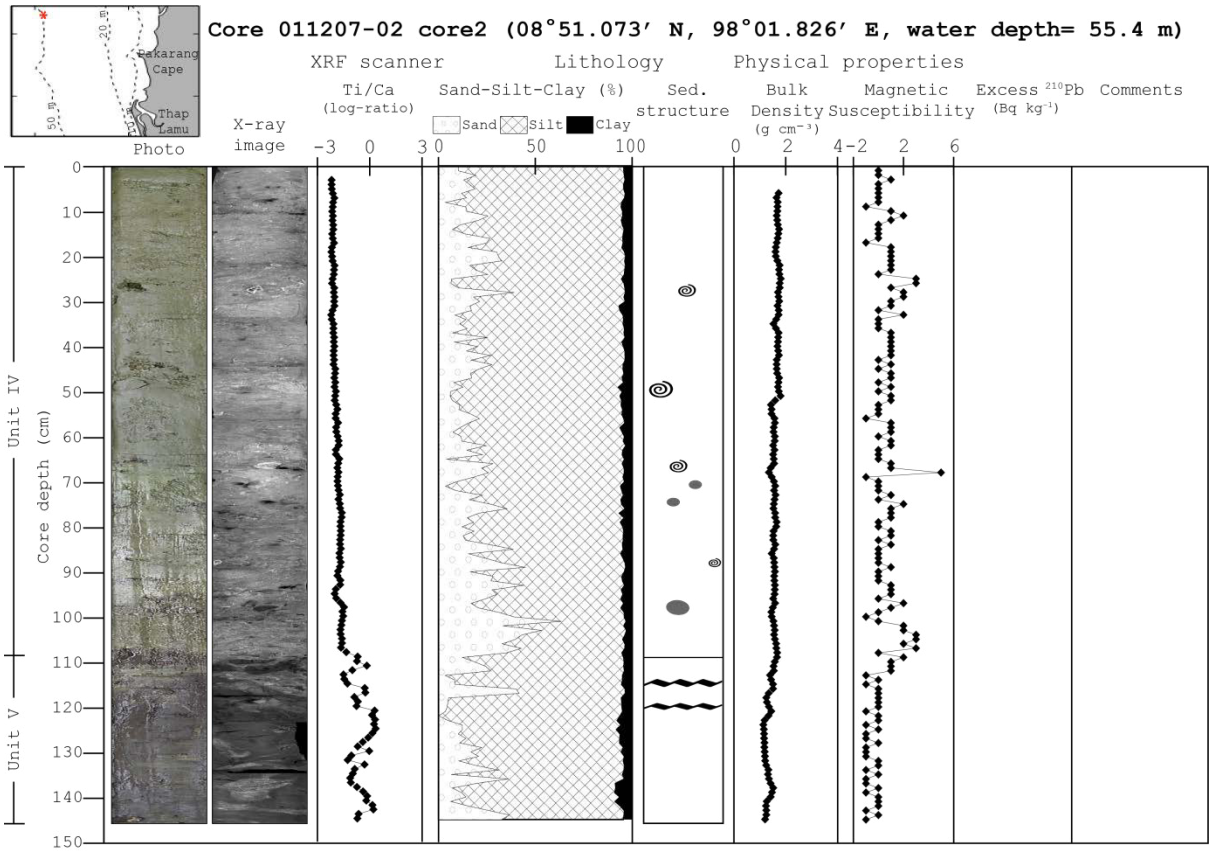
Core 011207-02 core2 (08°51.073′ N, 98°01.826′ E, water depth= 55.4 m)
XRF scanner
Lithology
Physical properties
Ti/Ca (log-ratio)
Sand-Silt-Clay (%)
Sand
Silt
Clay
Sed. structure
Bulk Density (g cm⁻³)
Magnetic Susceptibility
Excess ²¹⁰Pb (Bq kg⁻¹)
Comments
X-ray image
Photo
Core depth (cm)
Unit IV
Unit V
Pakarang Cape
Thap Lamu
20 m
50 m

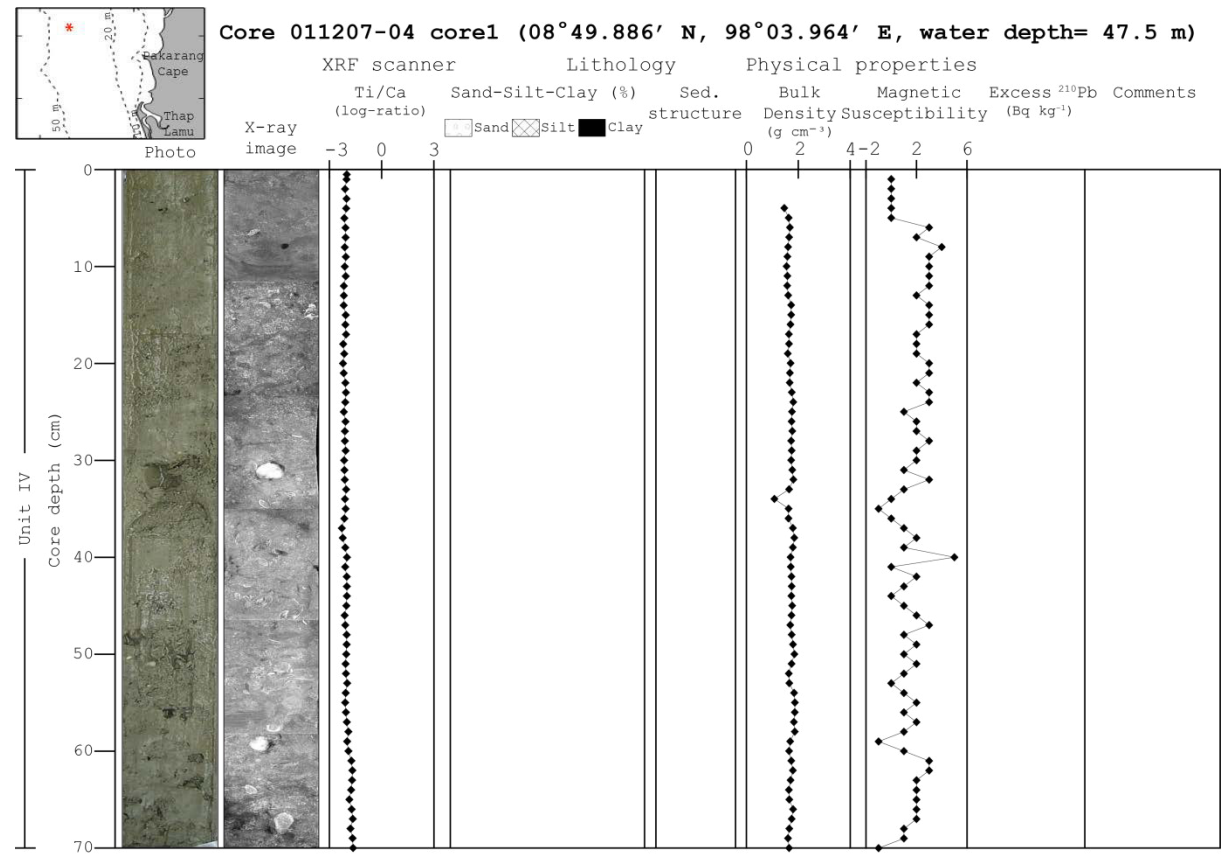
Core 011207-04 core1 (08°49.886′ N, 98°03.964′ E, water depth= 47.5 m)
XRF scanner
Lithology
Physical properties
Ti/Ca (log-ratio)
Sand-Silt-Clay (%)
Sand
Silt
Clay
Sed. structure
Bulk Density (g cm⁻³)
Magnetic Susceptibility
Excess ²¹⁰Pb (Bq kg⁻¹)
Comments
X-ray image
Photo
Unit IV
Core depth (cm)
Pakarang Cape
Thap Lamu
50 m
20 m

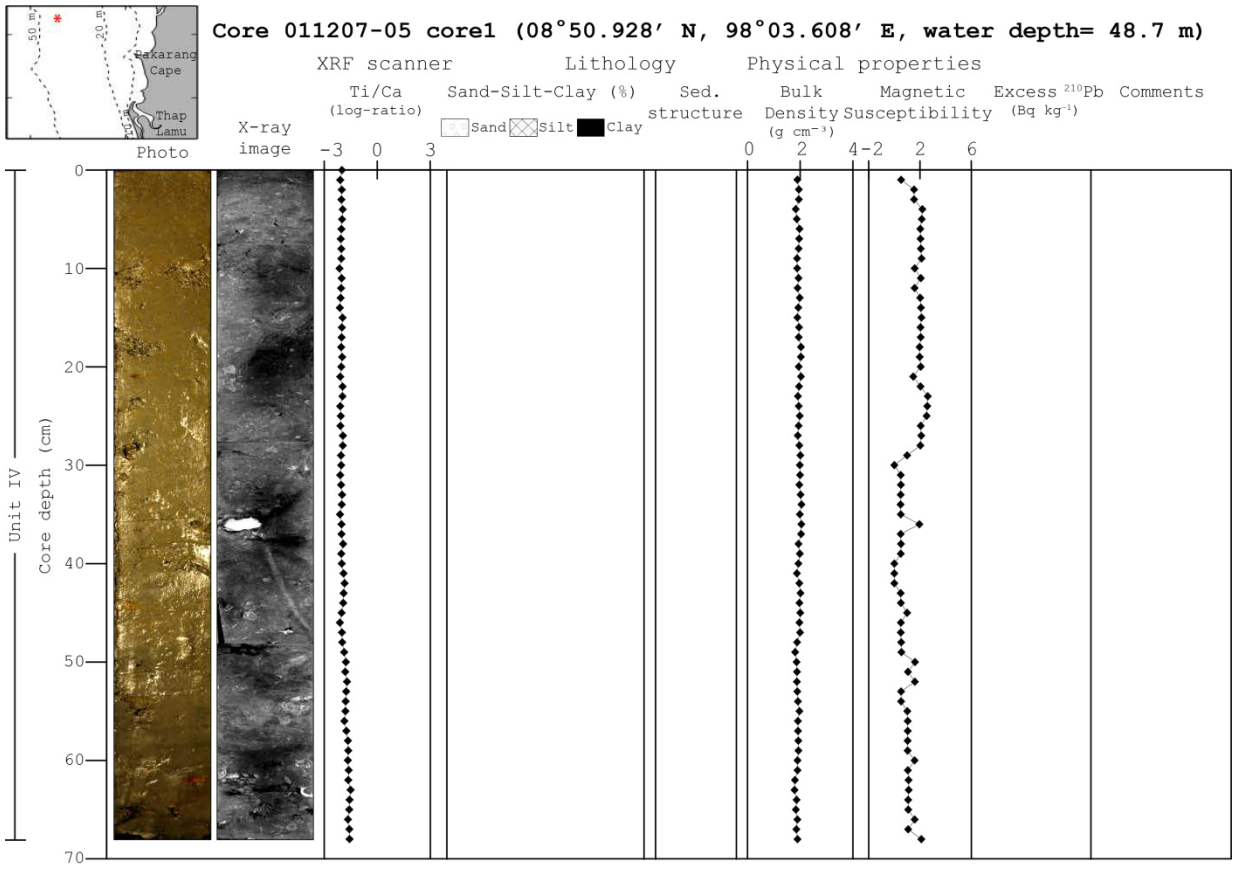
Core 011207-05 core1 (08°50.928′ N, 98°03.608′ E, water depth= 48.7 m)
XRF scanner
Lithology
Physical properties
Ti/Ca (log-ratio)
Sand-Silt-Clay (%)
Sand
Silt
Clay
Sed. structure
Bulk Density (g cm⁻³)
Magnetic Susceptibility
Excess ²¹⁰Pb (Bq kg⁻¹)
Comments
X-ray image
Photo
Unit IV
Core depth (cm)
Pakarang Cape
Thap Lamu
50 m
20 m

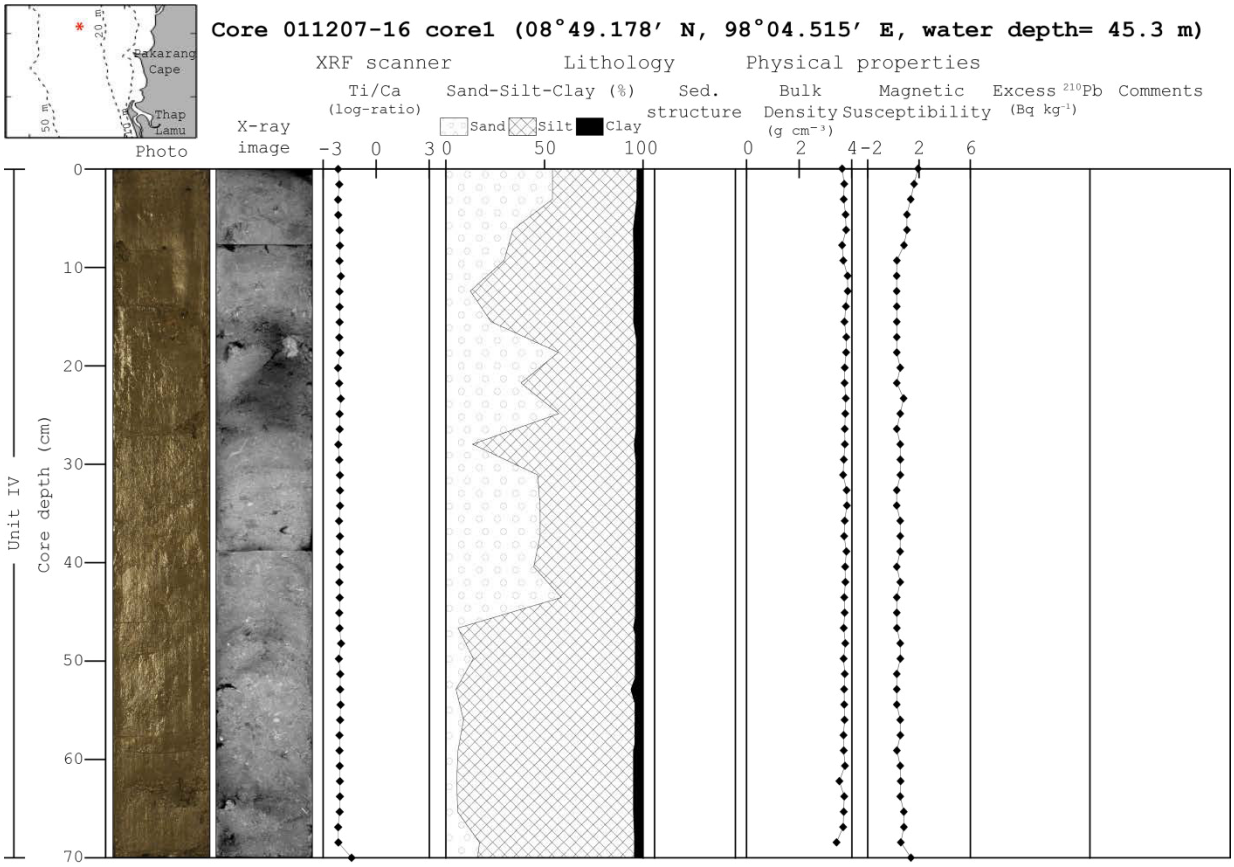
Core 011207-16 core1 (08°49.178′ N, 98°04.515′ E, water depth= 45.3 m)
XRF scanner
Lithology
Physical properties
Ti/Ca (log-ratio)
Sand-Silt-Clay (%)
Sand
Silt
Clay
Sed. structure
Bulk Density (g cm⁻³)
Magnetic Susceptibility
Excess ²¹⁰Pb (Bq kg⁻¹)
Comments
X-ray image
Photo
Core depth (cm)
Unit IV
Pakarang Cape
Thap Lamu
20 m
50 m

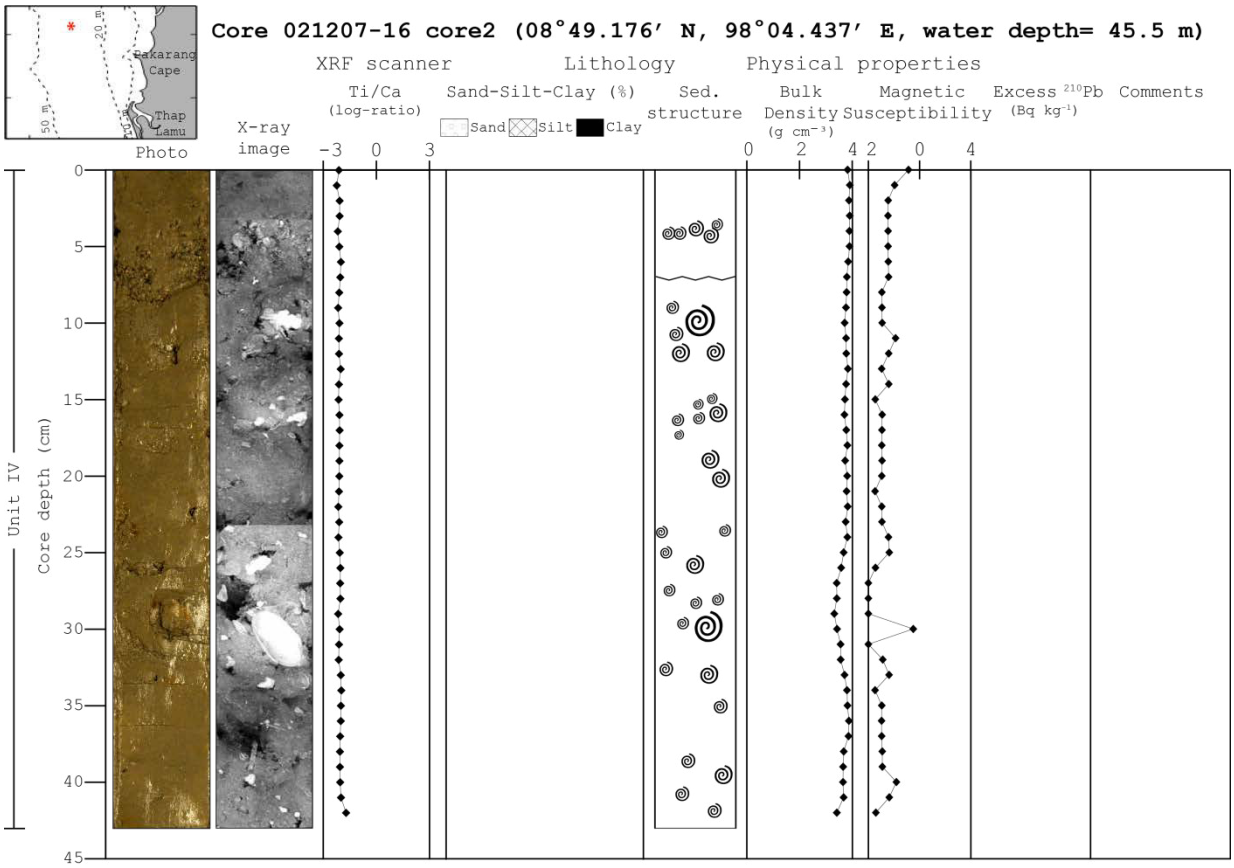
Core 021207-16 core2 (08°49.176′ N, 98°04.437′ E, water depth= 45.5 m)
XRF scanner
Lithology
Physical properties
Ti/Ca (log-ratio)
Sand-Silt-Clay (%)
Sand
Silt
Clay
Sed. structure
Bulk Density (g cm⁻³)
Magnetic Susceptibility
Excess ²¹⁰Pb (Bq kg⁻¹)
Comments
X-ray image
Photo
Core depth (cm)
Unit IV
Pakarang Cape
Thap Lamu
20 m
50 m

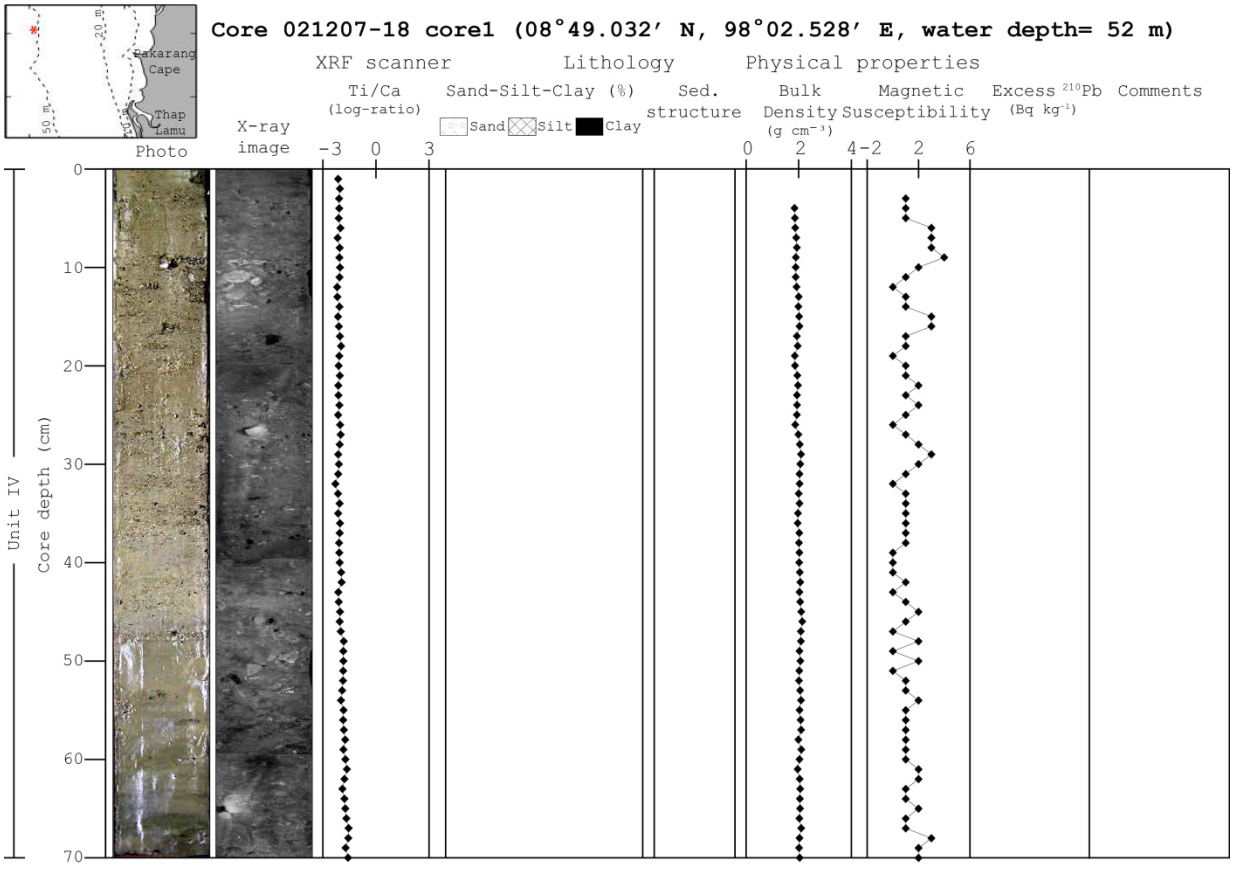
Core 021207-18 core1 (08°49.032′ N, 98°02.528′ E, water depth= 52 m)
XRF scanner
Lithology
Physical properties
Ti/Ca (log-ratio)
Sand-Silt-Clay (%)
Sand
Silt
Clay
Sed. structure
Bulk Density (g cm⁻³)
Magnetic Susceptibility
Excess ²¹⁰Pb (Bq kg⁻¹)
Comments
X-ray image
Photo
Core depth (cm)
Unit IV
Pakarang Cape
Thap Lamu
20 m
50 m

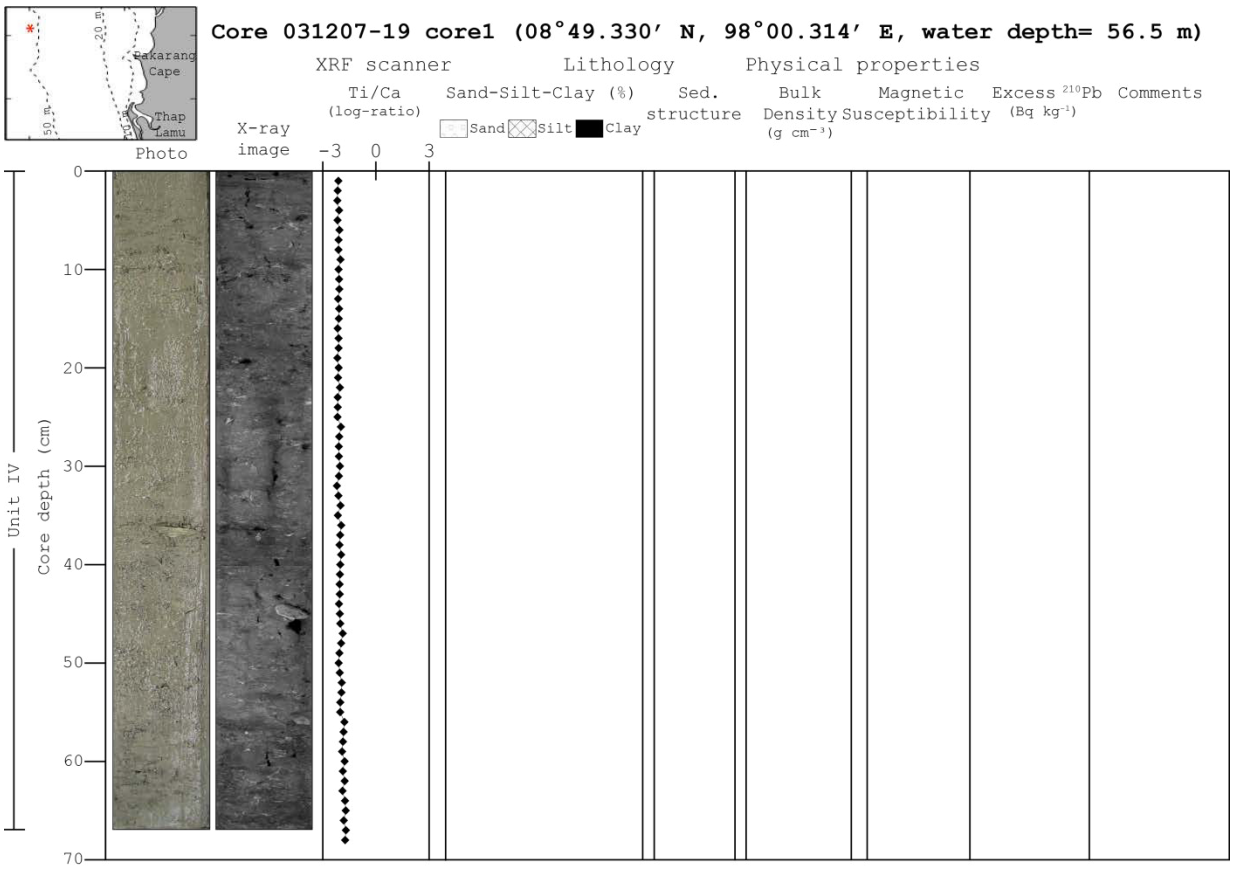
Core 031207-19 core1 (08°49.330′ N, 98°00.314′ E, water depth= 56.5 m)
XRF scanner
Lithology
Physical properties
Ti/Ca (log-ratio)
Sand-Silt-Clay (%)
Sand
Silt
Clay
Sed. structure
Bulk Density (g cm⁻³)
Magnetic Susceptibility
Excess ²¹⁰Pb (Bq kg⁻¹)
Comments
X-ray image
Photo
Core depth (cm)
Unit IV
Pakarang Cape
Thap Lamu
20 m
50 m

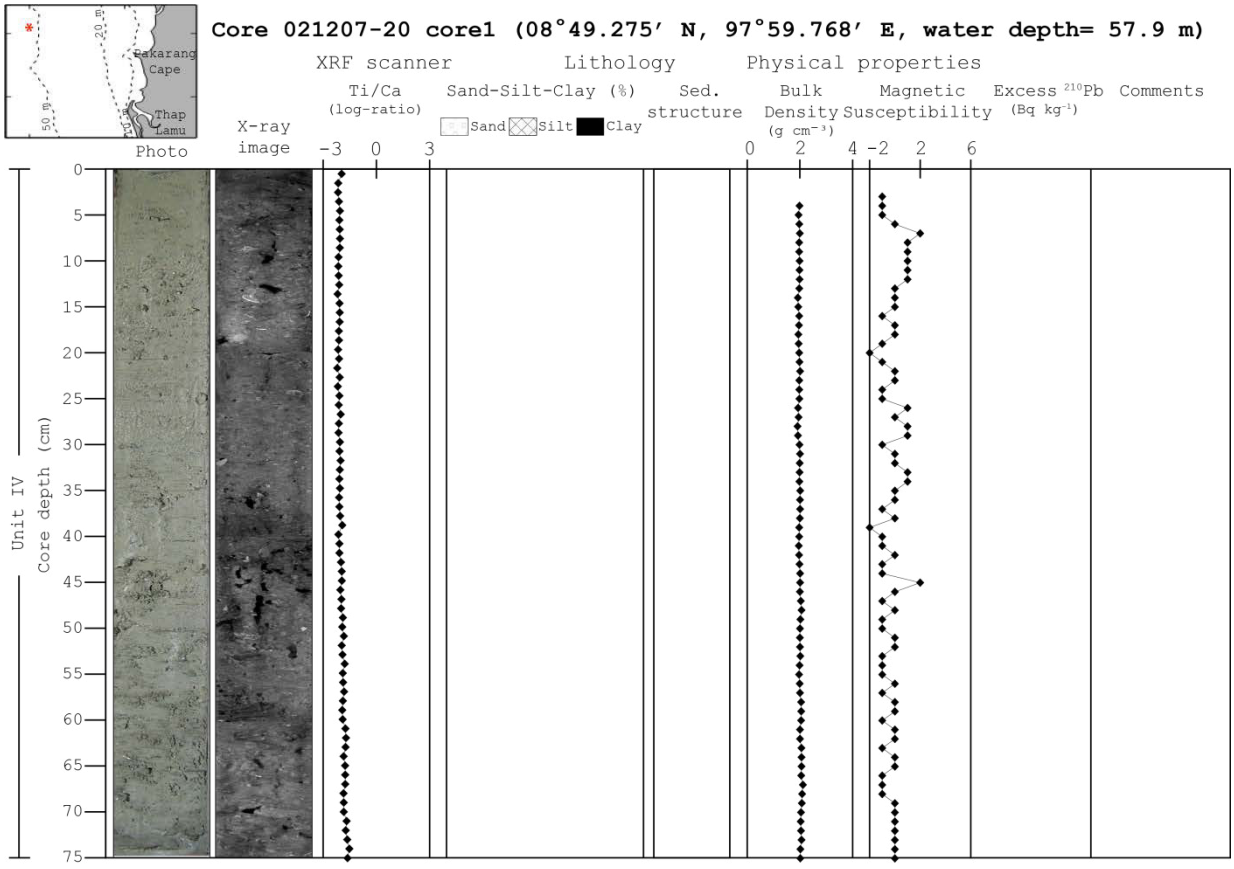
Core 021207-20 core1 (08°49.275′ N, 97°59.768′ E, water depth= 57.9 m)
XRF scanner
Lithology
Physical properties
Ti/Ca (log-ratio)
Sand-Silt-Clay (%)
Sand
Silt
Clay
Sed. structure
Bulk Density (g cm⁻³)
Magnetic Susceptibility
Excess ²¹⁰Pb (Bq kg⁻¹)
Comments
X-ray image
Photo
Core depth (cm)
Unit IV
Pakarang Cape
Thap Lamu
20 m
50 m

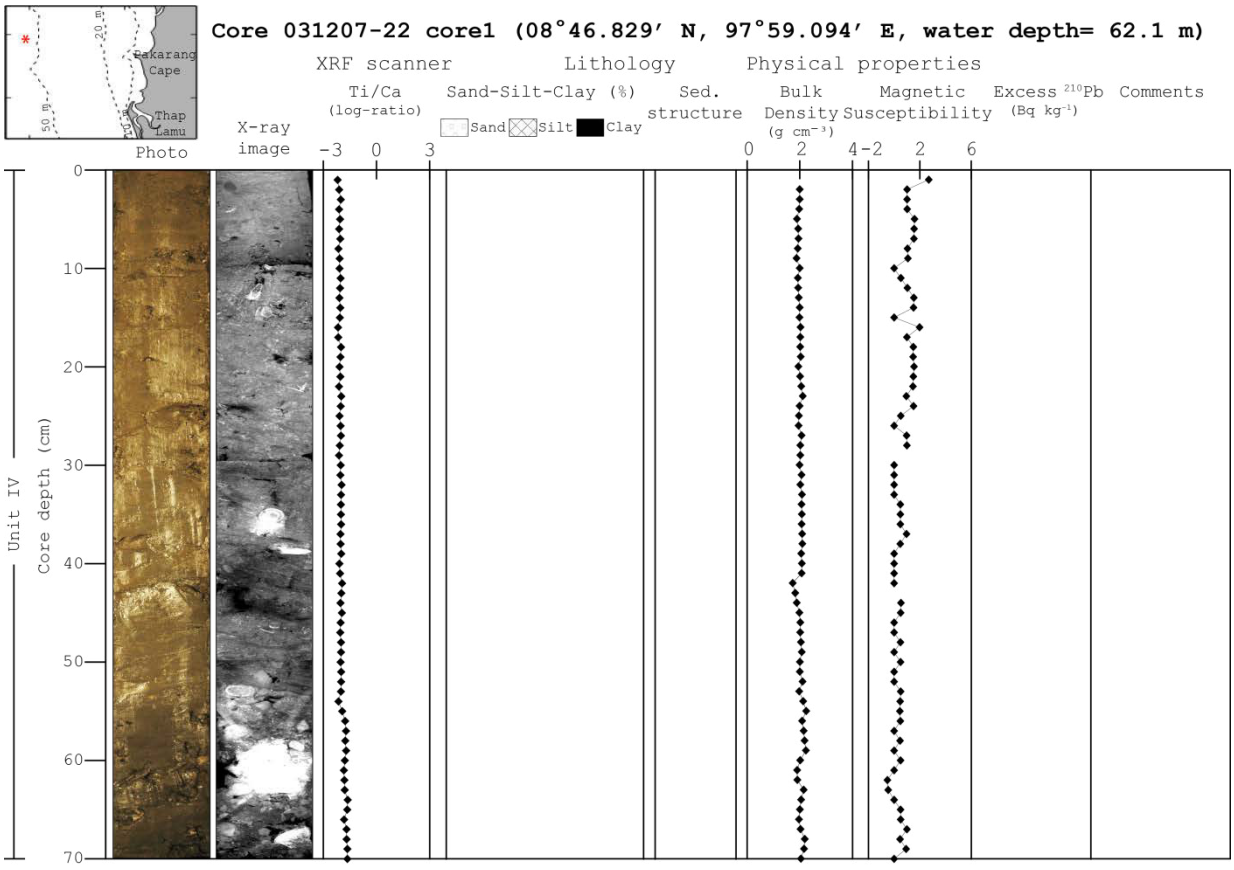
Core 031207-22 core1 (08°46.829′ N, 97°59.094′ E, water depth= 62.1 m)
XRF scanner
Lithology
Physical properties
Ti/Ca (log-ratio)
Sand-Silt-Clay (%)
Sand
Silt
Clay
Sed. structure
Bulk Density (g cm⁻³)
Magnetic Susceptibility
Excess ²¹⁰Pb (Bq kg⁻¹)
Comments
X-ray image
Photo
Core depth (cm)
Unit IV
Pakarang Cape
Thap Lamu
20 m
50 m

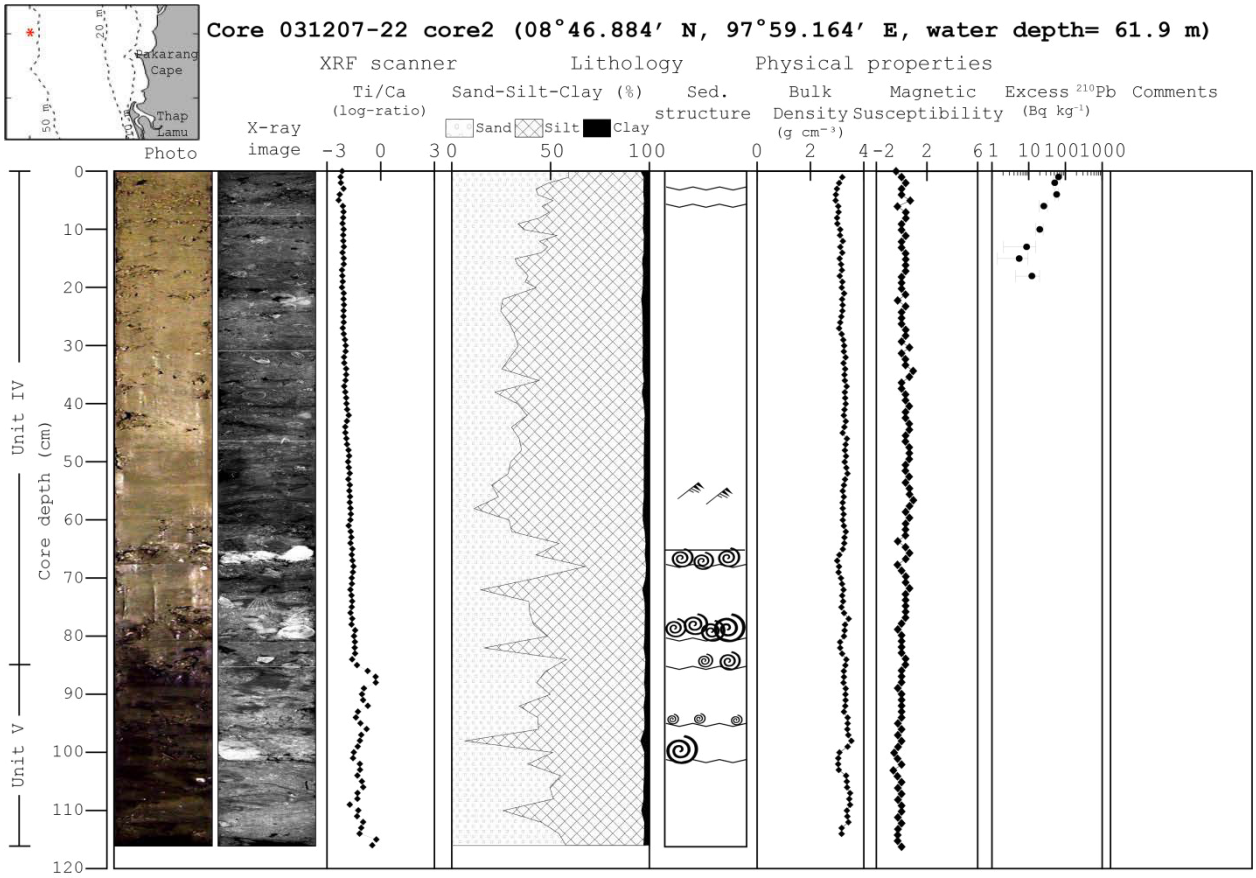
Core 031207-22 core2 (08°46.884′ N, 97°59.164′ E, water depth= 61.9 m)
XRF scanner
Lithology
Physical properties
Ti/Ca (log-ratio)
Sand-Silt-Clay (%)
Sand
Silt
Clay
Sed. structure
Bulk Density (g cm⁻³)
Magnetic Susceptibility
Excess ²¹⁰Pb (Bq kg⁻¹)
Comments
X-ray image
Photo
Pakarang Cape
Thap Lamu
20 m
50 m
Unit IV
Unit V
Core depth (cm)

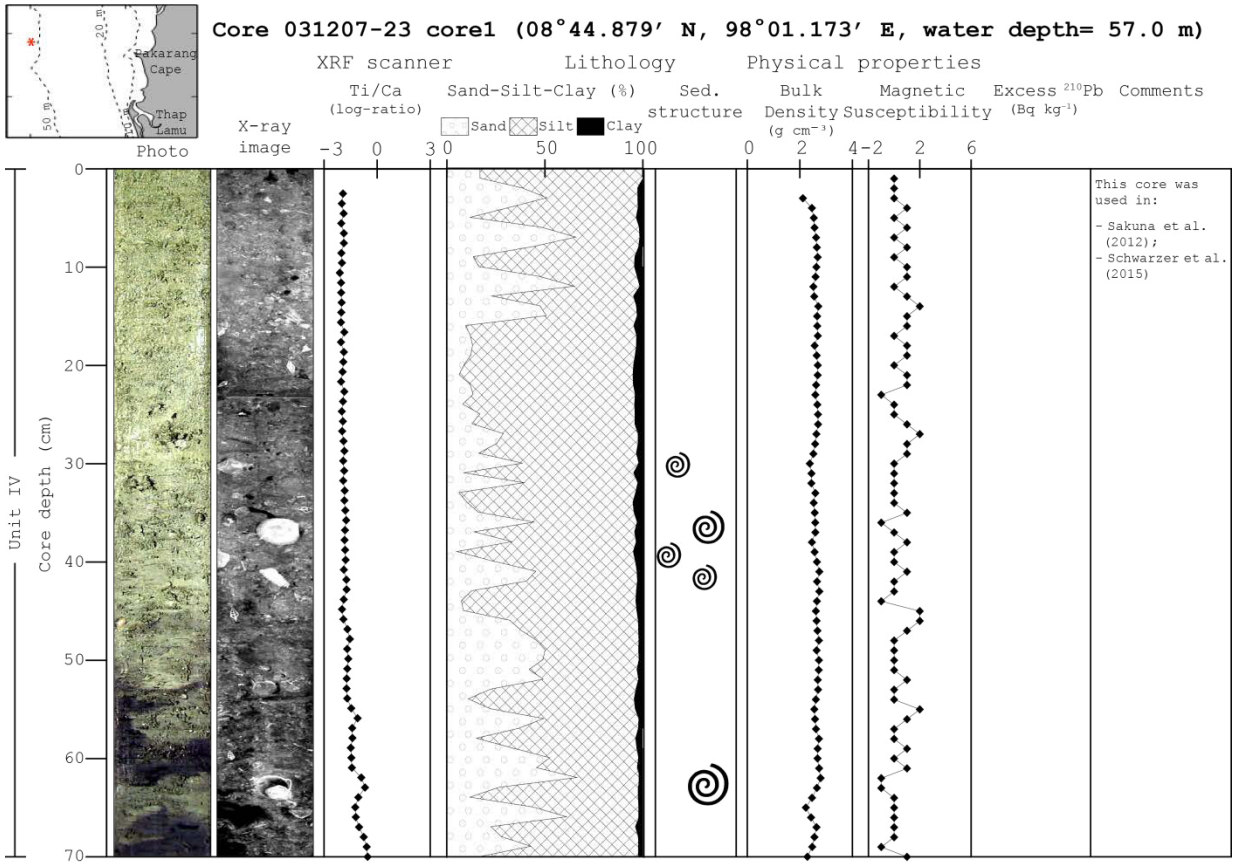
Core 031207-23 core1 (08°44.879′ N, 98°01.173′ E, water depth= 57.0 m)
XRF scanner
Lithology
Physical properties
Ti/Ca (log-ratio)
Sand-Silt-Clay (%)
Sand
Silt
Clay
Sed. structure
Bulk Density (g cm⁻³)
Magnetic Susceptibility
Excess ²¹⁰Pb (Bq kg⁻¹)
Comments
X-ray image
Photo
Pakarang Cape
Thap Lamu
20 m
50 m
Unit IV
Core depth (cm)
This core was used in:
- Sakuna et al. (2012);
- Schwarzer et al. (2015)

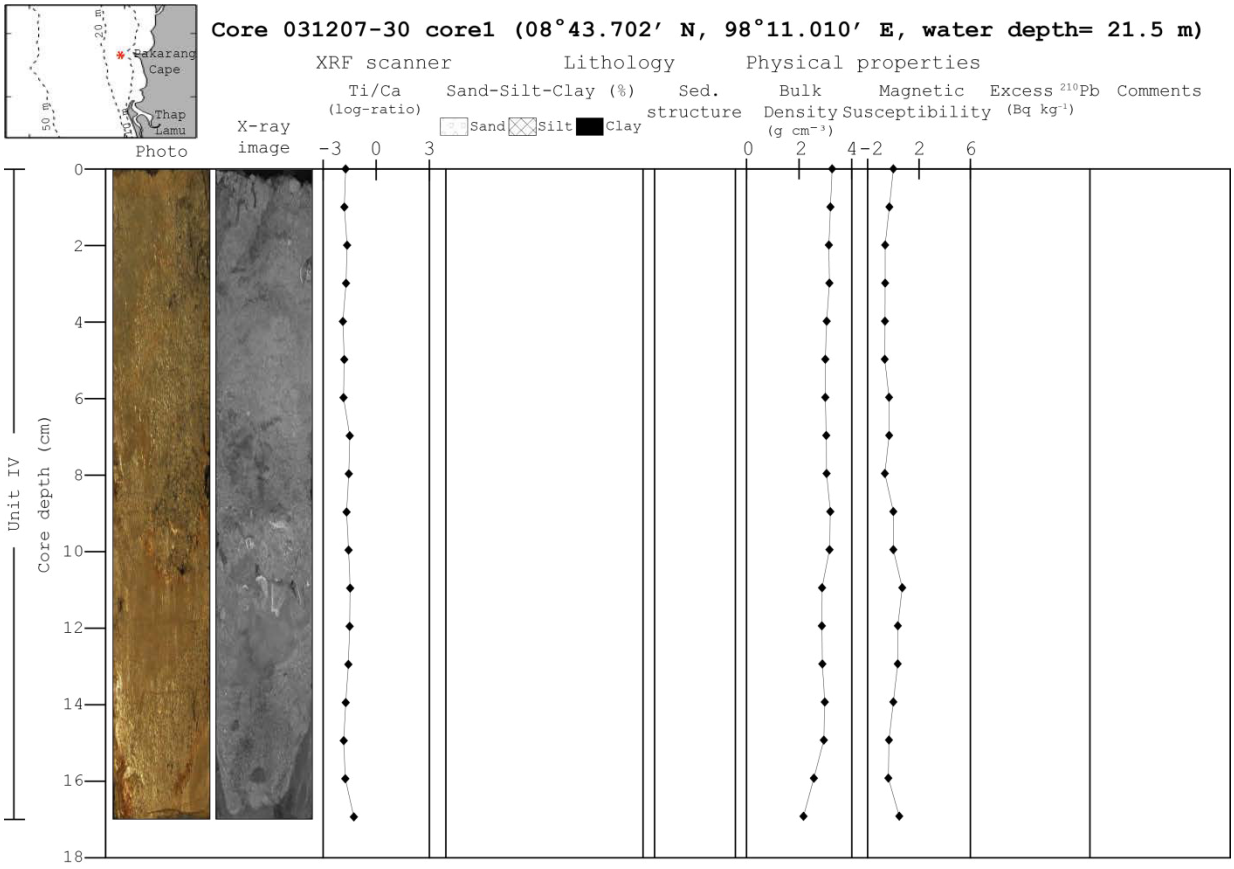
Core 031207-30 core1 (08°43.702′ N, 98°11.010′ E, water depth= 21.5 m)
XRF scanner
Lithology
Physical properties
Ti/Ca (log-ratio)
Sand-Silt-Clay (%)
Sand
Silt
Clay
Sed. structure
Bulk Density (g cm⁻³)
Magnetic Susceptibility
Excess ²¹⁰Pb (Bq kg⁻¹)
Comments
X-ray image
Photo
Core depth (cm)
Unit IV
Bakarang Cape
Thap Lamu
20 m
50 m

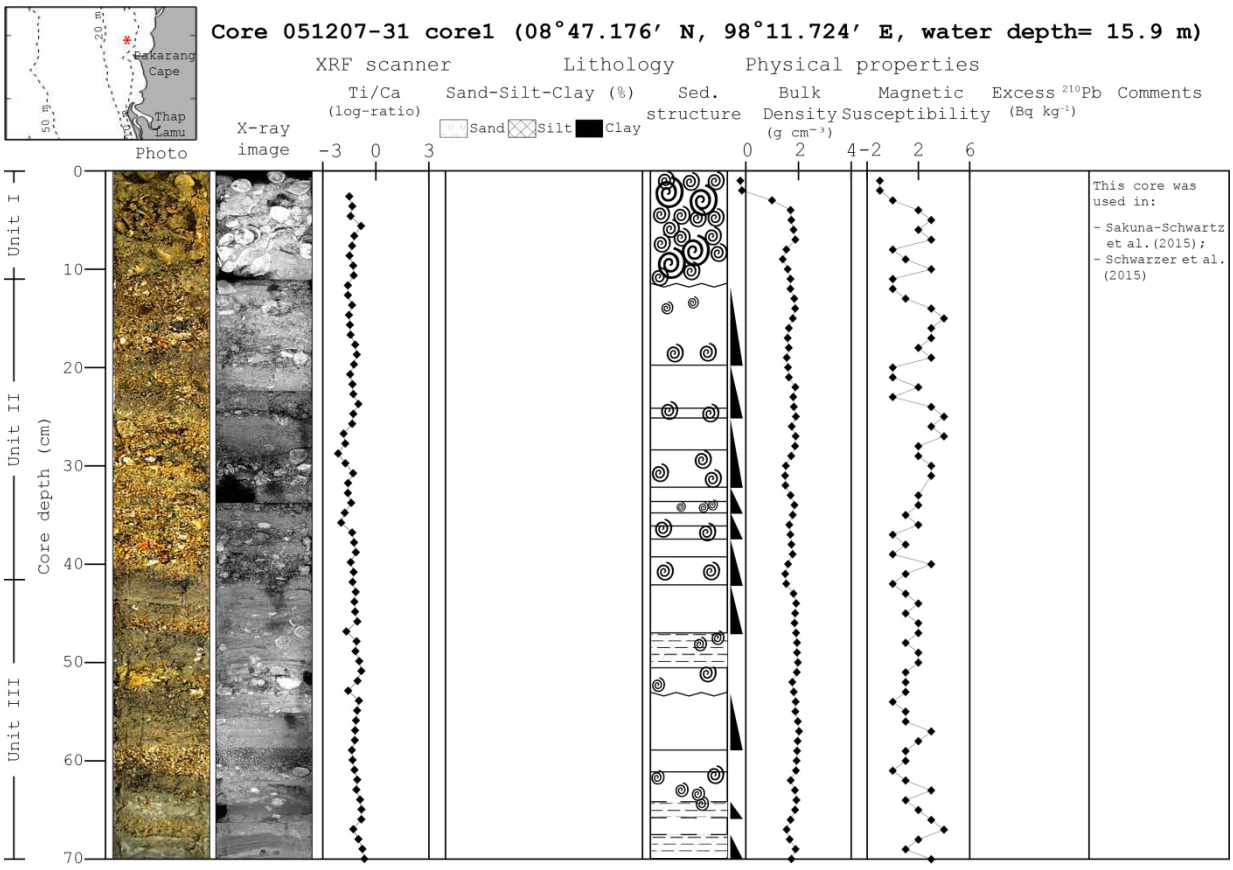
Core 051207-31 core1 (08°47.176′ N, 98°11.724′ E, water depth= 15.9 m)
XRF scanner
Lithology
Physical properties
Ti/Ca (log-ratio)
Sand-Silt-Clay (%)
Sand
Silt
Clay
Sed. structure
Bulk Density (g cm⁻³)
Magnetic Susceptibility
Excess ²¹⁰Pb (Bq kg⁻¹)
Comments
X-ray image
Photo
Core depth (cm)
Unit I
Unit II
Unit III
Bakarang Cape
Thap Lamu
20 m
50 m
This core was used in:
- Sakuna-Schwartz et al. (2015);
- Schwarzer et al. (2015)

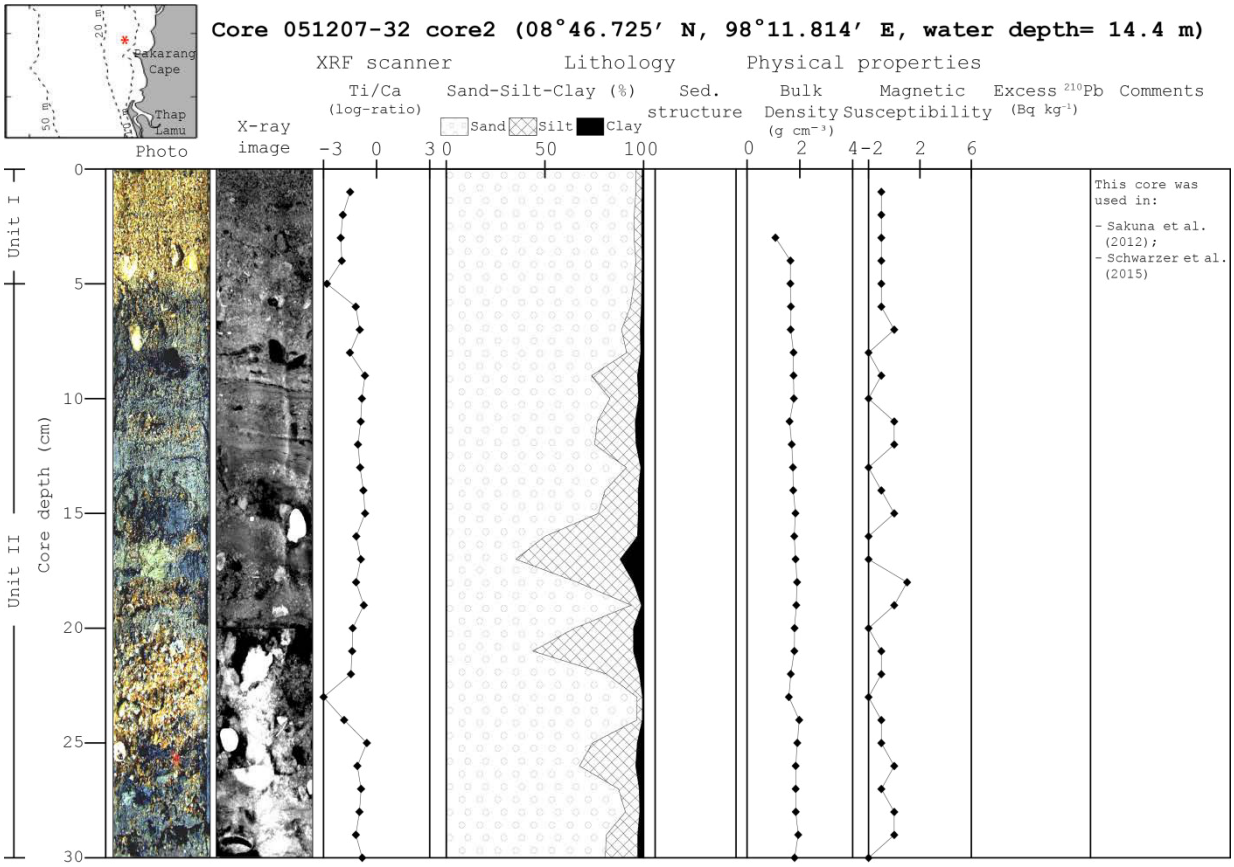
Core 051207-32 core2 (08°46.725′ N, 98°11.814′ E, water depth= 14.4 m)
XRF scanner
Lithology
Physical properties
Ti/Ca (log-ratio)
Sand-Silt-Clay (%)
Sand
Silt
Clay
Sed. structure
Bulk Density (g cm⁻³)
Magnetic Susceptibility
Excess ²¹⁰Pb (Bq kg⁻¹)
Comments
X-ray image
Photo
Core depth (cm)
Unit I
Unit II
This core was used in:
- Sakuna et al. (2012);
- Schwarzer et al. (2015)
Bakarang Cape
Thap Lamu
20 m
50 m

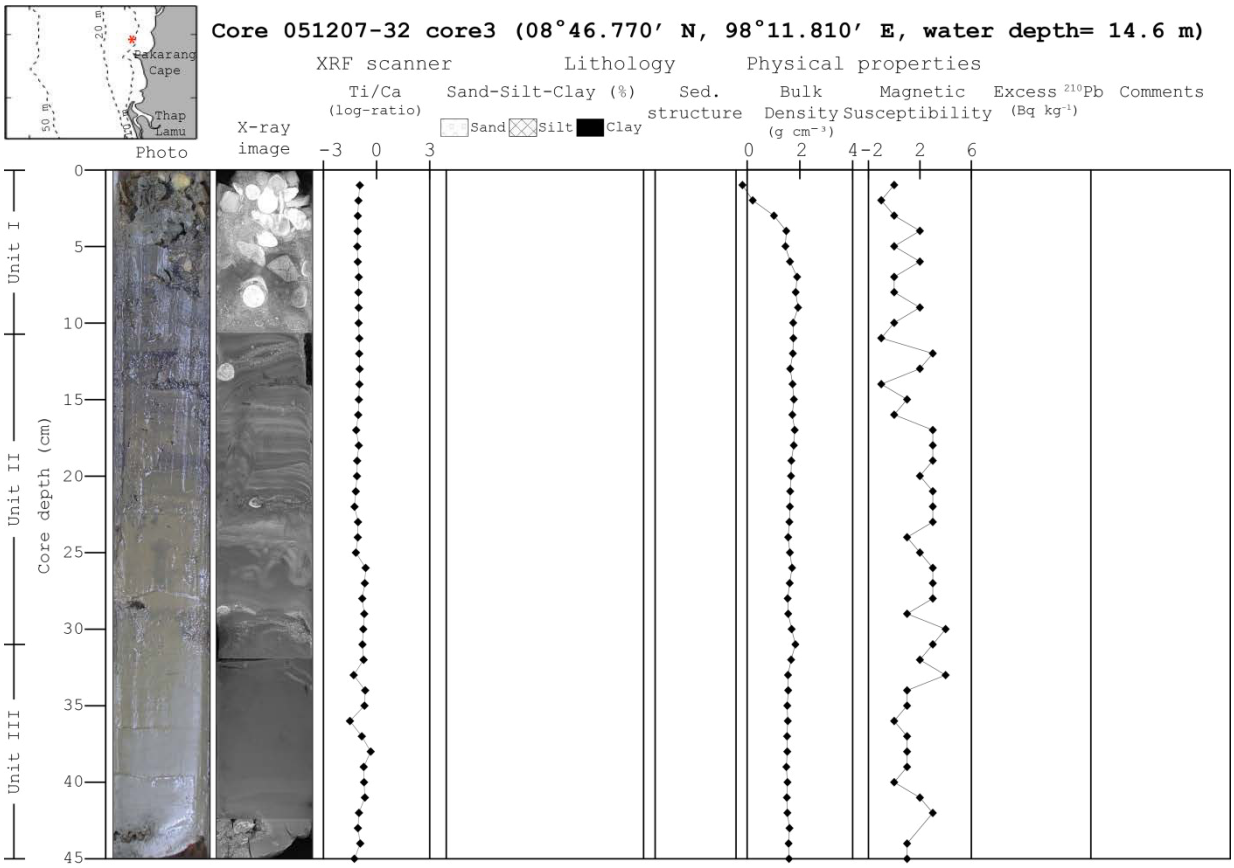
Core 051207-32 core3 (08°46.770′ N, 98°11.810′ E, water depth= 14.6 m)
XRF scanner
Lithology
Physical properties
Ti/Ca (log-ratio)
Sand-Silt-Clay (%)
Sand
Silt
Clay
Sed. structure
Bulk Density (g cm⁻³)
Magnetic Susceptibility
Excess ²¹⁰Pb (Bq kg⁻¹)
Comments
X-ray image
Photo
Core depth (cm)
Unit I
Unit II
Unit III
Bakarang Cape
Thap Lamu
20 m
50 m

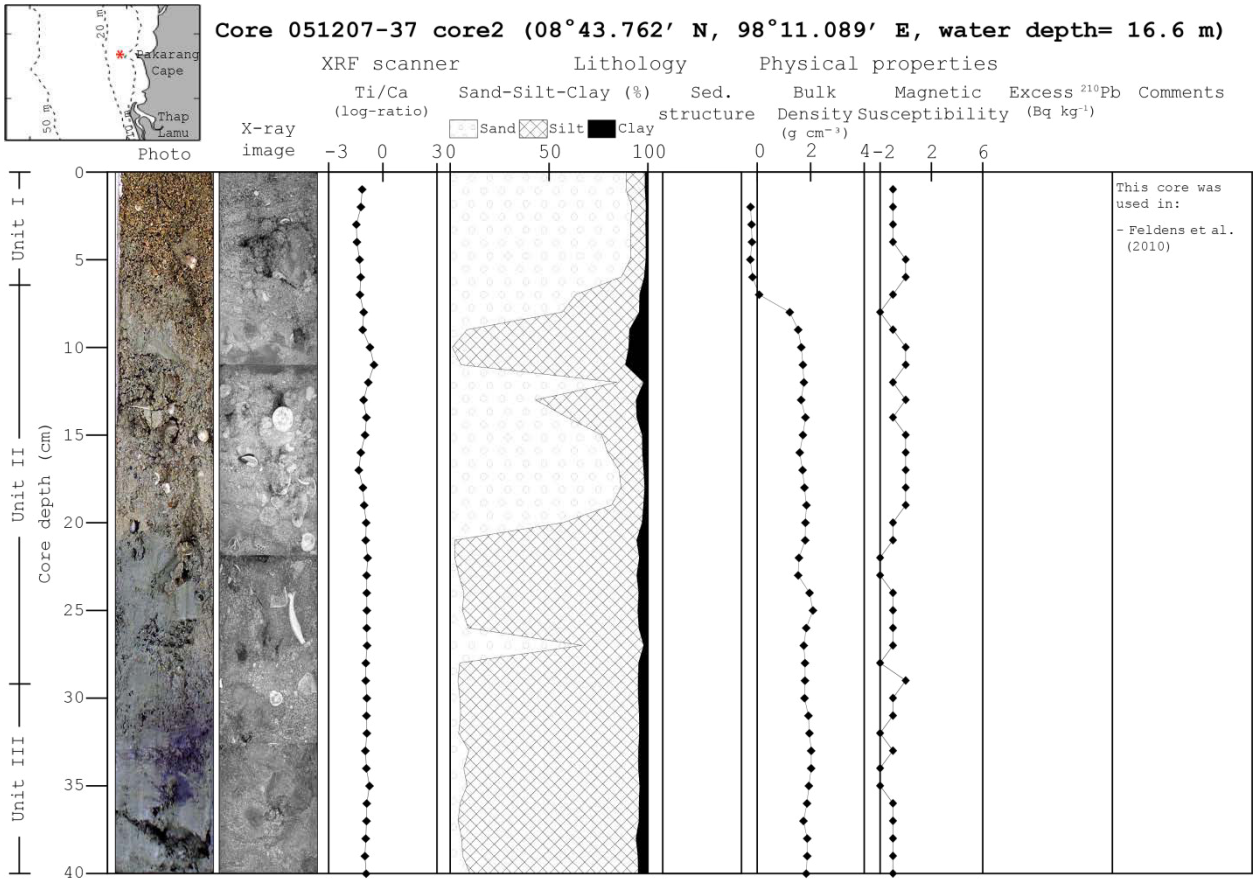
Core 051207-37 core2 (08°43.762′ N, 98°11.089′ E, water depth= 16.6 m)
XRF scanner
Lithology
Physical properties
Ti/Ca (log-ratio)
Sand-Silt-Clay (%)
Sand
Silt
Clay
Sed. structure
Bulk Density (g cm⁻³)
Magnetic Susceptibility
Excess ²¹⁰Pb (Bq kg⁻¹)
Comments
Photo
X-ray image
Pakarang Cape
Thap Lamu
20 m
50 m
Unit I
Unit II
Unit III
Core depth (cm)
This core was used in:
- Feldens et al. (2010)

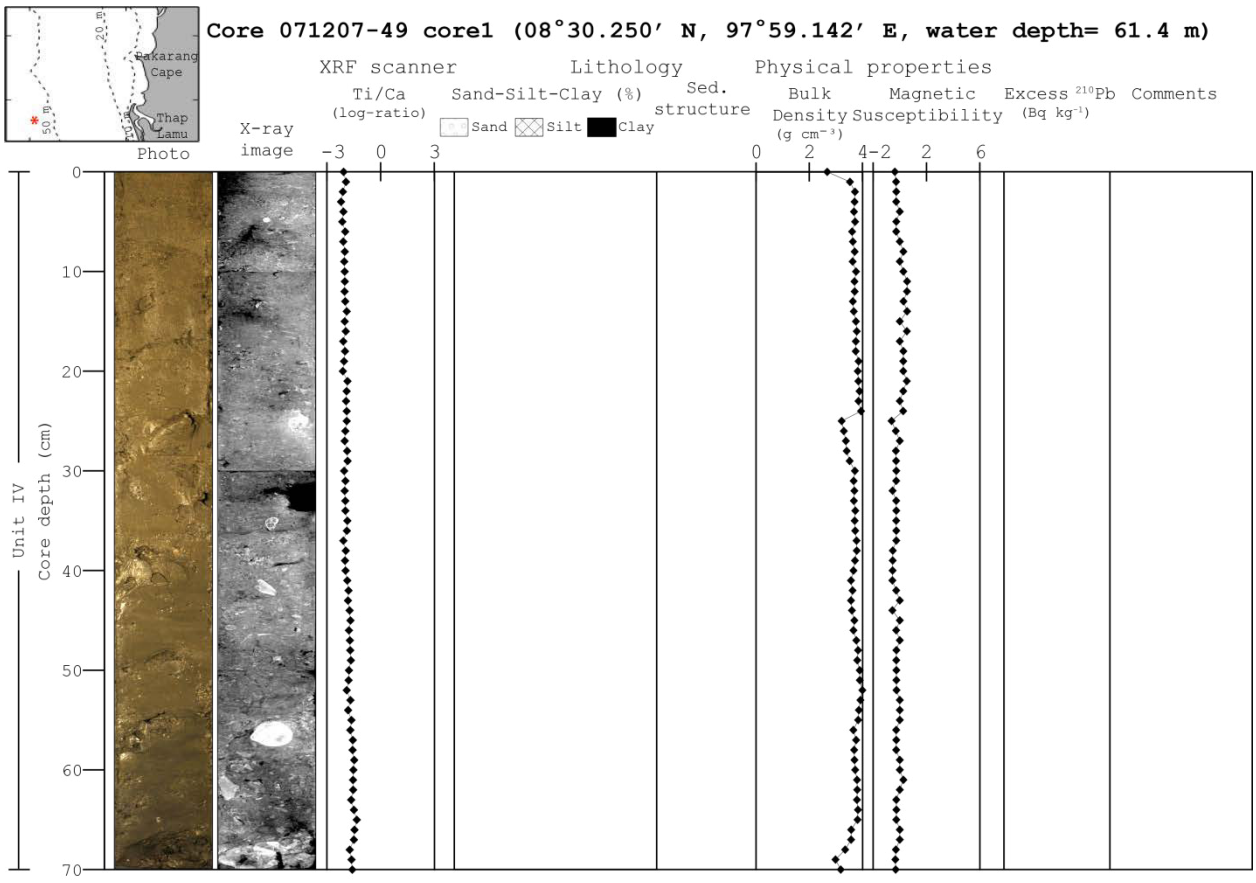
Core 071207-49 core1 (08°30.250′ N, 97°59.142′ E, water depth= 61.4 m)
XRF scanner
Lithology
Physical properties
Ti/Ca (log-ratio)
Sand-Silt-Clay (%)
Sand
Silt
Clay
Sed. structure
Bulk Density (g cm⁻³)
Magnetic Susceptibility
Excess ²¹⁰Pb (Bq kg⁻¹)
Comments
Photo
X-ray image
Pakarang Cape
Thap Lamu
20 m
50 m
Unit IV
Core depth (cm)

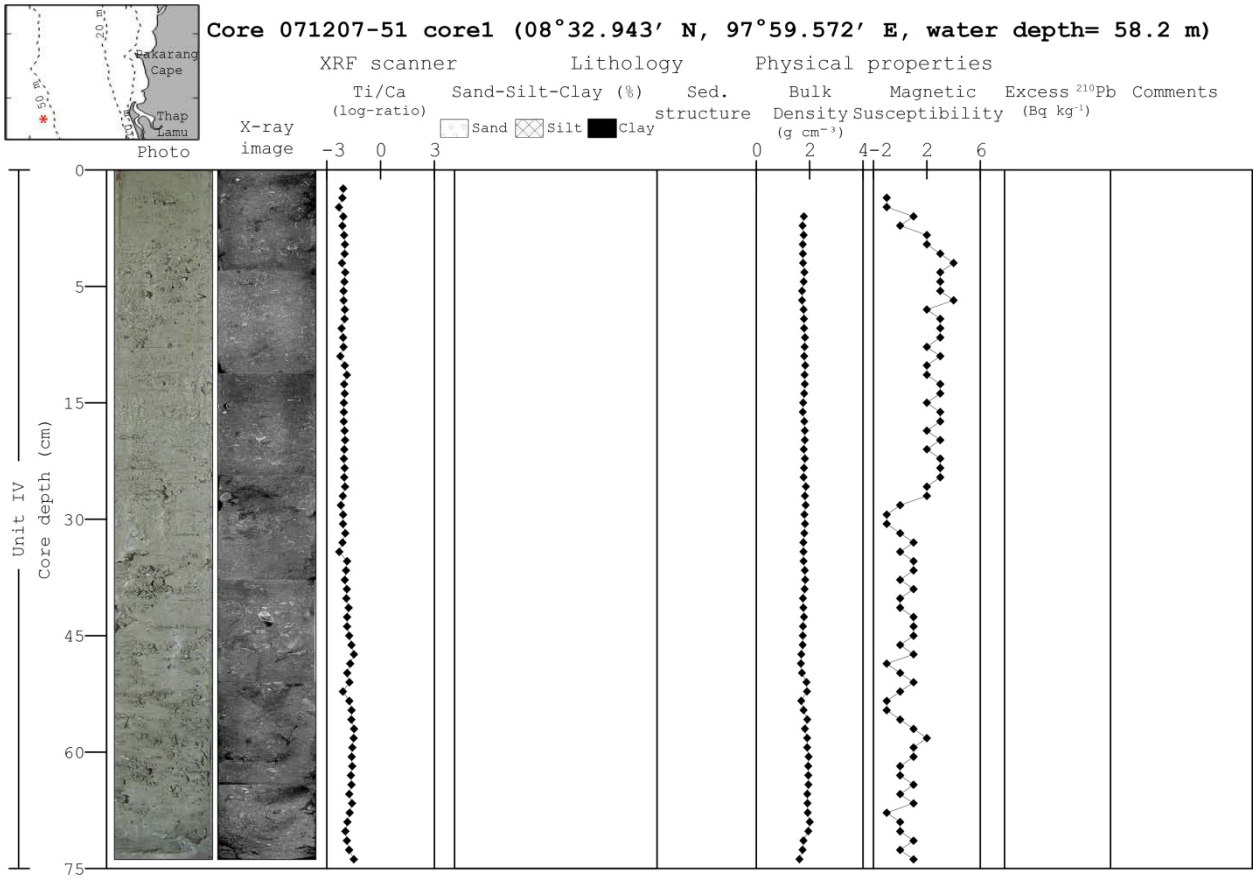
Core 071207-51 core1 (08°32.943′ N, 97°59.572′ E, water depth= 58.2 m)
XRF scanner
Lithology
Physical properties
Ti/Ca (log-ratio)
Sand-Silt-Clay (%)
Sand
Silt
Clay
Sed. structure
Bulk Density (g cm⁻³)
Magnetic Susceptibility
Excess ²¹⁰Pb (Bq kg⁻¹)
Comments
Photo
X-ray image
Pakarang Cape
Thap Lamu
20 m
50 m
Unit IV
Core depth (cm)
0
5
15
30
45
60
75
-3
0
3
0
2
4
-2
2
6

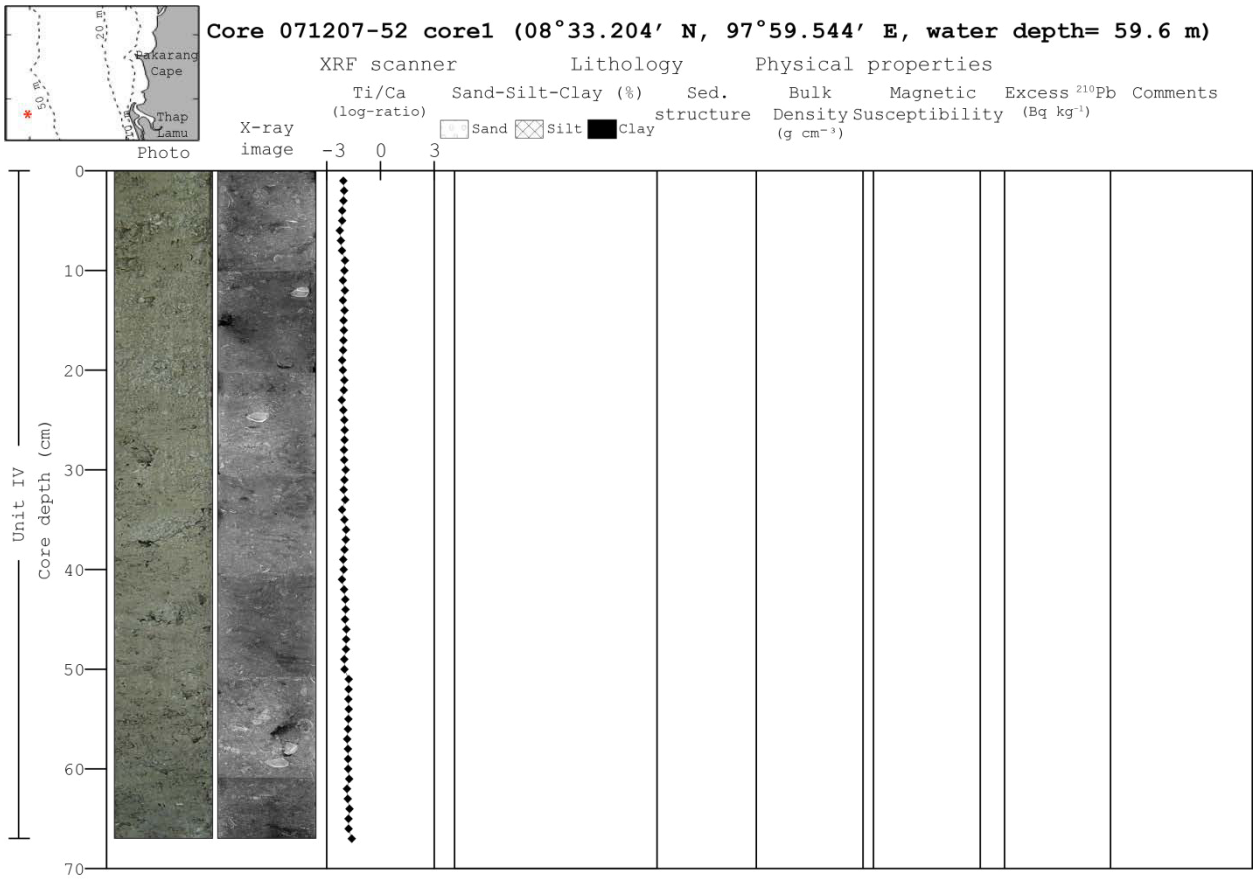
Core 071207-52 core1 (08°33.204′ N, 97°59.544′ E, water depth= 59.6 m)
XRF scanner
Lithology
Physical properties
Ti/Ca (log-ratio)
Sand-Silt-Clay (%)
Sand
Silt
Clay
Sed. structure
Bulk Density (g cm⁻³)
Magnetic Susceptibility
Excess ²¹⁰Pb (Bq kg⁻¹)
Comments
Photo
X-ray image
Pakarang Cape
Thap Lamu
20 m
50 m
Unit IV
Core depth (cm)
0
10
20
30
40
50
60
70
-3
0
3

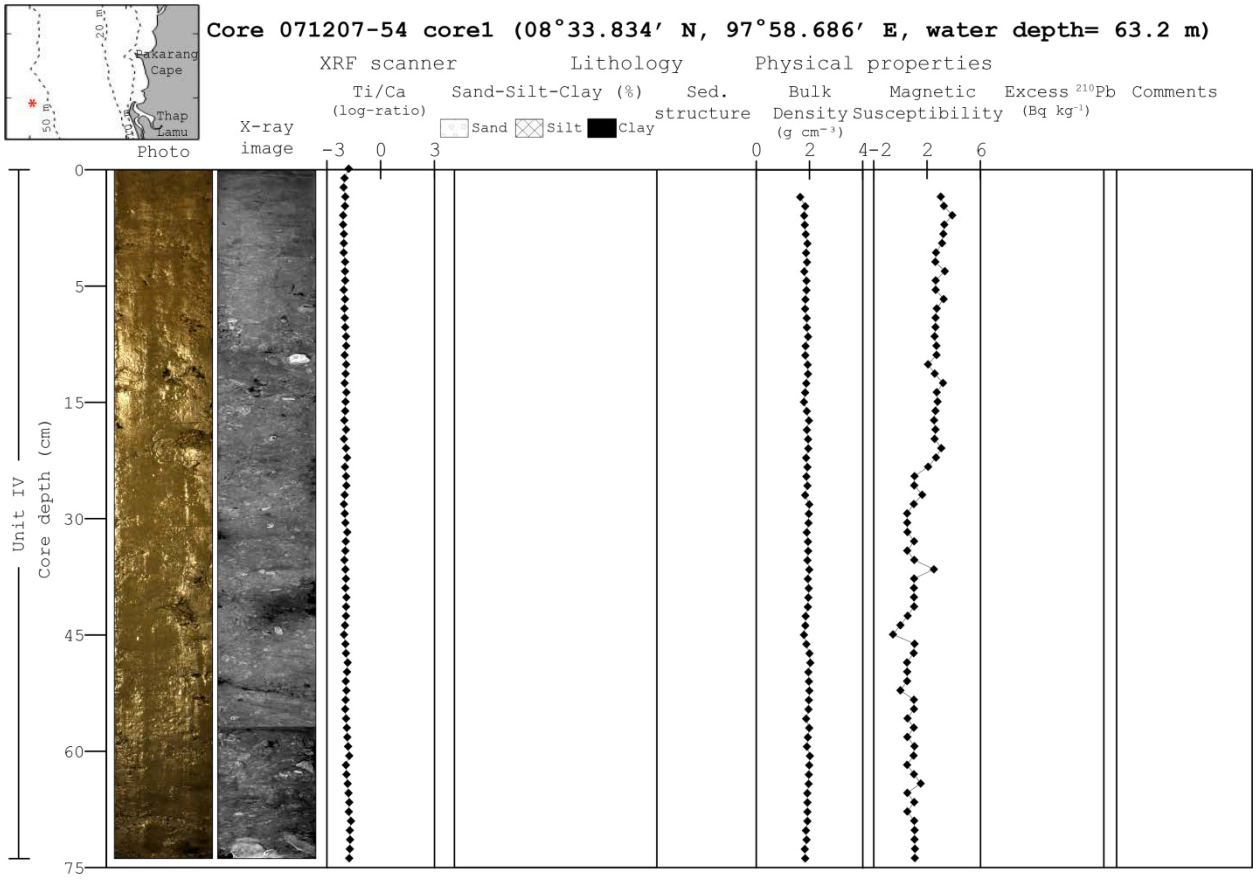
Core 071207-54 core1 (08°33.834′ N, 97°58.686′ E, water depth= 63.2 m)
Pakarang Cape
Thap Lamu
20 m
50 m
XRF scanner
Lithology
Physical properties
Ti/Ca (log-ratio)
Sand-Silt-Clay (%)
Sand
Silt
Clay
Sed. structure
Bulk Density (g cm⁻³)
Magnetic Susceptibility
Excess ²¹⁰Pb (Bq kg⁻¹)
Comments
Photo
X-ray image
-3 0 3
0 2
4-2 2 6
Unit IV
Core depth (cm)
0 5 15 30 45 60 75

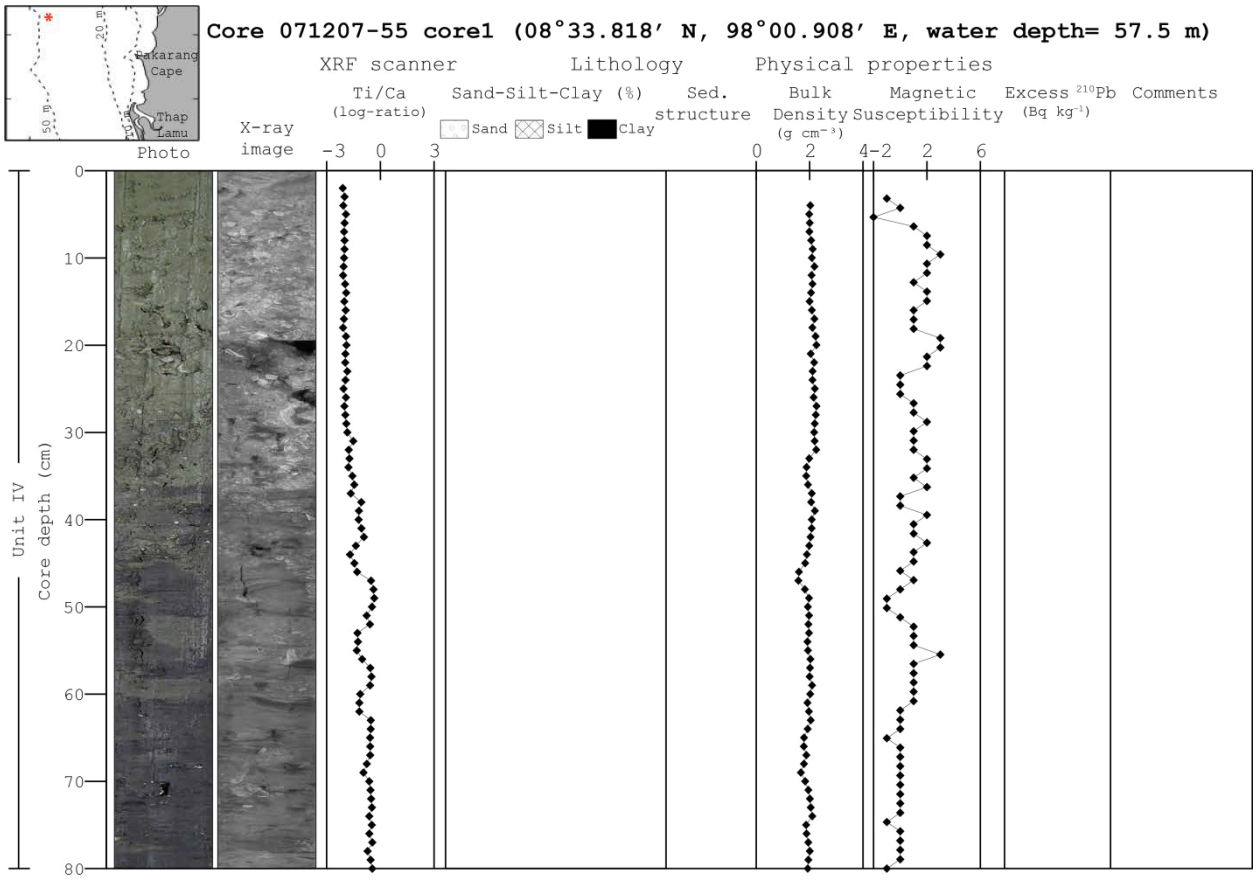
Core 071207-55 core1 (08°33.818′ N, 98°00.908′ E, water depth= 57.5 m)
Pakarang Cape
Thap Lamu
20 m
50 m
XRF scanner
Lithology
Physical properties
Ti/Ca (log-ratio)
Sand-Silt-Clay (%)
Sand
Silt
Clay
Sed. structure
Bulk Density (g cm⁻³)
Magnetic Susceptibility
Excess ²¹⁰Pb (Bq kg⁻¹)
Comments
Photo
X-ray image
-3 0 3
0 2
4-2 2 6
Unit IV
Core depth (cm)
0 10 20 30 40 50 60 70 80

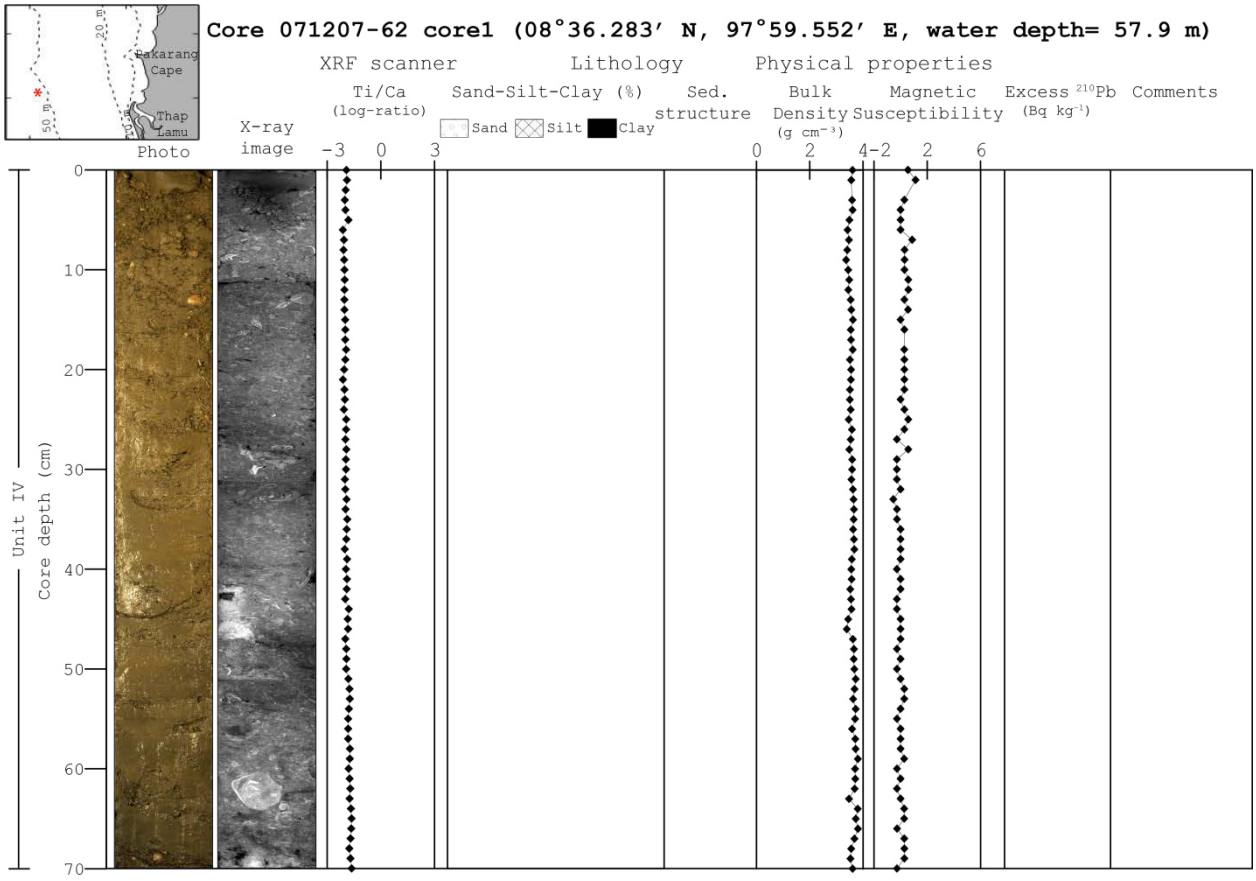
Core 071207-62 core1 (08°36.283′ N, 97°59.552′ E, water depth= 57.9 m)
XRF scanner
Lithology
Physical properties
Ti/Ca (log-ratio)
Sand-Silt-Clay (%)
Sand
Silt
Clay
Sed. structure
Bulk Density (g cm⁻³)
Magnetic Susceptibility
Excess ²¹⁰Pb (Bq kg⁻¹)
Comments
Photo
X-ray image
Pakarang Cape
Thap Lamu
20 m
50 m
Unit IV
Core depth (cm)

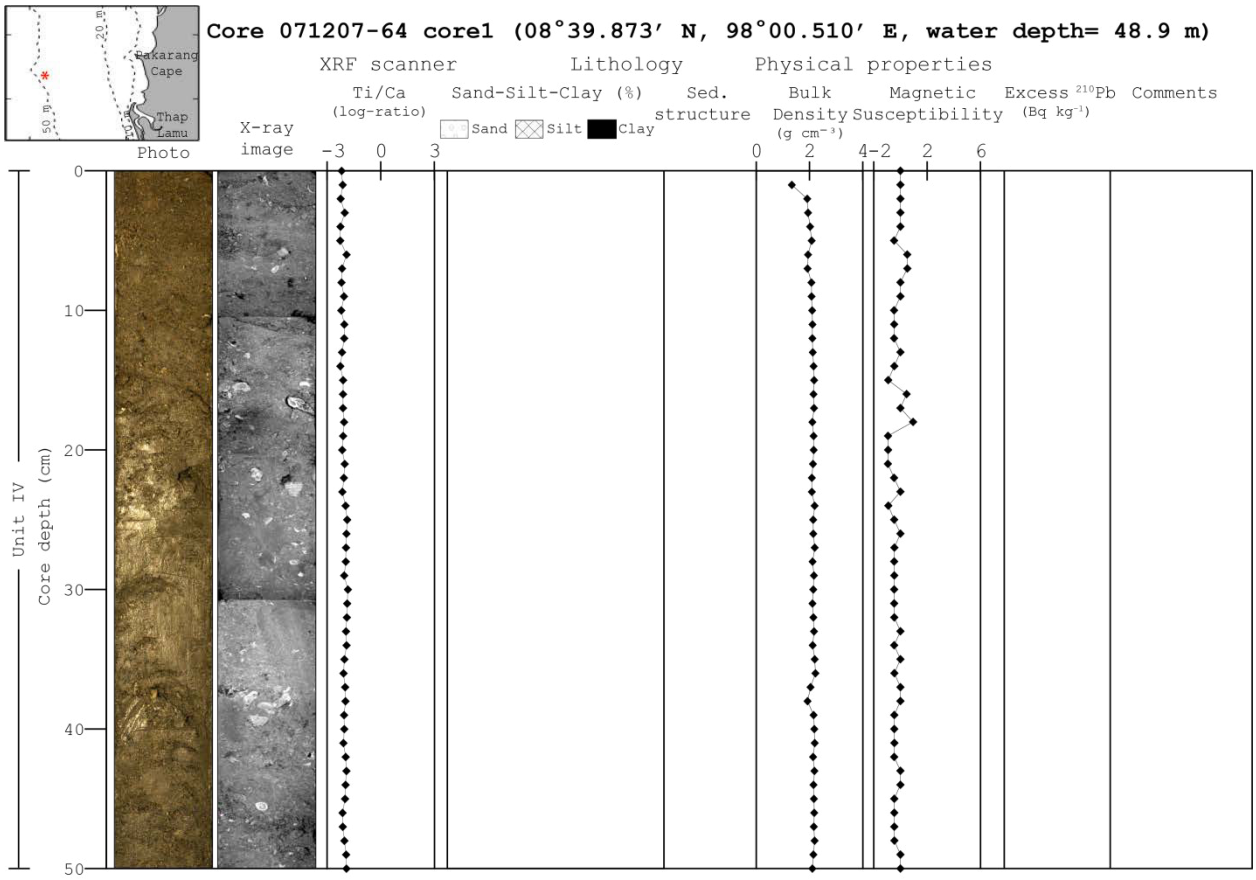
Core 071207-64 core1 (08°39.873′ N, 98°00.510′ E, water depth= 48.9 m)
XRF scanner
Lithology
Physical properties
Ti/Ca (log-ratio)
Sand-Silt-Clay (%)
Sand
Silt
Clay
Sed. structure
Bulk Density (g cm⁻³)
Magnetic Susceptibility
Excess ²¹⁰Pb (Bq kg⁻¹)
Comments
Photo
X-ray image
Pakarang Cape
Thap Lamu
20 m
50 m
Unit IV
Core depth (cm)

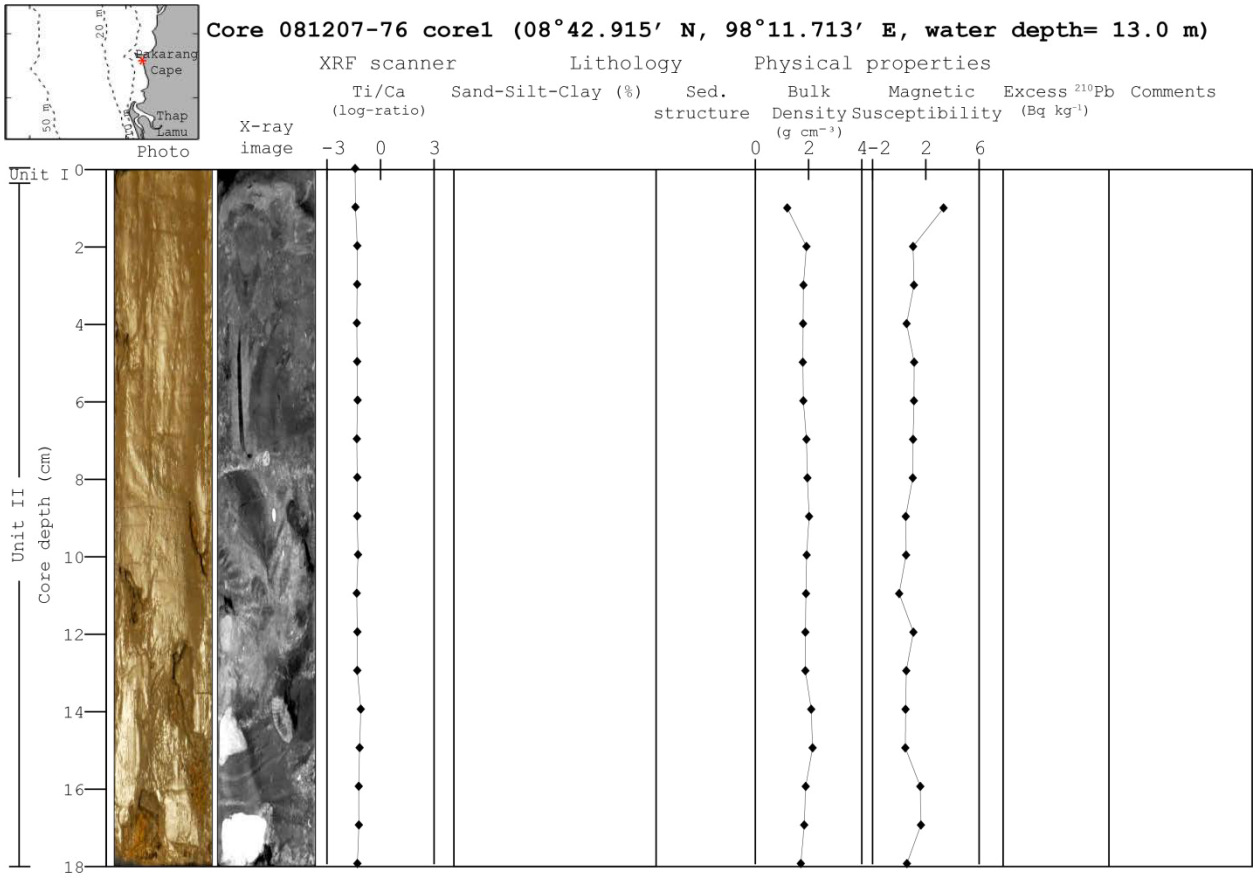
Core 081207-76 core1 (08°42.915′ N, 98°11.713′ E, water depth= 13.0 m)
XRF scanner
Lithology
Physical properties
Ti/Ca (log-ratio)
Sand-Silt-Clay (%)
Sed. structure
Bulk Density (g cm⁻³)
Magnetic Susceptibility
Excess ²¹⁰Pb (Bq kg⁻¹)
Comments
Photo
X-ray image
Pakarang Cape
Thap Lamu
20 m
50 m
Unit I
Unit II
Core depth (cm)

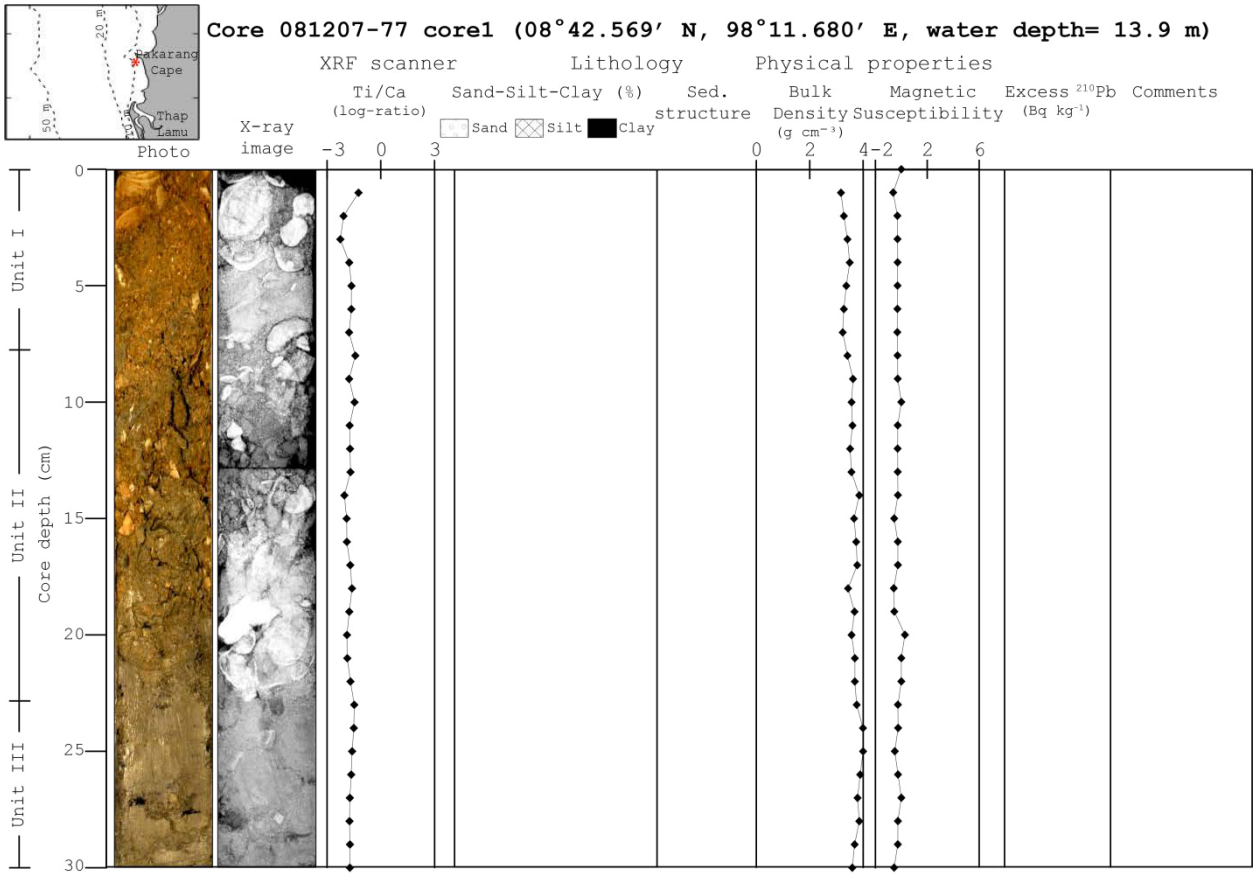
Core 081207-77 core1 (08°42.569′ N, 98°11.680′ E, water depth= 13.9 m)
XRF scanner
Lithology
Physical properties
Ti/Ca (log-ratio)
Sand-Silt-Clay (%)
Sand
Silt
Clay
Sed. structure
Bulk Density (g cm⁻³)
Magnetic Susceptibility
Excess ²¹⁰Pb (Bq kg⁻¹)
Comments
Photo
X-ray image
Pakarang Cape
Thap Lamu
20 m
50 m
Unit I
Unit II
Unit III
Core depth (cm)

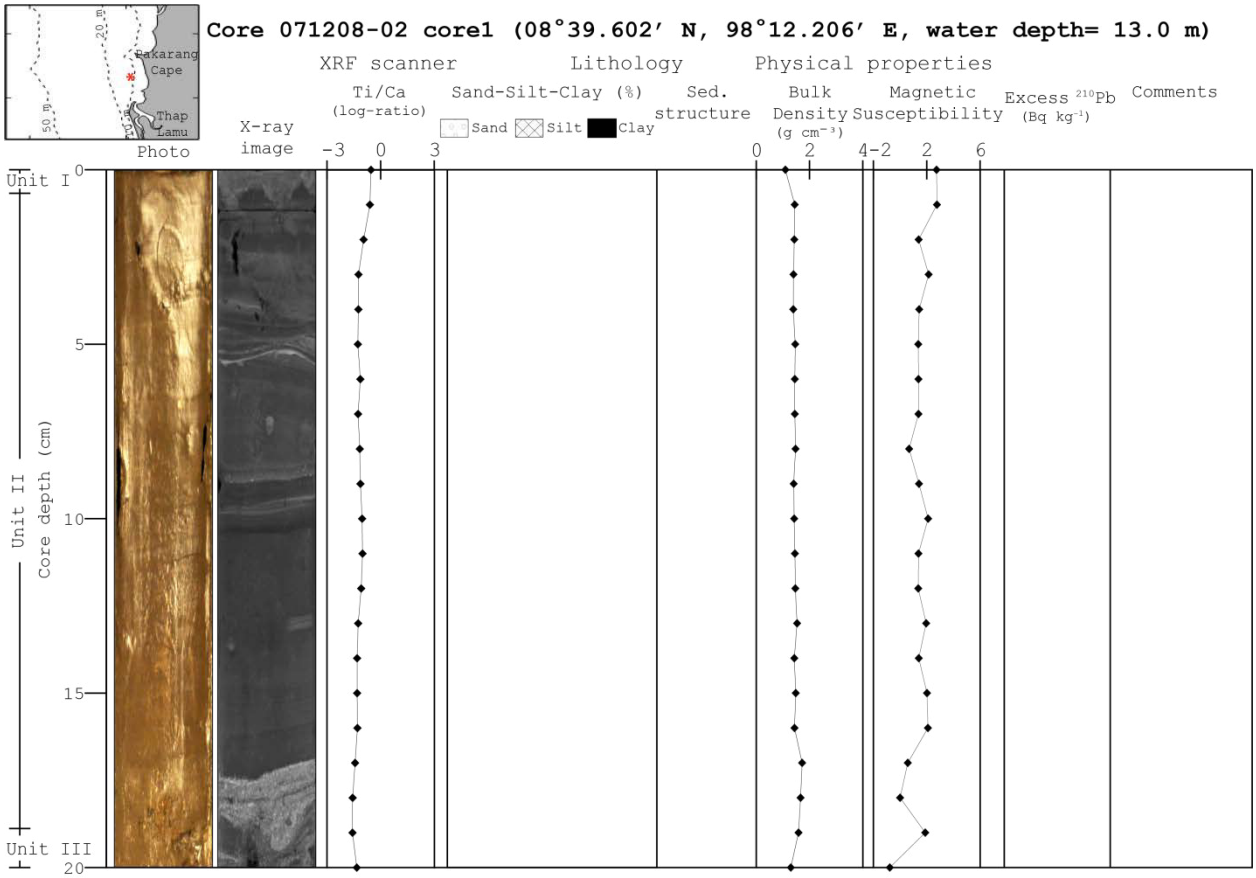
Core 071208-02 core1 (08°39.602′ N, 98°12.206′ E, water depth= 13.0 m)
XRF scanner
Lithology
Physical properties
Ti/Ca (log-ratio)
Sand-Silt-Clay (%)
Sand
Silt
Clay
Sed. structure
Bulk Density (g cm⁻³)
Magnetic Susceptibility
Excess ²¹⁰Pb (Bq kg⁻¹)
Comments
Photo
X-ray image
Pakarang Cape
Thap Lamu
20 m
50 m
Unit I
Unit II
Unit III
Core depth (cm)
-3 0 3
0 2
4-2 2 6
0 5 10 15 20

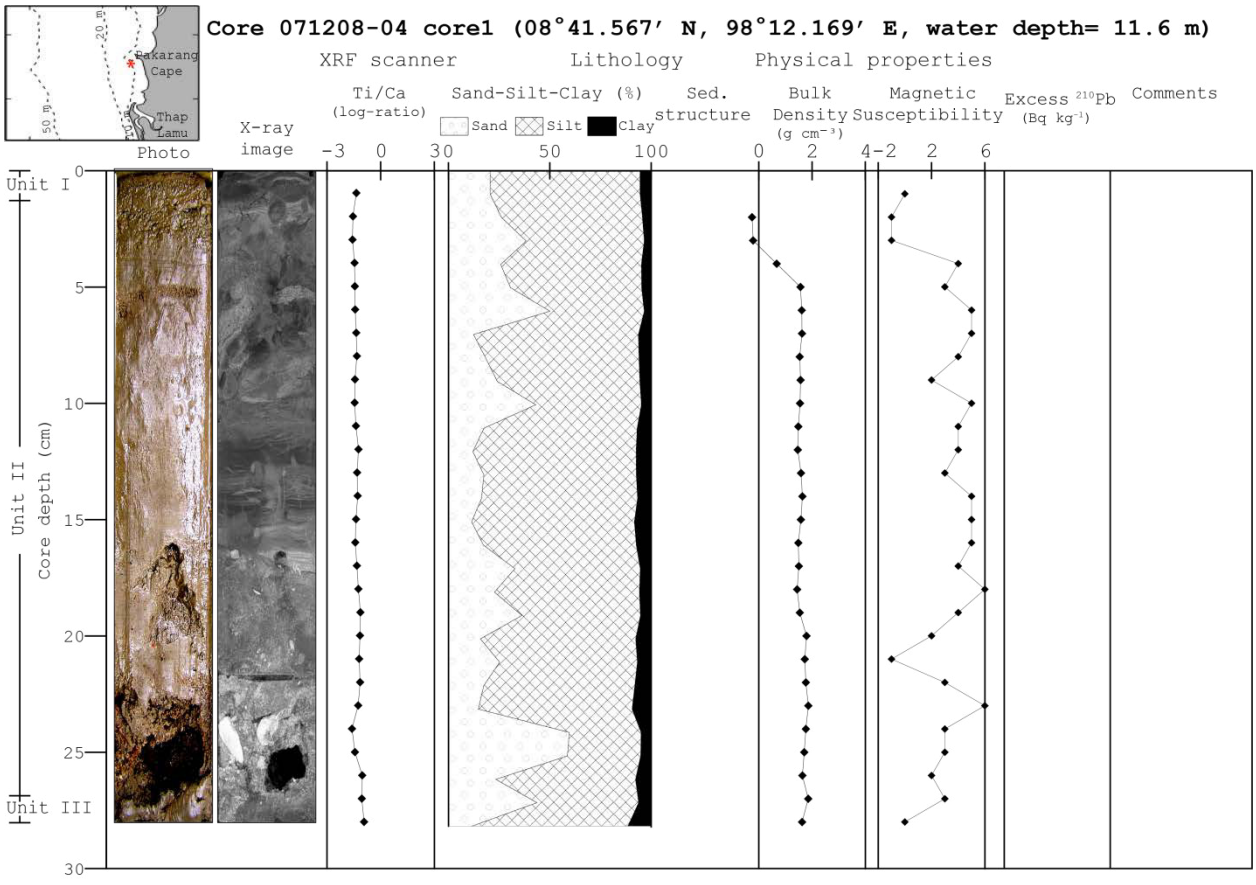
Core 071208-04 core1 (08°41.567′ N, 98°12.169′ E, water depth= 11.6 m)
XRF scanner
Lithology
Physical properties
Ti/Ca (log-ratio)
Sand-Silt-Clay (%)
Sand
Silt
Clay
Sed. structure
Bulk Density (g cm⁻³)
Magnetic Susceptibility
Excess ²¹⁰Pb (Bq kg⁻¹)
Comments
Photo
X-ray image
Pakarang Cape
Thap Lamu
20 m
50 m
Unit I
Unit II
Unit III
Core depth (cm)
-3 0 30
0 50 100
0 2
4-2 2 6
0 5 10 15 20 25 30

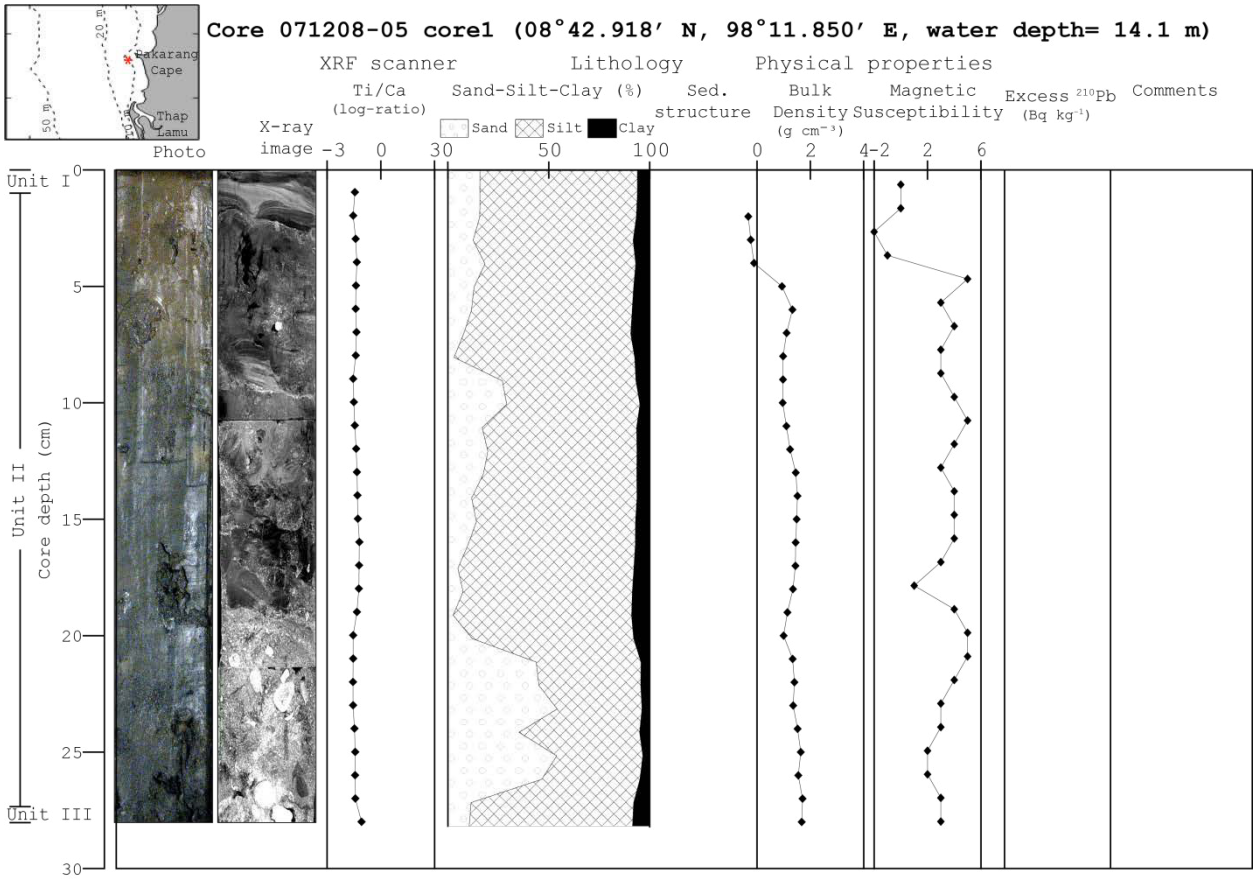
Core 071208-05 core1 (08°42.918′ N, 98°11.850′ E, water depth= 14.1 m)
XRF scanner
Lithology
Physical properties
Ti/Ca (log-ratio)
Sand-Silt-Clay (%)
Sand
Silt
Clay
Sed. structure
Bulk Density (g cm⁻³)
Magnetic Susceptibility
Excess ²¹⁰Pb (Bq kg⁻¹)
Comments
X-ray image
Photo
Pakarang Cape
Thap Lamu
20 m
50 m
Unit I
Unit II
Unit III
Core depth (cm)

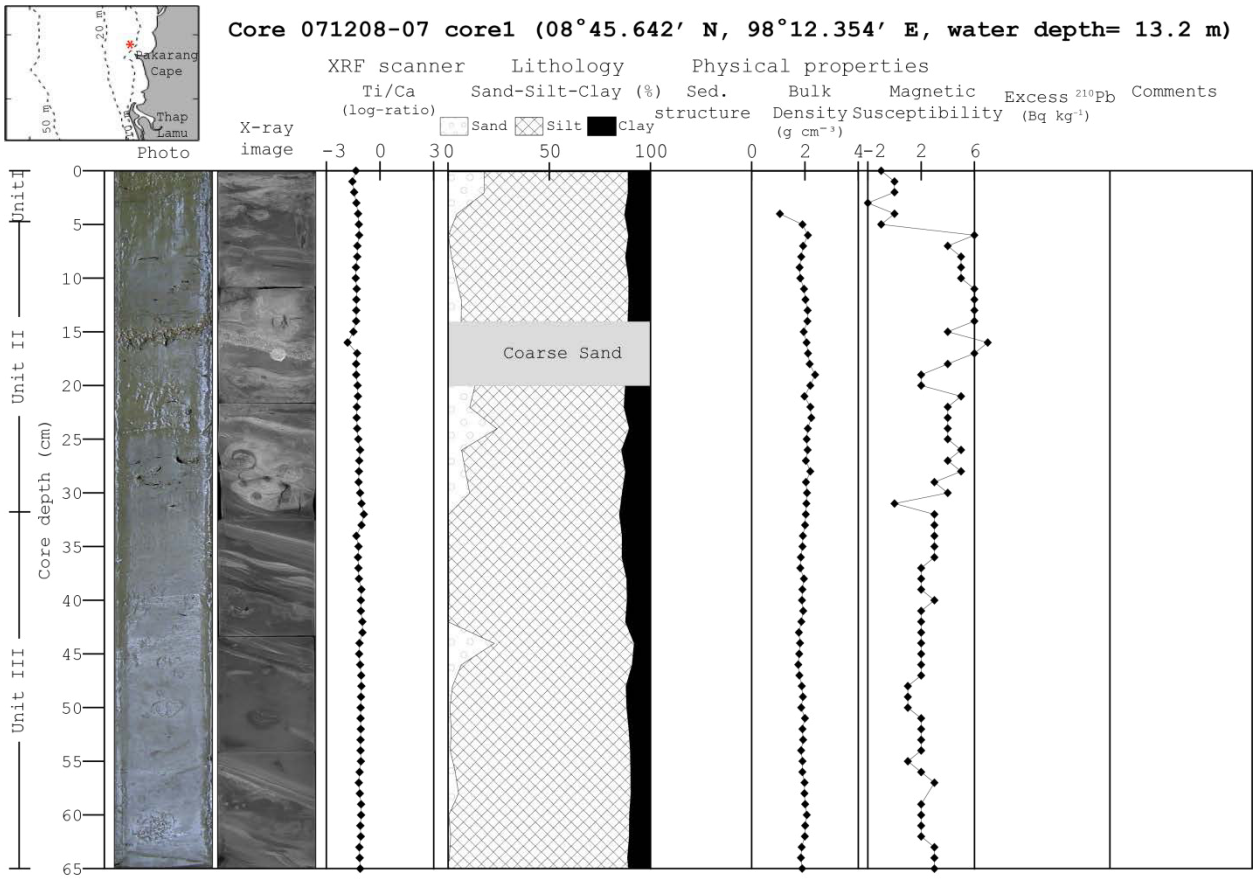
Core 071208-07 core1 (08°45.642′ N, 98°12.354′ E, water depth= 13.2 m)
XRF scanner
Lithology
Physical properties
Ti/Ca (log-ratio)
Sand-Silt-Clay (%)
Sand
Silt
Clay
Sed. structure
Bulk Density (g cm⁻³)
Magnetic Susceptibility
Excess ²¹⁰Pb (Bq kg⁻¹)
Comments
X-ray image
Photo
Coarse Sand
Pakarang Cape
Thap Lamu
20 m
50 m
Unit I
Unit II
Unit III
Core depth (cm)

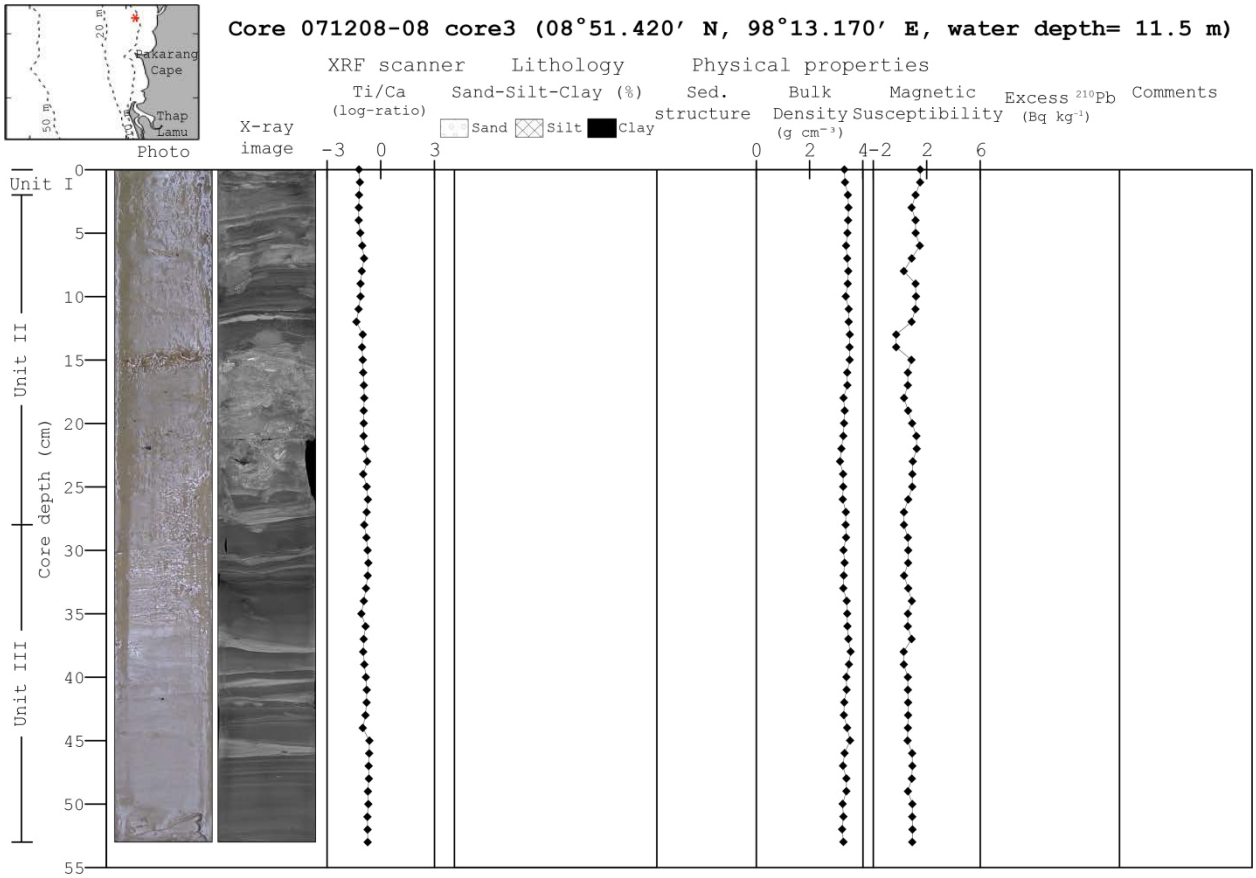
Core 071208-08 core3 (08°51.420′ N, 98°13.170′ E, water depth= 11.5 m)
XRF scanner
Lithology
Physical properties
Ti/Ca (log-ratio)
Sand-Silt-Clay (%)
Sand
Silt
Clay
Sed. structure
Bulk Density (g cm⁻³)
Magnetic Susceptibility
Excess ²¹⁰Pb (Bq kg⁻¹)
Comments
Photo
X-ray image
Pakarang Cape
Thap Lamu
20 m
50 m
Unit I
Unit II
Unit III
Core depth (cm)

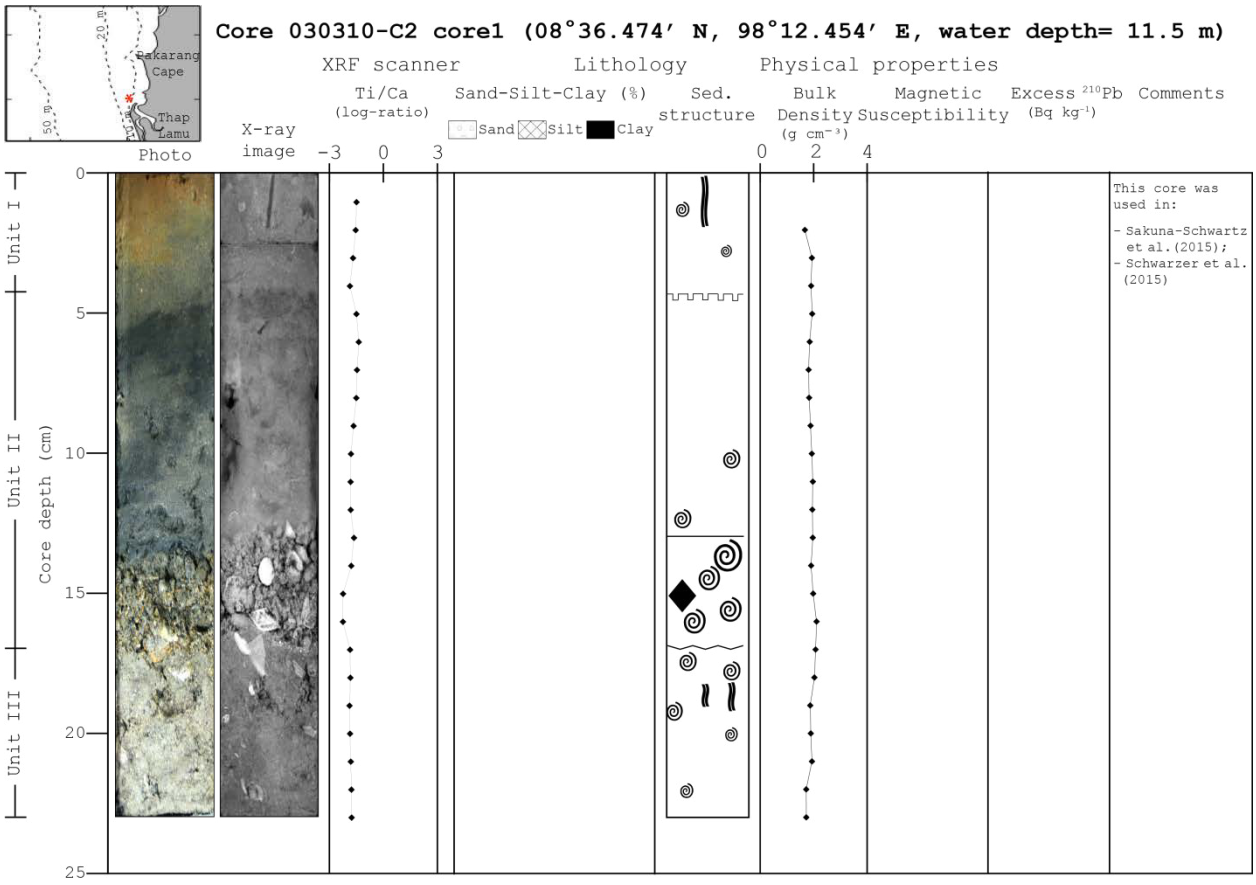
Core 030310-C2 core1 (08°36.474′ N, 98°12.454′ E, water depth= 11.5 m)
XRF scanner
Lithology
Physical properties
Ti/Ca (log-ratio)
Sand-Silt-Clay (%)
Sand
Silt
Clay
Sed. structure
Bulk Density (g cm⁻³)
Magnetic Susceptibility
Excess ²¹⁰Pb (Bq kg⁻¹)
Comments
Photo
X-ray image
Pakarang Cape
Thap Lamu
20 m
50 m
Unit I
Unit II
Unit III
Core depth (cm)
This core was used in:
- Sakuna-Schwartz et al.(2015);
- Schwarzer et al. (2015)

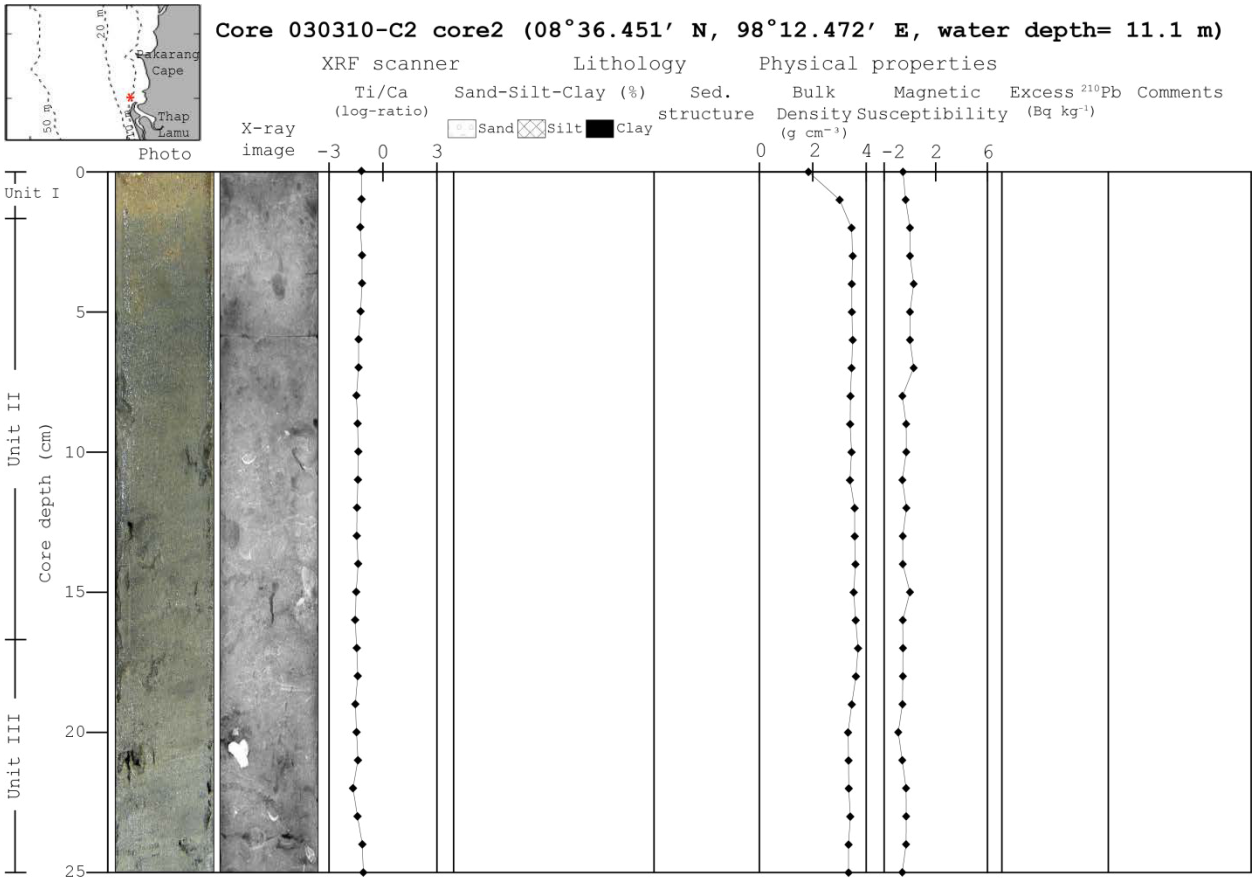
Core 030310-C2 core2 (08°36.451′ N, 98°12.472′ E, water depth= 11.1 m)
XRF scanner
Lithology
Physical properties
Ti/Ca (log-ratio)
Sand-Silt-Clay (%)
Sand
Silt
Clay
Sed. structure
Bulk Density (g cm⁻³)
Magnetic Susceptibility
Excess ²¹⁰Pb (Bq kg⁻¹)
Comments
Photo
X-ray image
Pakarang Cape
Thap Lamu
20 m
50 m
Unit I
Unit II
Unit III
Core depth (cm)

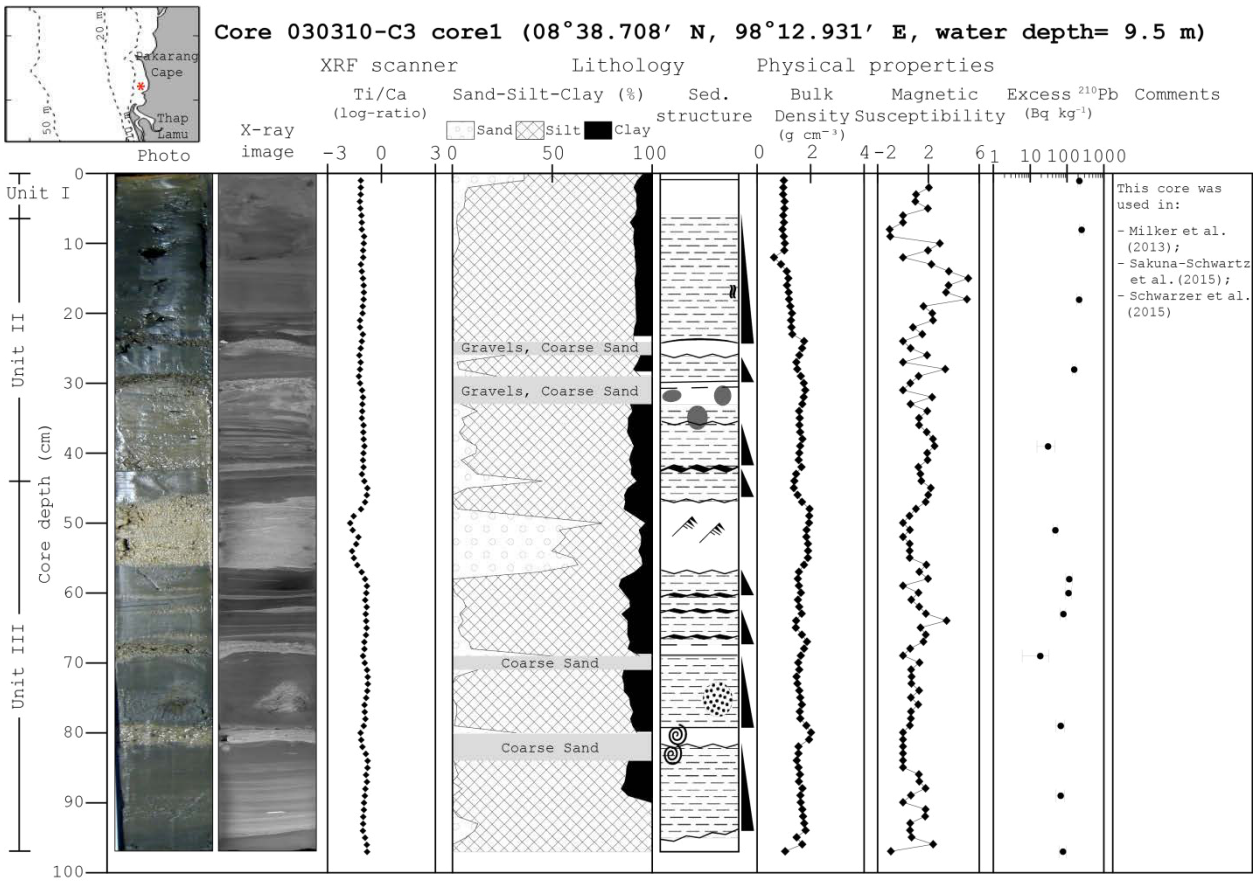
Core 030310-C3 core1 (08°38.708′ N, 98°12.931′ E, water depth= 9.5 m)
XRF scanner
Lithology
Physical properties
Ti/Ca (log-ratio)
Sand-Silt-Clay (%)
Sand
Silt
Clay
Sed. structure
Bulk Density (g cm⁻³)
Magnetic Susceptibility
Excess ²¹⁰Pb (Bq kg⁻¹)
Comments
Photo
X-ray image
Pakarang Cape
Thap Lamu
20 m
50 m
Unit I
Unit II
Unit III
Core depth (cm)
Gravels, Coarse Sand
Gravels, Coarse Sand
Coarse Sand
Coarse Sand
This core was used in:
- Milker et al. (2013);
- Sakuna-Schwartz et al.(2015);
- Schwarzer et al. (2015)

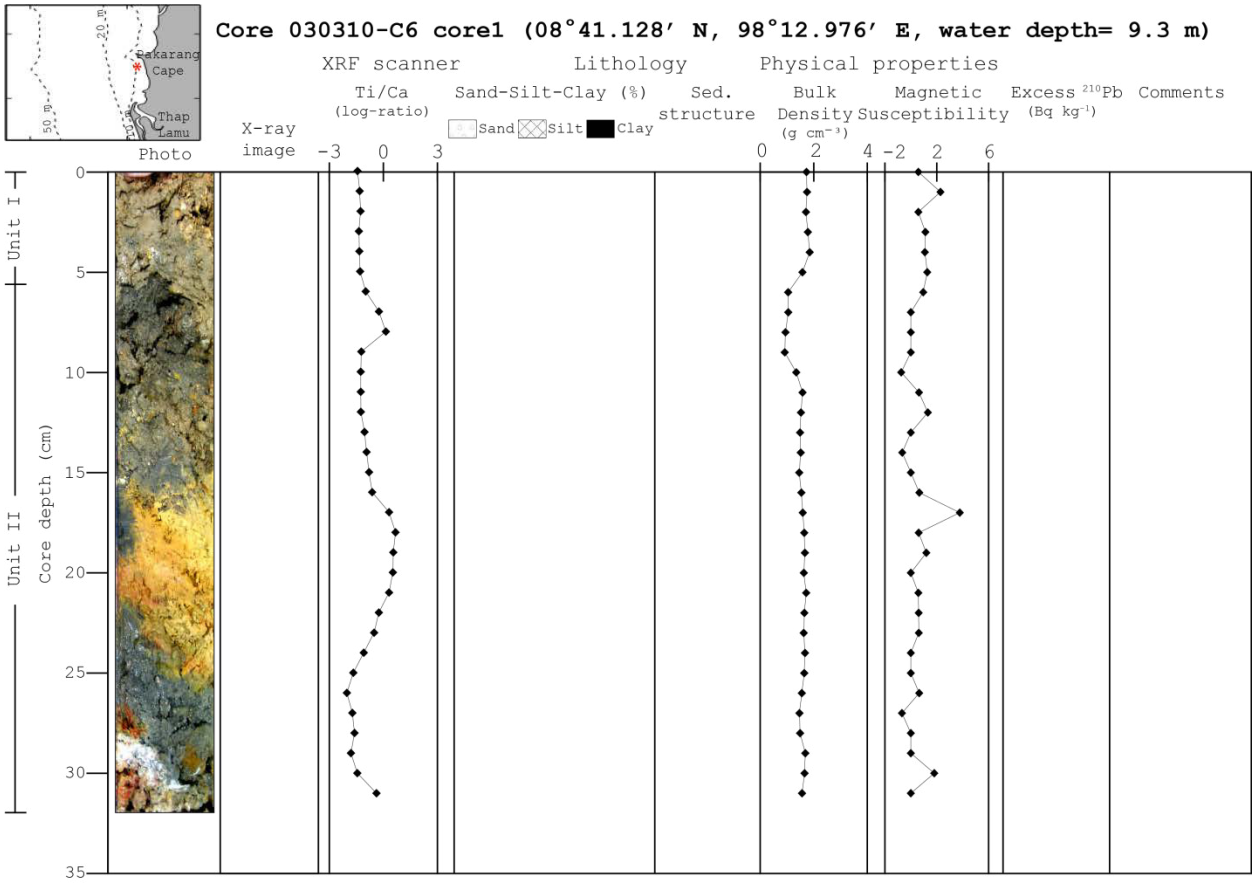
Core 030310-C6 core1 (08°41.128′ N, 98°12.976′ E, water depth= 9.3 m)
Pakarang Cape
Thap Lamu
20 m
50 m
XRF scanner
Lithology
Physical properties
Ti/Ca (log-ratio)
Sand-Silt-Clay (%)
Sand
Silt
Clay
Sed. structure
Bulk Density (g cm⁻³)
Magnetic Susceptibility
Excess ²¹⁰Pb (Bq kg⁻¹)
Comments
Photo
X-ray image
-3 0 3
0 2 4
-2 2 6
Unit I
Unit II
Core depth (cm)
0 5 10 15 20 25 30 35


Core 030310-C7 core1 (08°41.193′ N, 98°12.689′ E, water depth= 12.5 m)
Pakarang Cape
Thap Lamu
20 m
50 m
XRF scanner
Lithology
Physical properties
Ti/Ca (log-ratio)
Sand-Silt-Clay (%)
Sand
Silt
Clay
Sed. structure
Bulk Density (g cm⁻³)
Magnetic Susceptibility
Excess ²¹⁰Pb (Bq kg⁻¹)
Comments
Photo
X-ray image
-3 0 3
Unit I
Unit II
Core depth (cm)
0 5 10 15 20 25 30 35

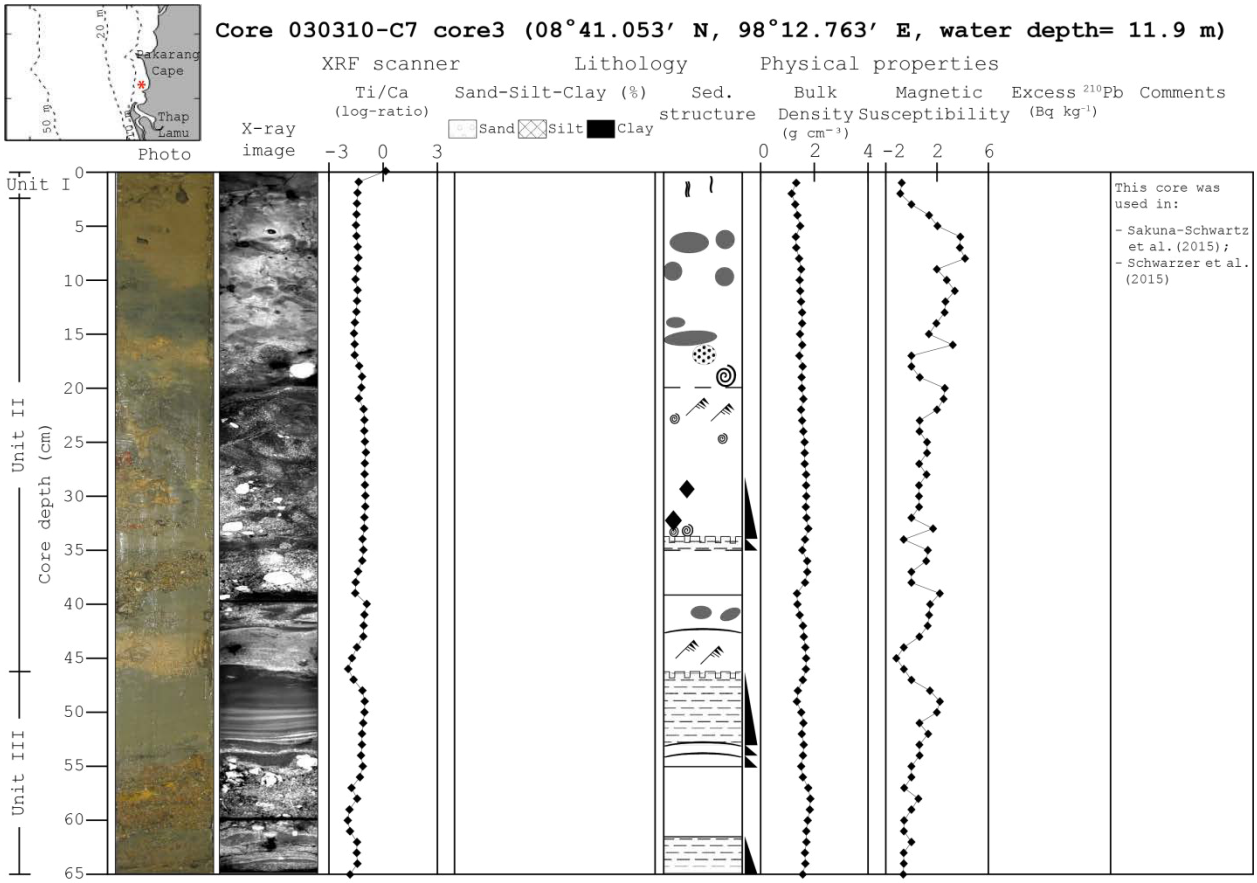
Core 030310-C7 core3 (08°41.053′ N, 98°12.763′ E, water depth= 11.9 m)
XRF scanner
Lithology
Physical properties
Ti/Ca (log-ratio)
Sand-Silt-Clay (%)
Sand
Silt
Clay
Sed. structure
Bulk Density (g cm⁻³)
Magnetic Susceptibility
Excess ²¹⁰Pb (Bq kg⁻¹)
Comments
Photo
X-ray image
Pakarang Cape
Thap Lamu
20 m
50 m
Unit I
Unit II
Unit III
Core depth (cm)
This core was used in:
- Sakuna-Schwartz et al. (2015);
- Schwarzer et al. (2015)

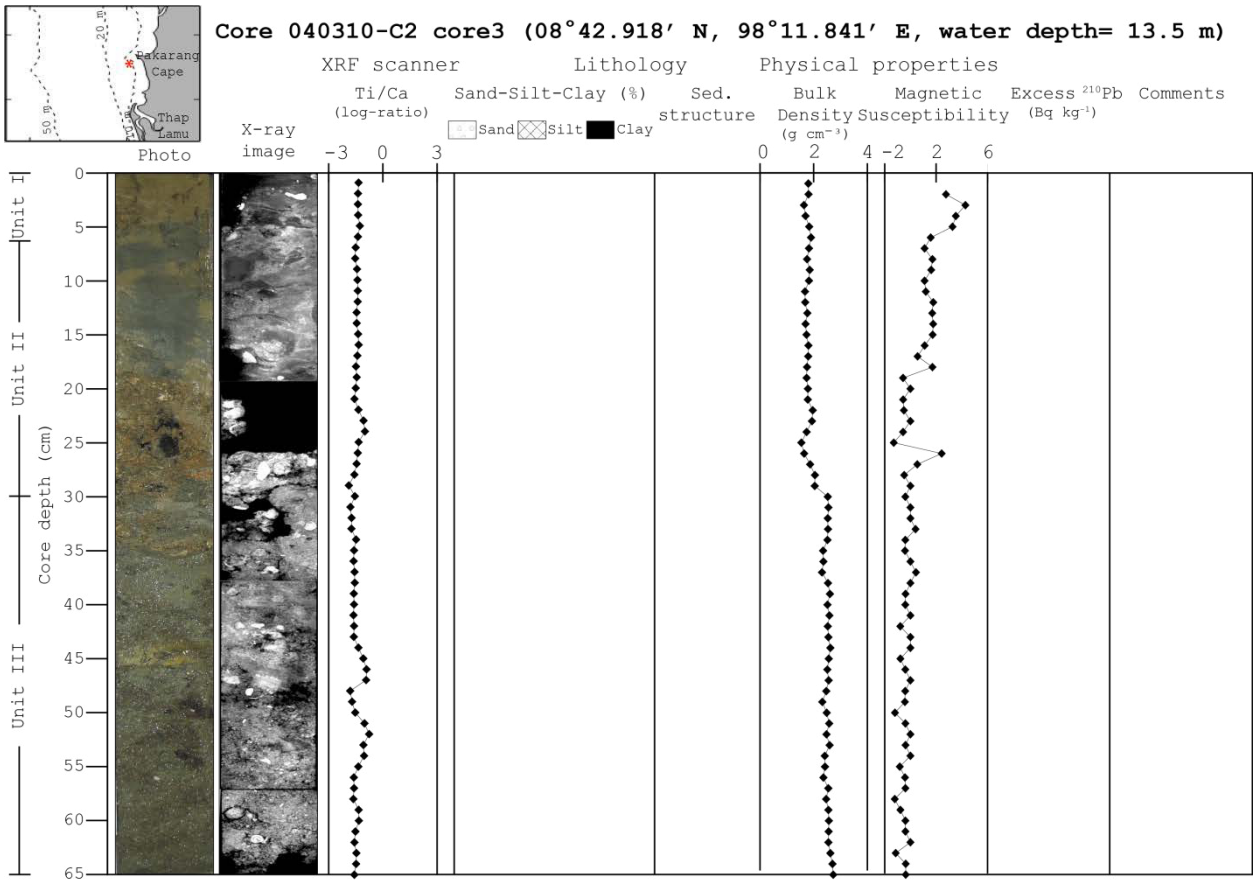
Core 040310-C2 core3 (08°42.918′ N, 98°11.841′ E, water depth= 13.5 m)
XRF scanner
Lithology
Physical properties
Ti/Ca (log-ratio)
Sand-Silt-Clay (%)
Sand
Silt
Clay
Sed. structure
Bulk Density (g cm⁻³)
Magnetic Susceptibility
Excess ²¹⁰Pb (Bq kg⁻¹)
Comments
Photo
X-ray image
Pakarang Cape
Thap Lamu
20 m
50 m
Unit I
Unit II
Unit III
Core depth (cm)

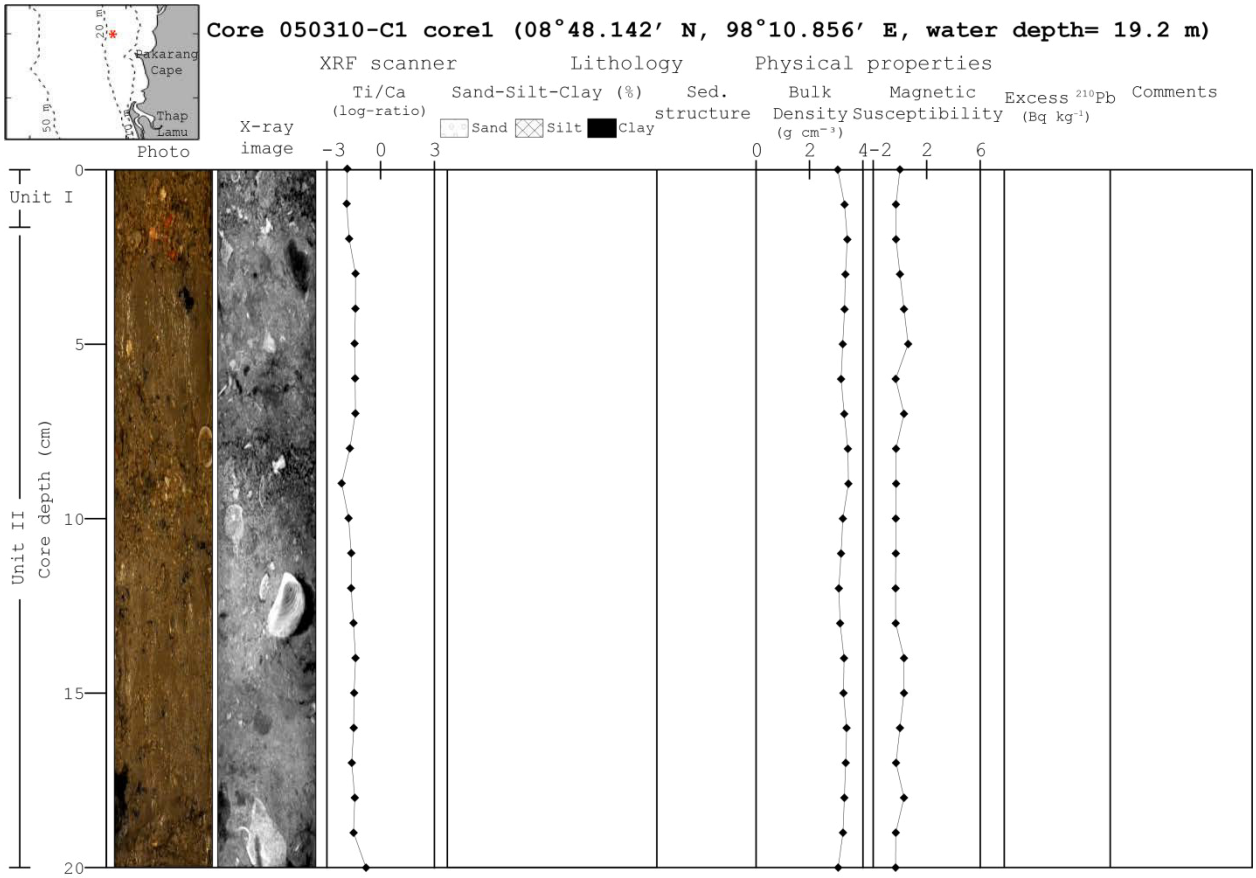
Core 050310-C1 core1 (08°48.142′ N, 98°10.856′ E, water depth= 19.2 m)
XRF scanner
Lithology
Physical properties
Ti/Ca (log-ratio)
Sand-Silt-Clay (%)
Sand
Silt
Clay
Sed. structure
Bulk Density (g cm⁻³)
Magnetic Susceptibility
Excess ²¹⁰Pb (Bq kg⁻¹)
Comments
Photo
X-ray image
Pakarang Cape
Thap Lamu
20 m
50 m
Unit I
Unit II
Core depth (cm)

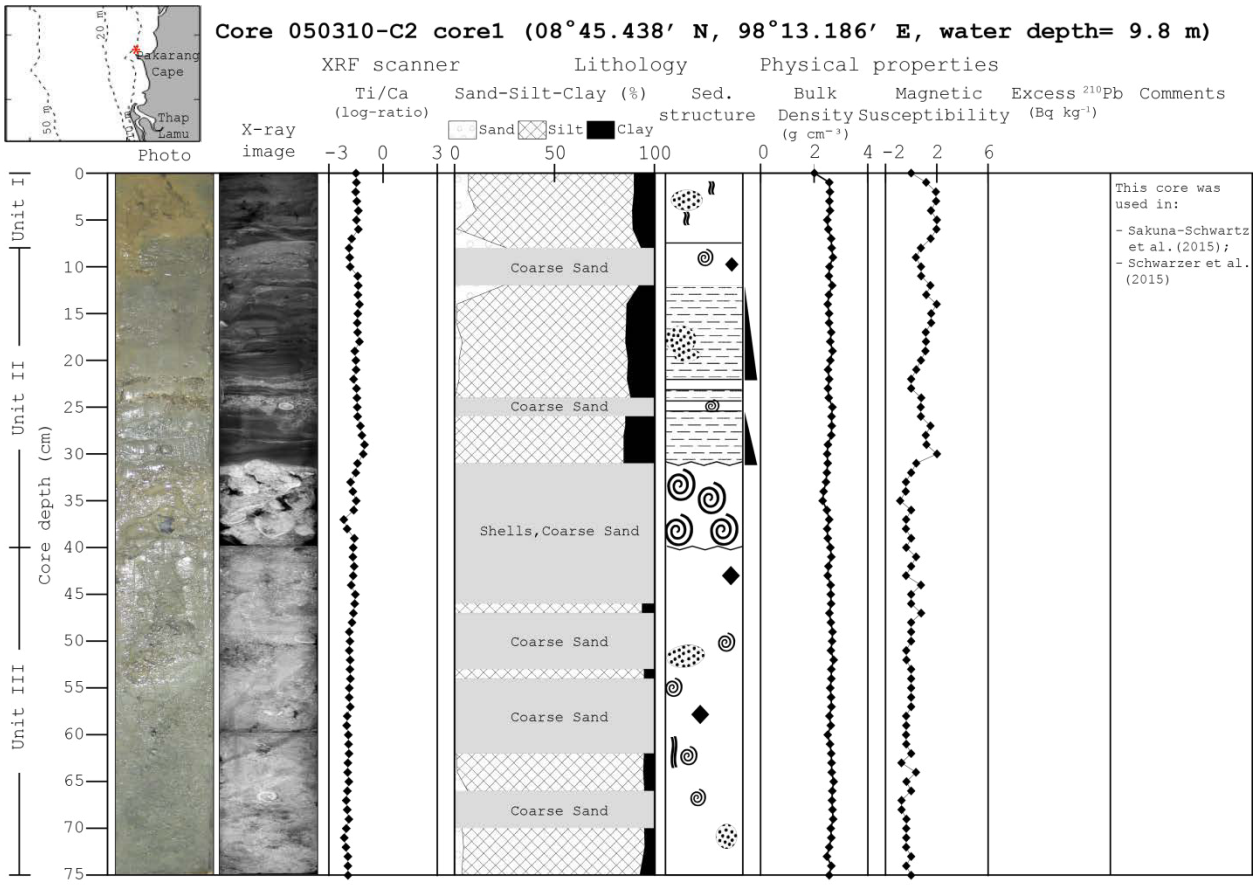
Core 050310-C2 core1 (08°45.438′ N, 98°13.186′ E, water depth= 9.8 m)
XRF scanner
Lithology
Physical properties
Ti/Ca (log-ratio)
Sand-Silt-Clay (%)
Sand
Silt
Clay
Sed. structure
Bulk Density (g cm⁻³)
Magnetic Susceptibility
Excess ²¹⁰Pb (Bq kg⁻¹)
Comments
Photo
X-ray image
Pakarang Cape
Thap Lamu
20 m
50 m
Unit I
Unit II
Unit III
Core depth (cm)
Coarse Sand
Coarse Sand
Shells,Coarse Sand
Coarse Sand
Coarse Sand
Coarse Sand
This core was used in:
- Sakuna-Schwartz et al.(2015);
- Schwarzer et al. (2015)

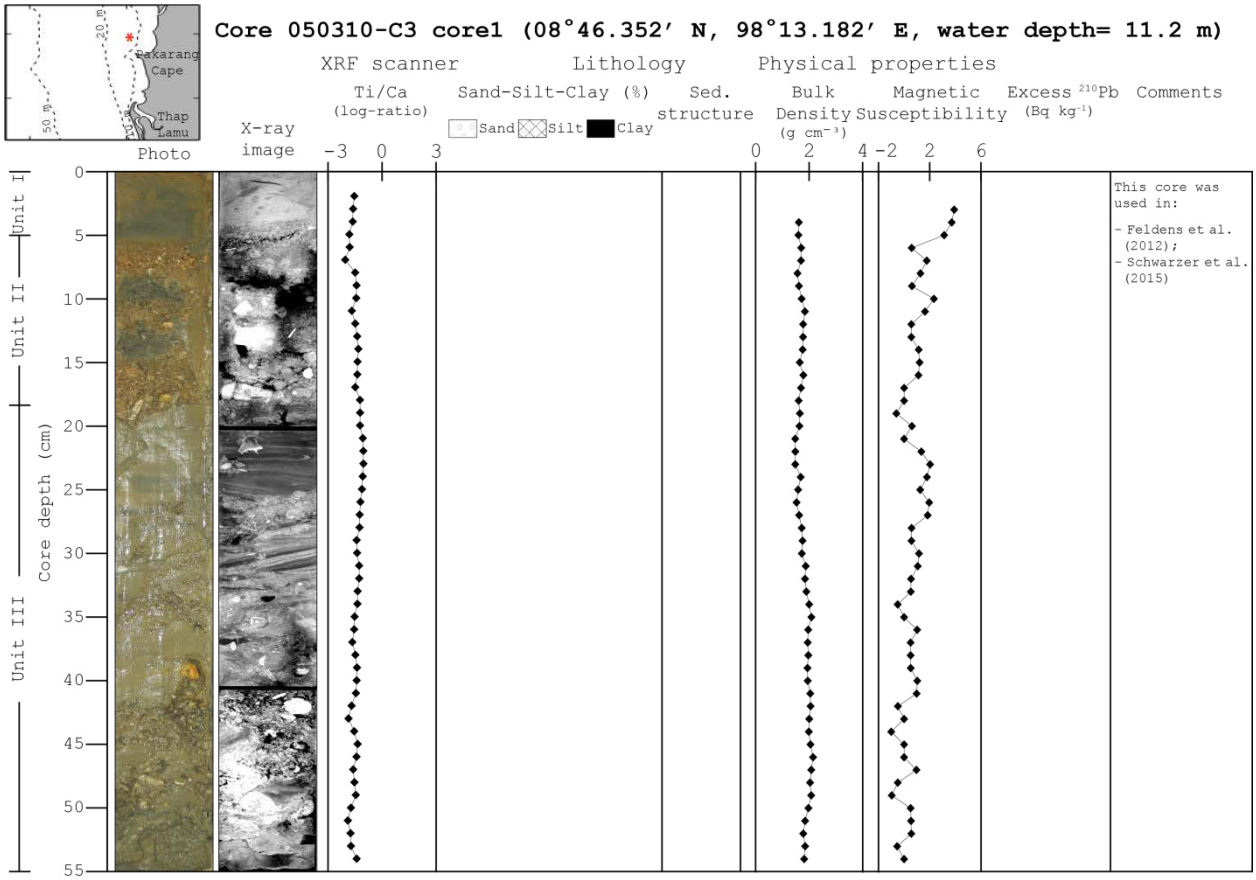
Core 050310-C3 core1 (08°46.352′ N, 98°13.182′ E, water depth= 11.2 m)
XRF scanner
Lithology
Physical properties
Ti/Ca (log-ratio)
Sand-Silt-Clay (%)
Sand
Silt
Clay
Sed. structure
Bulk Density (g cm⁻³)
Magnetic Susceptibility
Excess ²¹⁰Pb (Bq kg⁻¹)
Comments
Photo
X-ray image
Core depth (cm)
Unit I
Unit II
Unit III
Pakarang Cape
Thap Lamu
20 m
50 m
This core was used in:
- Feldens et al. (2012);
- Schwarzer et al. (2015)

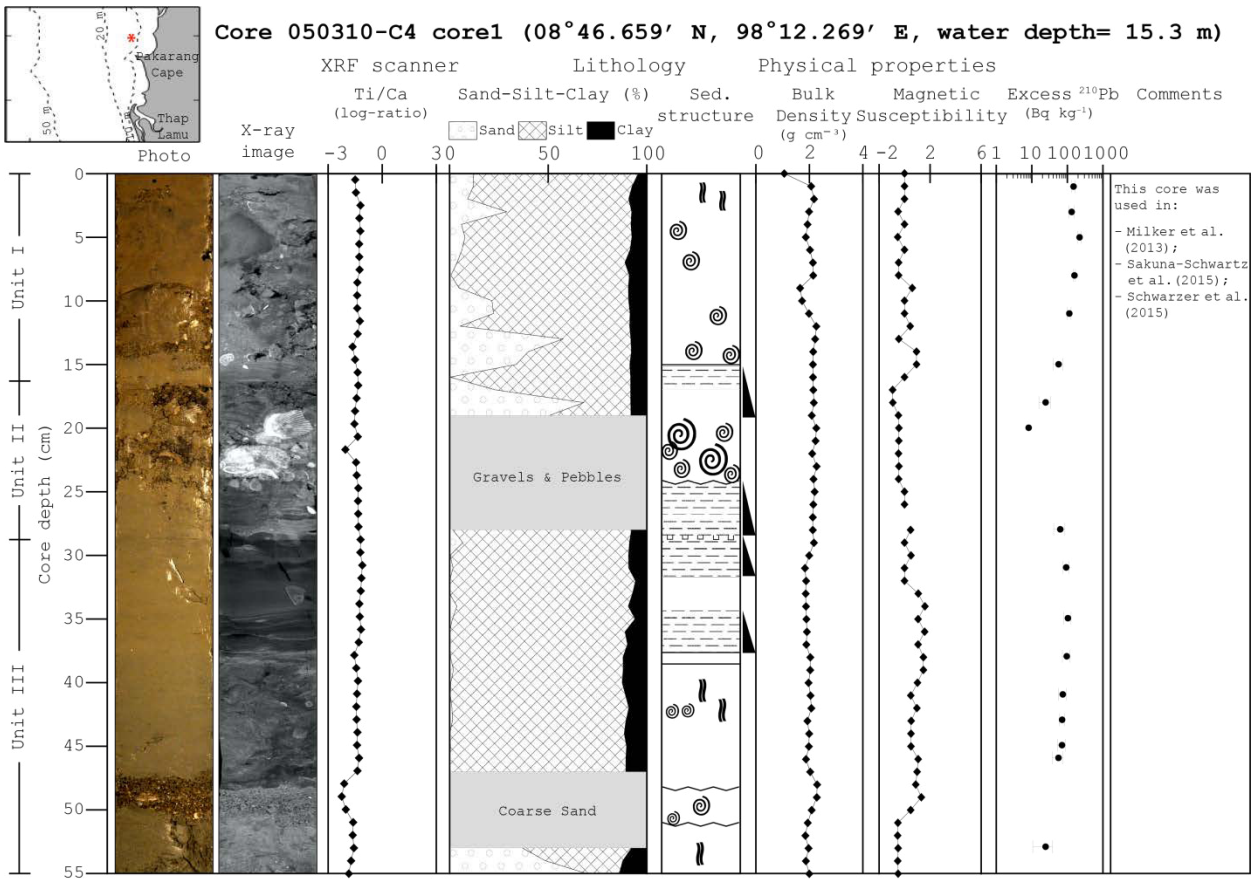
Core 050310-C4 core1 (08°46.659′ N, 98°12.269′ E, water depth= 15.3 m)
XRF scanner
Lithology
Physical properties
Ti/Ca (log-ratio)
Sand-Silt-Clay (%)
Sand
Silt
Clay
Sed. structure
Bulk Density (g cm⁻³)
Magnetic Susceptibility
Excess ²¹⁰Pb (Bq kg⁻¹)
Comments
Photo
X-ray image
Core depth (cm)
Unit I
Unit II
Unit III
Pakarang Cape
Thap Lamu
20 m
50 m
Gravels & Pebbles
Coarse Sand
This core was used in:
- Milker et al. (2013);
- Sakuna-Schwartz et al. (2015);
- Schwarzer et al. (2015)

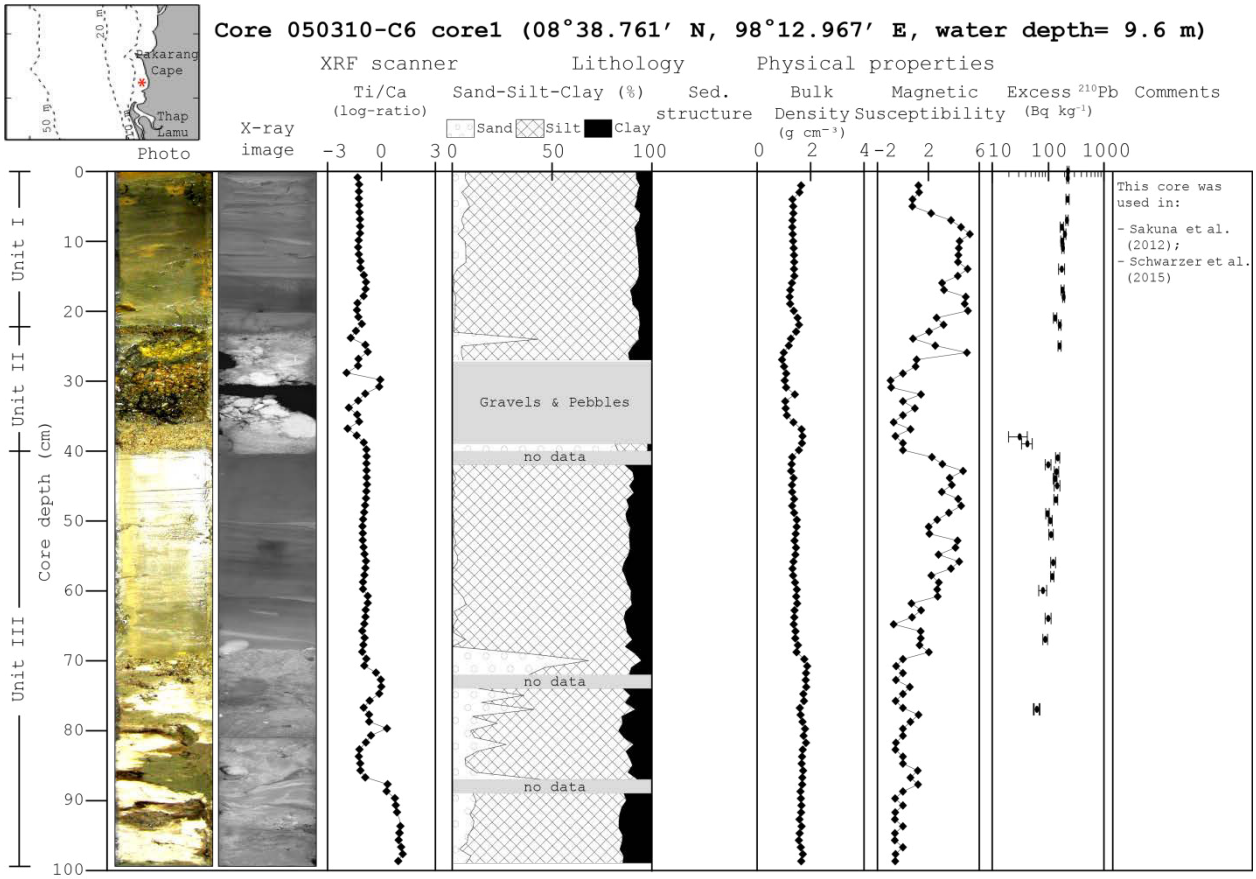
Core 050310-C6 core1 (08°38.761′ N, 98°12.967′ E, water depth= 9.6 m)
Pakarang Cape
Thap Lamu
20 m
50 m
XRF scanner
Lithology
Physical properties
Photo
X-ray image
Ti/Ca (log-ratio)
Sand-Silt-Clay (%)
Sand
Silt
Clay
Sed. structure
Bulk Density (g cm⁻³)
Magnetic Susceptibility
Excess ²¹⁰Pb (Bq kg⁻¹)
Comments
Core depth (cm)
Unit I
Unit II
Unit III
Gravels & Pebbles
no data
no data
no data
This core was used in:
- Sakuna et al. (2012);
- Schwarzer et al. (2015)

APPENDIX

ADDITIONAL PUBLICATIONS

Nat. Hazards Earth Syst. Sci., 13, 3095–3111, 2013
www.nat-hazards-earth-syst-sci.net/13/3095/2013/
doi:10.5194/nhess-13-3095-2013

Natural Hazards and Earth System Sciences
Open Access

Mapping tsunami impacts on land cover and related ecosystem service supply in Phang Nga, Thailand

G. Kaiser[1], B. Burkhard[2], H. Römer[3], S. Sangkaew[4], R. Graterol[2], T. Haitook[5], H. Sterr[6], and D. Sakuna-Schwartz[7,8]

[1]Norwegian Geotechnical Institute, Oslo, Norway
[2]Institute for Natural Resource Conservation, Christian-Albrechts-Universität zu Kiel, Kiel, Germany
[3]German Remote Sensing Data Center (DFD), German Aerospace Center (DLR), Oberpfaffenhofen, Germany
[4]Asian Institute of Technology, Bangkok, Thailand
[5]Department of Animal Science, Faculty of Agriculture, University of Khon Kaen, Khon Kaen, Thailand
[6]Institute of Geography, Christian-Albrechts-Universität zu Kiel, Kiel, Germany
[7]Institute of Geosciences Sedimentology, Coastal and Continental Shelf Research, Christian-Albrechts-Universität zu Kiel, Kiel, Germany
[8]Oceanography and Environment Unit, Phuket Marine Biological Center, Phuket, Thailand

Correspondence to: G. Kaiser (gka@ngi.no)

Received: 30 April 2012 – Published in Nat. Hazards Earth Syst. Sci. Discuss.: –
Revised: 5 July 2013 – Accepted: 16 July 2013 – Published: 5 December 2013

Abstract. The 2004 Indian Ocean tsunami caused damages to coastal ecosystems and thus affected the livelihoods of the coastal communities who depend on services provided by these ecosystems. The paper presents a case study on evaluating and mapping the spatial and temporal impacts of the tsunami on land use and land cover (LULC) and related ecosystem service supply in the Phang Nga province, Thailand. The method includes local stakeholder interviews, field investigations, remote-sensing techniques, and GIS. Results provide an ecosystem services matrix with capacity scores for 18 LULC classes and 17 ecosystem functions and services as well as pre-/post-tsunami and recovery maps indicating changes in the ecosystem service supply capacities in the study area. Local stakeholder interviews revealed that mangroves, casuarina forest, mixed beach forest, coral reefs, tidal inlets, as well as wetlands (peat swamp forest) have the highest capacity to supply ecosystem services, while e.g. plantations have a lower capacity. The remote-sensing based damage and recovery analysis showed a loss of the ecosystem service supply capacities in almost all LULC classes for most of the services due to the tsunami. A fast recovery of LULC and related ecosystem service supply capacities within one year could be observed for e.g. beaches, while mangroves or casuarina forest needed several years to recover. Applying multi-temporal mapping the spatial variations of recovery could be visualised. While some patches of coastal forest were fully recovered after 3 yr, other patches were still affected and thus had a reduced capacity to supply ecosystem services. The ecosystem services maps can be used to quantify ecological values and their spatial distribution in the framework of a tsunami risk assessment. Beyond that they are considered to be a useful tool for spatial analysis in coastal risk management in Phang Nga.

1 Introduction

1.1 Ecological impacts of the Indian Ocean tsunami in Phang Nga

The 2004 Indian Ocean tsunami left a path of destruction along the Andaman Sea coast of Thailand. The coastal areas of Phang Nga province suffered from an extraordinary high number of fatalities, structural damages and economic losses that affected or destroyed the livelihoods of coastal communities (United Nations and Worldbank, 2005). Although fatalities and damages to buildings and infrastructure were the most striking consequences of this tsunami disaster, environmental impacts and damages to ecosystems and related land use/land cover (LULC) also occurred. These included

uprooted coastal forests, beach erosion, impacts on coral reefs and sea-grass, pollution, contamination from tsunami deposits, and salt infiltration in ground- and surface water as well as in soils affecting vegetation and soil fertility (Choowong et al., 2009; DMCR, 2005a, b; Massmann, 2010; Paphavasit et al., 2009; Pongpiachan et al., 2013; Roemer et al., 2010; Szczucinski et al., 2006; UNEP, 2005; Vosberg, 2010). While the impacts on coral reefs and sea grass beds in the region were comparably small, the damages to coastal forests, e.g. mangroves, and plantations varied spatially, with more severe destruction close to the shore (FAO and MOAC, 2005; Römer, 2011).

Since the interconnection between coastal ecosystem degradation and communities' vulnerabilities has been widely recognized (Adger et al., 2005; Kallesøe et al., 2008; IUCN and UNEP, 2006), negative consequences were supposed to arise from the tsunami impacts due to the dependency of the coastal communities in Phang Nga on the local ecosystems. The economic, social and ecological linkages in the region are manifold, comprising fishing (e.g. shell fish, crab fish, oyster), aquaculture, agriculture, and tourism (Haitook et al., 2011; Willroth et al., 2011). It is therefore important to assess and quantify the ecological values and damages together with the socio-economic ones to evaluate the overall tsunami impact in the framework of a tsunami risk assessment and management.

A way to account for values of ecosystems is the consideration of the functions and services they provide as benefits to humans (MA, 2005; Daily, 1997; Costanza et al., 1997). The concept of ecosystem services (de Groot et al., 2010; Burkhard et al., 2012b) offers a methodological framework for the identification, quantification, evaluation and mapping of land use change on human societies (Burkhard et al., 2012a). It has evolved to a common framework in interdisciplinary ecological and socio-economic research and has high potential to be implemented in management and planning (Burkhard et al., 2012a; Kienast et al., 2009; MA, 2005; Müller and Burkhard, 2007). Ecosystem services also play an important role in risk mitigation of natural hazards and post disaster recovery. Costanza and Farley (2007) emphasised that part of the reason for the severe impacts of coastal disasters is the disregard of ecosystem services in coastal planning. Ecosystems with their functions and services are indeed supposed to reduce disaster impacts by providing natural capital that is essential for the preservation of livelihoods (IUCN and UNEP, 2006).

1.2 Mapping of ecosystem services

A common way to assess ecosystem services is the economic valuation (Costanza et al., 1997; MA, 2005; Bateman et al., 2010; Kumar, 2010). Beyond that the spatial analysis of ecosystem service values (Troy and Wilson, 2006) or the analysis of temporal dynamics of ecosystems services (Kroll et al., 2012) is used. Especially the assignment of ecosystem service supply capacities to spatially explicit biophysical units in maps provides useful aggregated information on current supply conditions and changes over space and time (Haines-Young et al., 2012; Burkhard et al., 2012a; Kienast et al., 2009). Spatio-temporal changes can be induced by human LULC changes, climatic change, or disturbances due to natural disasters. These visualisations of ecosystem services and their dynamics are useful tools for decision makers and environmental managers (Swetnam et al., 2011). However, before ecosystem services maps finally can be used for environmental risk management and related spatial planning, the methods need to be developed further and respective data and information have to be acquired in further studies (Daily and Matson, 2008; Burkhard et al., 2012a).

In this case study, we map ecosystem services in connection with impacts of the 2004 Indian Ocean tsunami in Phang Nga, Thailand. The aim is to identify tsunami-induced LULC changes and to assess and evaluate related alterations in ecosystem service supply capacities. The work has been conducted in the framework of the research project "Tsunami Risks, Vulnerability and Resilience in the Phang Nga and Phuket Provinces, Thailand – **T**sunami **R**isk **A**nd **I**nformation **T**ool (TRAIT)" and results will be integrated in an impact and vulnerability assessment for the region.

An approach is applied that indicates different LULC classes' capacities to supply ecosystem services on a relative scale, integrating local expert assessments (based on Burkhard et al., 2009, 2012a; MA, 2005; de Groot, 1992; Costanza, 1997). A similar approach was used by Maes et al. (2011) to map ecosystem services on a European scale, by Nedkov and Burkhard (2012) to map flood regulating ecosystem services in Bulgaria, by Kroll et al. (2012) in a central German peri-urban region, and by Vihervaara et al. (2010) studying the linkages between land use changes and ecosystem services in Lapland, Northern Finland. The approach is considered suitable here since people at the Phang Nga coast benefit from ecosystem services provided by the coastal areas, e.g. for eco-tourism, diving tourism, local farming, and fishery (IUCN and UNEP, 2006; Römer, 2011). Hence, socio-ecological aspects play a major role in the region's vulnerability and coping capacity.

The case study refers to changes in ecological integrity, provisioning, regulating and cultural ecosystem services on a local scale at three different points in time. Altogether, 17 ecosystem services of 18 LULC classes were assessed for pre-tsunami conditions and tsunami induced LULC change and related changes in ecosystem service supply capacities were mapped based on stakeholder interviews, field investigations, remote-sensing and GIS techniques in order to answer the following research questions:

– Does a combination of land cover data, stakeholder knowledge, field investigations, remote sensing, and GIS enable complex spatial assessments of multiple ecosystem services?

– Can the methods and the resulting maps be used for the evaluation of ecological impacts in the framework of a tsunami risk assessment?

– Can the methods and the resulting maps contribute to coastal risk management?

The paper is structured as follows: in Sect. 2 the study area is introduced. Section 3 describes the methodological approach comprising the development of an ecosystem services matrix, remote-sensing based damage and recovery assessment of LULC, and the development of multi-temporal ecosystem services maps. The resulting matrix and maps are presented in Sect. 4, followed by a discussion in Sect. 5 and conclusions in Sect. 6.

2 Study area

The study area covers a 50 km long, flat coastal stripe from Thai Mueang in the South to Ban Nam Khem in the North in the Phang Nga province, Thailand (Fig. 1). The whole area was devastated by the 2004 tsunami. Settlement structures and ecological characteristics in the area are diverse. Ban Nam Khem is a small community dominated by fishery and agriculture. Further south, Khao Lak has increasingly developed quality tourism structures including eco-tourism and is positioned in the global tourism market (Willroth et al., 2011). The Khao Lampi – Hat Thai Mueang National Park north of Thai Mueang city is located on a spit with a tidal inlet surrounded by mangrove belts, and populated by indigenous people. In all parts of the study area people live in close relation with their environment in terms of agriculture, fishery, or tourism. Dominating LULCs are casuarina forest, mixed beach forest, melaleuca forest, coconut plantations, mangroves, and grassland. *Casuarina equisetifolia* forms 20–50 m wide mono-specific stands at sandy coasts (Cochard et al., 2008). Mixed beach and melaleuca forests (*Melaleuca leucadendron*) are located in the Hat Thai Mueang National park in the south. Coconut plantations (*Cocos nucifera*) are spread all over the study area. According to Yanagisawa et al. (2009) dominant mangrove species found in the study area are *Rhizophora* sp. and *Bruguiera* sp. Beyond that grassland, open woodland, beaches, ponds, and build up areas are present (cf. Fig. 3, in Sect. 3.1).

The landscape in the study area is strongly shaped by human activities such as tin mining, shrimp aquaculture, and intensive agricultural use, dominated by the cultivation of rubber, oil palm, coconut, and cashew nut. Fishing and agriculture are a major source of income with 45 % of the population of Phang Nga employed in this sector (Willroth et al., 2011).

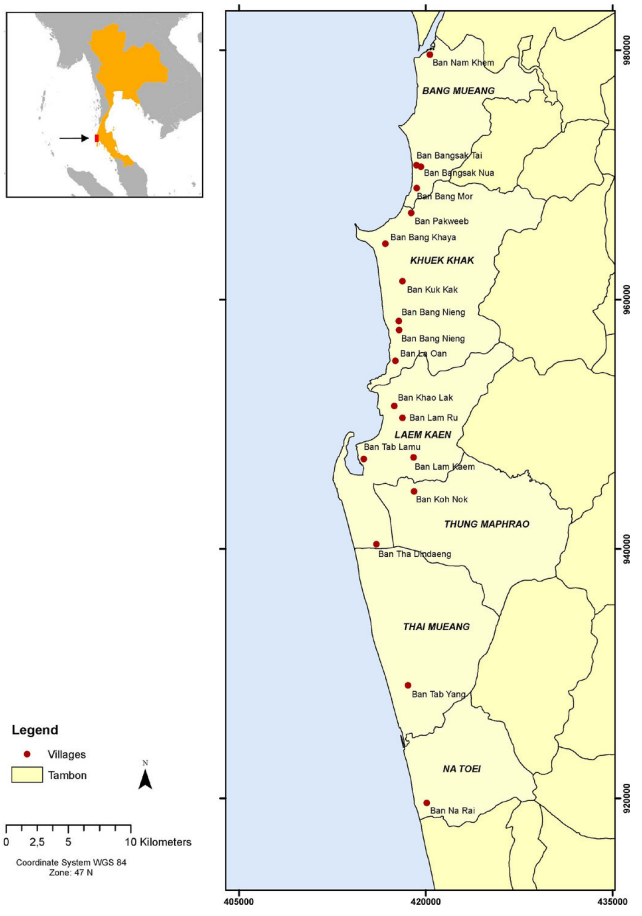

Fig. 1. The study area from Ban Nam Khem in the North, to Thai Mueang, Phang Nga in the South. The 18 villages where interviews took place are included in the map.

Moreover, due to the growing tourism sector, many natural forests have been cleared for development of large hotel complexes. In particular mangroves and coral reefs are under pressure due to marine and coastal development, including for example the expanding shrimp farm industry (Baird et al., 2005; UNEP, 2005; IUCN and UNEP, 2006). The tiger prawn industry, which developed in the 1990s, has led to a dramatic reduction of the mangrove area in South Thailand. By the mid 1990s the initial mangrove area was reduced by about 33 % (FAO and MOAC, 2005).

The 2004 tsunami led to a further impact on coastal ecosystems by destroying large patches of the exposed mangroves, casuarina forests, and coconut plantations and by causing indirect impacts such as defoliation or yellowing of leaves of mixed beach forests and melaleuca forests (Roemer et al., 2010). IUCN and UNEP (2006) estimated the overall economic loss due to damages on coastal ecosystems in the Phang Nga province to about USD 11 million, mainly arising from the destruction of mangroves.

3 Methods

The methodological approach for mapping tsunami impacts on ecosystem service supply includes three steps (Fig. 2):

1. LULC classification based on IKONOS satellite images (2003), and change detection analysis of LULC to detect tsunami damages after the event (2005) as well as recovery processes (2008).

2. Interviews with local stakeholders from coastal villages in Phang Nga as well as Thai governmental and non-governmental organisations to evaluate ecosystem services in the study area using a scoring approach. Development of a matrix for selected ecosystem functions and ecosystem service supply capacities in the study area based on a statistical analysis of the data gained from the interviews.

3. GIS-based mapping of tsunami-induced changes of ecosystem service supply capacities in the different LULC classes.

3.1 LULC classification, damage and recovery mapping

The LULC information for the study area was derived from high-resolution satellite images (IKONOS), taken before the tsunami in January 2003, using remote-sensing techniques. For the multi-temporal analysis on damages and recovery IKONOS images from January 2005 and February 2008 were included in the analysis. A rule-based object oriented classification approach was performed for the pre-tsunami image of 2003. The final classification has an overall accuracy of 93.6 % and a Kappa of 0.90, and can therefore be considered as very accurate. The resulting map for the coastal zone between Ban Nam Khem and Thai Mueang city consists of 37 different LULC classes including plantations, beaches, buildings and infrastructure, grassland, water bodies, and natural forests, such as mangroves, casuarina forest, or primary rain forest (Fig. 3). Details of the remote-sensing based LULC classification are provided in Römer (2011).

To derive LULC maps that show the changes that occurred due to the damaging effect of the tsunami, impacts and recovery processes were analysed for selected LULC classes by applying digital change detection techniques based on multi-temporal IKONOS imagery (Roemer et al., 2010; Römer et al., 2012b). A damage map (Fig. 4) was generated for January 2005 (post-tsunami) using the direct multi-date classification (DMC) method, which includes a supervised classification of a multi-temporal band composite (Roemer et al., 2010). Damages to LULC classes were categorised in: type 1 = no damage (no identifiable damage), type 0 = total damage (e.g. uprooted or removed vegetation), type 0.5 = indirect damage (degradation of understorey vegetation and soils, applicable to foliage of woody vegetation and to all non-woody vegetation). The damage analysis was conducted

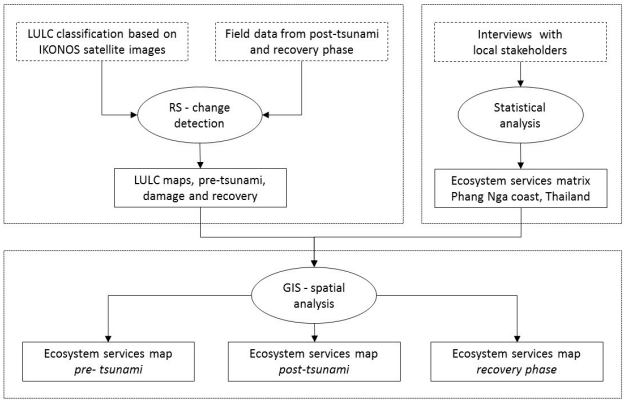

Fig. 2. Methodological approach for mapping changes in ecosystem service supply due to the impact of the 2004 Indian Ocean tsunami.

for the forest ecosystems mangroves, casuarina forest, coconut plantations, mixed beach forest, and melaleuca forest.

For a recovery map 3 yr after the tsunami (2008), the recovery rate was calculated based on multi-temporal Transformed Normalised Vegetation Index (TNDVI) images from three acquisition dates in 2003, 2005 and 2008 (for details see Römer et al., 2012a). The recovery rate was then binary coded in order to distinguish between areas that have recovered or were in a recovery state and those areas indicating persistent situations or even post-tsunami degradation not showing any recovery patterns. Field measurements from 2009 on vegetation recovery and succession were used for validating the change detection results (Römer et al., 2012a). Since the recovery assessment was conducted based on the NDVI, non-vegetated areas were not included in the analysis. The analysis included mangroves, casuarina forest, coconut plantations, and grassland.

Tsunami impacts on the beaches as well as beach recovery were added to the damage and recovery maps by applying a post-classification change detection analysis for beach areas (Vosberg, 2010).

From the LULC classification and the damage and recovery assessment, three maps were generated: (a) a LULC map representing LULC before the tsunami (2003) (Fig. 3), (b) a damage map including a quantification, classification, and spatial distribution of damages to LULC directly after tsunami (2005) (Fig. 4), and (c) a recovery map quantifying and classifying the spatial distribution of recovery from these damages until 2008 (not shown in this paper).

3.2 Stakeholder interviews and ecosystem services matrix

On a local scale the value of ecosystems is closely related to the dependencies of coastal communities on ecosystem services for their livelihoods. Therefore, to gain information on the ecosystem services provided and used in the region, interviews with local stakeholders and experts in

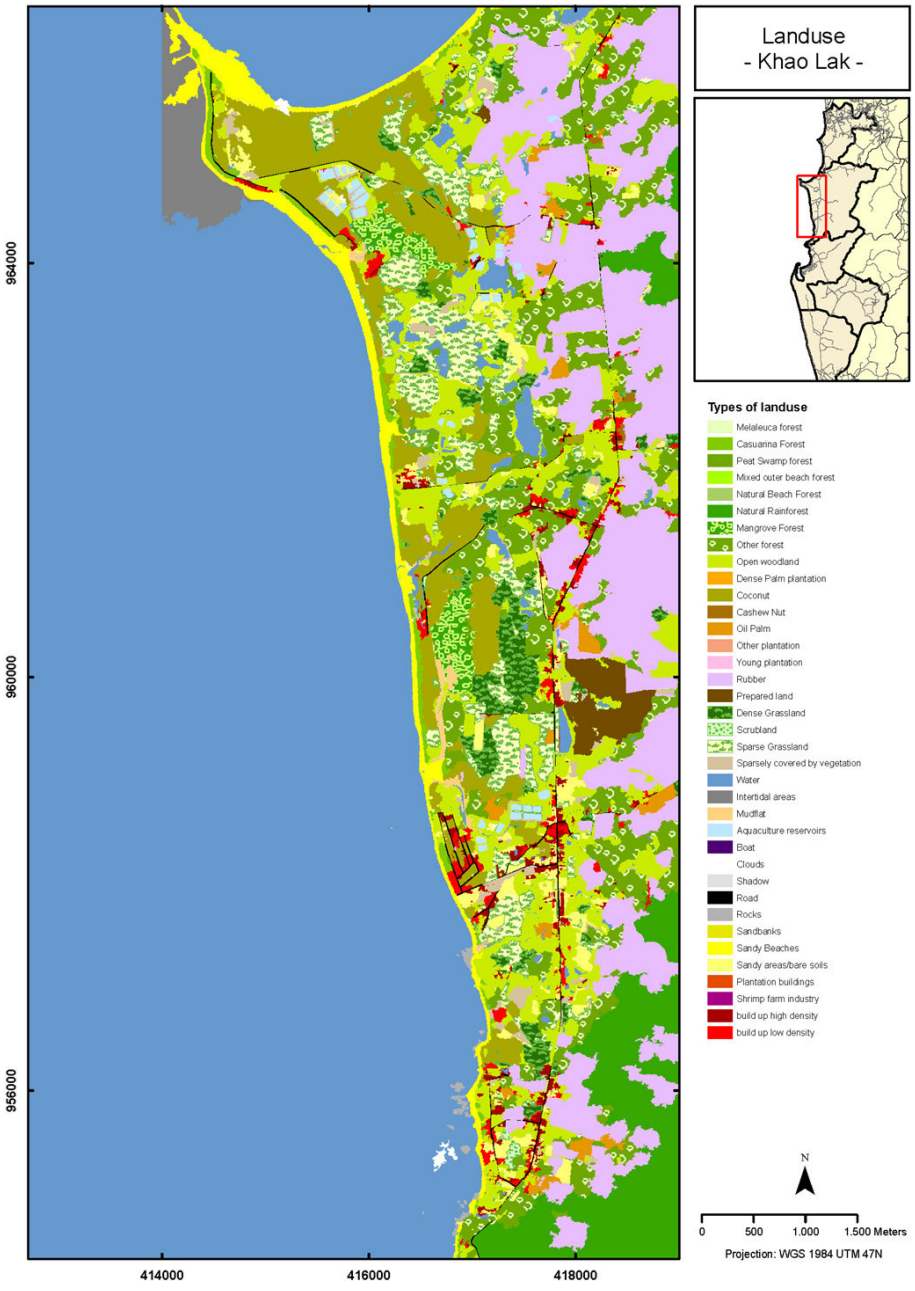

Fig. 3. LULC map exemplified for Khao Lak, based on IKONOS imagery from 13 January 2003.

the field of environmental management were conducted in 18 villages in the districts of Takuapa and Thai Mueang, Phang Nga Province (Fig. 1). Criteria for village selection included (a) a high degree of impact by the 2004 tsunami, and (b) a high degree of diversification of occupation and livelihoods of the people with a close link to coastal and marine resources (Haitook et al., 2011).

A questionnaire was distributed to 33 local stakeholders, whereof 18 persons were village chiefs or village chief assistants from Ban Nam Khem, Khao Lak, and Thai Mueang, nine persons were from governmental organisations and six persons from non-governmental international organizations. The standardised questionnaire included an empty ecosystem services matrix (see Table 2), where scores had to be given for each LULC class and each ecosystem service according to the respondents' local knowledge and experience.

The study covered 17 ecosystem functions and services of 18 LULC classes (Tables 1 and 2). The 18 LULC classes were (partly) merged from the original 37 LULC classes identified by the remote-sensing based classification (Fig. 3). The following ten LULC classes were excluded from the analysis: plantation buildings, shrimp farm industry

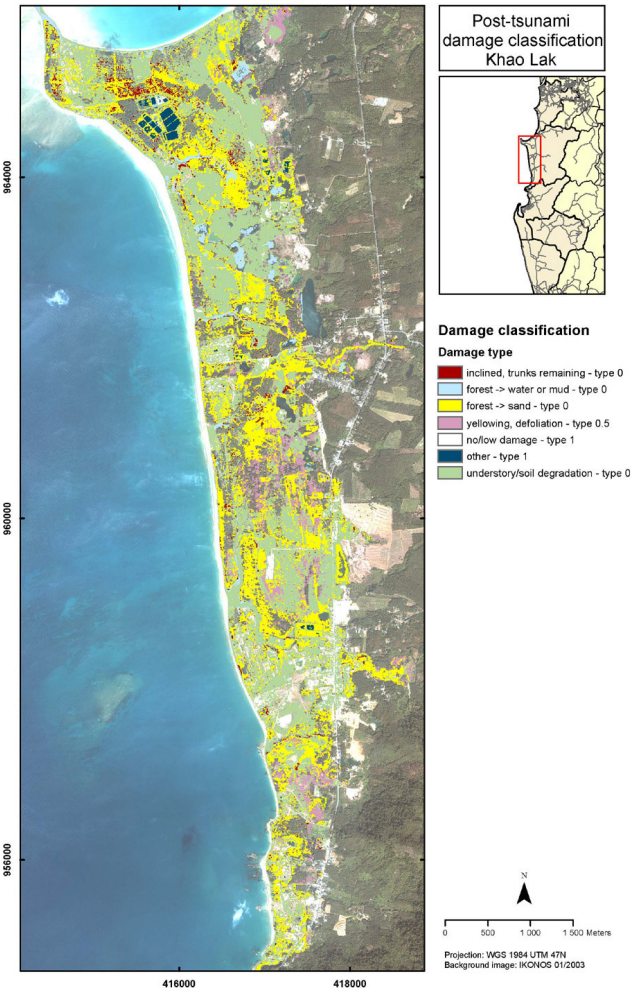

Fig. 4. Tsunami damage map for Khao Lak showing the spatial distribution and the type of damages to vegetation directly after the tsunami in 2005. Beach erosion is not included in the map. Areas with no/low damage are transparent. The method (Direct Multi-Date Classification) and data are described in Roemer et al. (2010). For the damage map applied in the ecosystem services maps, damage types have been summarised to type 1 (no damage), type 0 (total damage), and type 0.5 (indirect damage).

buildings, build up areas high density, build up areas low density, prepared land, boats, clouds, shadow, roads, and rocks. Some of the other categories were merged as follows: beach (sandy beaches, sandbanks), tidal inlet (mudflat, intertidal areas), rubber (rubber plantation, younger plantation), coconut plantation (coconut, other plantation), natural grassland (dense grassland, scrubland, sparse grassland, sparsely covered by vegetation, open woodland), oil plantation (dense palm plantation, oil palm), mixed beach forest (rain forest, other forest, mixed outer beach forest, natural beach forest).

The ecosystem functions and services were organised in the four categories: ecological integrity, provisioning services, regulating services, and cultural services (Burkhard et al., 2009, 2012a). Ecological integrity refers to ecosystem structures and processes responsible for ecosystem functioning and self-organisation (Müller, 2005; Müller and Burkhard, 2007; Barkmann et al., 2001). From the eight ecological integrity indicators initially suggested by Müller (2005), the ecosystem structure indicator "biodiversity" and the process indicator "nutrient cycling" were selected to be assessed in this study. The authors are aware that there are manifold categorisations for ecosystem functions and services and the related scientific debate, for example concerning problems of potential double counting, is not finished yet (Wallace, 2007). However, related studies are so singular, question- and context-related, so that perhaps a common classification framework is neither feasible nor really necessary (Burkhard et al., 2012b; Costanza, 2008). In this study, the focus was on illustrating spatial distributions of ecosystem function and service supply and their temporal changes. No "total ecosystem values" have been summed up in the end. Moreover, the two assessed ecological integrity components "biodiversity" and "nutrient cycling" are not considered in any of the other ecosystem service categories here. Therefore, problems of double counting were not involved.

Provisioning services include products that humans can derive from ecosystems, e.g. food or raw materials. Regulating services are ecological regulation mechanisms (such as coastal protection by coastal forests or ground water recharge) that are important for human activities. Cultural services are important for the quality of life and for spiritual inspiration, but also for economic aspects, i.e. tourism. The selection of ecosystem services in the three categories is mainly based on de Groot et al. (2010), Burkhard et al. (2009, 2012a), MA (2005) and suggestions from local stakeholders and experts for site-specific services. For example, the service "provisioning of shade" was highly recognised by the locals for their daily activities. Therefore, it was included in the study as a new and innovative aspect compared to existing ecosystem service categorisations.

In Table 1, an overview on the ecosystem functions and services assessed in this study is given.

The respondents were asked to rate each ecosystem service according to its overall importance in and for the communities in the region.

For the assessment of different LULC classes' capacities to support ecosystem integrity or to supply ecosystem services, the following rating scale was applied (after Burkhard et al., 2009, 2012a): 0 = no relevant capacity, 1 = low relevant capacity, 2 = relevant capacity, 3 = medium relevant capacity, 4 = high relevant capacity, and 5 = very high relevant capacity.

In addition, for a better interpretation of the results, further questions were included in the questionnaire on the respondents' evaluation of tsunami impacts on LULC and ecosystem service supply and their observations regarding the recovery progress in the region. The respondents were asked to categorise the damages to each LULC class according to

Table 1. Ecosystem functions and services investigated in this study.

	Short description	References
Ecological functions and integrity		
Biodiversity	The presence and absence of selected species, (functional) groups of species, biotic habitat components or species composition.	Müller (2005), MA (2005), Müller and Burkhard (2007), Burkhard et al. (2009),
Nutrient cycling	The capacity of an ecosystem to cycle nutrients and matter and thereby preventing the irreversible output of elements from the system.	De Groot (1992), Forbes and Broadhead (2007), Kandziora et al. (2013)
Provisioning services		
Food	Food obtained from: crops, livestock, captured fisheries, aquaculture, wild-foods and oil as well as presence of edible plants and animals.	Burkhard et al. (2009), de Groot et al. (2010)
Wood/fibre/oil/timber	Timber and fibre harvesting, e.g. for ornament making and tools. Presence of species or abiotic components with potential use for timber, fuel or raw material.	Burkhard et al. (2009), de Groot et al. (2010)
Medicine	Production of bio-chemicals, medicines and presence of species or abiotic components with potential chemical and/or medical use.	Burkhard et al. (2009), de Groot et al. (2010)
Energy/biomass	Presence of trees or plants with potential use as energy source, e.g. wood fuel cooking.	Burkhard et al. (2009)
Freshwater supply	Presence of fresh water from coastal aquifers or groundwater reservoirs.	Burkhard et al. (2009), Haitook et al. (2011), Graterol (2011)
Regulating services		
Local climate regulation	Changes in land cover can locally affect temperature, wind, radiation and precipitation.	Burkhard et al. (2009)
Coastal protection	Refers to natural elements that reduce the impact of extreme flood events, e.g. the role of forests in dampening wave impact.	Burkhard et al. (2009), de Groot et al. (2010)
Erosion regulation	In this study referring to the vegetation cover at the coast and the patches of sea-grass offshore that prevent beach erosion.	Haitook et al. (2011), Graterol (2011)
Water purification	Refers to the general capacity of ecosystems to purify fresh water.	Burkhard et al. (2009)
Provisioning of shade	Presence of trees along the streets and beaches and along the coastline that people use to protect themselves from the intense solar radiation.	Haitook et al. (2011), Graterol (2011), de Groot (1992)
Pollination	Ecosystem changes affect the distribution, abundance, and effectiveness of pollinators. Wind and bees are in charge of the reproduction of a lot of plants of cultural importance.	Burkhard et al. (2009), de Groot et al. (2010)
Ground water recharge	Changes in land cover strongly influence the timing and magnitude of runoff, flooding, and aquifer recharge.	Burkhard et al. (2009)
Cultural services		
Aesthetic value	Refers to the visual qualities of the area (beauty of the place). Aesthetic information has considerable influence on the quality of life.	de Groot (1992)
Recreation and tourism	Refers to the recreational activities that people can enjoy in the area (fun activities for relaxation, e.g. nature walks, hiking, snorkelling, guided tours, elephant rides) and available facilities (e.g. hotels, parks, restaurants, stores, swimming pools).	de Groot et al. (2010)
Education/research	Features with special educational and scientific value/interest, i.e. referring to the extent to which the area attract scientist to study certain phenomena and to the opportunities that area offers to teach about the natural system.	de Groot et al. (2010)

their local knowledge in "no/minor damage", "polluted/salt intrusion", and "destroyed/washed away/broken". Moreover they were asked to estimate the duration of the recovery process (Table 4). In addition, group discussions were conducted in some villages with about four to eight persons in each group to discuss these questions (Haitook et al., 2011).

When analysing the results it should be taken into account that the scoring was often difficult for the respondents and answers can be very subjective depending on peoples' personal experience (Fagerholm et al., 2012),

A descriptive statistical analysis was conducted to analyse the data from the scoring of the local stakeholders. For all LULC classes and all services, the scores were analysed using the statistical median. It has to be mentioned here, that not all 33 respondents ranked all services for all LULC classes. Very few answers were given for melaleuca forest (9), aquaculture (7), and natural grassland (2).

3.3 Creation of ecosystem services maps

To create the maps with the spatial distribution of ecosystem service supply capacities (pre-tsunami ecosystem services maps), the matrix (Table 2) was linked to the pre-tsunami LULC map in GIS by assigning the ecosystem service supply capacity scores to each polygon (biophysical unit) in the LULC map (after Burkhard et al., 2009, 2012a).

The post-tsunami ecosystem services maps were derived by combining the pre-tsunami ecosystem services maps with the damage classification, which was derived from the change detection analysis (Sect. 3.1). The percentage of the damage in each LULC polygon was multiplied by the pre-tsunami ecosystem service supply capacity score. The ecosystem service supply capacity score of the damaged part was then subtracted from the original score in order to get the ecosystem service supply capacity score, which was left after the tsunami (Eq. 1, Fig. 5).

$$\mathrm{ESSC}_{\mathrm{post}} = \mathrm{ESSC}_{\mathrm{s}} \cdot (1 - d) \quad (1)$$

where $\mathrm{ESSC}_{\mathrm{post}}$ = Ecosystem service supply capacity score post tsunami, $\mathrm{ESSC}_{\mathrm{s}}$ = ESSC score, d = damage in 2005.

Recovery refers to the potential and the rate at which vegetation reclaims its habitat by natural succession processes after being degraded or removed by the tsunami in 2004 (Römer et al., 2012a). To derive the ecosystem service supply capacity scores during recovery in 2008, the recovery was multiplied by the damages and the pre-tsunami ecosystem service supply capacity score, and added to each ecosystem service's post-tsunami ESSC score. This operation provided the respective ecosystem service supply capacity scores for 2008 (Eq. 2, Fig. 5).

$$\mathrm{ESSC}_{\mathrm{rec}} = r^{*}d^{*}\mathrm{ESSC}_{\mathrm{s}} + \mathrm{ESSC}_{\mathrm{post}} \quad (2)$$

where $\mathrm{ESSC}_{\mathrm{rec}}$ = Ecosystem service supply capacity score after recovery, r = recovery in 2008, d = damage in 2005, $\mathrm{ESSC}_{\mathrm{post}}$ = ESSC score post tsunami.

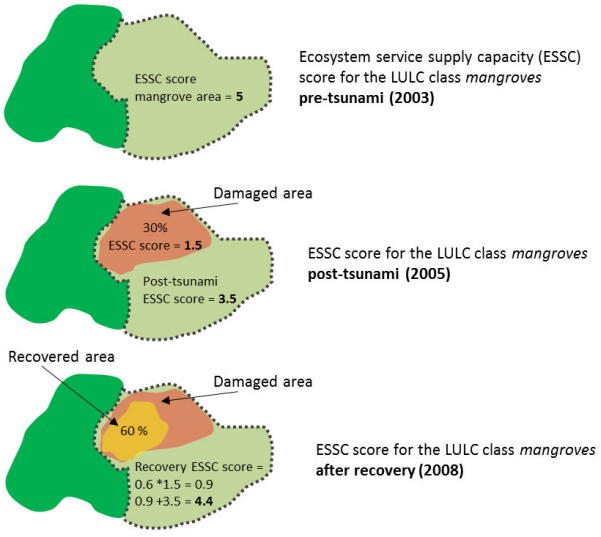

Fig. 5. Sketch describing the approach to calculate the ecosystem service supply capacity scores for the post-tsunami and the recovery phase (cf. Eqs. 1 and 2).

4 Results

4.1 Ecosystem services matrix

Results show, that the Phang Nga coast has a high capacity to support ecosystem functions and to supply services from a variety of LULC classes (Table 2). These can be considered of great importance for the livelihood of the local people and also for tourism and the economy of the region.

The ecosystem services matrix (Table 2), derived from the statistical analysis of the local stakeholder scoring shows that, according to the respondents' perception, mangroves, casuarina forest, mixed beach forest, coral reefs, tidal inlets, and wetlands (here peat swamp forest) provide the highest overall ecosystem service supply capacity. Lowest scores were given to plantations and aquaculture. In general the function "biodiversity" as well the services "food provisioning", "coastal protection" and all cultural services are considered to be particularly important in the region. This reflects the character of the study area, which is dominated by tourism and related activities, small business of local people at the beach, as well as fishery and agriculture.

Mangroves, which are known to be among the most valuable coastal ecosystems in the world (ten Brink, 2011), are also considered to be particularly important in almost all services. For mangroves the ecosystem functions "biodiversity" and "nutrient cycling" have been ranked with the highest score of 5. Mangroves are also considered to provide regulating services, such as "climate regulation" or "coastal protection" (also ranked with 5) by stabilising sediment and partly attenuating wave energy. Moreover, mangroves are an important food source as well as of cultural value for locals and

Table 2. Ecosystem services matrix for the coastal areas of the Phang Nga province, Thailand linking LULC classes to their capacities to support ecosystem functions and to supply ecosystem services on the scale: 0 = no relevant capacity, 1 = low relevant capacity, 2 = relevant capacity, 3 = medium relevant capacity, 4 = high relevant capacity, 5 = very high relevant capacity.

n: Mangroves = 24, Casuarina forest = 21, Rubber plantation = 20, Coconut plantation = 23, Orchard/Cashew nut = 12, Oil palm plantation = 20, Mixed beach forest = 21, Melaleuca forest = 9, Beach = 23, Tidal Inlet = 26, Coral reefs = 21, Sea grass = 19, Aquaculture = 7, Natural grassland = 2, Wetlands = 12, Ocean = 21, Pond = 20, Stream/river/channel = 17.

Code	LULC class	**Ecological Integrity**	Biodiversity/habitat function	Nutrient cycling	**Provisioning Services**	Food	Wood/fiber/oil/timber	Medicine	Energy/biomass	Fresh water	**Regulating Services**	Local climate regulation	Coastal protection	Erosion protection	Water purification	Provisioning of shade	Pollination	Ground water recharge	**Cultural Services**	Aesthetic value	Recreation and tourism	Education/reseach
1	Mangroves		5	5		5	4	3	2	0		5	5	5	4	4	4	4		4	4	5
2	Casuarina forest		3	4		2	3	0	2	0		4	5	4	3	4	4	4		4	5	4
3	Rubber plantation		1	4		0	5	0	2	0		4	0	2	2	4	2	3		3	3	3
4	Coconut plantation		2	3		4	3	2	1	0		3	3	3	3	3	3	3		4	3	2
5	Orchard/Cashew nut		1	3		3	0	0	0	0		3	0	2	2	3	3	2		3	2	2
6	Oil palm plantation		2	2		1	0	0	0	0		3	0	3	3	4	2	3		4	3	3
7	Mixed beach forest		4	4		4	3	2	2	0		5	5	5	4	4	4	4		5	5	4
8	Melaleuca forest		3	4		3	3	1	1	0		4	3	4	3	3	3	4		4	3	3
9	Beach		3	3		3	0	0	0	0		3	3	4	4	0	3	3		5	5	4
10	Tidal inlet		5	4		5	0	0	0	4		4	4	3	3	2	4	3		4	4	3
11	Coral reefs		5	4		5	0	0	0	0		4	3	4	4	1	5	3		5	5	5
12	Sea grass		5	4		5	0	1	0	0		4	3	4	3	1	4	3		4	3	4
13	Aquaculture		2	3		4	0	0	0	0		3	2	1	1	1	0	3		2	2	3
14	Natural grassland		3	4		4	0	0	0	0		4	4	4	4	1	4	4		4	4	4
15	Wetlands		4	5		4	2	2	1	3		4	3	3	4	3	3	4		4	3	4
16	Ocean		5	5		5	0	0	0	5		5	0	0	2	0	3	0		4	5	3
17	Pond		4	3		3	0	0	0	4		4	0	0	3	0	4	3		4	3	2
18	Stream/river/channel		4	4		3	0	0	0	4		4	0	2	3	0	4	3		4	4	3

Assessment scale	
0	No relevant capacity
1	Low relevant capacity
2	Relevant capacity
3	Medium relevant capacity
4	High relevant capacity
5	Very high relevant capacity

tourists in the area. The other coastal forests, i.e. casuarina forest or mixed beach forest, are considered to have a high ecosystem service supply capacity, especially in the regulating and cultural services.

According to the respondents, also local peat swamp forest (wetlands) is important for the supply of regulating services, such as "climate regulation", "water purification", or "ground water recharge".

Plantations are widely distributed in the study area. They are not natural forests and are considered to have only low and medium relevant capacities in most of the services. They are an important food source, though, and therefore play a major role for agriculture in the study area. Moreover, plantations are considered to provide cultural services as they contribute to the tropical scenery.

Grassland (open woodland, scrubland, dense and sparse grassland) makes up a large part of the study area. It was ranked high by the respondents in regulating and cultural services as well as ecological integrity. Grassland is considered to protect from erosion and flooding, but also to contribute to the aesthetic value of the region.

Coral reefs, the ocean, long tropical beaches, and water courses are important for recreation and tourism in the study area. Seaside tourism contributes significantly to the development and the income of the region (Willroth et al., 2011). Moreover, local people use the beach for their daily small business, e.g. selling of fruits or for relaxing from the heat in the shade of trees. Besides the cultural services coral reefs are considered to provide important regulating services.

Coastal aquacultures are increasing in the area and are therefore included in this study. They provide mainly food and are considered to have a function for education and research.

Table 3. Damage and recovery rates of coastal forests in the study area (derived from remote sensing techniques).

Ecosystem	Total area 2003 (ha)	Direct tsunami impacts		Recovery processes		
		area (ha)	% of exposed area	area (ha)	% of impacted area[a]	recovery rate[b]
Mangroves	980.17	59.59	6.15	33.49	54.10	Slow
Casuarina	98.06	37.24	37.98	20.78	61.60	Fast
Coconut plantation	494	124.61	25.22	97.32	78.10	None
Melaleuca forest	49.13	0.56	1.14	n/a	n/a	Fast
Mixed beach forest	193.05	1.72	0.89	n/a	n/a	Fast

[a] Derived from TNDVI-approach (Römer et al., 2012a). [b] Estimated from field observations conducted in 2009.

4.2 Pre-, post tsunami and recovery ecosystem services maps

Damage and recovery rates for coastal forests in the study area from the change detection analysis (Sect. 3.1) are shown in Table 3 (for details see Roemer et al., 2010; Römer et al., 2012b). Casuarina forests suffered the greatest damage with 38 % of trees destroyed in the inundated coastal zone. Also 25 % of all coconut plantations in the exposed area and about 6 % of the mangroves, but only small patches of melaleuca and mixed beach forest were destroyed. There has been a rapid recovery of casuarina forest and more than 60 % had recovered by 2008. Plantations are not natural ecosystems, so that recovery is related to undergrowth recovery or the plantation of new trees. A natural recovery of plantation patches would lead to a growth of casuarinas.

Based on the ecosystem services matrix (Table 2), the damage analysis, and the recovery analysis, pre-, post-tsunami, and recovery maps were produced using the method described in Sect. 3.3. The maps show the spatial distribution of ecosystem service supply capacities before the tsunami, as well as spatio-temporal changes of the supply capacities due to the tsunami impact.

Maps for the services "coastal protection" and "food provisioning" for Kao Lak are shown in Figs. 6 and 7.

The post-tsunami maps show that almost all biophysical units located in the inundated area were affected by a loss of ecosystem service supply capacities. Since the study area was flooded up to 1 km inland (Römer et al., 2012b), vast patches of coastal forest have been washed away or damaged, beaches were eroded and there was intrusion of salt water into the ground. With the loss of vegetation and soil, the services provided by the affected LULC were reduced.

Among the exposed forest ecosystems in the study area, mangroves and casuarina forest were mostly affected by the tsunami. When washed away, their coastal and erosion protection service was lost after the event. Moreover their capacity to provide food and other goods was disrupted. Also large patches of grassland lost some of their services due to damage to vegetation and salt water intrusion. The recovery maps show a recovery in all biophysical units in 2008. However, recovery rates vary spatially. In some areas in Khao Lak mangroves showed almost no recovery until 2008, while other patches completely recovered. Results also suggest that rubber and coconut plantations had a faster recovery or reafforestation rate than mangroves and casuarina forest. The results gained from the multi-temporal satellite analysis and ecosystem services mapping match with the results from the interviews conducted with local experts on damages and recovery processes in the region (Haitook et al., 2011, Table 4).

Comparing the pre-/post-/ and recovery maps for the service "coastal protection" (Fig. 6) shows high to very high supply capacities in the pre-tsunami state, where coastal forests are located. Casuarina forests are located parallel to the coast, building a natural green belt that shields the hinterland from impacts from the sea. Two mangrove patches, located in tidal inlets are also supposed to serve as protection.

The post-tsunami map shows that all biophysical units in the inundated area suffered from a decrease or loss of the coastal protection service. The overall reduction of the coastal protection service is mainly due to the damage of coastal forests.

The recovery map indicates that large parts of the study area recovered to some extent until 2008. However, the coastal protection service of the casuarina forest and the northern mangrove patch is still significantly reduced, while the southern patch is fully recovered. Beaches have recovered in almost all parts of the area, but are still smaller in more exposed areas in the North. Moreover tidal inlets were not fully recovered in 2008 (Vosberg, 2010). Therefore, also for beaches the coastal protection service supply capacity in 2008 varies locally.

Many LULC classes in the study area supply food (Fig. 7). Coconut plantations and mangroves have shown to have a very high relevant capacity for food provisioning, but also tidal areas and coral reefs are important food sources, e.g. fish. The post-tsunami map reveals that the service supply capacity for the provisioning of food has been strongly reduced, mainly due to the damage to agricultural areas (e.g. plantations). Some of the plantations have been completely reforested by 2008, but many still have a reduced service supply capacity. The spatial variations can be seen in Fig. 7.

Fig. 6. Map showing the spatial distribution of the ecosystem service "coastal protection" for Khao Lak before the tsunami 2003 (upper panel, left), after the tsunami (01/2005, upper panel, right), and after a recovery time (02/2008, lower panel). White areas represent areas not included in the analysis or no data available on damages or recovery of LULC classes (e.g. ocean, coral reefs, and sea-grass, rubber).

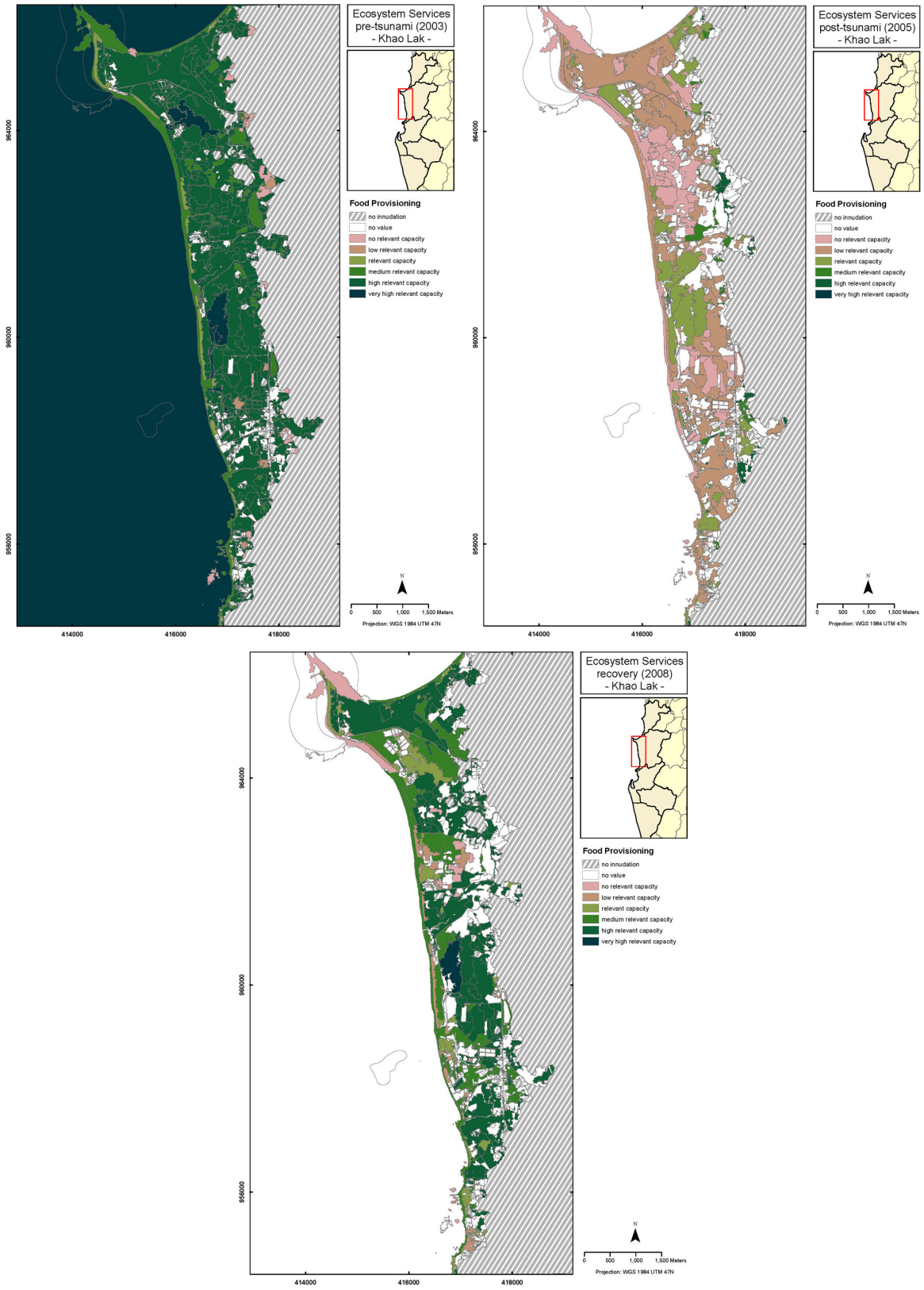

Fig. 7. Map showing the spatial distribution of the ecosystem service "food provisioning" before the tsunami 2003 (upper panel, left), after the tsunami (01/2005, upper panel, right) and after a recovery time (02/2008, lower panel). White areas represent areas not included in the analysis or no data available on damages or recovery of LULC classes (e.g. ocean, coral reefs, and sea-grass, rubber).

Table 4. Damage and recovery of ecosystem service supply capacities due to the tsunami. The values of the ecosystem services by LULC class are derived from the matrix in Table 2. Type of damage and recovery and duration of service reduction were derived from stakeholder interviews using the statistical median for all answers (modified from Haitook et al., 2011).

LULC class	Value of ecosystem services based on the matrix in Table 2	Type of damage to the ecosystem	Duration of service reduction due to the tsunami	Ecosystem service supply capacity in 2010 (% of pre-tsunami conditions)
Mangroves	High relevant capacity	Destroyed/washed away/broken	1–5 yr	75.83
Casuarina forest	High relevant capacity	Destroyed/washed away/broken	1–5 yr	85.24
Rubber plantation	Relevant capacity	No/minor damage	No influence	99.00
Coconut plantation	Medium relevant capacity	Pollution/salt intrusion	2 weeks–1 yr	89.13
Orchard/Cashew nut	Relevant capacity	Pollution/salt intrusion	2 weeks–1 yr	82.50
Oil palm plantation	Relevant capacity	No/minor damage	No influence	99.00
Mixed beach forest	High relevant capacity	Destroyed/washed away/broken	1–5 yr	77.62
Melaleuca forest	Medium relevant capacity	Pollution/salt intrusion	2 weeks–1 yr	95.56
Beach	Medium relevant capacity	Pollution/salt intrusion/erosion	2 weeks–1 yr	93.04
Tidal inlet	High relevant capacity	Pollution/salt intrusion/erosion	2 weeks–1 yr	88.46
Coral reefs	High relevant capacity	Destroyed/washed away/broken	1–5 yr	66.19
Sea-grass	Medium relevant capacity	Damage	1–5 yr	65.26
Aquaculture	Relevant capacity	Destroyed/washed away/broken	2 weeks–1 yr	97.14
Natural grassland	High relevant capacity	Pollution/salt intrusion	1–5 yr	100.00
Wetlands	Medium relevant capacity	Pollution/salt intrusion	No influence	97.50
Ocean	Medium relevant capacity	Pollution	2 weeks–1 yr	100.00
Pond	Medium relevant capacity	Pollution/salt intrusion	1–5 yr	90.50
Stream/river/channel	Medium relevant capacity	Pollution/salt intrusion	2 weeks–1 yr	96.47

Similar maps can be produced for all ecosystem services. With these maps spatial variations in changes of ecosystem service supply capacities for single biophysical units can be visualised and monitored. The additional questions in the questionnaire revealed that, according to the local respondents' experience, among the forest ecosystems, mangroves, casuarina forest and mixed beach forest had the longest period (1–5 yr) of reduction of ecosystem service supply capacities after the tsunami (Table 4). Also coral reefs and seagrass beds are considered to have a long recovery period. In contrast, a shorter recovery period of less than two weeks to maximum one year has been observed for salt water intrusion or pollution in coconut and cashew nut plantations, or melaleuca forest.

At the time of the survey in 2010, more than 5 yr after the tsunami, the respondents stated that most of the ecosystems were able to supply 80 % of their pre-tsunami services. They describe remaining ecosystem service supply capacity deficits for mangroves, mixed beach forest, coral reefs and sea grass.

5 Discussion

In this study, we used detailed high resolution spatial data and conducted stakeholder interviews to acquire very accurate spatio-temporal landscape patterns. Based on these data tsunami impacts on ecosystem service supply at the Phang Nga coast could be mapped.

Our results show, that the methodology of combining remote sensing techniques, field investigations, stakeholder interviews and GIS was a useful tool to (a) quantify the damages to ecosystems and related LULC in a spatially explicit way, (b) provide ecosystem service supply capacity scores for single LULC classes, and (c) visualise changes of ecosystem service supply capacities (losses as well as recovery processes). This yields a specific analysis of the local situation, the benefits local communities obtain from their environment as well as the losses of these benefits due to a tsunami impact.

GIS and remote-sensing based data and maps showing the spatial distribution of ecosystem services can be used in land-use planning and management (Troy and Wilson, 2006; Grêt-Regamey et al., 2008). The ecosystem services maps derived in this study can in addition be integrated in tsunami risk assessment and mapping since they can be used to quantify ecological values and their spatial distribution in the framework of an exposure analysis. In this way the maps can be combined with other spatial data such as maps with the distribution of economic values in a flood prone area. Moreover, the post tsunami mapping approach suggested in this study allows the quantification of damages to LULC by means of loss of ecosystem service supply capacities and related socio-economic consequences. Since the maps provide information for every biophysical unit, dynamics in LULC change and related potential losses of ecosystem service supply can be monitored for larger areas applying multi-temporal image analyses. This makes the maps also useful tools for tsunami risk management and coastal planning, for example by showing the correlation between

bio-shields and settlement structures, or by demonstrating the potential losses of services from mangroves when aquaculture or hotel complexes are planned to substitute them. This phenomenon has also been addressed by Tallis and Polasky (2009) who stated that decision-makers might overlook the variety of ecosystem services, when developing management plans. The interviews with the local stakeholders and discussions with the local people in our study area revealed that people do not use mangroves for wood as much as before the tsunami due to laws and management regulations as well as the increased awareness of the bio-shield function of mangroves and other coastal forests (Haitook et al., 2011). The maps produced in this study could contribute to this kind of management regulations.

Another example where the maps could be used is related to the growth of the shrimp farm industry and of tourism in Phang Nga which implicates direct short-term economic profit for the region, but does not consider the value losses by clearing coastal forests, which might cause negative economic consequences in the long-term perspective, for example, reduced flood protection or loss of food sources.

During this work some limitations of the methodology became obvious. The matrix is subjective which cannot be avoided because the interviews reflect the respondents experience, knowledge and attitude. Some services might have been underestimated because the scores assigned by the survey's participants indicate the services they know and use, but these scores do not necessarily consider the full potential of the ecosystems to supply their services, as proposed in the literature. This makes the matrix somewhat vulnerable to misinformation and misinterpretation (Burkhard et al., 2009; Hou et al., 2013). However, when comparing the scoring of the local stakeholders with a comprehensive literature review in Graterol (2011), a general good agreement could be observed for most of the LULC classes and their service supply capacities with other studies. Nevertheless there were some discrepancies. The local stakeholders ranked the coastal protection service of coastal forests, especially mangroves, very high (score = 5) in the study area. This was also confirmed by local experience during the 2004 tsunami (Haitook et al., 2011). However, on the other hand, there is an ongoing controversial discussion on the protective role of coastal forests against tsunami waves (Cochard et al., 2008). Although experiments and field investigations proved that there is a potential to reduce wave energy and flow velocities, it is still not clear to what degree and if this actually prevents severe damages (Dahdouh-Guebas et al., 2005; Danielsen et al., 2005; Das and Vincent, 2009; Kathiresan and Rajendran, 2005; Kerr et al., 2006; Strusińska-Correia et al., 2013; Tanaka, 2009).

The local respondents gave very low scores for the services "medicine", "energy/biomass" and "fresh water supply" for almost all LULC classes. This is assumed to be either due to a lack of knowledge or because people do not use these services in the region. However, casuarina forest, coral reefs or sea grass, for example, are actually known to provide substances that can be used for medical purpose (Ali et al., 2012; Birkeland, 1997; Whistler and Elevitch, 2006). Also the service "energy" provided for example by rivers was not mentioned here, most likely because rivers in the region are not used to gain hydropower. The provisioning of wood and other goods was perhaps underestimated by the locals since, according to their statements in the group discussions they do not cut trees to derive wood for construction and therefore do not consider the service important. They also do not use corals as market goods. "Pollination" was assessed very high from the locals also in water bodies, from coral reefs and sea-grass. However, pollination does not occur in water bodies or is known to be negligible (see also Costanza et al., 1997). Therefore, we assume a misunderstanding in the interviews here. Despite this mismatch with literature in some points, we find the locals' perspective relevant for a local assessment of tsunami impacts as perceived by those people who experienced the 2004 tsunami disaster and its consequences, e.g. in terms of loss of ecosystem services, for their personal livelihood.

Burkhard et al. (2009) emphasised that one weakness of this approach is, that it has so far been overlooking important aspects such as scale-dependencies (temporal and spatial), scale-interactions, and habitat heterogeneities. The method of calculating ecosystem service scores in the post tsunami and recovery maps, is based on the assumption that the loss and the recovery of ecosystem service supply capacities is directly related to the amount of damage of the biophysical units, i.e. a forest patch destroyed by 50 % of its area has also a reduction of its ecosystem service supply capacity by 50 %. This assumption neglects the complexity of the biophysical processes and spatial gradients and is only true for some of the services.

Like in all integrative interdisciplinary landscape assessments, uncertainties originate due to human-environmental system complexity as well as data and methodological uncertainties (Hou et al., 2013). For the interviews, more specific questions could be asked in order to effectively produce evaluations that are, for example, comparable from one ecosystem service to another. On the other hand, when carrying out interviews on such rather complex issues with the target to address all most relevant ecosystem functions, services and their linkages to land cover types, we argue that several generalisations and lack of some detail need to be accepted in order to gain thematic diversity. The use of additional spatial information such as maps or satellite images presented to the interview respondents could have been used in order to facilitate the assessments or to calibrate the results afterwards. Fagerholm et al. (2012) proved that stakeholders are able to identify and map different landscape-related values, perceptions and services.

Moreover, the use of binary damage and recovery maps to classify damages and recovery of LULC is a rather simple approach which does not include all processes of change.

Damage and recovery was indirectly estimated based on the spatial changes in LULC. These changes describe only the loss or increase of biomass but they do not indicate the quality of these changes (species composition, nutrient cycling, etc.). A more detailed damage analysis can be performed using sophisticated remote-sensing techniques, which allow a very accurate damage and recovery classification for small areas (as described in Roemer et al., 2010).

Despite this simplification the advantage of the approach is its applicability and transferability to other areas and other natural hazards as well as its potential to integrate additional data as soon as they are available. Moreover, it provides a spatial distribution of changes in ecosystems service supply capacities even for larger areas.

6 Conclusions

The paper presents a case study and a methodological approach to track LULC changes and to map related alterations in ecosystem service supply capacities due to an extreme event. The study revealed that, when sufficient data on LULC changes are available, the approach of combining a multi-temporal analysis of LULC changes, with an ecosystem services matrix facilitates a visualisation of the spatial distribution of ecosystem service supply capacities in maps, yielding valuable information on the consequences of the 2004 tsunami. Results have shown that coastal ecosystems in Phang Nga are vulnerable to LULC change (natural or anthropogenic) threatening the supply of multiple life-sustaining ecosystem services. Stakeholder interviews conducted to evaluate ecosystem service supply capacities provided useful insights in the locals' perception of natural goods and their use and therefore reflect on actual losses people in the region obtained from tsunami-induced damages to coastal ecosystems.

However, some limitations and uncertainties of the methodology have to be taken into account. Especially correlating the size of a damaged LULC patch with the loss of ecosystem service supply capacities needs further improvement.

It is believed here that the approach to quantitatively evaluate tsunami impacts on ecosystems with the loss of their capacity to supply services, a mapping of their spatial distribution, as well as monitoring recovery are useful tools for tsunami risk assessment and long-term coastal risk management, delivering reasonable outcomes with acceptable time and labour efforts.

Acknowledgements. The work presented in this paper was conducted in the project "Tsunami Risks, Vulnerability and Resilience in the Phang Nga Province, Thailand (TRAIT)" which was funded by the German Research Foundation (DFG) in the framework of the bilateral German-Thai research cooperation TRIAS. The authors would like to thank Christopher Dunbar and colleagues from WWF Thailand for their support in extensive field surveys and for giving us insights into the socio-ecological structures in the region, all the local stakeholders, NGOs and institutions involved in the interviews and group discussions for their support and contributions, as well as Birger Dircks and Johannes Tiffert for the GIS support. We gratefully acknowledge the support given by the Norwegian Geotechnical Institute (NGI) for the writing of this paper. Finally, we would like to thank the anonymous referees for their helpful comments to improve the paper.

Edited by: K. Schwarzer
Reviewed by: four anonymous referees

References

Adger, W. N., Hughes, T., Folke, C., Carpenter, S., and Rockström, J.: Socio-ecological resilience to coastal disasters, Science, 309, 5737, doi:10.1126/science.1112122, 2005.

Ali, M. S., Ravikumar, S., and Beula, J. M.: Bioactivity of seagrass against the dengue fever mosquito Aedes aegypti larvae, Asian Pac. J. Trop. Biomed., 2, 570–573, doi:10.1016/S2221-1691(12)60099-9, 2012.

Baird, A. H., Campbell, S. J., Anggoro, A. W., Ardiwijaya, R. L., Fadli, N., Herdiana, Y., Kartawijaya, T., Mahyiddin, D., Mukminin, A., Pardede, S. T., Pratchett, M. S., Rudi, E., and Siregar, A. M.: Acehnese Reefs in the Wake of the Asian Tsunami, Curr. Biol., 15, 1926–1930, doi:10.1016/j.cub.2005.09.036, 2005.

Barkmann, J., Baumann, R., Meyer, U., Müller, F., and Windhorst, W.: Ökologische Integrität: Risikovorsorge im nachhaltigen Landschaftsmanagement, GAIA, 10, 97–108, 2001 (in German).

Bateman, I. J., Mace, G. M., Fezzi, C., Atkinson, G., and Turner, R. K.: Economic analysis for ecosystem service assessments, Environ. Resour. Econ., 48, 177–218, doi:10.1007/s10640-010-9418-x, 2010.

Birkeland, C.: Life and Death of Coral reefs, Chapman and Hall, New York, 536 pp., 1997.

Burkhard, B., Kroll, F., Müller, F., and Windhorst, W.: Landscapes' Capacities to Provide Ecosystem Services – a Concept for Land-Cover Based Assessments, Landscape Online, 15, 1–22, 2009.

Burkhard, B., Kroll, F., Nedkov, S., and Müller, F.: Mapping supply, demand and budgets of ecosystem services, Ecol. Indic., 21, 17–29, doi:10.1016/j.ecolind.2011.06.019, 2012a.

Burkhard, B., de Groot, R. S., Costanza, R., Seppelt, R., Jørgensen, S. E., and Potschin, M.: Solutions for Sustaining Natural Capital and Ecosystem Services, Ecol. Indic., 21, 1–6, doi:10.1016/j.ecolind.2012.03.008, 2012b.

Choowong, M., Phantuwongraj, S., Charoentitirat, T., Chutakosikanon, V., Yumuang, S., and Charusiri, P.: Beach recovery after 2004 Indian Ocean tsunami from Phang Nga, Thailand, Geomorphology, 104, 134–142, 2009.

Cochard, R., Ranamukhaarachchi, S. L., Shivakoti, G. P., Shipin, O. V., Edwards, P. J., and Seeland, K. T.: The 2004 tsunami in Aceh and Southern Thailand: A review on coastal ecosystems, wave hazards and vulnerability, Perspect. Plant. Ecol., 10, 3–40, 2008.

Costanza, R.: Ecosystem services: Multiple classification systems are needed, Biol. Conserv., 141, 350–352, 2008.

Costanza, R. and Farley, J.: Ecological economics of coastal disasters: Introduction to the special issue, Ecol. Econ., 63, 249–253, 2007.

Costanza, R., d'Arge, R., de Groot, R., Farber, S., Grasso, M., Hannon, B., Limburg, K., Naeem, S., O'Neill, R. V., Paruelo, J., Raskin, R. G., Sutton, P., and van den Belt, M.: The value of the world's ecosystem services and natural capital, Nature, 387, 253–260, 1997.

Dahdouh-Guebas, F., Jayatissa, L. P., Di Nitto, D., Bosire, J. O., Lo Seen, D., and Koedam, N.: How effective were mangroves as a defence against the recent tsunami, Curr. Biol., 15, 443–447, 2005.

Daily, G. C.: Nature's services: societal dependence on natural ecosystems, Island Press, Washington DC, 392 pp., 1997.

Daily, G. C. and Matson, P. A.: Ecosystem Services: From theory to implementation, P. Natl. Acad. Sci. USA, 105, 9455–9456, 2008.

Danielsen, F., Sørensen, M. K., Olwig, M. F., Selvam, V., Parish, F., Burgess, N. D., Hiraishi, T., Karunagaran, V. M., Rasmussen, M. S., Hansen, L. B., Quarto, A., and Suryadiputra, N.: The Asian tsunami: a protective role for coastal vegetation, Science, 310, 5748, p. 643, 2005.

Das, S. and Vincent, J. R.: Mangroves protected villages and reduced death toll during Indian super cyclone, P. Natl. Acad. Sci. USA, 106, 7357–7360, doi:10.1073/pnas.0810440106, 2009.

De Groot, R. S.: Functions of Nature: Evaluation of nature in environmental planning, management and decision-making, Wolters, Nordhoff BV, Groningen, The Netherlands, 1992.

De Groot, R. S., Alkemade, R., Braat, L., Hein, L., and Willemen, L.: Challenges in integrating the concept of ecosystem services and values in landscape planning, management and decision making, Ecol. Complexity, 7, 260–272, 2010.

DMCR (Department of Marine and Coastal Resources and Thammasat University): Post tsunami impact on mangrove community and status quo of surrounding community: The case study in the area of Mangrove Resource Development Center, Phang Nga, Department of Marine and Coastal Resources, Ministry of natural Resources and Environment, Bangkok, Thailand, 100 pp., 2005a.

DMCR (Department of Marine and Coastal Resources): Rapid Assessment of the Tsunami Impact on Marine Resources in the Andaman Sea, Thailand, Phuket Marine Biological Center (PMBC), Phuket, Thailand, 76 pp., 2005b.

Fagerholm, N., Käyhkö, N., Ndumbaro, F., and Khamis, M.: Community stakeholders' knowledge in landscape assessments – Mapping indicators for landscape services, Ecol. Indic., 18, 421–433, 2012.

FAO and MOAC (Food and Agriculture Organisation of the United Nations and Ministry of Agriculture & Cooperation): Report of Joint FAO/MOAC Detailed Technical Damages and Needs Assessment Mission in Fisheries and Agriculture Sectors in Tsunami Affected Six Provinces in Thailand, 11–14 January 2005, available at: http://www.apfic.org/apfic_downloads/tsunami/FAO_MOAC_thai.pdf, last access: 12 August 2010, 2005.

Forbes, K. and Broadhead, J.: The role of coastal forests in the mitigation of tsunami impacts, FAO, Food and Agriculture Organization of the United Nations, Regional Office for Asia and the Pacific, Bangkok, 30 pp., 2007.

Graterol, R. M.: The utility of the ecosystem services approach in disaster risk reduction: a case study in the Phang Nga province, Thailand, MSc thesis, University of Kiel, Germany, 2011.

Grêt-Regamey, A., Bebi, P., Bishop, I. D., and Schmid, W. A.: Linking GIS-based models to value ecosystem services in an Alpine region, J. Environ. Manage., 89, 197–208, 2008.

Haines-Young, R., Potschin, M., and Kienast, F.: Indicators of ecosystem service potential at European scales: mapping marginal changes and trade-offs, Ecol. Indic., 21, 39–53, 2012.

Haitook, T., Sangkaew, S., and Dunbar, C.: Post-tsunami recovery assessment, Phang Nga Province, Thailand, unpublished TRAIT project report, 2011.

Hou, Y., Burkhard, B., and Müller, F.: Uncertainties in landscape analysis and ecosystem service assessment, J. Environ. Manage., 127, S117–S131, doi:10.1016/j.jenvman.2012.12.002, 2013.

IUCN and UNEP: Counting the Environmental Costs of Natural Disasters: Evaluating Tsunami-Related Damages to Coastal Ecosystems in Thailand. Ecosystems and Livelihoods Group Asia, Colombo, Sri Lanka, 36 pp., 2006.

Kallesøe, M. F., Bambaradeniya, C. N. B., Iftikhar, U. A., Ranasinghe, T., and Miththapala, S.: Linking Coastal Ecosystems and Human Well-Being: Learning from conceptual frameworks and empirical results, Colombo: Ecosystems and Livelihoods Group, Asia, IUCN, viii + 49 pp., 2008.

Kandziora, M., Burkhard, B., and Müller, F.: Interactions of ecosystem properties, ecosystem integrity and ecosystem service indicators – A theoretical matrix exercise, Ecol. Indic., 28, 54–78, 2013.

Kathiresan, K. and Rajendram, N.: Coastal mangrove forests mitigated tsunami, Estuar. Coast. Shelf S., 65, 601–606, 2005.

Kerr, A. M., Baird, A. H., and Campbell, S. J.: Comments on "Coastal mangrove forests mitigated tsunami" by K. Kathiresan and N. Rajendran [Estuar. Coast. Shelf S., 65, 601e606, 2005], Estuar. Coast. Shelf S., 67, 539–541, 2006.

Kienast, F., Bolliger, J., Potschin, M., de Groot, R. S., Verburg, P. H., Heller, I., Wascher, D., and Haines-Young, R.: Assessing Landscape Functions with Broad-Scale Environmental Data: Insights Gained from a Prototype Development for Europe, Environ. Manage., 44, 1099–1120, 2009.

Kroll, F., Müller, F., Haase, D., and Fohrer, N.: Rural-urban gradient analysis of ecosystem services supply and demand dynamics, Land Use Policy, 29, 521–535, 2012.

Kumar, P.: The Economics of Ecosystems and Biodiversity – Ecological and Economic Foundations, Earthscan, London, Washington, 2010.

MA (Millennium Ecosystem Assessment): Ecosystems and Human Well-being: Synthesis, Island Press, Washington, DC, World Resources Institute, 2005.

Maes, J., Paracchini, M. L., and Zulian, G.: A European assessment of the provision of ecosystem services: Towards an atlas of ecosystem services, Luxembourg: Publications Office of the European Union, 81 pp., doi:10.2788/63557, 2011.

Massmann, F.: Analyse der Vulnerabilität von Landwirtschaft und Fischerei an der Andamanküste Thailands im Kontext des Tsunamis von 2004, Diploma thesis, Institute of Geography, Christian-Albrechts-Universität Kiel, Germany, 2010 (in German).

Müller F.: Indicating ecosystem and landscape organisation, Ecol. Indic., 5, 280–294, 2005.

Müller, F. and Burkhard, B.: An ecosystem based framework to link landscape structures, functions and services, in: Multifunctional Land Use – Meeting Future Demands for Landscape Goods and Services, edited by: Mander, Ü., Wiggering, H., and Helming, K., Springer Berlin Heidelberg, 37–64, 2007.

Nedkov, S. and Burkhard, B.: Flood Regulating Ecosystem Services – Mapping Supply and Demand in the Etropole Municipality, Bulgaria, Ecol. Indic., 21, 67–79, doi:10.1016/j.ecolind.2011.06.022, 2012.

Paphavasit, N., Aksornkoae, S., and De Silvia, J.: Tsunami Impact on Mangrove Ecosystem, Thailand Environmental Institute, Nonthaburi, Thailand, 211 pp., 2009.

Pongpiachan, S., Tipmanee, D., Deelaman, W., Muprasit, J., Feldens, P., and Schwarzer, K.: Risk assessment of the presence of polycyclic aromatic hydrocarbons (PAHs) in coastal areas of Thailand affected by the 2004 tsunami, Mar. Pollut. Bull., doi:10.1016/j.marpolbul.2013.07.052, 2013.

Roemer, H., Kaiser, G., Sterr, H., and Ludwig, R.: Using remote sensing to assess tsunami-induced impacts on coastal forest ecosystems at the Andaman Sea coast of Thailand, Nat. Hazards Earth Syst. Sci., 10, 729–745, doi:10.5194/nhess-10-729-2010, 2010.

Römer, H.: Assessment of tsunami vulnerability and resilience of coastal ecosystems at the Andaman Sea coast of Thailand – potential and limitations of remote sensing and GIS techniques for a local scale approach, Ph.D. thesis, Christian-Albrechts-Universität zu Kiel, Germany, 186 pp., 2011.

Römer, H., Jeewarongkakul, J., Kaiser, G., Ludwig, R., and Sterr, H.: Monitoring post tsunami vegetation recovery in Phang Nga, Thailand – a remote sensing based approach, Int. J. Remote Sens., 33, 3090–3121, doi:10.1080/01431161.2011.628710, 2012a.

Römer, H., Willroth, P., Kaiser, G., Vafeidis, A. T., Ludwig, R., Sterr, H., and Revilla Diez, J.: Potential of remote sensing techniques for tsunami hazard and vulnerability analysis – a case study from Phang-Nga province, Thailand, Nat. Hazards Earth Syst. Sci., 12, 2103–2126, doi:10.5194/nhess-12-2103-2012, 2012b.

Swetnam, R. D., Fisher, B., Mbilinyi, B. P., Munishi, P. K. T., Willcock, S., Ricketts, T., Mwakalila, S., Balmford, A., Burgess, N. D., Marshall, A. R., and Lewis, S. L.: Mapping socio-economic scenarios of land cover change: A GIS method to enable ecosystem service modelling, J. Environ. Manage., 92, 563–574, 2011.

Strusińska-Correia, A., Husrin, S., and Oumeraci, H.: Tsunami damping by mangrove forest: a laboratory study using parameterized trees, Nat. Hazards Earth Syst. Sci., 13, 483–503, doi:10.5194/nhess-13-483-2013, 2013.

Szczucinski, W., Chaimanee, N., Niedzielski, P., Rachlewicz, G., Saisuttichai, D., Tepsuwan, T., Lorenc, S., and Siepak, J.: Environmental and Geological Impacts of the 26 December 2004 Tsunami in Coastal Zone of Thailand – Overview of Short and Long-Term Effects, Pol. J. Environ. Stud., 793–810, 2006.

Tallis, H. and Polasky. S.: Mapping and Valuing Ecosystem Services as an Approach for Conservation and Natural-Resource Management, Ann. NY Acad. Sci., 1162, 265–283, 2009.

Tanaka, N.: Vegetation bioshields for tsunami mitigation: review of effectiveness, limitations, construction, and sustainable management, Landsc. Ecol. Eng., 5, 71–79, 2009.

ten Brink, P.: The Economics of Ecosystems and Biodiversity in International and National Policy Making. An Output of TEEB: The Economics of Ecosystems and Biodiversity, Earthscan, London, Washington DC, 2011.

Troy, A. and Wilson, M. A.: Mapping ecosystem services: Practical challenges and opportunities in linking GIS and value transfer, Ecol. Econ., 60, 435–449, 2006.

UNEP (United Nations Environment Programme): After the Tsunami, Rapid Environmental Assessment, Nairobi, Kenia, 140 pp., 2005.

United Nations and Worldbank: Tsunami Thailand. One year later, United Nations Country Team, Bangkok, 2005.

Vihervaara, P., Kumpula, T., Tanskanen, A., and Burkhard, B.: Ecosystem services – A tool for sustainable management of human-environment systems, Case study Finnish Forest Lapland, Ecol. Complex., 8, 410–420, 2010.

Vosberg, Z.: Veränderung der Strandmorphologie an der thailändischen Andamankueste nach dem Tsunami 2004, BSc thesis, Institute of Geography, Christian-Albrechts-Universität Kiel, Germany, 2010 (in German).

Wallace, K.: Classification of ecosystem services: problems and solutions, Biol. Conserv., 139, 235–246, 2007.

Whistler, W. A. and Elevitch, C. R.: *Casuarina equisetifolia* (beach she-oak) *C. cunninghamiana* (river she-oak), Species Profiles for Pacific Island Agroforestry, The Traditional Tree Initiative, Hawaii, USA, available at: http://traditionaltree.org, last access: 7 October 2010, 2006.

Willroth, P., Revilla Diez, J., and Arunotai, N.: Modelling the economic vulnerability of households in the Phang Nga Province (Thailand) to natural disasters, Nat. Hazards, 58, 753–769, doi:10.1007/s11069-010-9635-1, 2011

Yanagisawa, H., Koshimura, S., Goto, K., Miyagi, T., Imamura, F., Ruangrassamee, A., and Tanavud, C.: The reduction effects of mangrove forest on a tsunami based on field surveys at Pakarang Cape, Thailand and numerical analysis, Estuar. Coast. Shelf S., 81, 27–37, 2009.

Nat. Hazards Earth Syst. Sci., 13, 3113–3128, 2013
www.nat-hazards-earth-syst-sci.net/13/3113/2013/
doi:10.5194/nhess-13-3113-2013

Natural Hazards and Earth System Sciences
Open Access

Sediment transport on the inner shelf off Khao Lak (Andaman Sea, Thailand) during the 2004 Indian Ocean tsunami and former storm events: evidence from foraminiferal transfer functions

Y. Milker[1], M. Wilken[1], J. Schumann[1], D. Sakuna[2], P. Feldens[2,3], K. Schwarzer[2], and G. Schmiedl[1]

[1]Center of Earth System Research and Sustainability, University of Hamburg, Hamburg, Germany
[2]Institute of Geosciences, Coastal and Shelf Research, University of Kiel, Kiel, Germany
[3]GEOMAR Helmholtz Centre for Ocean Research Kiel, Kiel, Germany

Correspondence to: Y. Milker (yvonne.milker@uni-hamburg.de)

Received: 29 March 2013 – Published in Nat. Hazards Earth Syst. Sci. Discuss.: 29 May 2013
Revised: 29 October 2013 – Accepted: 2 November 2013 – Published: 5 December 2013

Abstract. We have investigated the benthic foraminiferal fauna from sediment event layers associated with the 2004 Indian Ocean tsunami and former storms that have been retrieved in short sediment cores from offshore environments of the Andaman Sea, off Khao Lak, western Thailand. Species composition and test preservation of the benthic foraminiferal faunas exhibit pronounced changes across the studied sections and provide information on the depositional history of the tsunami layer, particularly on the source water depth of the displaced foraminiferal tests. In order to obtain accurate bathymetric information on sediment provenance, we have mapped the distribution of modern faunas in non-tsunamigenic surface sediments and created a calibration data set for the development of a transfer function. Our quantitative reconstructions revealed that the resuspension of sediment particles by the tsunami wave was restricted to a maximum water depth of approximately 20 m. Similar values were obtained for former storm events, thus impeding an easy distinction of different high-energy events.

1 Introduction

The devastating tsunami of 26 December 2004 that originated from a 9.3 magnitude submarine earthquake off the northwest coast of the Indonesian island Sumatra (Stein and Okal, 2005) (Fig. 1) had severe impacts on the coastlines of southeastern Asia (Bell et al., 2005; Tsuji et al., 2006). The highly energetic tsunami wave resulted in major coastal changes and is documented in on- and offshore erosion phenomena and deposits. Detailed topographic, sedimentological and geochemical investigations documented the complex nature of erosion and deposition processes of the tsunami wave and its backflow along the western coast of Thailand (Choowong et al., 2007; Fagherazzi and Du, 2007; Hawkes et al., 2007; Jankaew et al., 2008; Mard Karlsson et al., 2009; Feldens et al., 2009; Sakuna et al., 2012). However, little is known on the exact provenance and transport dynamics of sediment particles in tsunamigenic offshore deposits. Specific sedimentological characteristics such as thickness of the high-energy layer, its grain size distribution and sorting have been studied by several authors in order to distinguish between storm and tsunami events (e.g., Morton et al., 2007; Kortegaas and Dawson, 2007; Dahanayake and Kulasena, 2008). These studies also revealed that it is often difficult to separate a storm layer from a tsunami layer from the sedimentological record alone.

Among other microfossils, benthic foraminifers are frequently found in tsunami deposits, providing information on the provenance of the sediment components (review by Mamo et al., 2009). Size distribution, shape and preservation of foraminiferal tests document the hydrodynamics of the tsunami wave but are also influenced by rapid post-depositional taphonomic processes (Yawsangratt et al., 2011). The occurrence of certain marine taxa in onshore tsunamites allowed for an assessment of the water depth range from which sediment particles have been resuspended and incorporated into the tsunami wave (e.g., Nanayama and

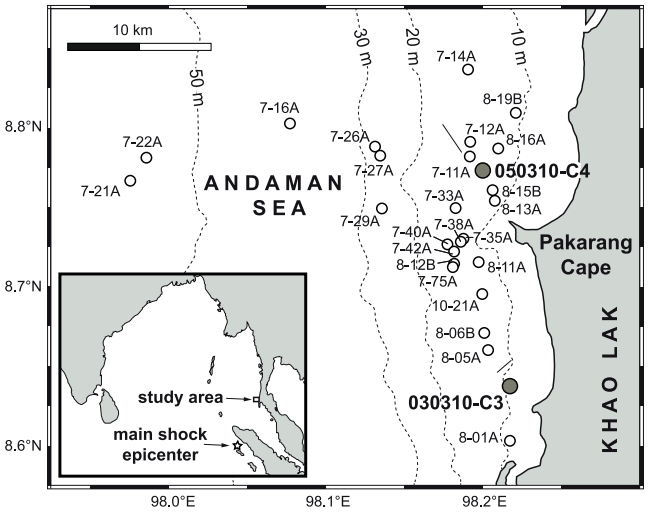

Fig. 1. Bathymetric map of the study area on the inner shelf of the eastern Andaman Sea off Cape Pakarang, Khao Lak, southwestern Thailand. Shown are the locations of the investigated surface sediment sites (small open circles) and the core sites (large grey circles) addressed in this study. See Table 1 for station details. The positions of the study area and the main shock of the 26 December 2004 earthquake are marked in the overview map of the northern Indian Ocean.

Shigeno, 2006; Uchida et al., 2010). Typically, the tsunamite assemblages contain open-shelf taxa, contrasting with lower diverse brackish faunas in under- and overlying marsh or other terrestrial sediments (Uchida et al., 2010). However, the published water depth estimates vary significantly, ranging from 30 m or shallower for a historical tsunami of southeastern India (Satyanarayana et al., 2007) up to 90 m for the 1992 tsunami of Hokkaido (Nanayama and Shigeno, 2006), and between 50 and 300 m for various tsunamites in Japan and southeastern Asia (Uchida et al., 2010). This compilation demonstrates that even tests from outer shelf to upper bathyal taxa have been documented in tsunamites (Dominey-Howes et al., 1998; Uchida et al., 2010). Sugawara et al. (2009) studied the foraminiferal content of offshore deposits of the southwest coast of Thailand related to the 2004 Indian Ocean tsunami on 4 stations from 4.5 m to 20.5 m water depth. The studied faunas reveal a significant backwash component but lack evidence for transport of particles from deeper to shallower water depth which might result from their sampling strategy. To date, all of these depth estimates have been based on qualitative information of bathymetric species ranges or hydrodynamic estimation of the tsunami wave and therefore remain relatively inaccurate.

In tropical and subtropical regions, the distribution of benthic shelf foraminifers depends on various factors, such as food availability and quality, substrate-type, bottom current velocity, temperature and salinity, vegetation and light penetration (e.g, Szarek et al., 2006; Murray, 2006; Parker and Gischler, 2011). The specific environmental setting is commonly reflected in a distinct depth zonation of shelf species. Of particular relevance are symbiont-bearing larger foraminifers that are adapted to limited depth intervals within the photic zone, depending on the specific light requirements of the algal symbiont and other habitat variables such as microscale environmental gradients within the substrate (Hohenegger et al., 1999; Beavington-Penney and Racey, 2004; Renema, 2006a, b). Different quantitative methods have been developed for water depth estimates, e.g, based on the ratio between benthic and planktonic foraminifers (Van der Zwaan et al., 1990), and the distribution patterns of certain faunas and benthic indicator taxa (Horton et al., 1999; Hohenegger, 2005; Milker et al., 2009). These methods have been successfully applied to paleobathymetric reconstructions in various sedimentary environments (e.g., Nelson et al., 2008; Rossi and Horton, 2009; Hawkes et al., 2010; Milker et al., 2011) and also bear a high potential for quantitative provenance studies of tsunami deposits.

The overall target of the present study is to generate quantitative data on the provenance of foraminiferal tests in high-energy event deposits from the inner shelf off Khao Lak, comprising layers of the 2004 tsunami and former storm events. For this, benthic foraminifers have been quantitatively analyzed from surface sediment samples and from two sediment cores retrieved from selected depositional systems of the inner shelf of the study area. The recent data set was used to establish a transfer function for water depth that was then applied to the fossil faunas. Our data will be particularly useful for sedimentological and modeling studies on hydrodynamics, wavelength and amplitude of tsunami waves. They will also contribute to the toolbox for distinguishing between storm and tsunami deposits.

2 Study area

The study area is situated 25 km off the Khao Lak region (Thailand) near Pakarang Cape (Andaman Sea) and covers an area of $\sim 1000\,km^2$ (Table 1, Fig. 1). The Andaman Sea is a marginal sea, separated from the Indian Ocean by the Nicobar and Andaman Islands. It is characterized by a relatively broad shelf region up to 200 km wide in the north, and a narrower shelf region in the south (Saidova, 2008). The absence of major riverine influence results in sedimentation of mixed siliciclastic–carbonate sediments, in many places dominated by coral–algal sand (Saidova, 2008; Feldens et al., 2009). The region is influenced by the monsoonal system with northeasterly winds during winter and southwesterly winds during summer. The monsoon system also accounts for the hydrologic properties of surface water masses. The summer monsoon results in stronger waves, influencing the coastal dynamics (Scheffers et al., 2012). In the southern Andaman Sea, the yearly range of surface water temperatures is 26–29 °C; surface salinities range between 31.5 and 33 psu (Levitus and Boyer, 1994; Varkey et al., 1996). The

Table 1. Surface sample and sediment core IDs, sampling year, longitude and latitude, and water depth of the investigated surface samples and sediment cores (see also Fig. 1).

Sample/core ID	Sampling period	Code in this study (RDA)	Type of material	Longitude	Latitude	Water depth (m)
021207-11A	12/2007	1	surface sample	08° 46.901	98° 11.512	20.1
021207-12A	12/2007	2	surface sample	08° 47.459	98° 11.528	20.1
021207-14A	12/2007	3	surface sample	08° 50.189	98° 11.433	18.7
021207-16A	12/2007	4	surface sample	08° 48.147	98° 04.652	44.7
031207-21A	12/2007	5	surface sample	08° 45.989	97° 58.549	63.4
031207-22A	12/2007	6	surface sample	08° 46.860	97° 59.166	61.8
031207-26A	12/2007	7	surface sample	08° 47.278	98° 07.884	33.6
031207-27A	12/2007	8	surface sample	08° 46.932	98° 08.094	26.5
031207-29A	12/2007	9	surface sample	08° 44.938	98° 08.154	25.1
051207-33A	12/2007	10	surface sample	08° 44.958	98° 10.965	17.0
051207-35A	12/2007	11	surface sample	08° 43.796	98° 11.270	15.2
051207-38A	12/2007	12	surface sample	08° 43.682	98° 11.168	15.1
051207-40A	12/2007	13	surface sample	08° 43.584	98° 10.655	17.8
051207-42A	12/2007	14	surface sample	08° 43.319	98° 10.908	15.7
081207-75A	12/2007	15	surface sample	08° 42.744	98° 10.866	16.5
061208-01A	12/2008	16	surface sample	08° 36.181	98° 13.044	10.3
061208-05A	12/2008	17	surface sample	08° 39.600	98° 12.217	13.0
061208-06II-B2	12/2008	18	surface sample	08° 40.250	98° 12.067	13.3
061208-11A	12/2008	19	surface sample	08° 42.917	98° 11.850	14.9
061208-12B	12/2008	20	surface sample	08° 42.860	98° 10.922	19.4
061208-13A	12/2008	21	surface sample	08° 45.233	98° 12.460	12.6
061208-15B	12/2008	22	surface sample	08° 45.639	98° 12.372	14.0
061208-16A	12/2008	23	surface sample	08° 47.200	98° 12.592	15.4
061208-19B	12/2008	24	surface sample	08° 48.548	98° 13.265	13.0
030310-21A	03/2010	25	surface sample	08° 41.720	98° 11.982	15.2
030310-C3	03/2010		sediment core	08° 38.708	98° 12.931	9.5
050310-C4	03/2010		sediment core	08° 46.659	98° 12.269	15.3

Andaman Sea is influenced by micro- to mesotidal semidiurnal tides with a tidal range from 1.1 to 3.6 m (Thampanya et al., 2006). This coastal region of the Andaman Sea is relatively unaffected by strong tropical cyclones. Typhoons can occur in the study area but their frequency is low (Kumar et al., 2008; Phantuwongraj and Choowong, 2012). The absence of larger riverine discharge (Feldens et al., 2009) as well as the absence of large storm events between the deposition of the 2004 tsunami deposits and the sampling campaigns from 2007 to 2010 (Regional Specialized Meteorological Centre (RMSC), New Delhi) allows for the investigation of depositional processes prior to, during and after the tsunami event in 2004.

3 Material and methods

3.1 Surface sediment samples and sediment cores

For this study, a total of 25 surface samples and two sediment cores, taken from the investigation area during three research cruises (November–December 2007, November–December 2008, February–March 2010), were investigated (Fig. 1, Table 1). The surface samples were collected with a grab sampler from water depth ranging from 10.3 to 63.4 m. The sites were selected based on detailed sea-floor mapping (Feldens et al., 2009, 2012) with high-resolution hydroacoustic systems (side-scan sonar, shallow seismic systems, multibeam echosounder) and an underwater video camera in order to cover a maximum variety of substrates and to get a clear picture of sediment distribution patterns and morphological features. The two sediment cores were recovered with a Rumohr gravity corer at 9.5 m water depth (core 030310-C3, length 97 cm) and 15.3 m water depth (core 050310-C4, length 56 cm) (Fig. 1; Table 1).

According to different lithological units of the cores, nine samples of 1 cm thickness were investigated from core 030310-C3 and eight samples from core 050310-C4 (for sampling position see Fig. 2). Six samples of core 030310-C3 and four samples of core 050310-C4 were taken from layers characterized by coarser-grained units. Three samples from core 030310-C3 and four samples from core 050310-C4 were taken from finer-grained layers deposited under normal background sedimentation. Two surface samples were taken onshore to investigate specimens redeposited during the 2004 tsunami.

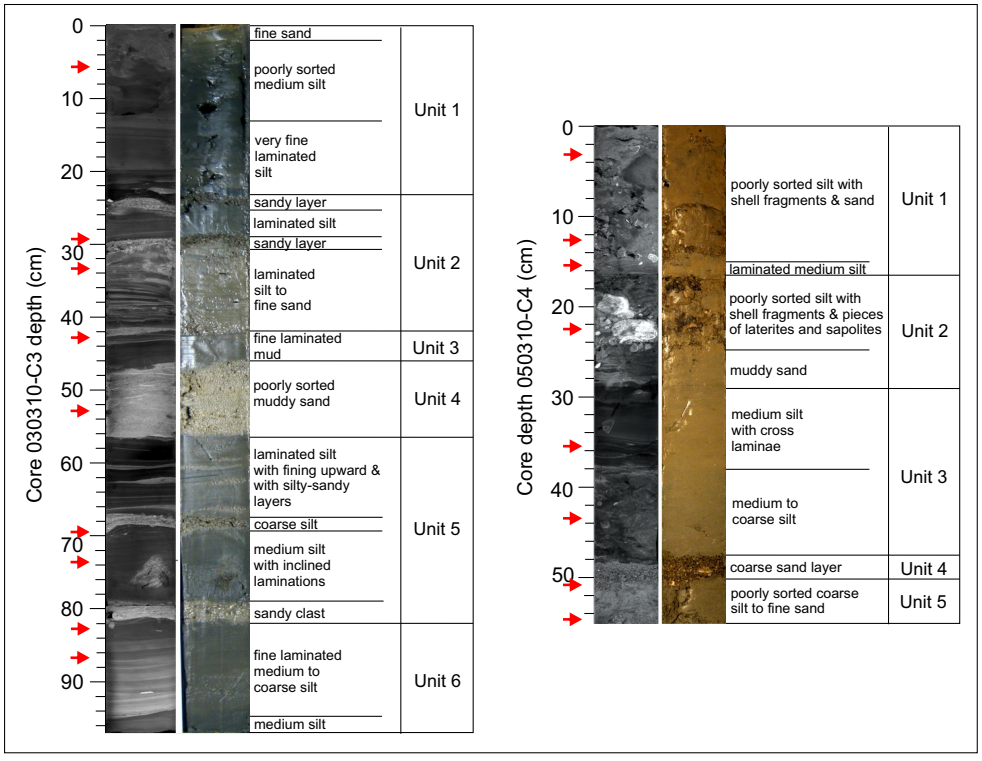

Fig. 2. Photographs, X-radiographs and definition of lithological units of sediment cores 030310-C3 and 050310-C4 versus core depth. The red arrows mark sample positions investigated in the frame of this study.

3.2 Foraminiferal and environmental data

Both the surface and core samples were wet-sieved with a 63 µm sieve. The fraction > 63 µm was dried at 40 °C for later foraminiferal analysis. The modern and fossil faunas were investigated from the > 125 µm fraction using representative splits containing approximately 300 benthic foraminiferal specimens. The identification of the foraminifera on the species level was mainly based on the studies of Hottinger et al. (1993), Jones (1994) and Hohenegger et al. (1999). Rare species or specimens that could not be identified on the species level were grouped into their genus or family. Potentially relocated benthic foraminifera (broken tests, tests fragments, and tests with yellowish-brown coloration) were counted separately.

In order to extract the dominant modern and fossil benthic foraminiferal assemblages, a principal component analysis (PCA) in Q-mode and with varimax rotation was carried out on the surface samples. A total of 53 modern foraminiferal taxa having relative minimum abundances of 0.5 % on the total fauna and being present in at least 3 samples were included into analysis. All potentially relocated specimens were excluded. The number of principal components (PCs) was selected based on eigenvalues > 1. PC loadings ≥ 0.4 for each axis were defined as significant (Malmgren and Haq, 1982; Backhaus et al., 2006).

In order to examine the relationship between the modern species in the data set of the surface samples and environmental parameters, a redundancy analysis (RDA) was carried out using Canoco (version 4.5) (Ter Braak and Smilauer, 2002; Leps and Smilauer, 2003). We selected the water depth and the percentages of silt and clay (< 63 µm), fine sand (63–125 µm) and coarser-grained sediment (> 125 µm) as environmental parameters. We used a reduced surface data set with 23 species having percentages exceeding 5 % in the total assemblage. Species counts were square-root-transformed and environmental parameters were standardized before analysis. Partial RDAs (with each environmental variable as the only variable) were calculated to evaluate the individual influence of the environmental parameters on the foraminiferal assemblages.

3.3 Development of foraminiferal-based transfer functions

We applied the detrended canonical correspondence analysis (DCCA) on the same reduced modern data set used for RDA (containing 23 species with percentages higher than 5 %) on the total fauna to analyze whether the species show a linear or unimodal distribution in relation to water depth (Birks, 1998, 1995). Birks (1995) suggests the use of linear regression methods for DCCA gradient lengths below 2 SD

standard deviation (SD) units, and unimodal methods for gradient lengths larger than 2 SD units. For this approach, we used the CANOCO software package (version 4.5) (Leps and Smilauer, 2003; Ter Braak and Smilauer, 2002).

For the development of the transfer function, the modern (training) data set was reduced to benthic foraminifera, identified on the species level, and with relative abundances of $> 0.5\,\%$ on the total dead assemblages. The fossil data sets were reduced to benthic species present in the surface data set. Potentially relocated specimens were removed from the training data set. The final modern data set consisted of 25 surface samples with a total of 49 dead species, ranging from 10.3 to 63.4 m water depth. In the fossil data sets, a total of 37 species from core 030310-C3 and 38 species from core 050310-C4 were used for reconstruction.

The modern analog technique (MAT) was applied to test whether the fossil samples provide good analogs for the modern samples by calculating dissimilarity coefficients (MinDC (minimum distance to closest analog) dissimilarity coefficients) (Birks, 1995). We selected the square chord distance as the dissimilarity coefficient (Overpeck et al., 1985) and the seven most similar modern samples. Coefficients lower than the 10th percentile have been defined as good analogs, coefficients between the 10th and 20th percentile have been considered as fair analogs and coefficients larger than the 20th percentile as poor analogs (Horton and Edwards, 2006; Birks, 1995; Kemp et al., 2009). For all calculations we used the C^2 software package (version 1.7.2) (Juggins, 2003).

We tested three methods for the paleo-water depth estimates in the sediment cores: the partial least squares (PLS) method that is based on a linear species–environment relationship, the weighted averaging (WA) that is based on a unimodal species–environment relationship and finally the combination of both methods, the WA-PLS method. The latter is presented here. The WA-PLS method creates new components from a data set by maximizing the covariance between the scores of the independent variable (water depth) and the dependent variables (species abundances) (Birks, 1998; Ter Braak and Juggins, 1993).

In order to obtain a normal distribution, species counts were square-root-transformed. In order to evaluate the performance of the transfer functions, we used the apparent coefficient of determination (R^2), allowing for an evaluation of the strength of the linear relationship between the observed and estimated water depths in the surface data set. In order to calculate the coefficient of determination of prediction (R^2_{jack}) and the root mean squared error of prediction (RMSEP) in the surface data set, we used the "jack-knifing" (leave one out) cross-validation technique (Horton and Edwards, 2006; Ter Braak and Juggins, 1993). Bootstrapping cross-validation (1000 cycles) was selected to evaluate the sample-specific errors of prediction in the fossil data sets (Birks et al., 1990; Horton and Edwards, 2006). The number of components for WA-PLS was selected according to the lowest RMSEP values if the reduction in prediction error exceeds 5 % for this component compared to the next lower component (Ter Braak and Juggins, 1993). All calculations were performed with the C^2 software, version 1.7.2 (Juggins, 2003).

4 Results

4.1 Lithology and sediment characteristics of sediment cores

The surface sediments are composed of a mixture of siliciclastic and carbonate particles of varying proportions and grain sizes. The biogenic components predominantly comprise coral and algal fragments, mollusc shells, echinoid fragments and benthic foraminifers. Differences are also characterized by the sand content ($> 63\,\mu$m) ranging from approximately 6 and to almost 100 % (Table S1). Most samples exhibit high sand contents exceeding 90 %. Local exceptions are restricted to several shallow mud-dominated sites (6–32 % sand) and the deepest sites (67–68 % sand).

The sediment cores were subdivided into different lithological units based on grain-size distributions and sedimentary structures, identified by visual inspection and/or by X-radiography images of the cores (Fig. 2).

Core 030310-C3 has been subdivided into six units (Fig. 2). Unit 6 consists of medium to coarse silt, with well-sorted medium silt in its lower part and finely laminated medium to coarse silt in its upper part. The contact to unit 5 is sharp and erosional. Unit 5 is mainly composed of very fine sand and silt. At its base a sandy clast, two cm in diameter, was found. The lower part of unit 5 consists of coarse silt followed by a subunit with medium silt showing some laminations, and a subunit of coarse silt. The upper part of unit 5 consists of laminated silt, showing a fining upward, and contains some mm-thick layers of coarse silt to very fine sand. Unit 4 is composed of a poorly sorted muddy sand layer and unit 3 consists of finely laminated mud. Unit 2 is composed of laminated clayey silt and contains two sand layers with laterites and shell fragments. The lower part of unit 2 consists of laminated silt to fine sand and the upper part is composed of slightly inclined laminated silt. The uppermost unit 1 consists of poorly sorted silt with a finely laminated silt subunit in the lower part and a medium silt subunit in the upper part.

Sediment core 050310-C4 has been subdivided into five units (Fig. 2). Unit 5 is composed of very poorly sorted coarse silt to fine sand and contains some shells. Unit 4 consists of a layer of coarse sand containing shell fragments. Unit 3 is composed of poorly sorted silt with medium-coarse silt in the lower part and medium silt in the upper part. The lower part of unit 2 is composed of muddy sand, while the upper part is an admixture of poorly to very poorly sorted silt, sand, gravels and shell fragments, clasts of sapolite, quartz and laterites. Unit 1, in the uppermost part of the core, consists of a laminated medium silt layer in the lowermost part followed by a subunit consisting of an admixture of poorly to very poorly sorted silt, sand, and shell fragments.

4.2 Distribution of foraminifera in the surface sediments

In the surface sediments, we identified a total of 59 different species. The shallow sites contain a significant amount of larger foraminifera with higher percentages of *Amphistegina radiata*, *Pararotalia stellata*, *Dentritina ambigua*, *Operculina ammonoides*, *Operculina complanata*, *Amphistegina lessonii*, *Amphistegina* sp. 1 and *Neorotalia calcar* (Fig. 3, Appendix A). Further dominant taxa include *Siphonaperta* sp. 2 (with a maximum of 32.1 %), *Quinqueloculina* sp. 1 (14.7 %), *Discorbinella bertheloti* (19.3 %), *Neoeponides praecinctus* (16.8 %),*Saidovina subangularis* (14.1 %), *Cibicidoides pseudoungerianus* (17.2 %) and *Quinqueloculina seminula* (9.1 %). Most of these taxa show a distinct bathymetric zonation, with species occurring with higher numbers at the shallower stations such as *P. stellata, Borelis schlumbergeri, A. lessonii, S. elliptica, D. ambigua* and *N. calcar*; at stations with intermediate water depths such as *A. radiata, O. ammonoides* and *N. praecinctus*; and at stations with higher water depths such as *S. subangularis* and *C. pseudoungerianus* (Fig. 3).

We observed relatively high amounts of potentially redeposited specimens with maximum percentages of 24 % (mean of 10.5 %) on the total assemblages at the shallower sites from approximately 10 to 30 m water depth, while the deeper sites contained lower amounts (mean of 3 %).

The PCA explains 89.1 % of the total variance in the surface data set for the first six principal components (PCs) (Table 2). The stations deeper than ∼ 45 m water depth are dominated by a *Neoeponides praecinctus–Operculina complanata* assemblage (PC2) with *S. subangularis*, *C. pseudoungerianus* and *D. bertheloti* as associated species (Fig. 4, Table 2). This assemblage explains 10 % of the total variance. The stations at intermediate water depths (between 16 and 34 m) are characterized by the *Amphistegina radiata* assemblage, containing *O. ammonoides* and *N. praecinctus* as associated taxa (PC1) (Fig. 4, Table 2). This PC explains 14.3 % of the total variance. The shallower stations, between 13 and 26 m water depth in the northern and middle part of the study area, are dominated by the *Siphonaperta* sp. 2 assemblage (PC3), with *A. radiata, Quinqueloculina* sp. 1 and *O. ammonoides* as associated species (Fig. 4, Table 2). This PC explains 38.5 % of the total variance. The shallowest stations in the study area, with water depths between 10 and 15 m, are characterized by three assemblages, each of them explaining almost 9 % of the total variance in the data set (Fig. 4, Table 2). The *Discorbinella bertheloti* assemblage (PC4) appears in the southern part of the study area and includes *Rosalina* spp., *Q. seminula, T. oblonga* and *A. tepida* as associated taxa. The *Operculina ammonoides–Dentritina ambigua* assemblage (PC5) occurs in the northern part of the study area and contains *A. lessonii* as the most important associated species. Finally, the *Pararotalia stellata* assemblage (PC6) occurs in the southernmost part of the study area (Fig. 4). Associated species of this assemblage are *A. radiata* and *B. schlumbergeri*.

Table 2. Results of the principal component analysis (see also Fig. 4) with the total variance explained by each principal component (PC) and the scores of the most important species. The species in bold, having the highest scores, are eponymous for the assemblages extracted from the surface samples.

PC axis	Explained variance (%)	Species	Scores
1	14.29	***Amphistegina radiata***	5.71
		Operculina ammonoides	1.31
		Neoeponides praecinctus	1.24
		Discorbinella bertheloti	0.89
		Amphistegina sp.	0.74
		Amphistegina lessonii	0.62
		Siphonaperta sp. 1	0.57
2	10.08	***Neoeponides praecinctus***	3.32
		Operculina complanata	3.03
		Saidovina subangularis	2.85
		Cibicidoides pseudoungerianus	2.78
		Discorbinella bertheloti	2.26
		Anomalinoides colligerus	0.89
		Reussella spinulosa	0.70
		Bolivina sp.	0.56
		Siphonaperta sp. 2	0.54
3	38.50	***Siphonaperta* sp. 2**	5.80
		Amphistegina radiata	2.80
		Quinqueloculina sp. 1	1.84
		Operculina ammonoides	1.11
4	8.86	***Discorbinella bertheloti***	4.28
		Rosalina spp.	3.88
		Quinqueloculina seminula	1.96
		Triloculina oblonga	1.65
		Ammonia tepida	1.05
5	8.86	***Operculina ammonoides***	3.49
		Dentritina ambigua	3.24
		Amphistegina lessonii	3.20
		Siphonaperta sp. 3	1.38
		Amphistegina sp.	1.24
		Borelis schlumbergeri	1.23
		Discorbinella bertheloti	1.02
		Pararotalia stellata	1.02
6	8.56	***Pararotalia stellata***	6.13
		Amphistegina radiata	1.89
		Borelis schlumbergeri	1.31
		Quinqueloculina sp. 1	0.95
		Elphidium craticulatum	0.65
		Quinqueloculina seminula	0.61

The results of the redundancy analysis (RDA) applied on the surface samples show that the water depth, explaining a total of 22 % of the variance ($p > 0.001$) in the data set, is the most important environmental parameter, followed by the proportion of silt and clay (pelite) (20.5 %, $p < 0.002$), fine sand (19.5 %, $p < 0.002$) and the coarser fraction (17.0 %,

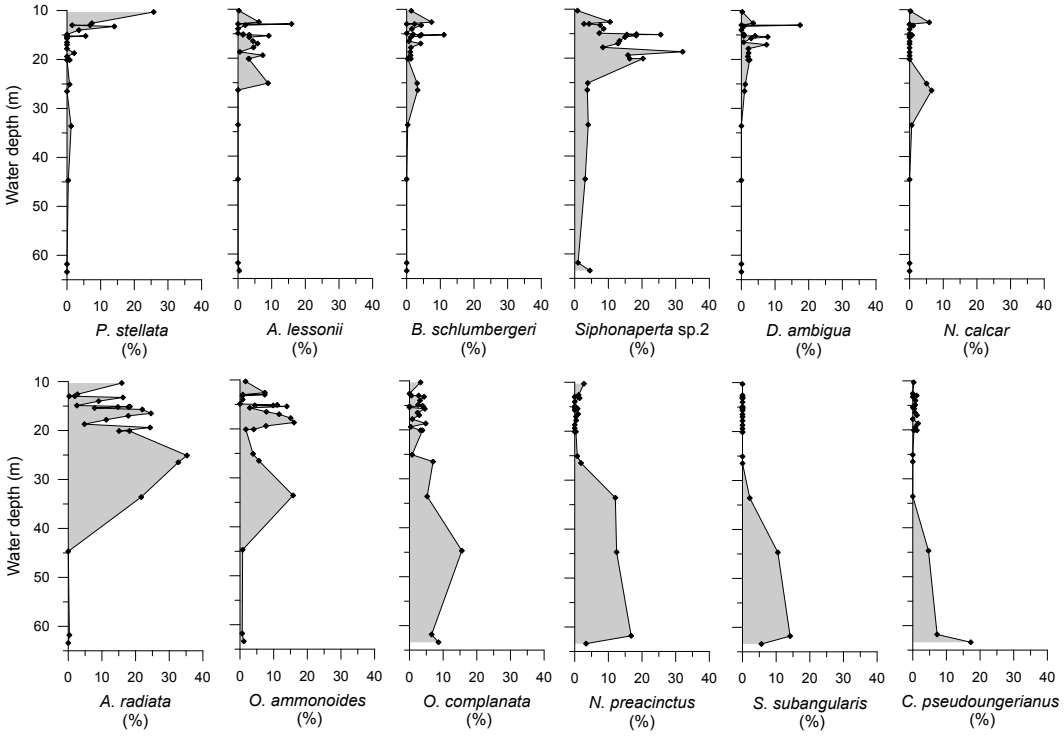

Fig. 3. Relative abundance of selected recent benthic foraminifera from surface sediments versus water depth, showing a distinct bathymetric zonation. Only species having a relative abundance of $> 5\,\%$ on the recent assemblages are presented.

Table 3. Results of the redundancy analysis (RDA).

Axes	1	2	3	4	Captured variance (%)	p value
Eigenvalues	0.296	0.135	0.068	0.014		
Species–environment correlations	0.905	0.945	0.802	0.529		
Cumulative percentage variance						
of species data	29.60	43.10	49.80	51.20		
of species–environment relation	57.80	84.10	97.30	100.00		
Correlation						
Water depth	0.685	−0.567	0.210	−0.001	22.2	<0.001
Fraction < 63 mum	0.699	0.245	−0.426	−0.123	20.5	< 0.002
Fraction > 125 mum	−0.627	−0.394	0.038	0.310	17.0	<0.001
Fraction 63–125 mum	0.643	0.438	0.398	0.098	19.5	<0.002

$p < 0.001$) (Table 3). Water depth, pelite and fine sand are positively correlated to the first RDA axis, while the content of coarser-grained sediment is negatively correlated to the first RDA axis (Fig. 5, Table 3). This axis explains a total of 29.6 % of the total variance in the data set (Table 3). Species of the PC2 assemblage, such as *S. subangularis*, *C. pseudoungerianus*, *Anomalinoides colligerus*, *N. praecinctus, and O. complanata,* show a clear correlation with increasing water depths, while other species, such as *B. schlumbergeri* and *N. calcar,* exhibit an association with lower water depths (Figs. 4 and 5). The species of the PC4 assemblage, such as *D. bertheloti*, *T. oblonga, Q. seminula* and *A. tepida,* show a correlation to finer-grained substrate. In contrast, *O. ammonoides, Siphonaperta* sp. 1 and *Siphonaperta* sp. 2 show a close relation to coarser-grained material. The species of the PC5 assemblage (*A. lessonii, D. ambigua* and *Siphonaperta* sp. 3) together with *A. radiata* and *Quinqueloculina* sp. 1 exhibit a relation both to shallow water and to coarser-grained material (Figs. 4 and 5).

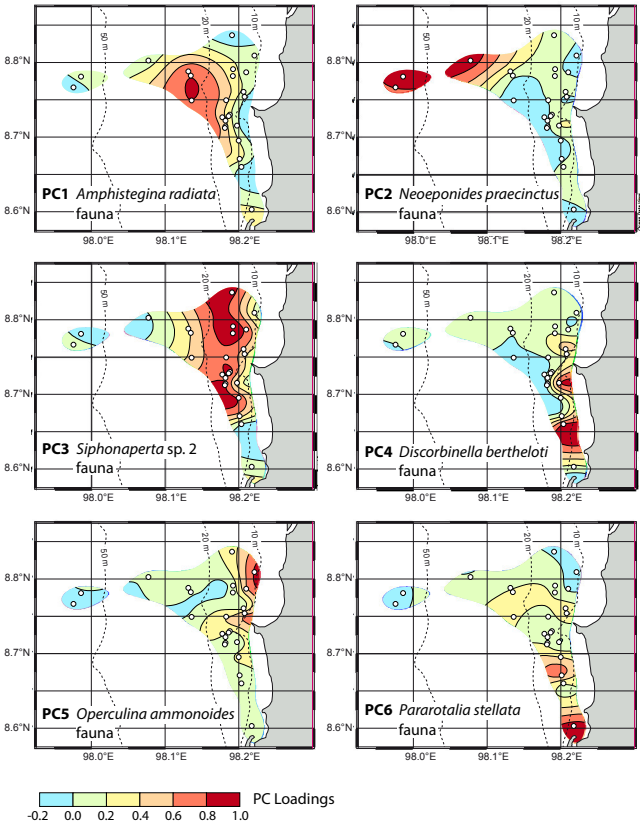

Fig. 4. Distribution of recent benthic foraminiferal assemblages extracted with Q-mode principal component analysis. Shown are PC loadings. Loadings > 0.4 indicate statistically significant influence of the respective fauna (Malmgren and Haq, 1984). Ocean Data View (Schlitzer, 2012) was used for data interpolation. For scale bar see Fig. 1.

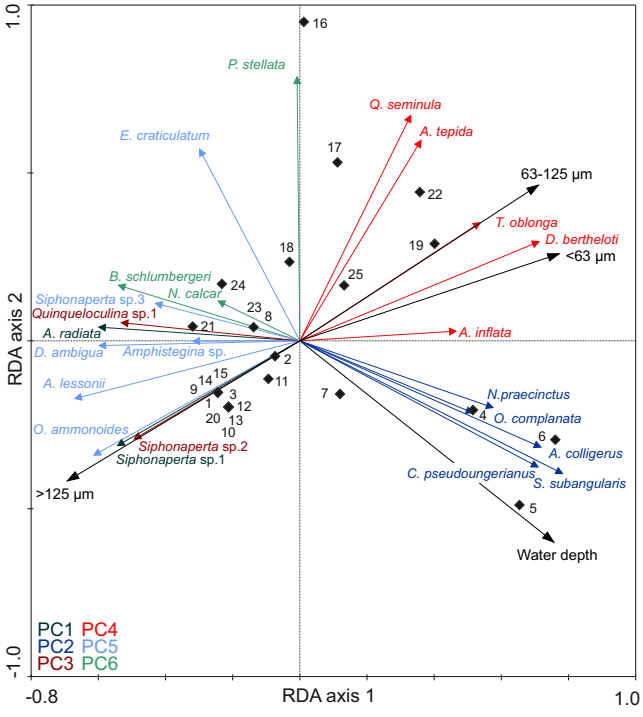

Fig. 5. Results of the redundancy analysis (RDA) applied on the surface samples (see also Table 3). The species arrows are colorized according to their membership to the principal components (PC) extracted from PCA (compare with Fig. 4). The distribution of recent foraminifers exhibits a strong relation to water depth but also to the grain size of the substrate. Species of the PC2 assemblage have a relation to deeper water depths and species of the PC6 assemblages occur more frequently at shallower water depths. For surface sample codes see Table 1.

4.3 Distribution of fossil foraminifera in the sediment cores

Sediment core 030310-C3 contains a total of 48 fossil species, each with percentages larger than 1 % on the total assemblages. The most abundant species in this core are *Amphistegina radiata* (with a maximum relative abundance of 21.4 %), *Siphonaperta* sp. 2 (19.4 %), *Discorbinella bertheloti* (17.8 %) and *Parrellina hispidula* (11.9 %) (Fig. 6a, Appendix A). In addition, species with percentages between 5 and 10 % include (in descending order) *Quinqueloculina* sp. 1, *Elphidium craticulatum*, *Quinqueloculina seminula* and *Borelis schlumbergeri* (Fig. 6a). Core 030310-C3 contains a very high content of redeposited tests with a mean value of 76 %. A maximum with 95 % redeposited specimens was found in the lowermost part of the core at 86.5 cm, and minimum values with 43–48 % redeposited specimens were observed in the upper part of the core at 5.5 and 33.5 cm (Fig. 8).

Sediment core 050310-C4 contains a total of 33 fossil species, each with percentages larger than 1 % on the total assemblages. The most dominant species in this core are *D. bertheloti* (with a maximum relative abundance of 21.2 %) and *Siphonaperta* sp. 2 (13.2 %) (Fig. 6b, Appendix A). Further species with relative abundances between 5 and 10 % are (in descending order) *Amphistegina* sp. 1, *A. radiata, Quinqueloculina* sp. 1, *Quinqueloculina seminula, Spiroloculina communis* and *Elphidium craticulatum* (Fig. 6b). The content of potentially relocated specimens in core 050310-C4 is lower than that observed in core 030310-C3, with a mean value of 48 % (Fig. 8).

4.4 Quantitative paleo-water depth reconstructions

The short gradient length of 1.74 SD for the first axis of the DCCA implies a more linear distribution of the species in relation to water depth (Table 4). This can be explained by the limited water depth range (approximately 10 to 63 m) included in this study, masking the common unimodal bathymetric species distributions. Although the weighted

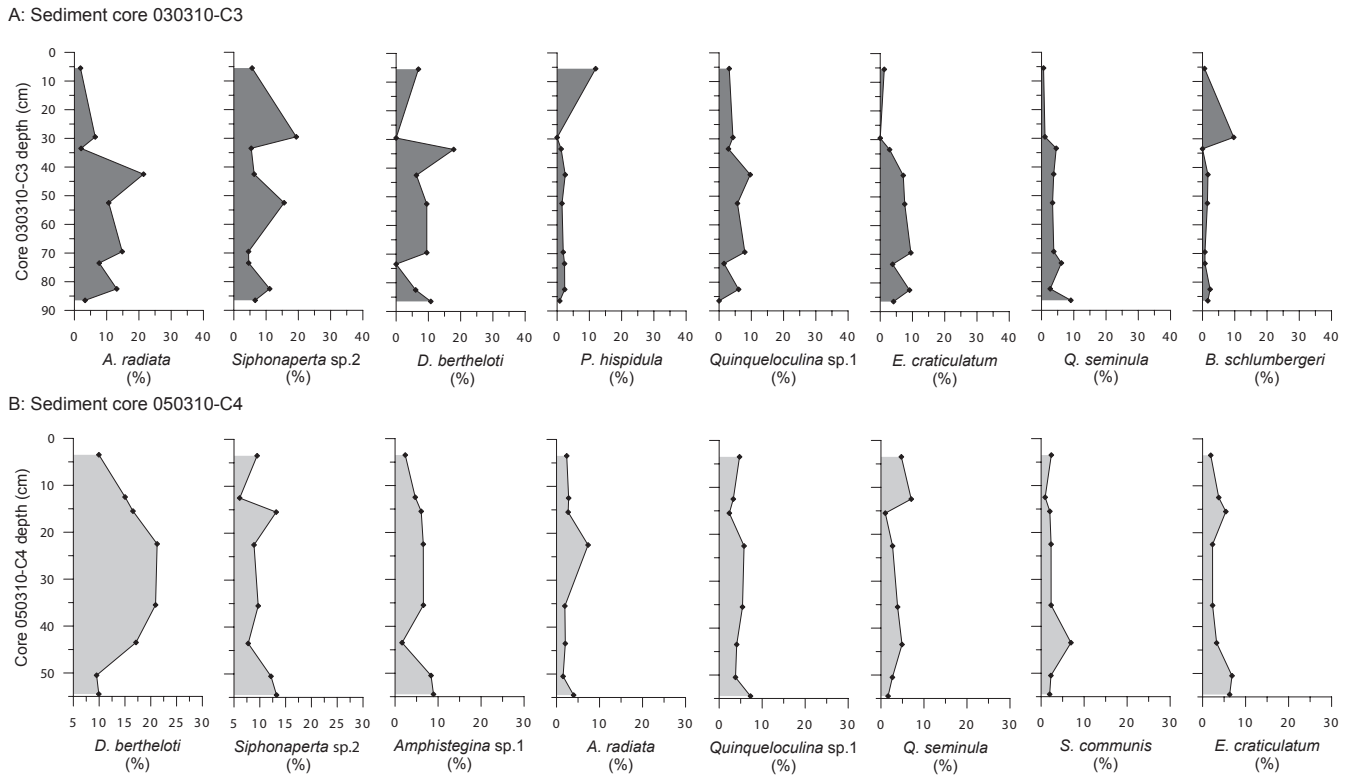

Fig. 6. Distribution of the most abundant fossil benthic foraminifera in sediment cores 030310-C3 **(A)** and 050310-C4 **(B)**. Only species with a relative abundance of $> 5\,\%$ on the fossil assemblages in the sediment cores are presented.

Table 4. Results of the detrended canonical correspondence analysis (DCCA). The short length of gradient for the first axis indicates a linear species–water-depth relationship in the surface samples.

	1	2	3	4
Eigenvalues	0.236	0.123	0.07	0.017
Lengths of gradient (SD)	1.738	1.723	1.112	0.706

averaging–partial least square (WA-PLS) method theoretically works better for gradient lengths of 2 and higher (Birks, 1998; Ter Braak et al., 1993), this method provided the best prediction potential from all methods applied. Moreover, this method can detect the influence of additional parameters such as substrate (Birks, 1998; Horton and Edwards, 2006).

The transfer function created by the WA-PLS method reveals a significant linear correlation ($R^2 = 0.97$ and cross-validated $R^2_{\text{jack}} = 0.92$) between the observed and the estimated water depths in the surface data set for the selected second component (Table 5, Fig. 7). The residuals in the surface data set range between -5.06 m and 2.71 m with a mean of 2.25 m (Fig. 8). The apparent root mean squared error (RMSE) and jack-knifed root mean squared error of prediction (RMSEP) for this component is ± 2.45 m and ± 4.09 m, respectively, showing a relatively good predictive potential of the transfer function (Table 5).

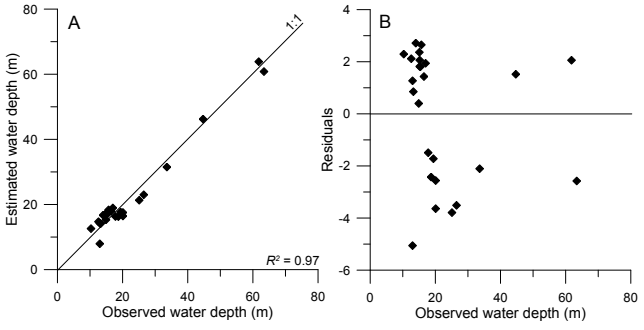

Fig. 7. Observed water depths versus estimated water depths by the WA-PLS transfer function in the surface samples **(A)** and their residuals **(B)**.

To test the robustness of the transfer function, the application of the MAT method showed that, in core 030310-C3, one good analog and four fair analogs, but also four poor analogs with MinDC values above the 20th percentile, were found (Fig. 8). In core 050310-C4, two samples have good analogs with MinDC values below the 10th percentile and the remaining six core samples have fair analogs with values between the 10th and 20th percentile (Fig. 8).

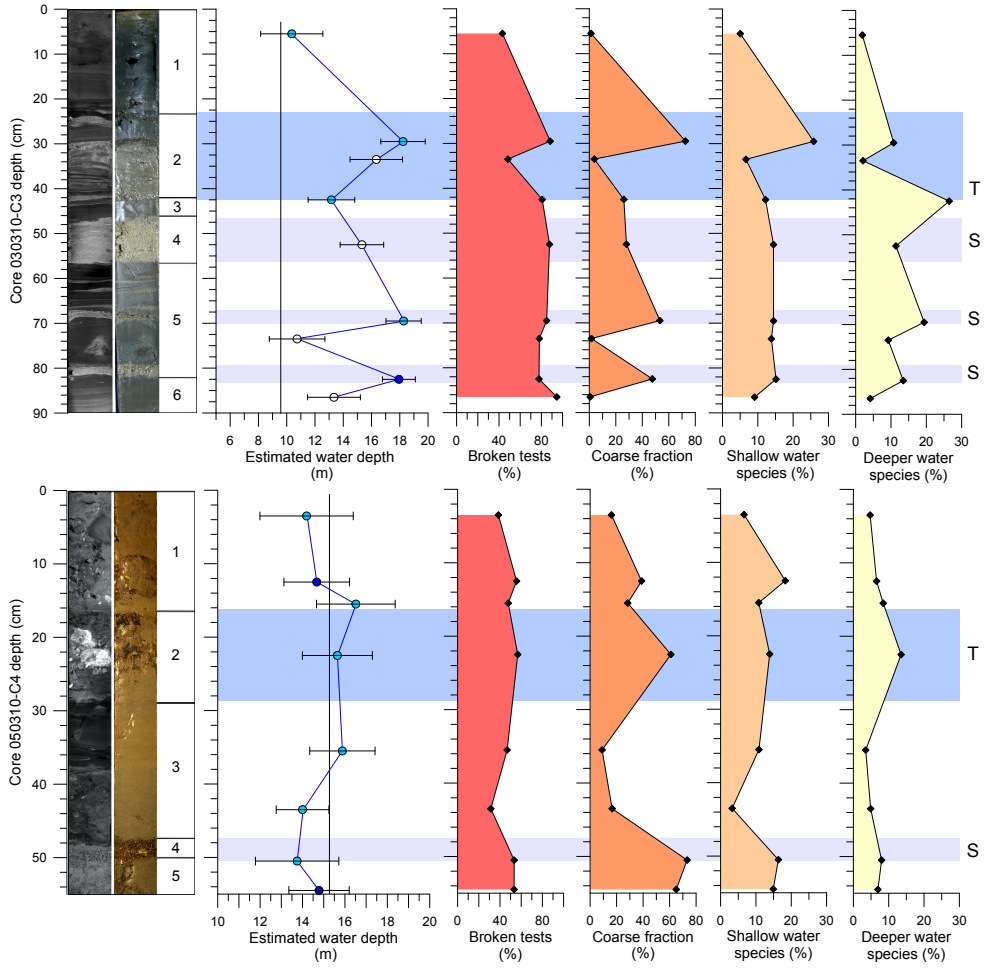

Fig. 8. Sediment core images with their lithological units (see also Fig. 2) and paleo-water depths in cores 030310-C3 and 050310-C4 estimated with the WA-PLS transfer function (open circles = bad analogs; light blue circles = fair analogs; blue circles = good analogs; calculated by modern analog technique). The vertical black lines mark the water depth where the sediment cores were taken. Further are shown the percentages of broken foraminiferal tests, proportion of the coarse fraction, and total relative abundances of species indicative for shallower water (*B. schlumbergeri, P. stellata, A. lessonii, N. calcar, D. ambigua* and *Amphistegina* sp.) and deeper water (*A. radiata* and *O. ammonoides*) in the study area (see also Figs. 3, 4 and 5). The shaded areas indicate storm layers (S) and the 2004 tsunami deposits (T).

Table 5. Results of the WA-PLS transfer function with the root mean squared error, the apparent coefficient of determination (R^2), the cross-validated coefficient of determination (R^2_{jack}), the root mean squared error of prediction (RMSEP) calculated by cross-validation, and the reduction in RMSEP (% change). The selected component for the paleo-water depth estimates in cores 030310-C3 and 050310-C4 is shown in bold.

Component	RMSE	R^2	R^2_{jack}	RMSEP	% change
1	4.50	0.90	0.85	5.46	
2	**2.45**	**0.97**	**0.92**	**4.09**	**25.12**
3	1.67	0.99	0.92	3.98	2.69
4	1.07	0.99	0.92	4.05	−1.65
5	0.79	1.00	0.92	3.94	2.63

The paleo-water depths estimated with the transfer function range from 10.36 (±2.54) m to 18.27 (±1.51) m for core 030310-C3 and from 14.40 (±1.91) m to 17.80 (±2.00) m for core 050310-C4 (Fig. 8). The mean sample-specific error, calculated by bootstrapping, is 1.88 m for core 030310-C3 and 1.59 m for core 050310-C4.

5 Discussion

5.1 Ecology of benthic foraminifera in the study area

Our results imply that both water depth and substrate act as relevant factors on the distribution of benthic foraminifers in the study area, explaining a large part of the observed faunal variability (Fig. 5). Similar relations have been reported from comparable environments of the lower photic zone on

a mixed siliciclastic–carbonate inner shelf (e.g., Renema, 2006a). Many species and the majority of the identified faunas exhibit a distinct bathymetric zonation (Figs. 3 and 4). All faunas except for PC 4 (*D. bertheloti* fauna) contain symbiont-bearing larger benthic foraminifers as dominant or associated components. The relative bathymetric zonation and habitats of larger foraminifers off Khao Lak are comparable to other areas of the Indo-Pacific realm and, thus, are likely controlled by various physical and biological factors, most of which are related to the requirements of the species-specific symbiotic algae (Hallock, 1981; Hohenegger et al., 1999; Beavington-Penney and Racey, 2004; Renema, 2006b). The main factors include water temperature, light penetration, nutrient concentration, food availability and transport, energy at the benthic boundary layer and substrate type and grain size.

In the shallowest environments of the study area, between approximately 10 and 15 m water depth, three distinctive faunas are observed: the larger foraminifers *O. ammonoides, D. ambigua* and *A. lessonii,* which dominate PC5 in the shallow northern parts of the study area (Fig. 4), are typically associated with strong to medium light intensity, moderate to low water energy, and sands or rubble with sand on the reef flat (Hohenegger et al., 1999; Renema, 2006b). The distribution maximum of *A. lessonii* commonly occurs between 10 and 20 m water depth (Renema, 2006b), which is consistent with its occurrence in our study area (Fig. 3). In contrast, *O. ammonoides* has been reported from a wider depth interval, including distribution maxima between 10 and 30 m (Renema, 2006a), in other areas between 40 and 60 m (Hohenegger, 2004). Further to the south, this fauna is replaced by PC4, dominated by the non-symbiont-bearing *D. bertheloti* and *Rosalina* spp. (Figs. 3 and 4). The cosmopolitan species *D. bertheloti* inhabits various shelf and deep-sea environments and has a clear preference for fine-grained substrates (Milker et al., 2009), where it likely profits from specific biogeochemical conditions and the availability of sufficient food particles on and below the sediment surface. In the study area, this fauna is confined to depressions in the reef flat that operate as sediment traps for muddy sediments (Feldens et al., 2012). To the south, this fauna is replaced by the *Pararotalia stellata* fauna. Little is known on the ecology of this species, but it seems to be associated with sandy substrates and has been reported as typical inner-shelf taxon in the study area (Hawkes et al., 2007; Yawsangratt et al., 2011).

The environments at intermediate water depths are dominated by the *Siphonaperta* sp. 2 fauna between 15 and 25 m, and the *Amphistegina radiata* fauna between 20 and 30 m water depth (Figs. 3 and 4). The larger foraminifer *A. radiata* is a characteristic taxon in both faunas and prefers firm substrates with maximum abundances between 20 and 40 m water depth, where it is adapted to variable light intensities and moderate to low water energy (Hohenegger et al., 1999; Hohenegger, 2004). This species commonly avoids the reef flat but is typical for rubble and macroalgal environments at the reef slope (Renema, 2006a). A similar adaption can be also inferred for the miliolid *Siphonaperta* sp. 2.

The deepest environments of the study area, below 30 m water depth, are characterized by *N. praecinctus* and *O. complanata*. The latter species typically replaces *O. ammonoides* at deeper sites and has been reported from sandy substrates between 30 and 90 m (in some areas down to 150 m) water depth, where it is likely adapted to low light intensities and low water energy (Hohenegger, 2004; Renema, 2006b).

5.2 Quantitative reconstruction of redeposition processes during the 2004 Indian Ocean tsunami

Our results demonstrate significant redeposition of sediment particles in the offshore sediments during the 2004 Indian Ocean tsunami, including site-specific uprush and back-wash processes (Fig. 8). Our results are in general agreement with previous observations documenting the severe impacts of the tsunami event on coastal and shallow-water environments from the study area and adjacent regions (Bell et al., 2005; Tsuji et al., 2006; Hawkes et al., 2007). The tsunami-induced run-up at Pakarang Cape reached more than 15 m in height and resulted in the deposition of a few-centimeter-thick sand-rich tsunamite layer (Szczucinski et al., 2005; Choowong et al., 2007; Hori et al., 2007, Jankaew et al., 2008, Brill et al., 2012). Goto et al. (2007) estimated that about 12 500 m^2 of Pakarang Cape were eroded by the 2004 Indian tsunami and a high amount of boulders were transported from offshore into the intertidal zone during the uprush. Hawkes et al. (2007) have shown that the shoreline of Thailand and Malaysia was influenced by up to three waves and a run-up of up to 2 km to the inland. Lay et al. (2005) reported inundation heights of up to 13 m for Sumatra, Thailand and Sri Lanka. On the inner shelf of the study area (9–15 m water depth), event layers of commonly 20–25 cm in thickness were identified as tsunami deposits (Sakuna et al., 2012). Based on the sedimentological observations and 210 Pb dating, assessing the decline in the excess of 210 Pb activities from the nearby area (Sakuna et al., 2012), the 2004 tsunami deposits are 18 cm thick in core 030310-C3 (lithological unit 2) and 13 cm thick in core 050310-C4 (lithological unit 2) (Figs. 2 and 8). Downcore, below the tsunami layers, we observed distinct sand layers in both cores, which were interpreted as storm layers. Core 030310-C3 contains three event layers, with one thicker layer in lithological unit 4 and two thinner layers in lithological unit 5. Core 050310-C4 contains one relatively thin event layer (lithological unit 4) (Figs. 2 and 8). The paleo-water depth estimates for core 030310-C3 indicate a sediment transport from deeper waters to the core location, similar for both the storm layers and the tsunamite (Fig. 8). The paleo-water depths estimated in the storm layers are 15.32 ± 1.54 m for the storm layer in lithological unit 4, and 17.94 ± 1.42 m and 18.27 ± 1.50 m for the lower and upper layer in lithological unit 5, respectively. In the tsunami layer,

we estimated paleo-water depths between 13.16 ± 1.90 m and 18.23 ± 1.68 m. Based on the modern water depth of 9.5 m at this site our results demonstrate a net transport from deeper to shallower environments but also limit the reworking and resuspension of particles to a maximum water depth of approximately 20 m. This result is supported by the low proportion of foraminifera (between two and four percent) in the core that in the present ocean occur in higher percentages at deeper water depths (~ 25 to ~ 60 m) (Fig. 3). Based on the regional seafloor topography (Fig. 1), particles have been transported over approximately 5 km distance. The reconstructed maximum water depth of 20 m is lower than most previous reconstructions based on foraminifers that inferred resuspension depths of 45–300 m (Dominey-Howes et al., 1998; Nanayama and Shigeno, 2006; Uchida et al., 2010). Obviously, the energies and depth impacts of tsunami waves can vary significantly, based on the distance to the source area and the specific coastal morphology (Rabinovich et al., 2011). On the other hand, the majority of existing reconstructions are simply based on general assumptions and observations of benthic foraminiferal distribution ranges, lacking regional reference data sets and a robust statistical assessment. As a consequence, at least some of the reported maximum water depths could be overestimated since many species from middle and deeper shelf environments can also inhabit inner-shelf ecosystems, depending on the local presence of suitable (fine-grained) substrates and related microhabitats (Milker et al., 2009; Mojtahid et al., 2010; Goineau et al., 2011).

Within the tsunami layer of core 030310-C3, changes to deeper paleo-water depths can be observed, likely representing changes in water energy and/ or an admixture of uprush and backwash events during successive tsunami waves (Fig. 8). The estimated deeper water depths in co-occurrence with a sand layer in the upper part of the tsunamite (around 30 cm) may represent a subsequent uprush event, i.e., during a subsequent tsunami wave reaching the coastal area around Cape Pakarang. Our interpretation is supported by frequent occurrences of various species, such as *O. complanata* and *A. radiata,* in the surface samples from deeper water depths. At present, these species preferentially occur between 10 and 45 m water depth, and reach their optima at around 25 m and 35 m water depth, respectively (Figs. 3 and 8). However, the coeval occurrence of species that commonly prefer shallower water depths in the present ocean (*B. schlumbergeri, N. calcar, P. stellata, D. ambigua, A. lessonii* and *Amphistegina* sp.) do not support a clear provenance signal for this potential uprush event in the core (Figs. 3 and 8). Similarly, Hawkes et al. (2007) concluded from microfossil distributions in the Pulau Penang region of northern Malaysia that uprush events related to the 2004 tsunami are indicated by specimens derived from the inner shelf, while backwash layers contain more specimens recently found in mangrove sediments. Furthermore, Nanayama and Shigeno (2006) observed higher percentages of redeposited benthic foraminifera from water depths shallower than 45 m in uprush deposits of the 1993 Hokkaido tsunami.

Our paleo-water depth estimates in core 030310-C3, retrieved from 9.5 m water depth, reveal a provenance of particles in the tsunami layer from approximately 13 to 18 m water depth (Fig. 8). This result is in accordance with existing studies demonstrating that, within 8 km distance to the shoreline, the occurrence of the 2004 tsunami layer was restricted to a maximum water depth of 9 to 18 m (Feldens et al., 2012; Sakuna et al., 2012). These studies also attributed different lithologies and structures within the tsunamite to various phases of the tsunami event; i.e., marine sand layers were related to uprush and intercalated muddy intervals to backwash phases.

Our paleo-water depth reconstructions of core 050310-C4 show that the particles within the tsunamite were derived from slightly deeper water depths of 16.94 ± 1.56 m (Fig. 8). However, our reconstructions show a higher variability for this core, hampering a straightforward reconstruction of redeposition processes from the paleo-water depth estimates alone. The higher variability in the estimated paleo-water depths in core 050310-C4 could be a consequence of the lower amount of larger foraminifera in this core. Larger foraminifera are particularly suitable for paleo-water depth estimations due to their stronger vertical zonation, which can be related to the light dependence of their symbionts and their dependence on hydrodynamic and trophic conditions, which can be linked to water depth (e.g., Hohenegger et al., 1999). In contrast, non-symbiont-bearing foraminifera occur over a wider depth range depending on the surrounding environmental conditions (Milker et al., 2009).

The sediments found in lithological unit 2, interpreted as the 2004 tsunami layer, contain terrestrial particles such as laterites, which indicates that this layer contains a mixture of particles derived from both uprush and backwash processes, inhibiting a clear distinction of the different phases of the tsunami event. The relatively high content of redeposited *A. radiata* and *O. ammonoides* in the middle part of the tsunami layer indicates sediment redeposition from water depths similar to that in core 030310-C3 (Fig. 8). The different percentages of redeposited specimens from deeper water in the two cores can be attributed to the different water depth of the core sites, representing different distances between source and deposition areas of the transported particles. This interpretation, however, is biased by the background redeposition processes that influence sedimentation of inner-shelf environments. The presence of bottom currents and wave action accounts for the overall significant percentages of relocated benthic foraminiferal tests in the recovered sediments of the study area (Fig. 8). Similar observations were also made by Yordanova and Hohenegger (2002) and Briguglio and Hohenegger (2011), indicating that downslope transport of larger benthic foraminifera due to normal wave activity can have significant influence on the accuracy of paleo-depth estimates because the real zonation of foraminifera can be

masked by such redeposition processes. More specifically, Yordanova and Hohenegger (2007) observed that the buoyancy and entrainment potential of larger foraminiferal tests varies depending on their test shape and density.

Based on preliminary datings, a storm layer has been identified in the lower part of the core (unit 4). This layer is characterized by sandy sediment, whose high content of coarse particles contrasts with the adjacent sediments (Fig. 2). Our paleo-water depth reconstruction indicates a sediment transport from slightly shallower to deeper water (14.04 ± 1.78 m). This result contrasts with observations from other areas, where sediment particles during comparable storm surges were preferentially transported from deeper to shallower water depths and where no backflow was observed (Nanayama et al., 2000).

Our data demonstrate that is not possible to distinguish tsunami deposits from background sedimentation based on the relative proportion of reworked particles. Instead, additional information on species composition is required for proper identification of high-energy events, particularly considering comprehensive data on the species distribution in the background sediment for comparison with the event layers.

6 Conclusions

For the first time, a transfer function for water depth reconstruction was developed on benthic foraminifers and applied to the reconstruction of redeposition processes and dynamics associated with the 2004 Indian Ocean tsunami. From our results we can extract the following conclusions:

- The distribution of recent benthic foraminifera on the inner shelf of the southeastern Andaman Sea off Khao Lak (Thailand) is typical for a tropical Indo-Pacific mixed siliciclastic–carbonate environment. The faunas exhibit not only a distinct bathymetric zonation but also a relation to the grain size of the substrate reflecting gradients in light intensity and water energy as well as specific microhabitats. A total of six assemblages have been distinguished, most of which including symbiont-bearing larger foraminifera as dominant and associated constituents. The shallowest sites, between 10 and 15 m, are inhabited by three assemblages, comprising the *Operculina ammonoides* fauna, the *Pararotalia stellata* fauna, and the *Discorbinella bertheloti* fauna. The last is associated with muddy sediments trapped in depressions on the reef flat. The sandy sediments at intermediate water depth are inhabited by the *Siphonaperta* sp. 2 fauna (between 15 and 25 m) and the *Amphistegina radiata* fauna (between 20 and 30 m). The deepest sites (below 30 m) are characterized by the *Neoeponides praecinctus* fauna adapted to low light intensities and low water energy.
- The distinct bathymetric zonation of most recent species allowed the development of a transfer function for quantitative water depth reconstructions with a high prediction potential. Our reconstructions for the 2004 Indian Ocean tsunami layer and pre-dating storm layers from two sites in the study area limit the maximum water depth of resuspension to approximately 20 m. This value is considerably lower than most previous estimates for various tsunami events in the Indo-Pacific realm. On the other hand, the differentiation between storm and tsunami layers in the study area based on foraminifera remains problematic because both events reveal similar characteristics and redeposition processes.

Appendix A

Species list

Ammonia tepida (Cushman, 1926) – Melis and Violanti (2006), p. 98, pl. 1, Figs. 1–2

Amphistegina lessonii (d'Orbigny, 1843) – Jones (1994), p. 109, pl. 111, Figs. 4–7; Hohenegger et al. (1999), p. 144, Fig. 19

Amphistegina radiata (Fichtel and Moll, 1798) – Hohenegger et al. (1999), p. 145, Fig. 20; Jones (1994), pl. 111, Fig. 3

Amphistegina sp. 1

Anomalinoides colligerus (Chapman and Parr, 1937) – Jones (1994), p. 98, pl. 94, Figs. 2–3

Borelis schlumbergeri (Reichel, 1937) – Hottinger et al. (1993), p. 68, pl. 75, Figs. 1–17

Cibicidoides pseudoungerianus (Cushman, 1922) – Cushman (1931), p. 123, pl. 22, Figs. 3–7; Milker and Schmiedl (2012), p. 106, Fig. 24.5–8

Dendritina ambigua (Fichtel and Moll, 1798) – Hohenegger et al. (1999), p. 131, Fig. 10

Discorbinella bertheloti (d'Orbigny, 1839) – Hottinger et al. (1993), p. 114, pl. 150, Figs. 1–4

Elphidium craticulatum (Fichtel and Moll, 1798) – Hottinger et al. (1993), p. 147, pl. 208, Figs. 1–10; Hawkes et al. (2007); p. 178, pl. 2, Fig. 8

Neoeponides praecinctus (Karrer 1868) – Jones (1994), p. 99, pl. 95, Figs. 1–3

Neorotalia calcar (d'Orbigny, 1839) – Hottinger et al. (1993), p. 140, pl. 199, Figs. 1–10; Hohenegger et al. (1999), p. 146, Fig. 21

Operculina ammonoides (Gronovius, 1781) – Hohenegger et al. (1999), p. 155, Fig. 28

Operculina complanata (Defrance, 1822) – Jones (1994), p. 110, pl. 112, Figs. 3–9

Pararotalia stellata (de Férussac, 1827) – Jones (1994), p. 107, pl. 108, Fig. 3; Hawkes et al. (2007), p. 176, pl. 1, Figs. 1–3

Parrellina hispidula (Cushman, 1936) – Melis and Violanti (2006), p. 98, pl. 1, Fig. 13; Berkeley et al. (2009), p. 84, pl. 3, Fig. 7a, b

Quinqueloculina seminula (Linné, 1758) – Jones (1994), p. 21, pl. 5, Fig. 6

Quinqueloculina sp. 1

Saidovina subangularis (Brady, 1881) – Jones (1994), p. 59, pl. 53, Figs. 30, 31

Siphonaperta sp. 1

Siphonaperta sp. 2

Siphonaperta sp. 3

Spiroloculina communis Cushman and Todd (1944) – Jones (1994), p. 25, pl. 9, Figs. 5–6

Triloculina oblonga (Montagu, 1803) – Berkeley et al. (2009), p.84, pl. 2, Fig. 5a, b, c

Supplementary material related to this article is available online at http://www.nat-hazards-earth-syst-sci.net/13/3113/2013/nhess-13-3113-2013-supplement.pdf.

Acknowledgements. For technical support during preparation of samples we thank Eva Vinx and Jutta Richarz at the Center of Earth System Research and Sustainability, Hamburg University. We further want to thank Johann Hohenegger and an anonymous reviewer for their constructive comments helping to improve the manuscript. The project from which the samples originate was funded by Deutsche Forschungsgemeinschaft (DFG) grant SCHW 572/11 and the National Research Council of Thailand (NRCT).

Edited by: H. Sterr
Reviewed by: J. Hohenegger and one anonymous referee

References

Backhaus, K., Erichson, B., Plinke, W., and Weiber, R.: Multivariate Analysemethoden, 11th Edn., Springer, Berlin, Heidelberg, New York, 2006.

Beavington-Penney, S. J. and Racey, A.: Ecology of extant nummulitids and other larger benthic foraminifera: applications in palaeoenvironmental analysis, Earth-Sci. Rev., 67, 219–265, 2004.

Bell, R., Cowan, H., Dalziell, E., Evans, N., O'Leary, M., Rush, B., and Yule, L.: Survey of impacts on the Andaman coast, southern Thailand following the great Sumatra-Andaman earthquake and tsunami of December 26, 2004, Bull. New Zealand Soc. Earth. Eng., 38, 124–148, 2005.

Berkeley, A., Perry, C. T., Smithers, S. G., Horton, B. P., and Cundy, A. B.: Foraminiferal biofacies across mangrove-mudflat environments at Cocoa Creek, north Queensland, Australia, Mar. Geol., 263, 64–86, 2009.

Birks, H. J. B.: Quantitative palaeoenvironmental reconstructions, in: Statistical Modelling of Quaternary Science Data, edited by: Maddy, D. and Brew, J. S., Cambridge, 161–254, 1995.

Birks, H. J. B.: Numerical tools in palaeolimnology – Progress, potentialities, and problems, J. Paleolimnol., 20, 307–332, 1998.

Birks, H. J. B., Line, J. M., Juggins, S., Stevenson, A. C., and Ter Braak, C. J. F.: Diatoms and pH reconstruction, Phil. Trans. R. Soc. Lond., B 327, 263–278, 1990.

Brill, D., Klasen, N., Jankaew, K., Brückner, H., Kelletat, D., Scheffers, A., and Scheffers, S.: Local inundation distances and regional tsunami recurrence in the Indian Ocean inferred from luminescence dating of sandy deposits in Thailand, Nat. Hazards Earth Syst. Sci., 12, 2177–2192, doi:10.5194/nhess-12-2177-2012, 2012.

Briguglio, A. and Hohenegger, J.: How to react to shallow water hydrodynamics: The larger benthic foraminifera solution, Mar. Micropalaeontol., 81, 63–76, doi10.1016/j.marmicro.2011.07.004, 2011.

Choowong, M., Murakoshi, N., Hisada, K., Charusiri, P., Daorerk, V., Charoentitirat, T., Chutakositkanon, V., Jankaew, K., and Kanjanapayont, P.: Erosion and deposition by the 2004 Indian Ocean tsunami in Phuket and Phang-nga provinces, Thailand. J. Coastal Res., 23, 1270–1276, 2007.

Cushman, J. A.: The foraminifera of the Atlantic Ocean, Part 8: Rotaliidae, Amphisteginidae, Calcarinidae, Cymbalporettidae, Globorotallidae, Anomalinidae, Planorbulinidae, Pupertidae and Homotremidae, Smithonian Institution, United States National Museum, Bulletin 104, Washington, 1931.

Dahanayake, K. and Kulasena, N.: Recognition of diagnostic criteria for recent- and paleo-tsunami sediments from Sri Lanka, Mar. Geol., 254, 180–186, doi:10.1016/j.margeo.2008.06.005, 2008.

Dominey-Howes, D., Dawson, A., and Smith, D.: Late Holocene coastal tectonics at Falasarna, western Crete: a sedimentary study, in: Coastal Tectonics, edited by: Stewart, I. and Vita-Finzi, C., Special Publications, Geological Society, London, 343–352, 1998.

Fagherazzi, S. and Du, X.,: Tsunamigenic incisions produced by the December 2004 earhquake along the coasts of Thailand, Indonesia and Sri Lanka, Geomorphology, 99, 120–129, doi:10.1016/j.geomorph.2007.10.015, 2007.

Feldens, P., Schwarzer, K., Szczuciński, W., Stattegger, K., Sakuna, D., and Somgpongchaiykul, P.: Impact of 2004 tsunami on seafloor morphology and offshore sediments, Pakarang Cape, Thailand, Polish J. Environ. Stud, 18, 63–68, 2009.

Feldens, P., Schwarzer, K., Sakuna, D., Szczucinski, W., and Sompongchaiyakul, P.: Sediment distribution on the inner continental shelf off Khao Lak (Thailand) after the 2004 Indian Ocean tsunami, Earth Planet. Space, 64, 875–887, 2012.

Goineau, A., Fontanier, C., Jorissen, F. J., Lansard, B., Buscail, R., Mouret, A., Kerhervé, P., Zaragosi, S., Ernoult, E., Artéro, C., Anschutz, P., Metzger, E., and Rabouille, C.: Live (stained) benthic foraminifera from the Rhône prodelta (Gulf of Lion, NW Mediterranean): Environmental controls on a river-dominated shelf, J. Sea Res., 65, 58–75, 2011.

Goto, K., Chavanich, S. A., Imamura, F., Kunthasap, P., Matsui, T., Minoura, K., Sugawara, D., and Yanagisawa, H.: Distribution, origin and transport process of boulders deposited by the 2004 Indian Ocean tsunami at Pakarang Cape, Thailand, Sediment. Geol., 202, 821–837, 2007.

Hallock, P.: Algal symbiosis: A mathematical analysis, Mar. Biol., 62, 249–255, 1981.

Hawkes, A. D., Bird, M., Cowie, S., Grundy-Warr, C., Horton, B. P., Tan Shau Hwai, A., Law, L., Macgregor, C., Nott, J., Eong Ong, J., Rigg, J., Robinson, R., Tan-Mullins, M., Tiong Sa, T., Yasin, Z., and Wan Aik, L.: Sediments deposited by the 2004 Indian Ocean Tsunami along the Malaysia–Thailand Peninsula, Mar. Geol., 242, 169–190, 2007.

Hawkes, A. D., Horton, B. P., Nelson, A. R., and Hill, D. F.: The application of intertidal foraminifera to reconstruct coastal subsidence during the giant Cascadia earthquake of AD 1700 in Oregon, USA, Quaternary Int., 122, 116–140, 2010.

Hohenegger, J.: Depth coenoclines and environmental considerations of western pacific larger foraminifera, J. Foramin. Res., 34, 9–33, 2004.

Hohenegger, J.: Estimation of environmental paleogradient values based on presence/absence data: a case study using benthic foraminifera for paleodepth estimation, Palaeogeogr. Palaeocl., 217, 115–130, 2005.

Hohenegger, J., Yordanova, E., Nakano, Y., and Tatzreiter, F.: Habitats of larger foraminifera on the upper reef slope of Sesoko Island, Okinawa, Japan, Mar. Micropalaeontol., 36, 109–168, 1999.

Hori, K., Kuzumoto, R., Hirouchi, D., Umitsu, M., Janjirawuttikul, N., and Patanakanog, B.: Horizontal and vertical variation of 2004 Indian tsunami deposits: An example of two transects along the western coast of Thailand, Mar. Geol., 239, 163–172, doi:10.1016/j.margeo.2007.01.005, 2007.

Horton, B. P. and Edwards, R. J.: Quantifying Holocene sea-level change using intertidal foraminifera: Lessons from the British Isles, Cushman Foundation for Foraminiferal Research, Special publication No. 40, 1–97, 2006.

Horton, B. P., Edwards, R. J., and Lloyd, J. M.: A foraminiferal-based transfer function: Implications for sea-level studies, J. Foramin. Res., 29, 117–129, 1999.

Hottinger, L., Halicz, E., and Reiss, Z.: Recent foraminiferida from the Gulf of Aqaba, Red Sea, Academia Scientarum et Artium Slovenica, Classis IV: Historia Naturalis, Lubljana, 179 pp., 1993.

Jankaew, K., Atwater, B. F., Sawai, Y., Choowong, M. Charoentitirat, T., Martin M. E., and Prendergast, A.: Mediveal forewarning of the 2004 Indian Ocean Tsunami in Thailand, Nature, 455, 1228–1231, 2008.

Jones, R. W.: The Challenger Foraminifera, 1st Edn., Oxford University Press Inc., New York, 149 pp., 1994.

Juggins, S.: Software for ecological and palaeoecological data analysis and visualisation, Tutorial Version 1.3, 1–24, 2003.

Kemp, A. C., Horton, B. P., Corbett, R., Culver, S. J., Edwards, R. J., and van de Plassche, O.: The relative utility of foraminifera and diatoms for reconstructing late Holocene sea-level change in North Carolina, USA, Quaternary Res., 71, 9–21, 2009.

Kortegaas, S. and Dawson, A. G.: Distinguishing tsunami and storm deposits: An example from Martinhal, SW Portugal, Sediment. Geol., 200, 208–221, doi:10.1016/j.sedgeo.2007.01.004, 2007.

Kumar, V. S., Babu, V. R., Babu, M. T., Dhinakaran, G., and Rajamanickam, G. V.: Assessment of storm surge disaster potential for the Andaman Islands, J. Coastal Res., 24, 171–177, doi:10.2112/05-0506.1, 2008.

Lay, T., Kanamori, H., Ammon, C. J., Nettles, M., Ward, S. N., Aster, R. C., Beck, S. L., Bilek, S. L., Brudzinski, M. R., Butler, R., DeShon, H. R., Ekström, G., Satake, K., and Sipkin, S.: The great Sumatra-Andaman Earthquake of 26 December 2004, Science, 308, 1127–1132, 2005.

Leps, J. and Smilauer, P.: Multivariate analysis of ecological data using CANOCO, Cambridge University Press, Cambridge, 269 pp., 2003.

Levitus, S., and Boyer, T. P.: World Ocean Atlas 1994, Volume 4. Temperature, National Environmental Satellite, Data, and Information Service, Washington, DC (United States), 1994.

Malmgren, B. A. and Haq, B. U.: Assessmant of quantitative techniques in paleobiogeography, Mar. Micropaleontol., 7, 213–230, 1982.

Mamo, B., Strotz, L., and Dominey-Howes, D.: Tsunami sediments and their foraminiferal assemblages, Earth-Sci. Rev., 96, 263–278, 2009.

Mard Karlsson, J., Skelton, A., Sandén, M, Ioualalen, M., Kaewbanjak, N., Pophet, N., Asavanant, J., and von Matern, A.: Reconstructions of the coastal impact of the 2004 Indian Ocean tsunami in the Khao Lak area, Thailand, J. Geophys. Res., 114, C10023, doi:10.1029/2009JC005516, 2009.

Melis, R. and Violanti, D.: Foraminiferal biodiversity and Holocene evolution of the Phetchaburi coastal area (Thailand Gulf), Mar. Micropalaeontol., 61, 94–115, 2006.

Milker, Y. and Schmiedl, G.: A taxonomic guide to modern benthic shelf foraminifera of the western Mediterranean Sea., Palaeontol. Electron., 15, 1–134, 2012.

Milker, Y., Schmiedl, G., Betzler, C., Römer, M., Jaramillo-Vogel, D., and Siccha, M.: Distribution of Recent benthic foraminifera in neritic carbonate environments of the Western Mediterranean Sea, Mar. Micropalaeontol., 73, 207–225, doi:10.1016/j.marmicro.2009.10.003, 2009.

Milker, Y., Schmiedl, G., and Betzler, C.: Paleobathymetric history of the Western Mediterranean Sea shelf during the latest glacial period and the Holocene: Quantitative reconstructions based on foraminiferal transfer functions, Palaeogeogr. Palaeocl., 307, 324–338, doi:10.1016/j.palaeo.2011.05.031, 2011.

Mojtahid, M., Jorissen, F., Lansard, B., and Fontanier, C.: Microhabitat selection of benthic foraminifera in sediments off Rhone river mouth (NW Mediterranean), J. Foram. Res., 40, 231–246, doi:10.2113/gsjfr.40.3.231, 2010.

Morton, R. A., Gelfenbaum, G., and Jaffe, B. E.: Physical criteria for distinguishing sandy tsunami and storm deposits using modern examples, Sediment. Geol., 200, 184–207, doi:10.1016/j.sedgeo.2007.01.003, 2007.

Murray, J. W.: Ecology and Applications of Benthic Foraminifera, Cambridge University Press, Cambridge, 2006.

Nanayama, F. and Shigeno, K.: Inflow and outflow facies from the 1993 tsunami in southwest Hokkaido, Sediment. Geol., 187, 139–158, 2006.

Nanayama, F., Shigeno, K., Satake, K., Shimokawa, K., Koitabashi, S., Miyasaka, S., and Ishii, M.: Sedimentary differences between the 1993 Hokkaido-nansei-oki tsunami and the 1959 Miyakojima typhoon at Taisei, southwestern Hokkaido, northern Japan, Sediment. Geol., 135, 255–264, 2000.

Nelson, A. R., Sawai, Y., Jennings, A. E., Bradley, L.-A., Gerson, L., Sherrod, B. L., Sabean, J., and Horton, B. P.: Great-earthquake paleogeodesy and tsunamies of the past 2000 years at Alsea Bay, central Oregon coast, USA, Quaternary Sci. Rev., 27, 747–768, 2008.

Overpeck, J. T., Webb III., T., and Prentice, I. C.: Quantitative interpretation of fossil pollen spectra: Dissimilarity coefficients and the method of Modern Analogs, Quaternary Res., 23, 87–108, 1985.

Parker, J. H. and Gischler, E.: Modern foraminiferal distribution and diversity in two atolls from the Maldives, Indian Ocean, Mar. Micropaleontol., 78, 30–49, 2011.

Phantuwongraj, S., and Choowong, M.: Tsunamis versus storm deposits from Thailand, Nat. Hazards, 63, 31–50, 2012.

Rabinovich, A. B., Candella, R. N., and Thomson, R. E.: Energy Decay of the 2004 Sumatra Tsunami in the World Ocean, Pure Appl. Geophys, 168, 1919–1950, 2011.

Renema, W.: Large benthic foraminifera from the deep photic zone of a mixed siliciclastoc-carbonate shelf off East Kalimantan, Indonesia, Mar. Micropaleontol., 58, 73–82, 2006a.

Renema, W.: Habitat variables determining the occurrence of large benthic foraminifera in the Berau area (East Kalimantan, Indonesia), Coral Reefs, 25, 351–359, 2006b.

Rossi, V. and Horton, B. P.: The application of subtidal foraminifera-based transfer function to reconstruct Holocene paleobathymetry of the Po Delta, northern Adriatic Sea, J. Foramin. Res., 39, 180–190, 2009.

Saidova, K. M.: Benthic foraminifera communities of the Andaman Sea (Indian Ocean), Oceanology, 48, 517–523, 2008.

Sakuna, D., Szczucinski, W., Feldens, P., Schwarzer, K., and Khokiattiwong, S.: Sedimentary deposits left by the 2004 Indian Ocean tsunami on the inner continental shelf offshore of Khao Lak, Andaman Sea (Thailand), Earth Planet. Space, 64, 931–943, 2012.

Satyanarayana, A., Nallapa Reddy, A., Jaiprakash, B. C., and Chidambaram, L.: A note on foraminifera, grain size and clay mineralogy of tsunami sediments from Karaikal-Nagore-Nagapattinam beaches, Southeast coast of India, J. Geol. Soc. India, 69, 70–74, 2007.

Scheffers, A., Brill, D., Kelletat, D., Brückner, H., Scheffers, S., and Fox, K.: Holocene sea levels along the Andaman Sea coast of Thailand, Holocene, 22, 1169–1180, 2012.

Stein, S. and Okal, E. A.: Speed and size of the Sumatra earthquake, Nature, 434, 581–582, 2005.

Sugawara, D., Minoura, N., Tsukawaki, S., Goto, K., and Imamura, F.: Foraminiferal evidence of submarine sediment transport and deposition by backwash during the 2004 Indian Ocean tsunami, Isl. Arc, 18, 513–525, 2009.

Szarek, R., Kuhnt, T., Kawamura, H., and Kitazato, H.: Distribution of recent benthic foraminifera on the Sunda Shelf (South China Sea), Mar. Micropaleontol., 61, 171–195, 2006.

Ter Braak, C. J. F. and Juggins, S.: Weighted averaging partial least squares regression (WA-PLS): an improved method for reconstructing environmental variables from species assemblages, Hydrobiologia, 269/270, 485–502, 1993.

Ter Braak, C. J. F. and Smilauer, P.: CANOCO Reference manual and CanoDraw for Windows User's guide (version 4.5), Microcomputer power Ithaka, NY, USA, 500 pp., 2002.

Ter Braak, C. J. F., Juggins, S., Birks, H. J. B., and Van der Voet, H.: Weighted Averaging Least Squares regression (WA-PLS): definition and comparison with other methods for species-environment calibration, in: Multivariate Environmental Statistics, edited by: Patil, G. P. and Rao, C. R., Elsevier Science Publishers B.V. (North Holland), Amsterdam, 525–560, 1993.

Thampanya, U., Vermaat, J. E., Sinsakul, S., and Panapitukkul, N.: Coastal erosion and mangrove progradation of Southern Thailand, Estuar. Coast. Shelf S., 68, 75–85, 2006.

Tsuji, Y., Namegaya, Y., Matsumoto, H., Iwasaki, S.-I., Kanbua, W., Sriwichai, M., and Meesuk, V.: The 2004 Indian tsunami in Thailand: Surveyed runup heights and tide gauge records, Earth Planet. Space, 58, 223–232, 2006.

Uchida, J.-I., Fujuwara, O., Hasegawa, S., and Kamataki, T.: Sources and depositional processes of tsunami deposits: Analysis using foraminiferal tests and hydrodynamic verification, Isl. Arc, 19, 427–442, 2010.

Van der Zwaan, G. J., Jorissen, F. J., and de Stigter, H. C.: The depth dependency of planktonic/benthic foraminiferal ratios: Constraints and applications, Mar. Geol., 95, 1–16, 1990.

Varkey, M. J., Murty, V. S. N., and Suryanarayana, A.: Physical oceanography of the Bay of Bengal and Andaman Sea, Oceanogr. Mar. Biol. Ann. Rev, 34, 1–70, 1996.

Yawsangratt, S., Szczucinski, W., Chaimanee, N., Chatprasert, S., Majewski, W., and Lorenc, S.: Evidence of probable paleotsunami deposits on Kho Khao Island, Phang Nga Province, Thailand, Nat. Hazards, 23, 1270–1276, doi:10.2112/05-0561.1, 2011.

Yordanova, E. K. and Hohenegger, J.: Taphonomy of larger foraminifera: Relationships between living individuals and empty tests on flat reef slopes (Sesoko Island, Japan), Facies, 46, 169–203, doi:10.1007/BF02668080, 2002.

Yordanova, E. K. and Hohenegger, J.: Studies on settling, traction and entrainment of larger benthic foraminiferal tests: implications for accumulation in shallow marine sediments, Sedimentology, 54, 1273–1306, doi:10.1111/j.1365-3091.2007.00881.x, 2007.

Schwarzer, Schrottke & Stattegger (eds.):
From Brazil to Thailand – New Results in Coastal Research
***Coastline Reports 16 (2010)**, ISSN 0928-2734, ISBN 978-3-9811839-9-3*
S. 15-24

Shallow water sediment structures in a tsunami-affected area (Pakarang Cape, Thailand)

Peter Feldens[1], Daroonwan. Sakuna[1,2], Penjai Somgpongchaiyakul[3] & Klaus Schwarzer[1]

[1]Kiel University, Germany
[2]Phuket Marine Biological Centre, Thailand
[3]Biogeochemical and Environmental Change Research Unit, Prince of Songkla University, Thailand

Abstract

The influence of tsunami on the seafloor is poorly understood. Detailed hydroacoustic surveys and sediment sampling campaigns were carried out in 2007 and 2008 offshore Pakarang Cape (Thailand) to catalogue the geomarine effects of the 2004 Indian Ocean tsunami. A major problem in determining tsunami influence in offshore deposits is the lack of pre-tsunami mappings. Starting in 15 m water depth, a system of sand ridges composed of coarse sand exists offshore Pakarang Cape. Elongated sediment transport structures on the NW-flanks of the sand ridges, slowly fading during the annual cycle, indicate the presence of a current oblique to the coastline. This current might coincide with the 2004 Indian Ocean Tsunami. A several cm-thick event layer found at the base of a sand ridge is composed of silty sediment, which could be related to the tsunami backwash or strong floods during the monsoon. These event deposits are covered by coarse sand. They might enter the geological record.

1 Introduction

Tsunamis are among the largest catastrophic events in the world. They are recorded since historical times and numerous investigations have been done about their origin, wave distribution and energy release along coastlines. On December 26th, 2004 an M 9.3 submarine earthquake was generated off the northwest coast of the Indonesian island Sumatra due to a complex tectonic activity between the Indo-Australian plate and the Sunda-Plate. This generated a giant tsunami which had an impact over many SE Asian coastlines, reaching to the East-coast of Africa (Lay et al. 2005).

Compared to the influence of the 2004 Indian Ocean Tsunami to onshore areas, the impact to the offshore environment is not well understood. Only few studies document tsunami effects offshore (e.g. Van den Bergh et al. (2003), Noda et al. (2007), Abrantes et al. (2008), Feldens et al. (2009), Paris et al. (2009), but influence and physical properties of the sediment-loaded tsunami backwash are largely unknown. Dawson & Stewart (2007) propose that offshore tsunami deposits are more common in the geological record than onshore deposits. A secure identification of offshore tsunami deposits would therefore be of great value for the recognition of paleotsunamis. A major, but common problem is the missing data about pre-tsunami conditions when working on recent tsunamigenic structures on continental shelf areas. It has to be carefully considered, if observed structures have existed before a tsunami hit the area, were created during the tsunami event or were altered by the tsunami impact. We present observations and first results of selected sedimentological and morphological features, recorded during cruises in the framework of the TUNWAT project (Tsunami deposits in near-shore- and coastal waters of Thailand; funded by the Human Research Foundation (DFG), Grant: SCHW/11-1) offshore the tsunami impacted coastline of Khao Lak, Phang Nga Province, Thailand.

2 Investigation area

The continental shelf of the Andaman Sea adjacent to the Malay Peninsula is narrow and slightly inclined; the 50 m isobaths is reached approximately 7 km offshore Phuket and about 30 km offshore Phang Nga Province located towards north. The coastal area is dominated by rocky cliffs altering with sandy lowlands and pocket beaches. From December to February the NE-monsoon dominates while the SW-monsoon is active from May to September (Khokiattiwong et al. 1991). The influence of storms and typhoons on this part of Thailand's coastline is low (Kumar et al. 2008, Jankaew et al. 2008). The tide is mixed semidiurnal, ranging between 1.1 m and 3.6 m (Thampanya et al. 2006).

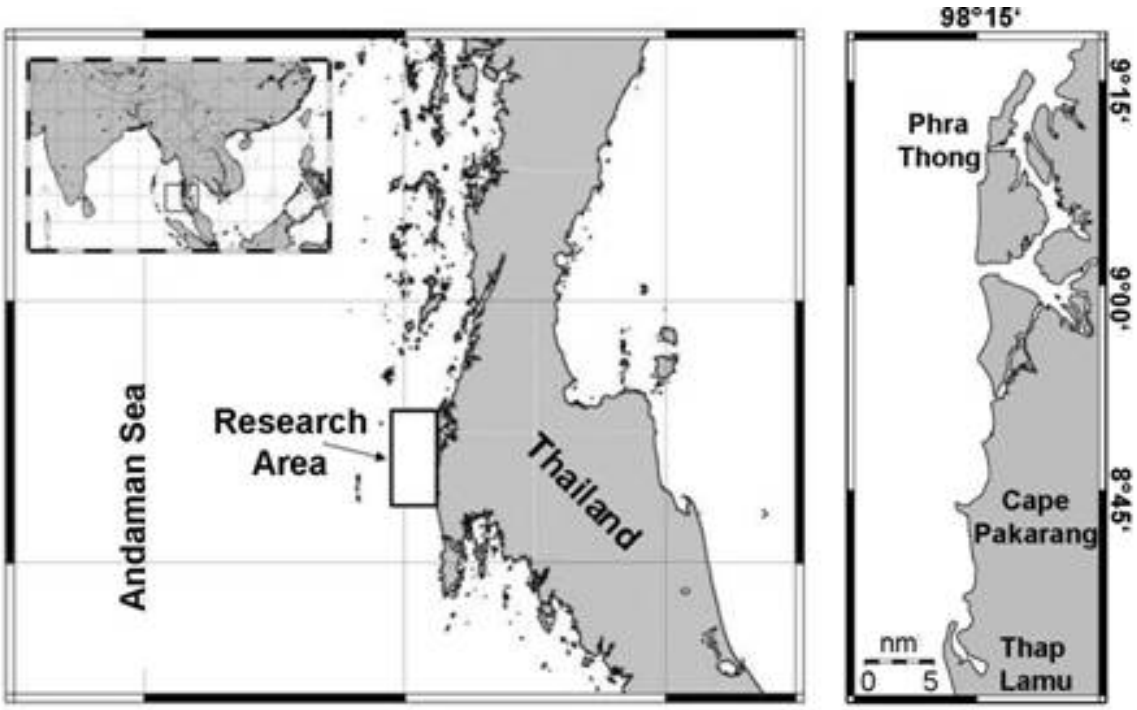

Figure 1: The research area is located in front of Khao Lak, Phang Nga province, Thailand.

The research area, between Thap Lamu and Phra Thong Island comprises of approximately 1.000 km² (figure 1). It was selected as it was hit severely by the 2004-Indian-Ocean-Tsunami (Bell et al. 2005, Tsuji et al. 2006). The wave run-up heights reached more than 15 m at Pakarang Cape (Siripong 2006) and up to 20 m at Phra Thong Island (Jankaew et al. 2008). At Pakarang Cape an area of about 12.500 m² was eroded by the tsunami (Synolakis & Kong 2006) and hundreds of reef rocks could be observed on the intertidal area after the event (Goto et al. 2007). For the investigation area the fluvial discharge is small, which increases the preservation potential of tsunamigenic features on the seafloor.

3 Methods

Two cruises have been carried out; a first one in Nov./Dec. 2007 with RV CHAKRATONG TONGYAI and a second with RV BOONLERT PASOOK in Nov./Dec. 2008. Both ships are operated by the Phuket Marine Biological Center (PMBC). Different side scan sonar systems were applied; a Klein 595 with digital data acquisition in 2007 and a Benthos 1624 digital side scan sonar system in 2008. Side scan sonar systems measure acoustical properties of the seafloor, which mainly depend on grain size distribution, seafloor roughness and the angle of the seafloor slope (Lurton 2002). Features protruding from the seafloor, e.g. boulders, but as well large ripples are easily recognized in side scan sonar images due to the acoustic shadow formed behind them. In this study, fine grained deposits

appear in lighter colours, while coarse grained material is represented by darker colours. For ground-truthing of the side-scan sonar data grab samples were taken on selected positions.

A shallow water multibeam echosounder (ELAC SeaBeam 1185) was used to acquire bathymetric data. Multibeam echo sounders provide many simultaneous depth measurements over a narrow section of the seafloor. The SeaBeam 1185 system is working with a frequency of 180 kHz, which is suitable for a high resolution mapping in shallow waters. The acoustic beam of the system has a fan width of 153°, giving a theoretical swath width of 8.3 times the water depths. Calibration for tidal fluctuations was done by using the software WX-Tide32 (www.wxtide32.com), as no direct water level measurements are available in or close to the research area.

Shallow water high resolution reflections seismics (C-Boom System), in combination with the recovery of short gravity cores, was used to obtain information about the uppermost layers of the seafloor. X-radiography images of thin slabs taken from the core surface were prepared to detect sedimentary structures that cannot be seen otherwise (Jackson et al. 1996). The database of the cruises carried out in 2007 and 2008 include about 1500 nautical miles (nm) of hydroacoustic profiles, 112 Surface sediment samples and 42 short sediment cores.

4 Results

Side scan sonar images offshore Khao Lak show several different sedimentary structures in depths from 7 to 30 m (figure 2). In water depths between 7 and 15 m, extended patches of fine grained sediments are deposited. Connected to these patches is a small scale channel system starting at 10 m water depth. Here we focus on structures appearing at 15 m water-depth. Elongated SW-NE striking morphological ridges are visible in the hydroacoustic data (Figure 2). These structures are common along the whole coastline between Thap Lamu and Pakarang Cape, and up to Phra Thong Island towards north. The continuation of the ridges into deeper waters is yet unknown. The ridges, with a steep NW- and a gently dipping SE flank reach heights of about 2 m, while their length exceeds several kilometres. The distance between two ridge crests varies from several hundred meters to several kilometres. In front of the steep north-eastern side of these ridges, small channels with incision depths of approximately 1 m are sometimes cut into the seafloor. According to seismic data, the ridges are not connected to subsurface structures, but are clearly separated from the sedimentological structures below by an unconformity (figure 5).

For one ridge, a side scan sonar mosaic was draped over the bathymetry (figure 3) to correlate sedimentology and morphology. Grab samples taken around the ridge (figure 3) reveal the presence of different sediment properties in a small area: Generally, the south-western, landward flank of the ridge and the surface of the seafloor surrounding the ridge are composed of coarse sand. Bright elongated sediment structures are deposited on the seaward flank of the ridge and are composed of well sorted fine to medium sand. The patches are separated from each other by thin bands of coarser sediment. From their appearance in the side scan sonar image, the structures resemble large-scale flaser beddings. However, as the genesis of the observed features is different to flaser beddings, which are formed due to tidal activities, the term will not be used.

The sediment patches are commonly observed on the seaward, northern flank of sand ridges along the coastline. Rarely, they are found on the flat seafloor. Boulders are sometimes exposed in close vicinity (figure 3, figure 4). At the base of the ridge flank shown in figure 3, grab samples contain muddy material just a few centimetres below the seafloor.

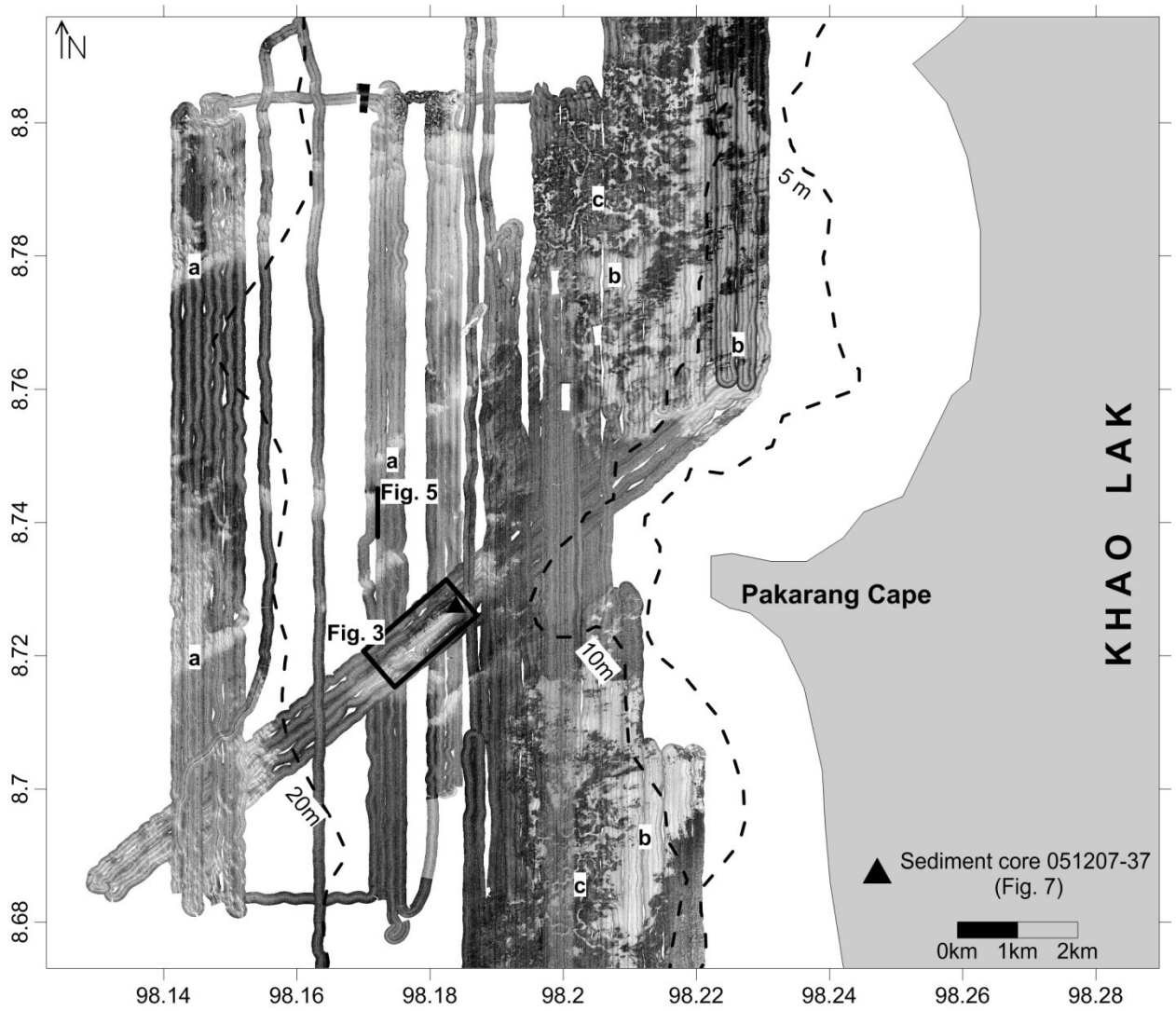

Figure 2: Side scan sonar data around Pakarang Cape. Sampling stations and the positions of fig. 3 and fig. 4 are indicated. Sediment core 051207-37 is shown in fig. 7. This article is focusing on SW-NE striking sediment structures visible as lighter-coloured bands in the side-scan sonar image (a). Closer to the coastline, extended areas of fine grained sediment (b) and a small scale channels (c) are visible.

Core 051207-37 (figure 7) is divided in four sedimentary units. Unit 1 (0-8 cm core depth) is mainly composed of brown sand, including some shell fragments. Between 8 and 11 cm, a layer composed of silt, containing no sand, is apparent (unit 2). The lower boundary of unit 2 is sharp, while its upper boundary is not well defined. Between app. 11 to 12 cm core depth, unit 3A is composed of well sorted sand. Below, unit 3B (12 to 20 cm core depth) contains higher amounts of clay and silt. Various shell fragments are abundant in unit 3B. From 20 cm to the base of the core, unit 4 is composed of sandy silt, and includes some shell fragments. Partly, layers containing higher amounts of sediments in the sand fraction are recognized in the x-ray images.

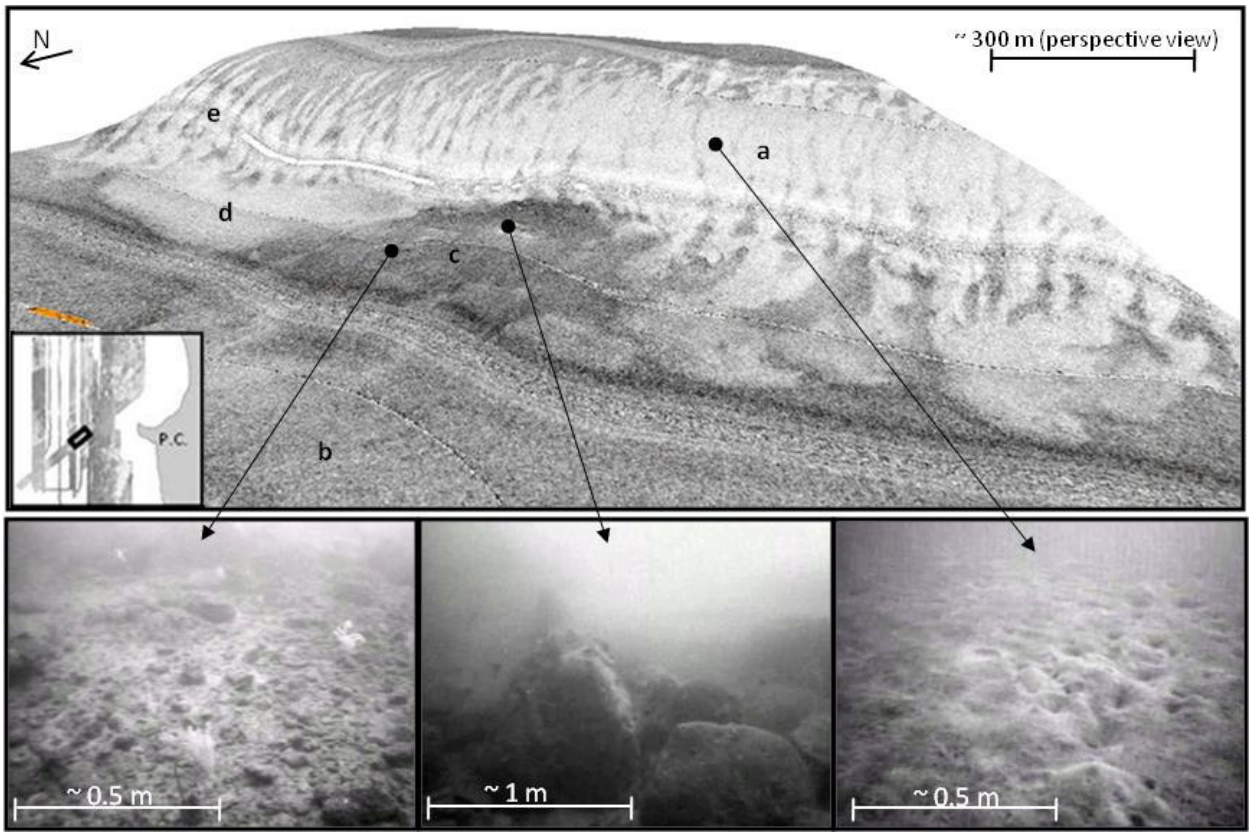

Figure 3: Side scan sonar draped over the bathymetric dataset. For position see figure 2. The length of the ridge is approx. 1500 m (perspective view). a) elongated sediment patches, consisting of fine to medium sand b) coarse sand c) carbonatic gravel and boulders (notice video image) d) sand at the surface, muddy material below e) position of short core (051207-37, fig. 7), composed of sandy material on top and a fine grained layer at 10 cm depth.

5 Discussion

Sand ridges are formed due to regular hydrodynamic processes, e.g. tidal currents in inlets, ocean currents at the shelf margin or during storms (Ernstsen et al. 2006, Flemming 1978, Holland & Elmore 2008), although moribund ridges as remnants from times with a lower sea level are known (Dyer & Huntley 1999). Goff et al. (1999) report that sand ridges on the northeast US Atlantic shelf are asymmetric, having steeper seaward flanks. Holland & Elmore (2008) report that grain sizes across sand ridges typically range from coarse to fine sand. The typical height of storm generated sand ridges is given with 3 to 12 m (van de Meene & van Rijn 2000). Commonly, sand ridges are oblique to the coastline, with the acute angle opening into the prevailing flow direction (Swift et al. 1978, Holland & Elmoore 2008). Most of these features are found in the observed ridge system. The strike direction of the ridges indicates an approximately south-north directed current which was responsible for their formation. This was not the main current direction observed during the tsunami (images of the IKONOS satellite, Goto et al. 2007). Therefore, the ridge system existed prior to the tsunami, although the definite process responsible for its formation has not yet been identified.

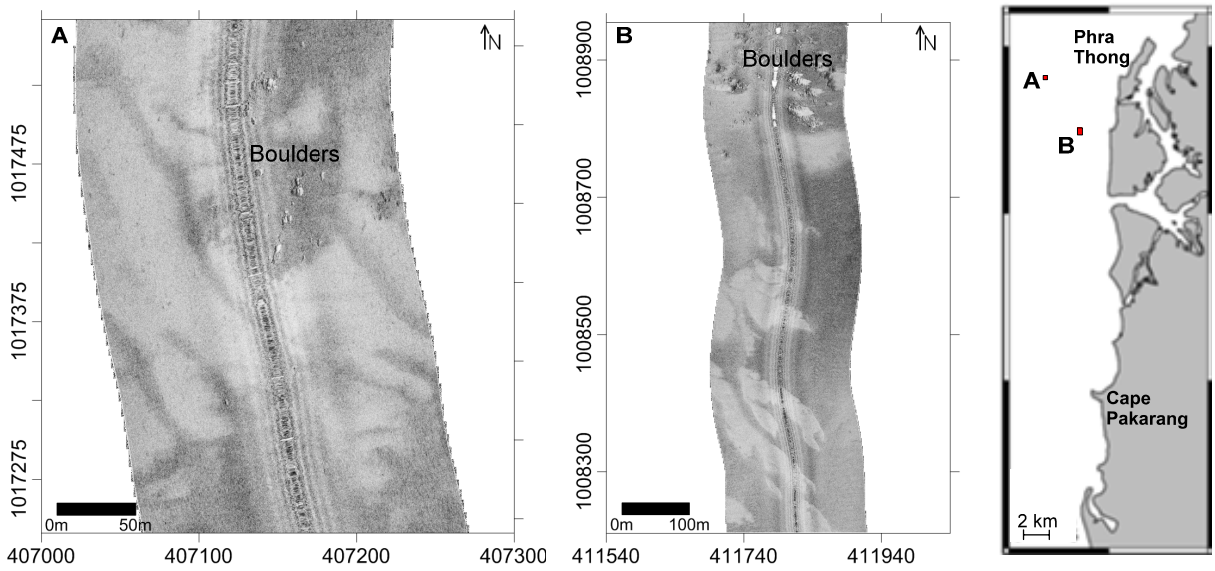

Figure 4: Elongated sedimentary structures offshore Phra Thong. Frequently, boulders are exposed in close vicinity to these structures. Water depth at A: 27 m. Water depth at B: 21 m.

Notable are elongated sediment patches commonly found on the northern flanks of the sand ridges. While finer sediment on the steeper slope of asymmetrical sand ridges is common, in front of storm dominated coasts (Holland & Elmore 2008). Here fine sediments are not visible over the entire length of the flank, but instead they are deposited in small patches separated by coarser sediment. Similar bedforms on the continental shelf offshore Brazil have been formed due to storm events (Moscon & Bastos 2010). The comparison of side scan sonar images from 2007 and 2008 (figure 6) indicates that the general shape of the patches is preserved, but smaller parts begin to fade during one annual cycle, indicating an out-of-equilibrium event based deposition and ongoing reworking of the sediment. Additionally, the existence of identical sediment structures on the flat seafloor further indicates that their formation is not connected with the formation of the sand ridges. Therefore these elongated patches of fine grained sediment have to be interpreted as bedforms created by currents along the north-east/south-west direction. The general stability of these bedforms, combined with the slow fading of delicate structures suggests that no frequently occurring event is responsible for their formation. Since strong storms are rare in the area, and none occurred between the 2004 tsunami and our measurements (based on tracks published by the Regional Specialised Meteorological Centre – Tropical Cyclones (RMSC), New Delhi), it is reasonable to assume that the observed sediment pattern was influenced by the 2004 tsunami, either during the run-up or the backwash.

It is assumed that the muddy material frequently found in grab samples at the base of the sand ridge corresponds to unit 2 in core 051207-37. Therefore, such material is present over a larger area at the base of the sand ridge, and not only locally in one core. Considering the silt separating two units of coarse sand, its deposition likely corresponds to a single event. Similar deposits in cores offshore the Eel River have been described by Crocket & Nittrouer (2004) as flood deposits, which could be generated in the research area by strong monsoon events. But also a tsunami backwash transports large amounts of fine-grained material offshore (Shi & Smith 2003). The process responsible for the formation cannot be determined with certainty. However, a deposition of this material during the monsoon is unlikely, as more regularly occurring structures would be expected. Regardless of the origin of their formation, these event deposits were preserved in the comparably sheltered environments at the base of the sand ridges. They are covered by coarse sand (unit 1), typical for this area of the shelf, indicating some sediment dynamics in the area. This agrees to the change of sedimentological boundaries observed in side scan sonar mosaics between 2007 and 2008 (figure 6). A

potential deposition of the sediments beneath unit 2 during an event, indicated for instance by the marked change in sand content of unit 3A compared to unit 3B, or the abundance of shell fragments in unit 3B, is uncertain. Further analysis is needed to identify the origin and the spatial extension of these potential tsunami deposits, especially closer towards the shoreline.

Interesting are frequent observations of boulders close to the elongated patches deposited at the seaward flank of the sand ridges. Many of these boulders show no connection to structures in the subsurface, and must have been transported to their current position. Potentially, this could have happened during the tsunami, either during the run-up from source areas in deeper waters, or during the backwash (compare Paris et al. 2009)

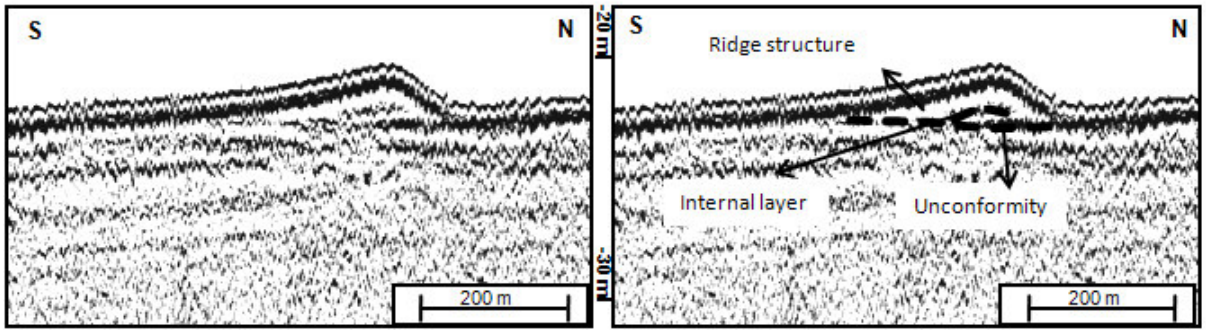

Figure 5: Seismic profile crossing a sand ridge (for position see Figure 2). Clearly visible is the asymmetric form of the ridge which is indicating a transport direction from South to North. Additionally, the ridge is separated from the older surface below by an unconformity.

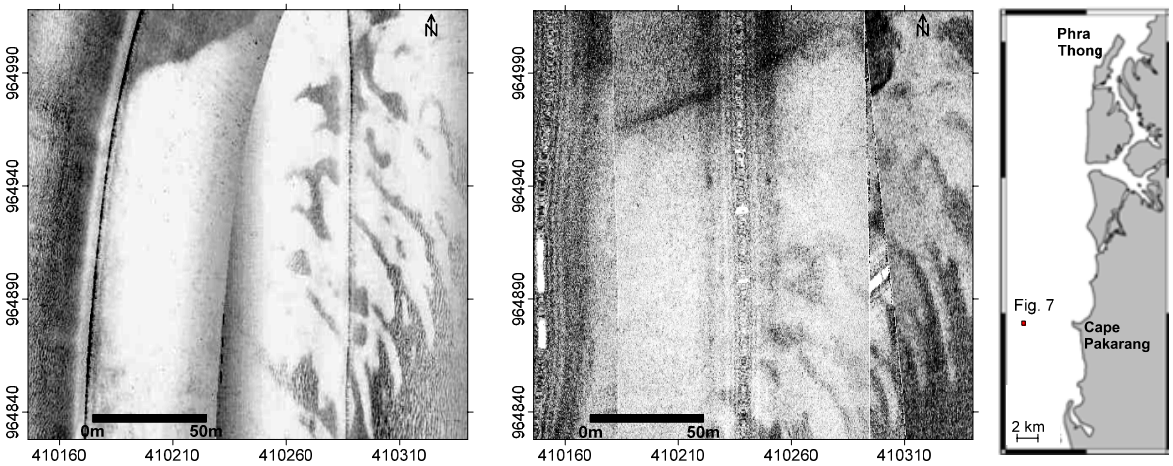

Figure 6: Two side-scan sonar images showing a comparison of a detail of the sand ridge shown in figure 3. The left image was recorded in 2007, the right image in 2008. Small differences are visible. The contours of the elongated sedimentary structures are more pronounced in 2007.

During the tsunami run-up, many boulders were transported towards the intertidal area on Pakarang Cape (Goto et al. 2007). The backwash at Pakarang Cape was modelled by Goto et al. (2007). The authors show that the current speed of the backwash was in the order of 3m/s. This is strong enough to move the observed boulders (Goto et al. 2007, Imamura et al. 2008), which have a diameter of less than 1 meter according to underwater images. Taking into account a channelized backwash (Le Roux & Vargas 2005, Fagherazzi & Du 2007), it is possible that in some areas the current speed was strong enough to transport boulders downslope from the reef platform fringing Pakarang Cape back towards

the sea. However, this cannot explain the presence of boulders found several kilometers offshore (Fig. 4).

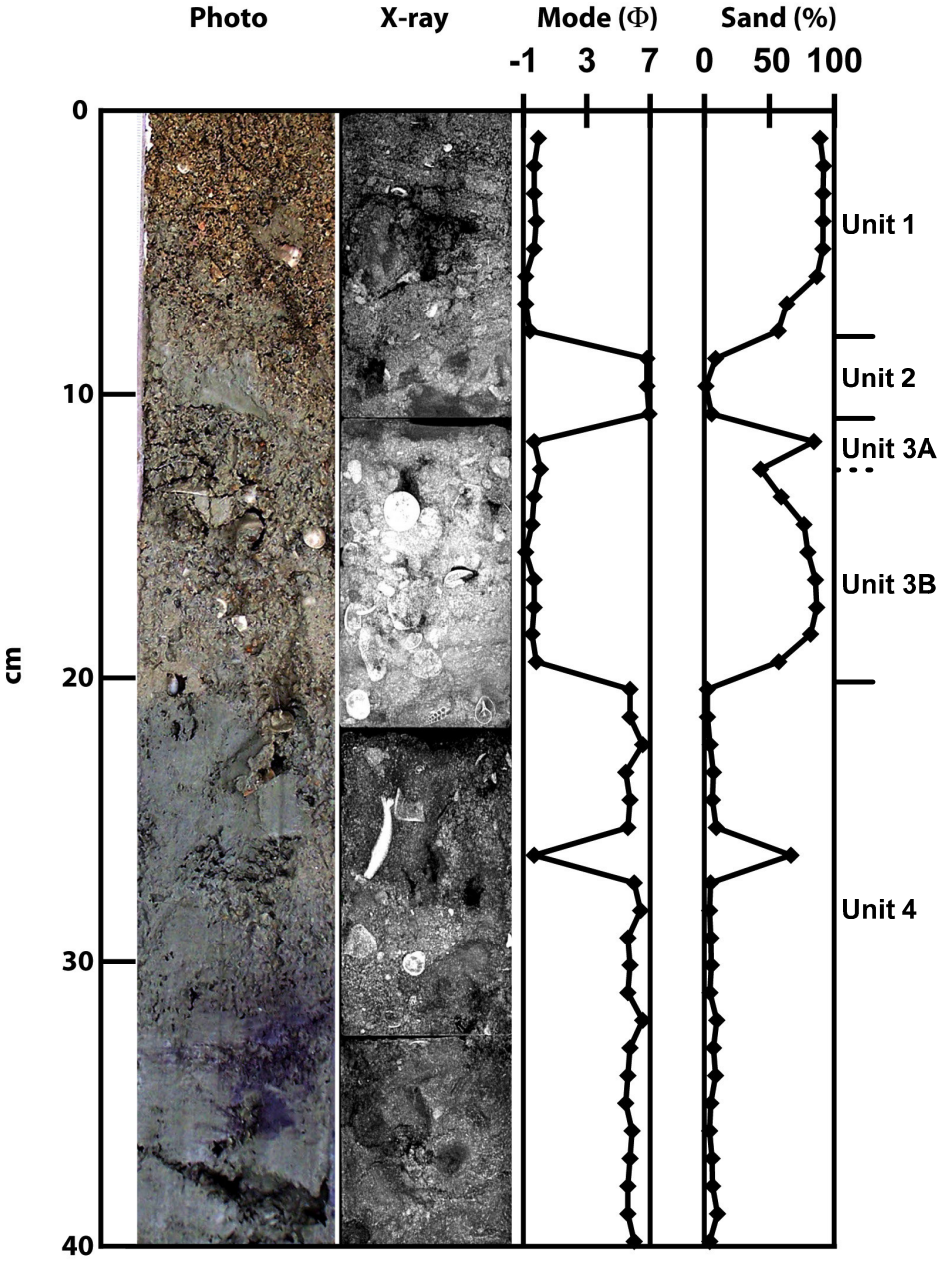

Figure 7: Properties of core 051207-37. From left to right, photo, x-ray image, first mode in phi-degrees, sand content and sedimentary units are presented. For position, refer to Fig.2.

6 Conclusion

Detailed hydroacoustic surveys have been carried out offshore Phang Nga province (Thailand) in 2007 and 2008 and sediment samples have been collected. Starting at 15 m water depth, a system of sand ridges, formed by coarse sand, was discovered. The sand ridges existed prior to the 2004 Indian Ocean Tsunami. Elongated sediment patches on the seaward flank of the sand ridges consist of fine to medium sand, and indicate a current oblique to the coastline. They fade slowly during the annual cycle, and were potentially reworked during the 2004 Indian Ocean Tsunami. An event layer found at the base of a sand ridge is composed of silty sediment, which could be related to the tsunami backwash or floods during the monsoon. These event deposits are covered by coarse sand, and might enter the geological record.

References

Abrantes, F., U. Alt-Epping, S. Lebreiro, A. Voelker & R. Schneider (2008): Sedimentological record of tsunamis on shallow-shelf areas: The case of the 1969 AD and 1755 AD tsunamis on the Portugese Shelf off Lisbon. In: Marine Geology 249: 283–293.

Bell, R., H. Cowan, E. Dalziell, N. Evans, M. O`Leary, B. Rush & L. Yule (2005): Survey of impacts on the Andaman Coast, Southern Thailand following the great Sumatra-Andaman earthquake and tsunami of December 26, 2004. In: Bull. of The New Zealand Soc. For Earthquake Eng. 38 (3), 123–148.

Crockett, J.S. & C.A. Nittrouer (2004): The sandy inner shelf as a repository for muddy sediment: an example from Northern California. In: Continental Shelf Research 24: 55–73.

Dawson, A.G. & I. Stewart (2007): Tsunami deposits in the geological record. In: Sedimentary Geology 200: 166–183.

Dyer, K.R. & D.A. Huntley (1999): The origin, classification and modelling of sand banks and ridges. In: Continental Shelf Research 19 (10), 1285–1330.

Ernstsen, V.B., R. Noormets, C. Winter, D. Hebbeln, A. Bartholomä, B.W. Flemming & J. Bartholdy (2006): Qunatification of dune dynamics during a tidle cycle in an inlet channel of the Danish Wadden Sea. In: Geo-Mar Lett 26 (3): 151–163.

Fagherazzi, S. & X. Du (2007): Tsunamigenic incisions produced by the December 2004 earthquake along the coasts of Thailand, Indonesia and Sri Lanka. In: Geomorphology 99: 120–129.

Feldens, P., K. Schwarzer, W. Sczcuciński, K. Stattegger, D. Sakuna & P. Sompongchaiykul (2009): Impact of 2004 Tsunami on seafloor morphology and offshore sediments, Pakarang Cape, Thailand. In: Polish J. of Environ. Stud. 18: 63–68.

Flemming, B.W. (1978): Underwater sand dunes along the southeast African continental margin – observations and implications. In: Mar. Geol. 26: 177–198

Geronimo, I.D., M. Choowong, S. Phantuwongraj (2009): Geomorphology and superficial bottom sediments of Khao Lak coastal area (SW Thailand). In: Polish J. of Environ. Stud. 18(1): 111–121.

Holland, K.T. & P.A. Elmore (2008): A review of heterogenous sediments in coastal environments. In: Earth-Science Reviews 89: 116–134.

Goff, J.A., D.J.P. Swift, C.S. Duncan, L.A. Mayer & J. Hughes-Clarke (1999): High-resolution swath sonar investigation of sand ridge, dune and ribbon morphology in the offshore environment of the New Jersey margin. In: Marine Geology 161: 307–337.

Goto, K. S.A. Chavanich, F. Imamura, P. Kunthasap, T. Matsui, K. Minoura, D. Sugawara & H. Yanagisawa (2007): Distribution, origin and transport process of boulders deposited by the 2004 Indian Ocean tsunami at Pakarang Cape, In: Thailand. Sed. Geol. 202: 821–837.

Imamura, F., K. Goto & S. Ohkubo (2008): A numerical model for the transport of a boulder by tsunami. In: Journal of Geophysical Research 113, C01008, doi:10.1029/2007JC004170.

Jackson, P.D., K.B. Briggs & R.C. Flint (1996): Evaluation of sediment heterogeneity using microresistivity imaging and X-radiography. In: Geo-Marine Latters 16: 219–225.

Jankaew, K., B.F. Atwater, Y. Sawai, M. Choowong, T. Charoentitirat, M.E. Martin & A. Prendergast (2008): Medieval forewarning of the 2004 Indian Ocean tsunami in Thailand. In: Nature 455: 1228–1231.

Kelletat, D., S.R. Scheffers & A. Scheffers (2007): Field signatures of the SE-Asian Mega-Tsunami along the West Coast of Thailand compared to Holocene Paleo-Tsunami from the Atlantic Region. In: Pure appl. Geophys. 164: 413–431.

Khokiattiwong, S., P. Limpsaichol, S. Petpiroon, P. Sojisuporn & B. Kjerfve (1991): Oceanographic variations in Phangnga Bay, Thailand under monsoonal effects. In: Phuket Marine Biological Center Research Bulletin, 55: 43–76.

Kumar, V.S, V. Ramesh Babu, M.T. Babu, G. Dhinakaran & G.V. Rajamanickam (2008): Assessment of Storm Surge Disaster Potential for the Andaman Islands. In: Journal of Coastal Research 24(2):171–177.

Lay, T., H. Kanamori, J.C. Ammon & M. Nettles (2005): The great Sumatra-Andaman earthquake of 26 December 2004. In: Science 306: 1127–1133.

Le Roux, J.P. & G. Vargas (2005): Hydraulic behaviour of tsunami backflows: insights from their modern and ancient deposits. In: Environ. Geol 49: 65–75.

Lurton, X. (2002): Underwater Acoustics: An introduction. Springer (Berlin) 347 S.

Moscon, D.M.C. & A.C. Bastos (2010): Occurence of storm-generated bedforms along the inner continental shelf - southeastern Brazil. In: Brazilian Journal of Oceanography 58: 45–56.

Noda A., H. Katayama, T. Sagayama, K. Suga, Y. Uchida, K. Satake, K. Abe & Y. Okamura (2007): Evaluation of tsunami impacts on shallow marine sediments: An example from the tsunami caused by the 2003 Tokachioki earthquake, northern Japan. In: Sed. Geol. 200: 314–327.

Paris, R., J. Fournier, E. Poizot, S. Etienne, J. Morin, F. Lavigne & P. Wassmer (2010): Boulder and fine sediment transport and deposition by the 2004 tsunami in Lhok Nga (western Banda Aceh, Sumatra, Indonesia): A coupled offshore-onshore model. In: Marine Geology 268 (1-4): 43–54

Pälike, H., N.J. Shackleton & U. Röhl (2001): Astronomical forcing in Late Eocene marine sediments. In: Earth Planet. Sci. Lett. 193: 589–602.

Shi, S. & D.E. Smith (2003): Coastal tsunami geomorphological impacts and sedimentation processes: Case studies of modern and prehistorical events. International Conference on Estuaries and Coasts. November 9-11, 2003, Hangzhou, China

Siripong, A. (2006): Andaman Seacoast of Thailand Field Survey after the December 2004 Indian Ocean Tsunami. In: Earthquake Spectra 22 (S3): 187–202.

Swift, D.J.P., G. Parker, N.W. Lanfredi, G. Perillo & K. Figge (1978): Shoreface-connected Sand Ridges on American and European Shelves: A Comparison. In: Estuarine and Coastal Marine Science 7: 257–271.

Synolakis, C.E. & L. Kong (2006): Runup measurements of the December 2004 Indian Ocean Tsuanmi. In: Earthquake Spectra 22 (S3): 67–91.

Thampanya, U., J.E. Vermaat, S. Sinsakul & N. Panapitukkul (2006): Coastal erosion and mangrove progradation of Southern Thailand. In: Estuar., Coast. Shelf Sci. 68: 75–85.

Tsuji, Y., Y. Namegaya, H. Matsumoto, S.I. Iwasaki, W. Kanbua, M. Sriwichai & V. Meesuk (2006): The 2004 Indian tsunami in Thailand. Surveyed runup heights and tide gauge records. In: Earth Planets Space 58: 223–232.

Van Den Bergh G.D., W. Boer, H. De Haas, TJ.C.E. Van Weering & R. Van Wijhe (2003): Shallow marine tsunami deposits in Teluk Banten (NW Java, Indonesia), generated by the 1883 Krakatau eruption. In: Marine Geology 197: 13–34.

Van de Meene, J.W.H. & L.C. van Rijn (2000): The shoreface-connected ridges along the central Dutch coast – part 1: field observations. In: Continental Shelf Research 20: 2295–2323.

Weiss, R. & H. Bahlburg (2006): The Coast of Kenya Field Survey after the December 2004 Indian Ocean Tsunami. In: Earthquake Spectra 22 (S3): 235–240.

Acknowledgement

We are grateful to NRCT (National Research Council Thailand) and PMBC (Phuket Marine Biological Center) for providing us with the research vessels CHAKRATONG TONGAI and BOONLERT SOOK. We thank masters and crew of both vessels for their outstanding support during the cruise. The German part of this study was supported by DFG through research grant SCHW/11-1. Many thanks go to Witold Sczcuciński and Karl Stattegger for good discussions.

Address

Peter Feldens
University of Kiel - Institute of Geosciences
Otto-Hahn Platz 1
24418 Kiel, Germany

pfeldens@gpi.uni-kiel.de

Polish J. of Environ. Stud. Vol. 18, No. 1 (2009), 63-68

Original Research

Impact of 2004 Tsunami on Seafloor Morphology and Offshore Sediments, Pakarang Cape, Thailand

P. Feldens[1]*, K. Schwarzer[1], W. Szczuciński[2], K. Stattegger[1], D. Sakuna[1], P. Somgpongchaiykul[3]

[1]Institute of Geosciences, Coastal and Shelf Research, Kiel University, Olshausenstrasse 40, 24118 Kiel, Germany
[2]Institute of Geology, Adam Mickiewicz University in Poznań, Maków Polnych 16, 61-606 Poznań, Poland
[3]Biogeochemical and Environmental Change Research Unit, Prince of Songkla University, P.O. Box 50, Kho Hong, hat Yai, Songkhla 90112, Thailand

Received: 8 October, 2008
Accepted: 25 November, 2008

Abstract

This study documents seafloor morphology and sediments based on multibeam, side-scan sonar and boomer surveys, as well as sediment samples taken on the inner to mid shelf of the Andaman Sea after the 2004 Indian Ocean tsunami. Preservation of submarine relief in former underwater mining areas points to limited impact of the tsunami, while channel structures parallel to the observed tsunami backwash indicate a possible higher impact. Therefore, the tsunami impact seems to be focused on some areas. The impact was probably most effective during the backwash, when stiff mud deposits containing grass, wood fragments and shells were transported by high density backwash flows. Moreover, several boulders, which might have been deposited during the tsunami backwash flow, were found in the channels in front of Pakarang Cape.

Keywords: 2004 Indian Ocean tsunami, seafloor mapping, tsunami backwash, inner continental shelf, Andaman Sea

Introduction

Most of the research published about erosion and deposition of recent tsunamis focus on the onshore areas. The offshore effects, although theoretically significant [1] and more common in older geological records compared to onshore deposits [2], have only been documented in a few studies [3-5]. Surprisingly, offshore impacts of the well studied 2004 Indian Ocean tsunami are also almost unknown. Few authors reported offshore deposition of muddy sediments [6-8]. Offshore was postulated through analyses of microfossils in onshore tsunami deposits [9-12].

This article presents results of a four-week research cruise, undertaken in November and December 2007, focussing on the inner continental shelf next to Pakarang Cape (Phang Nga province, Thailand). During this cruise, hydroacoustic data (side-scan sonar, multibeam echo sounder, shallow water reflection seismic) as well as sediment samples were collected to obtain further insight about the impact of the 2004 tsunami on the shallow seafloor.

*e-mail: pfeldens@gpi.uni-kiel.de

The Research Area

The Andaman Sea continental shelf adjacent to the Malay Peninsula is narrow and slightly inclined. The area is dominated by two monsoonal winds: the northeast monsoon from mid October to March and the southwest monsoon from May to September. The southwest monsoon generates the highest waves along the coast. The tide is mixed semidiurnal with a tidal range between 1.1 and 3.6 m, taking into account spring and neap tide [13]. The research area, about

1,000 km², is situated off Khao Lak (Phang Nga province), in water depths between 10 and 70 meters. For decades, tin mining activities took place in parts of the studied area [14], but ceased about 20 years ago. This study focuses on a part of the shelf next to Phang Nga province, especially around Cape Pakarang (Fig. 1). The research area was chosen because tsunami-induced change of the seafloor can be expected in this area, as the coastline was highly damaged during the tsunami [15, 16]. Furthermore, the absence of large river mouths in this area increases the visibility of tsunami-induced structures on the seafloor in hydroacoustic data. The run-up at Pakarang Cape reached a height of more than 15 m [17] due to shoaling processes and the interaction of the tsunami wave with the seabottom. During the tsunami event a layer of a few cm to about 0.5 m thickness, composed of sand and silty sand, was deposited over almost the whole inundation zone [7, 18-20]. According to eyewitnesses reports, the tsunami wave arrived from three different directions at Pakarang Cape [17]. The backwash pattern was documented by satellite images taken after the tsunami (indicated in Fig. 2). Obviously, the waves were forming a complex run-up and backwash pattern, heavily influenced by the nearshore bathymetry [7]. At the tip of Pakarang Cape, an area of about 12,500 m² was completely eroded during the tsunami [21]. Hundreds of reef rocks more than 1 m in diameter were transported landwards by the tsunami and deposited in shallow waters around Pakarang Cape [22, 23]. Tsunamigenic incisions, with a spacing between 50 and 200 m at the coastline of Khao Lak, were created during the run-up, and enlarged during the backwash of the tsunami [24]. Furthermore, it was observed that the channels are fan-shaped, and are wider at the coastline and narrower further inshore. This indicates a control of spacing and dimension of these return channels by the wave height of the tsunami. [24]. Westward of the research area, about 2 m sand from the seafloor have been eroded around a coral reef boulder in 30 m water depth, probably due to the tsunami [6].

Methods

Material for the study was collected during a research cruise on RV CHAKRATONG TONGYAI in November and December 2007. Acoustic properties of the seafloor sediment were measured using a side scan sonar (500 kHz) with digital data acquisition. A shallow water multibeam echo sounder with a working frequency of 180 kHz was welded to the portside of the research vessel to record bathymetric data. Shallow water reflection seismic data were obtained using a high resolution EG&G boomer system (about 500-15000 Hz). The covered area is shown in Fig. 1. For ground-truthing of the hydroacoustic data and for further sediment analysis, 77 grab samples were taken using a Van-Veen-type grab sampler. 40 short sediment cores of up to 125 cm in length were obtained using a gravity corer. However, for the present study only grab sample material was analyzed. To determine the grain-size parameters, sediment samples were dried and sieved. The grain-size statistics were calculated using Gradistat software [25].

Results

Bathymetry

The obtained bathymetric map of the area in front of Pakarang Cape is shown in Fig. 2. Down to 18 m, the slope is inclined with an angle of about 0.8°. Below this depth, the overall slope angle decreases (to about 0.1°), and the seafloor shows a “step like” morphology (Figs. 2 and 3). At the base of the southern slope of these steps, SW-NE striking channels, with a width of several hundred meters

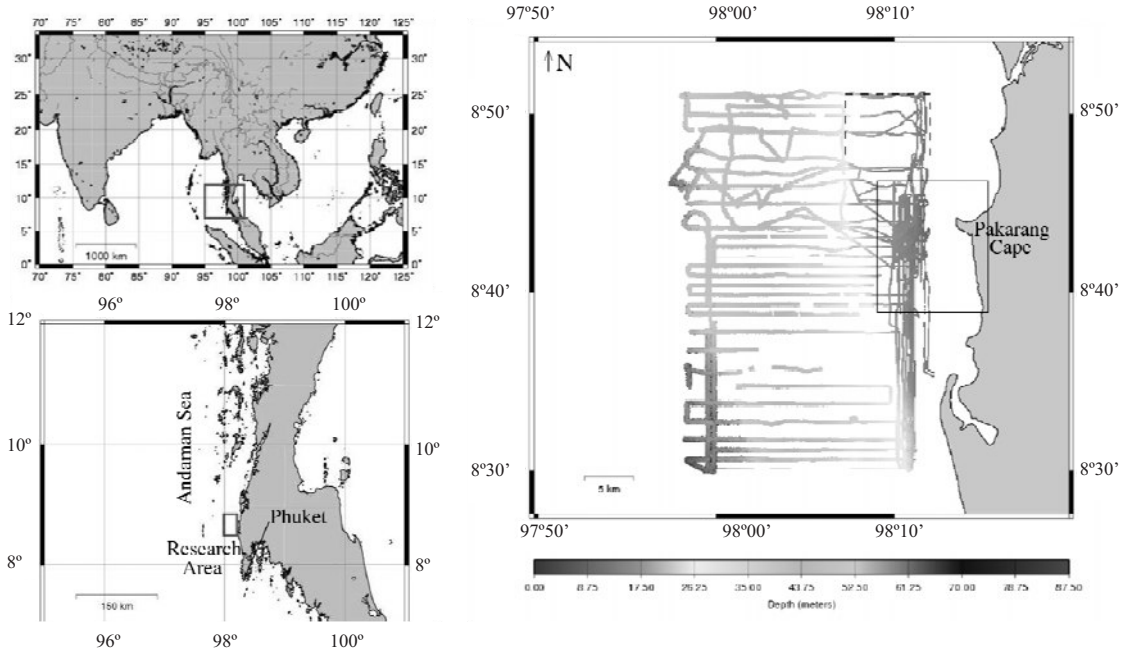

Fig. 1. The research area offshore Phang Nga province.

and a depth between 0.5 to 2 m are cut in the seafloor. Bathymetric cross sections (Fig. 3) reveal that the channels are asymmetrical, with the deepest incisions situated close to their southern slope. The dipping angles of the channels are low, reaching 1 to 1.2° at the southern slopes and about 0.2° at the northern slope. Towards the coastline, corresponding with the onset of the steeper slope angle in water depths between 14 and 18 m, the number of channels increases. The continuation of these channels both in deeper and shallower water is unknown, although first data from shallow water reflection seismics suggests a continuing propagation of the channels further offshore. The seismic data does not show any connection between the channels and subsurface structures. Remnants of these tin mining activities in this area (indicated in Fig. 1) are visible in the form of steep holes up to 7 m deep.

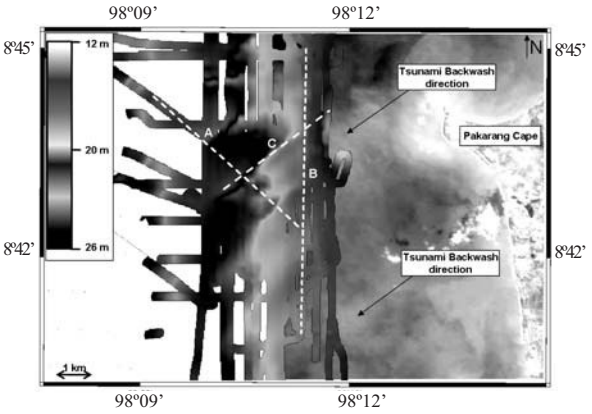

Fig. 2. Bathymetry around Pakarang Cape merged with a satellite image taken shortly after the 2004 tsunami. The dashed lines indicate the profiles shown in Fig. 3. (satellite image: Images acquired and processed by CRISP, National University of Singapore. IKONOS image © 2004. www.crisp.nus.edu.sg/tsunami/tsunami.html, modified.)

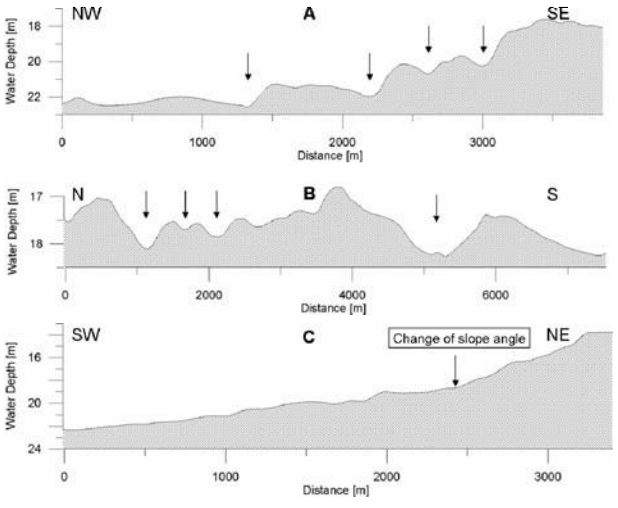

Fig. 3. Cross sections from several parts of the seafloor. Channels are marked by arrows. For the positions, refer to Fig. 2.

Seafloor Sediments

Large elongated sediment patches, appearing nearly white in the side-scan sonar images, with the same strike direction as the aforementioned channels, were documented in front of Pakarang Cape. There is a distinct transition between these areas and the surrounding seafloor (appearing darker in the side-scan sonar image shown in Fig. 4). Light-coloured areas in the side scan sonar data correspond to finer or non-consolidated sediment, while darker areas correspond to coarser or more consolidated sediment. The southern boundary of the elongated patches is very irregular and appears "flame-shaped" (Fig. 5). A combination of side-scan sonar and multibeam echo sounder data indicates that the large elongated areas of fine sediment are situated at the steeper southern slopes of the channels. In many cases, it was not possible to distinguish between the layers of fine to medium sand in the seismic data, taken simultaneously with the side scan sonar data. When it was possible to recognize these layers in the seismic data, their thickness appeared to be on the order of a few decimetres. Small patches of the same, fine sediment are visible closer to the coastline and are commonly situated in smaller channels and depressions (Fig. 6).

The results of the grain size analysis are incorporated in Fig. 4. The elongated sediment patches are composed of fine to medium sand, while the surrounding seafloor consists of coarse sand. Both types of sediment are poorly to moderately sorted. In one grab sample, taken from about 16 m water depth a stiff mud, covered by a 3 cm thick layer of coarse, well sorted sand was found. It contained terrestrial organic remnants: grass and pieces of wood, moreover, clasts of clay were found. Additionally, side-scan sonar data revealed the presence of numerous boulders with diameters around 1 m, as determined on the basis of their acoustic shadows in the side-scan sonar images. Most of these boulders appear between the aforementioned sediment patches close to the

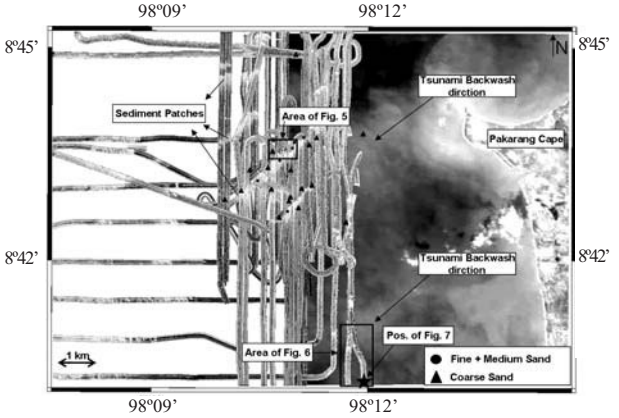

Fig. 4. Side Scan Sonar data merged with a satellite image taken shortly after the 2004 tsunami. Indicated are sediment types based on grain size analysis, as well as the locations of the following figures. (satellite image: Images acquired and processed by CRISP, National University of Singapore. IKONOS image © 2004. www.crisp.nus.edu.sg/tsunami/tsunami.html, modified.)

coastline (Fig. 7). However, some boulders, located at a distance of about 4 to 6 km from the tip of Pakarang Cape, are situated within a larger channel directly north of an elongated sediment patch (Fig. 5).

Discussion

Although the survey took place three years after the 2004 Indian Ocean tsunami, it is likely that several of the observed features may be ascribed to this impact. For instance, the channels and elongated sediment patches observed in front of Pakarang Cape have a striking resemblance to the backwash pattern observed in the satellite images taken after the tsunami event (Fig. 4). The erosion potential of a tsunami run-up and backwash is commonly mentioned in the literature [26, 27]. The impacts of the backwash depend on the amount of water flowing back into the sea, which itself depends on wave height [24], and on the formation of high density hyperpycnal flows [28]. High tsunami run-up heights at Pakarang Cape and the local presence of stiff mud with grass and wood found in offshore sediment samples suggest that both conditions enhancing the erosion potential of the backwash were met. Therefore, it is possible that the observed channels were formed mainly during the channelized tsunami backflow. Although due to a lack of pre-tsunami data it is not possible to exclude that the channels already existed prior to that event, several features suggest their origin or at least reshaping during the tsunami. A good correlation between the spacing of onshore incisions, interpreted to be created during run-up and backwash, and tsunami wave height is reported [24]. River mouths in the Nam Khem plain (north from Pakarang Cape) changed into wedge-shaped channels [29] with a width of 50-200 m, mainly due to the effect of a concentrated tsunami backwash. As the onshore return channels of the tsunami are wedge-shaped, and widening towards the coastline, it could be assumed that a connection between the onshore incisions and the wider channels, observed in shallow waters, exists. The rapid transition of these channels into the deeper, and even wider, channels in water depths of about 17 to 18 m might be caused by a change of the hydraulic behaviour of the backwash due to the changing slope angle of the seafloor (Figs. 2 and 3). The channels in deeper waters are asymmetrical in cross section. Related to this observation, it is interesting to note that regularly spaced, very shallow swales with asymmetrical profiles and filled by very fine-grained sandstones, and interpreted to be created during a paleotsunami event, have been reported [30].

Local erosion (adjacent to a large reef boulder where the formation of scour structures was possible) of up to 2 m

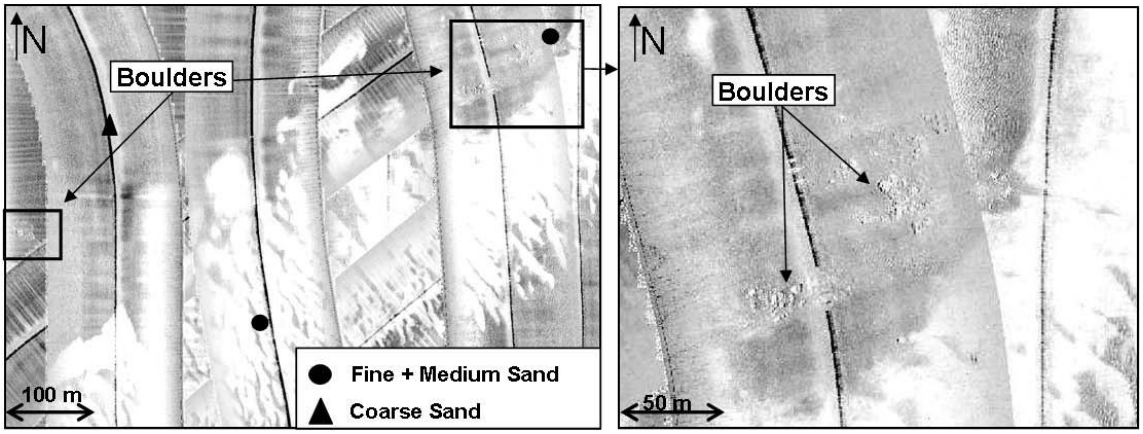

Fig. 5. Detailed view of one elongated sediment patch in front of Pakarang Cape. To the north of the patches, boulders are visible. For the location of the figure, refer to Fig. 4.

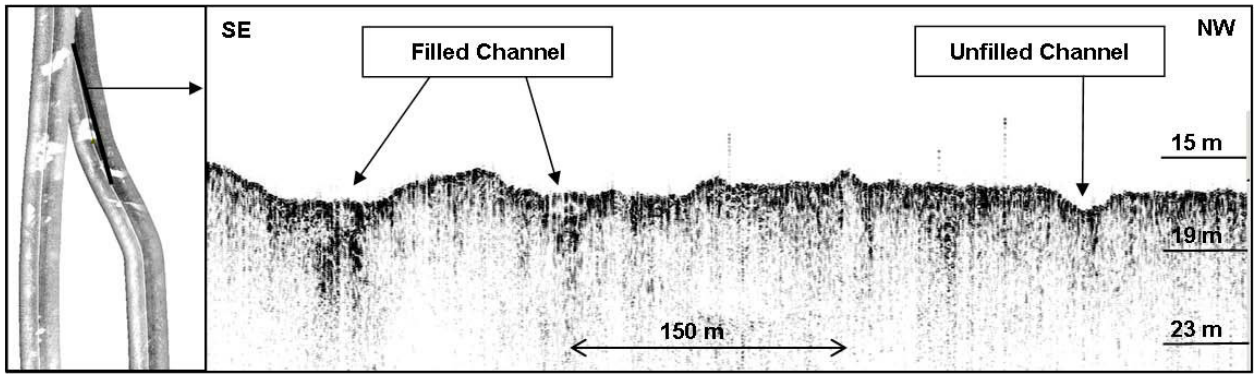

Fig. 6. Shallow seismic profiles close to the coastline with small channels. Some of these channels are filled with finer sediment, which appears white in the side scan sonar data. For the location of the figure, refer to Fig. 4.

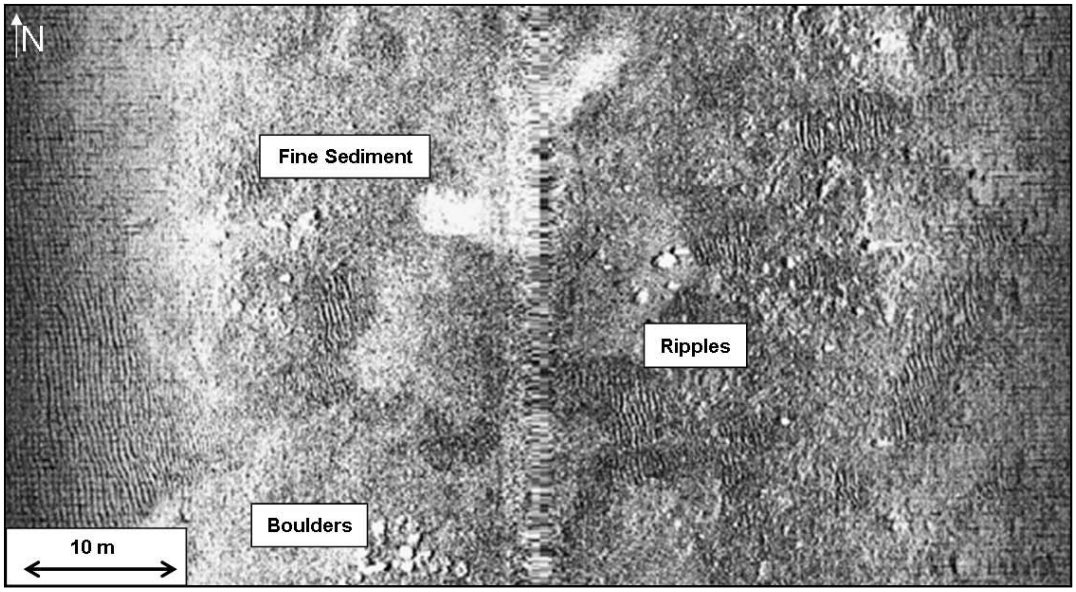

Fig. 7. Detailed view of side scan sonar data from a profile recorded close to the coastline. Different sediment types, including boulders, fine sediment and rippled sand, are deposited within a distance of a few meters. The location of this figure is indicated in Fig. 4.

during the tsunami event in a water depth of 30 m was reported [6]. Our data suggest erosion of a lower but comparable magnitude in the channels, and less erosion of the surrounding seafloor, as indicated by well preserved tin mining holes. This observation confirms previous suggestions [28] that tsunami effects are largely related to confined channelized flows during backwash and, possibly, run-up. The elongated areas and the small patches of fine and medium sand found in the channels and closer to the coastline could have been deposited during the backwash of the tsunami. If these sediments were deposited before the tsunami, one could expect that the tin mining holes would have been filled with the finer material during the past decades. However, the "flame-like" shape (indicating sediment transport) of the fine to medium sand sediment patches, as well as the presence of these sediments on the steeper southern slopes of the channels, may suggest their reworking during the post-tsunami period. In particular, their asymmetrical distribution in the channels may be a result of monsoon-related circulation and preservation of the finer sediments in relatively sheltered locations [8].

The existence of stiff muddy sediments containing pieces of grass and wood, which should be floating unless transported in a high turbidity and high density hyperpycnal flow, is strong supporting evidence of tsunami backwash and its potential erosion power. On the other hand, these deposits being covered by distinctly different coarse sand, typical for this part of the continental shelf, are already preserved in the geological record. This finding is promising for the search for paleotsunami evidence in this setting.

Interesting is the presence of boulders within the larger return channels in front of Pakarang Cape. The backwash velocity was modelled to be around 3.0 m/s at Cape Pakarang [22], slightly higher than the calculated critical velocity to move boulders. While some authors do not believe that the backwash, due to its short duration, transported boulders from the tidal flat back to the deeper waters, [22], it is very likely that boulders could easily be transported downhill from their original position on the coral reef slope during the tsunami backwash.

Conclusions

One of the first studies of offshore impacts of the 2004 tsunami indicates:

- Existence of a system of channels slightly oblique to the coastline, which are partly filled with finer sediments and could have been created during the backwash of the 2004 Indian Ocean tsunami.
- Variability in the channel system, which is changing with water depth and slope angle; probably as a result of changing hydrodynamic properties of the backwash (hyperpycnal flow).
- Validity of the assumptions on a channelized backwash, and maybe even run-up of the tsunami.
- Characteristic sediment deposition during the backwash, suggesting deposition from highly turbulent, high density flow.
- The backwash had enough power to transport boulders from the coral reef slope to deeper waters.

Acknowledgement

The study was supported by the DFG through research grant SCHW/11-1. W. Szczuciński was supported by a Foundation for Polish Science (FNP) fellowship. We are grateful to Phuket Marine Biological Center (PMBC) for providing us with RV CHAKRATONG TONGYAI. The help of cruise participants is greatly acknowledged.

References

1. WEISS R. Sediment grains moved by passing tsunami waves: Tsunami deposits in deep water. Mar. Geol. **250**, 251, **2008**.
2. DAWSON A. G., STEWART I. Tsunami deposits in the geological record. Sed. Geol. **200**, 166, **2007**.
3. VAN DEN BERGH G.D., BOER W., DE HAAS H., VAN WEERING TJ.C.E., VAN WIJHE R. Shallow marine tsunami deposits in Teluk Banten (NW Java, Indonesia), generated by the 1883 Krakatau eruption. Mar. Geol. **197**, 13, **2003**.
4. NODA A., KATAYAMA H., SAGAYAMA T., SUGA K., UCHIDA Y., SATAKE K., ABE K., OKAMURA Y. Evaluation of tsunami impacts on shallow marine sediments: An example from the tsunami caused by the 2003 Tokachi-oki earthquake, northern Japan. Sed. Geol. **200**, 314, **2007**.
5. ABRANTES F., ALT-EPPING U., LEBREIRO S., VOELKER A., SCHNEIDER R. Sedimentological record of tsunamis on shallow-shelf areas: The case of the 1969 AD and 1755 AD tsunamis on the Portuguese Shelf off Lisbon. Mar. Geol. **249**, 283, **2008**.
6. CHAVANICH S., SIRIPONG A., SOJISUPORN P., MENASVETA P. Impact of Tsunami on the seafloor and corals in Thailand. Coral Reefs **24**, 535, **2005**.
7. SZCZUCIŃSKI W., CHAIMANEE N., NIEDZIELSKI P., RACHLEWICZ G., SAISUTTICHAI D., TEPSUWAN T., LORENC S., SIEPAK J. Environmental and Geological Impacts of the 26 December 2004 Tsunami in Coastal Zone of Thailand – Overview of Short and Long-Term Effects. Polish J. Environ. Stud. **15** (5), 793, **2006**.
8. DI GERONIMO I., ROBBA E., CHARUSIRI P., CHOOWONG M., AGOSTINO I., MARTINO C., DI GERONIMO R., PHANTUWONGRAJ S. Marine modern sediments and rocky bottoms of Khao Lak coastal area, Changwat Phang Nga, Andaman Sea, SW Thailand. Color Map, 1:30.000, Catania, Bangkok, **2008**.
9. RAZZHIGAEVA N.G., GANZEI L.A., GREBENNIKOVA T.A., IVANOVA E.D., KAISTRENKO V.M. Sedimentation particularities during the tsunami of December 26, 2004, in northern Indonesia: Simelue Island and the Medan coast of Sumatra Island. Oceanology **46**, 875, **2006**.
10. HAWKES A.D., BIRD M., COWIE S., GRUNDY-WARR C., HORTON B.P., SHAU HWAI A.T., LAW L., MACGREGOR C., NOTT J., ONG J.E., RIGG J., ROBINSON R., TAN-MULLINS M., SA T.T., YASIN Z., AIK L.W. Sediments deposited by the 2004 Indian Ocean tsunami along the Malaysia-Thailand peninsula. Mar. Geol. **242**, 169, **2007**.
11. DAHANAYAKE K., KULASENA N. Recognition of diagnostic criteria for recent- and paleo-tsunami sediments from Sri Lanka. Mar. Geol. **254**, 180, **2008**.
12. KOKOCIŃSKI M., SZCZUCIŃSKI W., ZGRUNDO A., IBRAGIMOW A. Diatom assemblages in 26 December 2004 tsunami deposits from coastal zone of Thailand as sediment provenance indicators. Polish J. Environ. Stud. **18**, 93, **2009**.
13. THAMPANYA U., VERMAAT J.E., SINSAKUL S., PANAPITUKKUL N. Coastal erosion and mangrove progradation of Southern Thailand. Estuar., Coast. Shelf Sci. **68**, 75, **2006**.
14. USIRIPRISAN C. CHIEMCHINDARATANA S., SHOOSUWAN S., CHATRAPAKPONG Y. Offshore exploration for tin and heavy minerals in the Andaman Sea. Department of Mineral Resources, Thailand, pp. 224, **1987**.
15. BELL R., COW AN H., DALZI ELL E., EVANS N., O'LEARY M., RU SH B., YU LE L. Survey of impacts on the Andaman Coast, Southern Thailand following the great Sumatra-Andaman earthquake and tsunami of December 26, 2004. Bull. of The New Zealand Soc. For Earthquake Eng. **38** (3), 123, **2005**.
16. TSUJI Y.Y., NAMEGAYA H., MATSUMOTO S.I., IW ASZKI W., KANBUA M., SRIWI CHAI M., MEESUK V. The 2004 Indian tsunami in Thailand. Surveyed runup heights and tide gauge records. Earth Planets Space, **58**, 223, **2006**.
17. SIRIPONG A. Andaman Seacoast of Thailand Field Survey after the December 2004 Indian Ocean Tsunami. Earthquake Spectra **22** (S3), 187, **2006**.
18. SZCZUCIŃSKI W., NIEDZIELSKI P., RACHLEWICZ G., SOBCZYŃSKI T., ZIOŁA A., KOWALSKI A., LORENC S., SIEPAK J. Contamination of tsunami sediments in a coastal zone inundated by the 26 December 2004 tsunami in Thailand. Environ. Geol. **49**, 321, **2005**.
19. HORI K., KUZUMOTO R., HIROUCHI D., UMITSU M., JANJIRAWUTTIKUL N., PATANAKANOG B. Horizontal and vertical variation of 2004 Indian tsunami deposits: An example of two transects along the western coast of Thailand. Mar. Geol. **239**, 163, **2007**.
20. CHOOWONG M., MURAKOSHI N., HISADA K., CHARUSIRI P., DAORERK V., CHAROENTITIRAT T., CHUTAKOSITKANON V., JANKAEW K., KANJANAPAYONT P. Erosion and deposition by the 2004 Indian Ocean tsunami in Phuket and Phang-nga Provinces, Thailand. J. Coast. Res. **23**, 1270, **2007**.
21. SYNOLAKIS C.E., KONG L. Runup measurements of the December 2004 Indian Ocean Tsunami. Earthquake Spectra **22** (S3), 67, **2006**.
22. GOTO K., CHAVANICH S.A., IMAMURA F., KUNTHASAP P., MATSUI T., MINOURA K., SUGAWARA D., YANAGISAWA H. Distribution, origin and transport process of boulders deposited by the 2004 Indian Ocean tsunami at Pakarang Cape, Thailand. Sed. Geol. **202**, 821, **2007**.
23. GOTO K., IMAMURA F., KEERTHI N., KUNTHASAP P., MATSUI T., MINOURA K., RUANGRASSAMEE A., SUGAWARA D., SUPHARATID S. Distribution and significance of the 2004 Indian Ocean tsunami deposits: initial results from Thailand and Sri Lanka. In: Tsunamiites – Features and Implications. Shiki et al. (eds.) Elsevier, pp. 105-122, **2008**.
24. FAGHERAZZI S., DU X. Tsunamigenic incisions produced by the December 2004 earthquake along the coasts of Thailand, Indonesia and Sri Lanka. Geomorphology **99**, 120, **2008**.
25. BLOTT S.J., PYE K. Gradistat: a grain size distribution and statistics package for the analysis of unconsolidated sediments. Earth Surface Processes and Landforms **26**, 1237, **2001**.
26. DAWSON A. G. Geomorphological effects of tsunami run-up and backwash. Geomorphology **10**, 83, **1994**.
27. DAWSON A. G., SHI S. Tsunami deposits. Pure and Applied Geoph. **157**, 875, **2000**.
28. LE ROUX J. P., VARGAS G. Hydraulic behavior of tsunami backflow: insights from their modern and ancient deposits. Environ. Geol. **49**, 65, **2005**.
29. UMITSU M., TANAVUD C., PATANAKANOG B. Effects of landforms on tsunami flow in the plains of Banda Aceh, Indonesia, and Nam Khem, Thailand. Mar. Geol. **242**, 141, **2007**.
30. ROSETTI D.D.F., GÓES A.M., TRUCKENBRODT W., ANAISSE JR J. Tsunami-induced large scale scour-and-fill structures in Late Albian to Cenomanian deposits of the Grajaú Basin, northern Brazil. Sedimentology **47**, 309, **2000**.